The Dissertation Committee for Adam Bradley Powell
certifies that this is the approved version of the following Dissertation:

Synthesis and Applications of Poly N-Heterocyclic Carbenes and Investigation of Aldimine Coupling

Committee:

Alan H. Cowley, Supervisor

Christopher W. Bielawski

Richard A. Jones

Bradley J. Holliday

Christine E. Schmidt

Synthesis and Applications of Poly N-Heterocyclic Carbenes and Investigation of Aldimine Coupling

by

Adam Bradley Powell, B.S.

Dissertation

Presented to the Faculty of the Graduate School of

The University of Texas at Austin

in Partial Fulfillment

of the Requirements

for the Degree of

Doctor of Philosophy

The University of Texas at Austin

December 2010

Dedication

To my Mom and Dad, both of which encouraged me from a very young age to strive for excellence in all facets of my life. My Mom who put all her love and energy into helping me become the best scientist and overall person I could be. Also my Aunt Shirley for treating me like the grandson she never had. All of my members of my immense family encouraged me throughout college and graduate school and never doubted my success.

Acknowledgements

First and foremost I am grateful to my research advisor, Professor Alan H. Cowley for his confidence in my ideas and patience as we developed our project. His encouragement and guidance were critical to my progression as a scientist.

Another significant person in my growth as a scientist has been my distinguished and humble collaborator Professor Christopher W. Bielawski. Formulating a partnership with him and his research group allowed me to become accustomed with fields outside my sphere of familiarity and he has challenged me to conduct research in a systematic manner. This collaboration also enabled me to learn the delicate art of diplomacy in dealing with other research environments.

My undergraduates Jon Varias, Li Dinh, and Jaclyn Brown were also valuable in aiding the progression of my projects. Jaclyn Brown deserves special attention because she educated me on how to perform several lab techniques such as flash column chromatography that our lab previously had little experience in executing. Without these skills many of my reaction pathways would not have been successful and our progress would have stalled.

Professor Bradley J. Holliday was an essential asset to me in the early stages of our thiophene diimine project. Brent Norris, Evelyn Rosen, Michelle Mejia and Maria Cabezas were as well helpful in advancing my research.

November 4, 2010

Synthesis and Applications of Poly N-Heterocyclic Carbenes and Investigation of Aldimine Coupling

Adam Bradley Powell, PhD.

The University of Texas at Austin, 2010

Supervisor: Alan H. Cowley

The design, synthesis, characterization and application of carbene-based metallopolymers are described herein. Metallopolymers have found wide applications in the fields of photovoltaics, energy storage and electrochromic windows. The incorporation of N-heterocyclic carbene (NHC) functionalities into a polymerizable scaffold would allow for many different metals to be attached in a facile and high-yielding manner. Such complexes could be functionalized onto surfaces and utilized as either spectroscopic or antimicrobial devices.

Early attempts in our lab focused on utilizing bis(thiophene) diimines (instead of NHCs) as scaffolds for metal chelation and polymerization. This approach was unsuccessful due to the lability of the diimine moiety under electrochemical cycling and the thiophene moieties were not able to undergo polymerization. In order to more fully

understand the key transformation in synthesizing the thiophene-substituted diimines, a comprehensive investigation of the aldimine coupling transformation was undertaken. A high concentration of substrate and catalyst was determined to be the most important factor in obtaining high yields of the dimerized products. Green solvents such as acetonitrile and hexanes could be used for the dimerization reaction when the cyanide counteranion was changed from sodium to tetrabutylammonium. The steric limitations were systematically identified and a series of possible substrates have been ruled out as viable candidates for dimerization.

Applying the experience gleaned from earlier reports, the first example of an NHC polymer was prepared in which the monomer features an NHC functional group orthogonally connected to its main chain. A polymerizable imidazolylidene-AuCl complex containing pendant bithiophene moieties was prepared by a high yielding, multi-step procedure. Oxidative electropolymerization of this monomer afforded the desired polymer $(Au[NHC]Cl)_n$, which was characterized on the basis of electrochemical studies as well as by X-ray crystallography, photoelectron and UV-vis spectroscopy.

The methodology described above was expanded to develop a series of analogous poly(N-heterocyclic carbene) complexes with appended entities (M = Ir, Au, Ag, or S) and found to be electrochromic. Most of the polymers exhibit an intense absorbance wave at 700 nm under oxidative conditions which is attributable to the formation of polaron excitations along the polymer main chain. The presence of a transition metal significantly increased the electrochromic character of the polycarbene system. The iridium-containing polymer was found to possess significant near-infrared (NIR) absorbance at 1100 nm in which the metal moiety effectively functions as an electron sink. Electrochemical analysis of the polymer thin films revealed that they exhibit highly reversible electrochromic activities.

Table of Contents

List of Tables

List of Figures

List of Schemes

Chapter 1: Review of Electropolymizable Poly N-Heterocyclic Carbene Complexes

Well-defined transition metal complexes supported by N-heterocyclic carbenes (NHCs) have found tremendous utility in a broad range of catalytic[1] and antimicrobial applications over the past several decades.[2] However, less attention has been directed toward polymeric materials containing NHCs possibly due to synthetic limitations involved in their assembly. Due to their distinctive electronic and/or physical properties, such materials hold promise for enabling the aforementioned applications, in addition to creating new ones.[3] As illustrated in Figure 1, three types of polymeric NHCs are currently known. Tethered poly(NHC) complexes typically feature catalytically-active complexes connected via alkyl linkers to the main chains of synthetic polymers or Merrifield resins.[4] One notable advantage of these materials is that they can be conveniently recovered from various reaction mixtures and re-used. Another example is main-chain poly(NHC)s where carbene-metal complexes are integral components of the polymer main chain. Certain derivatives of these materials have been shown to be thermally reversible, which has helped to establish new concepts in self-healing electronics, self-assembly, and catalysis.[5] Recently, we reported the first examples of poly(NHC) complexes in which the carbene functionalities are orthogonally connected to the main chains of the respective polymers.[6] These materials feature a backbone virtually analogous to that of polythiophene, which renders them attractive for use as components in molecular electronics and redox-switchable catalysts.[3,7]

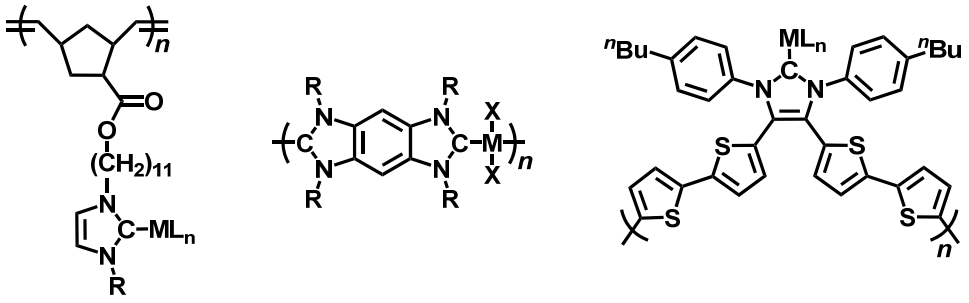

Figure 1.1. Representative examples of transition metal complexes supported by three different classes of poly(NHC)s. ML_n = transition metal complex. R = aryl or alkyl.

Three classes of poly(NHC)s have been reported in the literature and are illustrated in Figure 1.1. The synthetic strategy used to prepare the third class of polymers was based on a series of thiophene-substituted diimine ligands that were previously reported[8] by our group (see Figure 1.2). Due to their ability to accept up to two electrons, these diimine ligands and their transition metal complexes were envisioned to undergo electropolymerizaton. However, these monomers were found to be too unstable under oxidative conditions to undergo this process. Subsequent cyclic voltammetry studies revealed that the installation of electron-donating groups lowered the oxidation potential of the aforementioned diimines. It was surmised that the incorporation of bithiophene moieties might lower the oxidation potential enough to facilitate electropolymerization.

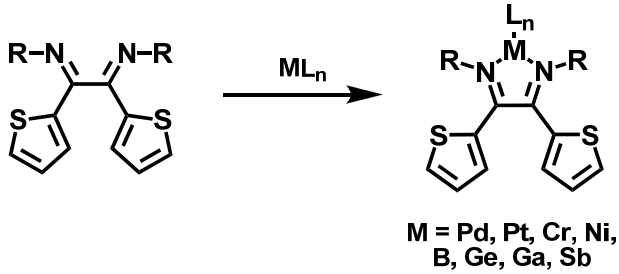

Scheme 1.1. Metallation of thiophene-substituted diimines with various main-group and transition metal complexes.

A bithiophene-substituted diimine (**1**) was synthesized in 77% overall yield by dimerizing and then oxidizing the monoimine formed from the condensation of 2,2′-bithiophene carboxaldehyde with 4-*n*-butylaniline. Continuous electrochemical cycling of a CH_2Cl_2 solution of **1** in a three-electrode cell resulted in the deposition of a yellow film of polymer. While the relationship between the oxidative current and the scan rate was found to be linear, an indicator that good films were being electrodeposited,[9] a reduction feature was evident at –0.2 V (see Figure 1.3) and the overall profile did not resemble that of a standard thiophene polymerization. Hence, the material appeared to undergo decomposition upon deposition, precluding its use an effective scaffold for ligating transition metals.

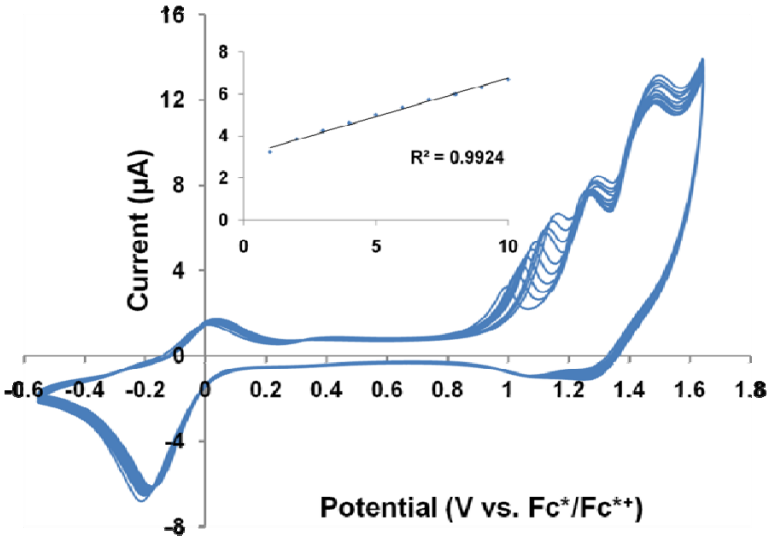

Figure 1.2. Overlay of continuous cyclic voltammograms of diimine **1** over time. Inset: plot of current maxima vs. number of cycles. Conditions: CH_2Cl_2, $[(n\text{-Bu})_4N^+][PF_6^-]$ (0.1 M), $[\mathbf{1}]_0 = 1 \times 10^{-3}$ M, $v = 100$ mV s^{-1}. The potentials were referenced to SCE by shifting Fc^{*0}/Fc^{*+} to −0.057 V.

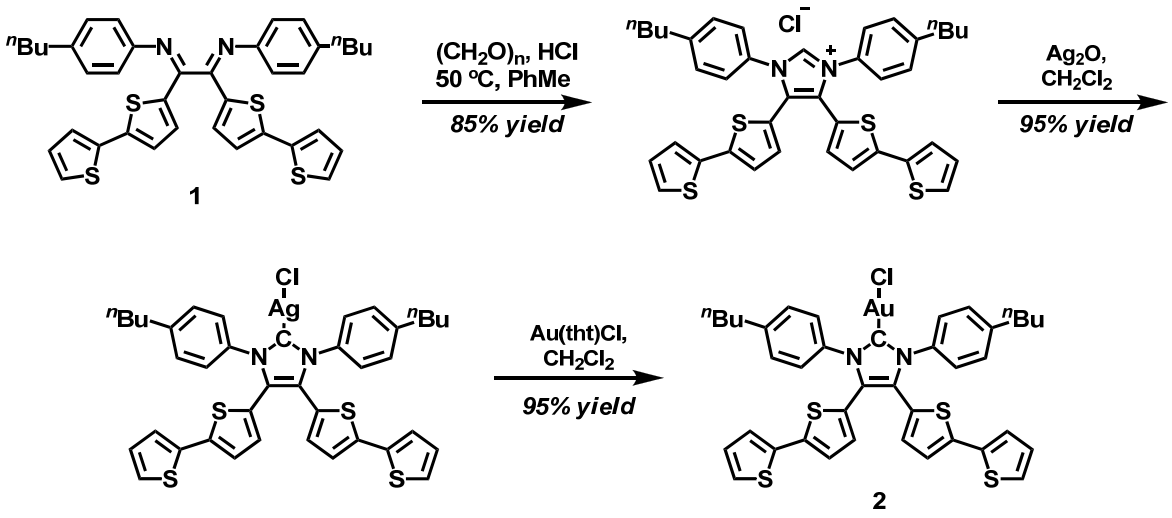

Scheme 1.2. Synthesis of electropolymerizable gold-NHC monomer **2**.

To overcome this decomposition problem, the aforementioned diimine (**1**) was transformed into the NHC-gold complex **2** as summarized in Scheme 1.2. This monomer was subsequently electropolymerized (Scheme 1.3) onto a platinum disc in a three-electrode cell. As shown in Figure 1.3, features attributable to the oxidation and reduction processes were clearly evident and easily assigned. Moreover, the current generated upon oxidation was found to vary linearly with scan rate, as anticipated. This enhancement in the electrochemical properties of the diimine upon metallation is consistent with previous reports on other systems[10] and it was surmised that the ligated metals effectively assisted the electron transfer processes. Furthermore, elemental analysis of poly(**2**) by XPS revealed the anticipated atomic ratios for sulfur, nitrogen and gold and the UV-vis profile of the polymer was shifted bathochromically with respect to its monomer, which is consistent with the formation of an electronically delocalized polymeric structure.

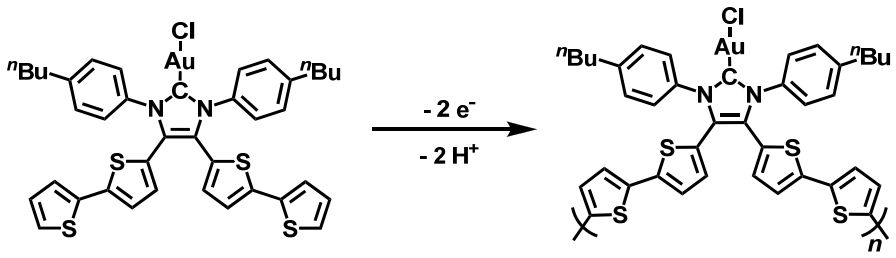

Scheme 1.3. Oxidative electropolymerizaton of **2**.

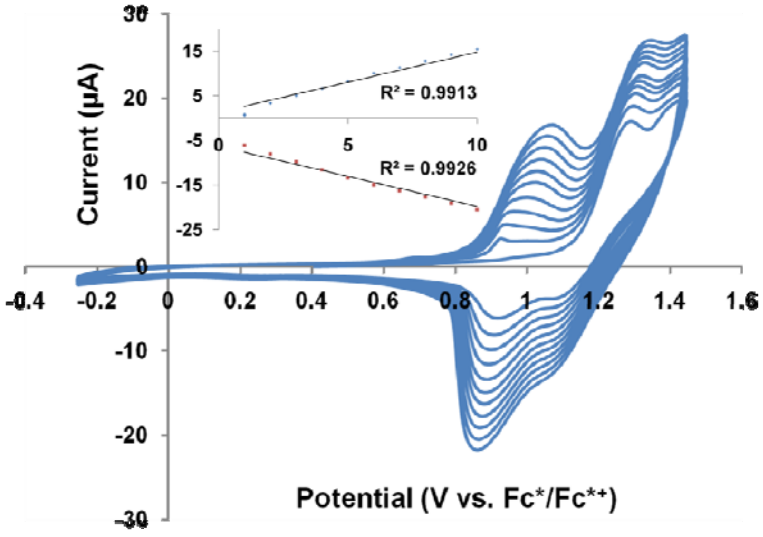

Figure 1.3. Overlay of continuous cyclic voltammograms of **2** over time. Inset: plot of current maxima vs. number of cycles. Conditions: CH_2Cl_2, $[(n\text{-}Bu)_4N^+][PF_6^-]$ (0.1 M), $[\mathbf{2}]_0 = 1 \times 10^{-3}$ M, $v = 100$ mV s^{-1}. The potentials were referenced to SCE by shifting Fc^{*0}/Fc^{*+} to −0.057 V.

As illustrated in Scheme 1.4, the aforementioned synthetic approach was recently extended to include five new polymeric NHCs of the general formula $[ML(NHC)]_n$.[11] These metallopolymers were found to undergo a reversible color change from yellow to

blue upon electrochemical oxidation, although the stability of these materials was found to depend on the identity of the incorporated ligated transition metal complex. The $Ir(CO)_2Cl$-substitued material was found to be the most stable electrochromic material studied and was also the only system capable of stabilizing both polarons and bipolarons. Moreover, excitations assigned to bipolaron formation, which were observed at 1100 nm by UV-vis-NIR spectroscopy, were relatively discrete when compared with those of other polythiophene-based materials.[12] As shown in Figure 1.8, the polarons and bipolarons formed are believed to exist along the quarterthiophene chains that connect the NHC metal moieties. The metals act as electron sinks, which facilitates the formation of positive charges along the oligothiophene linkers. Although organic polymers are known to exhibit electrochromic properties,[13] examples that feature transition metals are rare.[14] Further study of the aforementioned metallopolymers is currently underway with a view to exploring the possibility of additional applications.

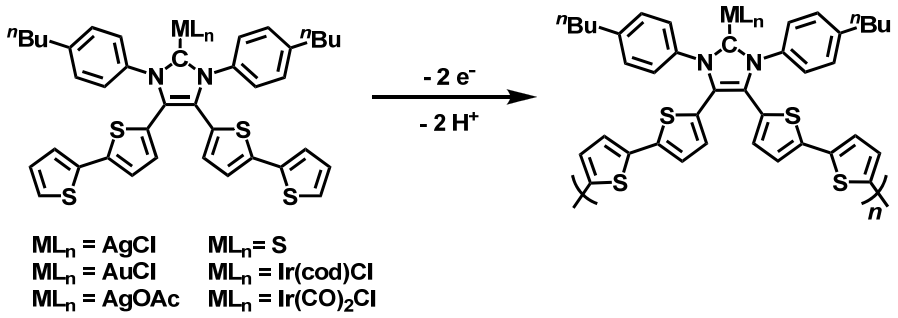

Scheme 1.4. Oxidative electropolymerizaton of various NHC supported transition metal and main group complexes.

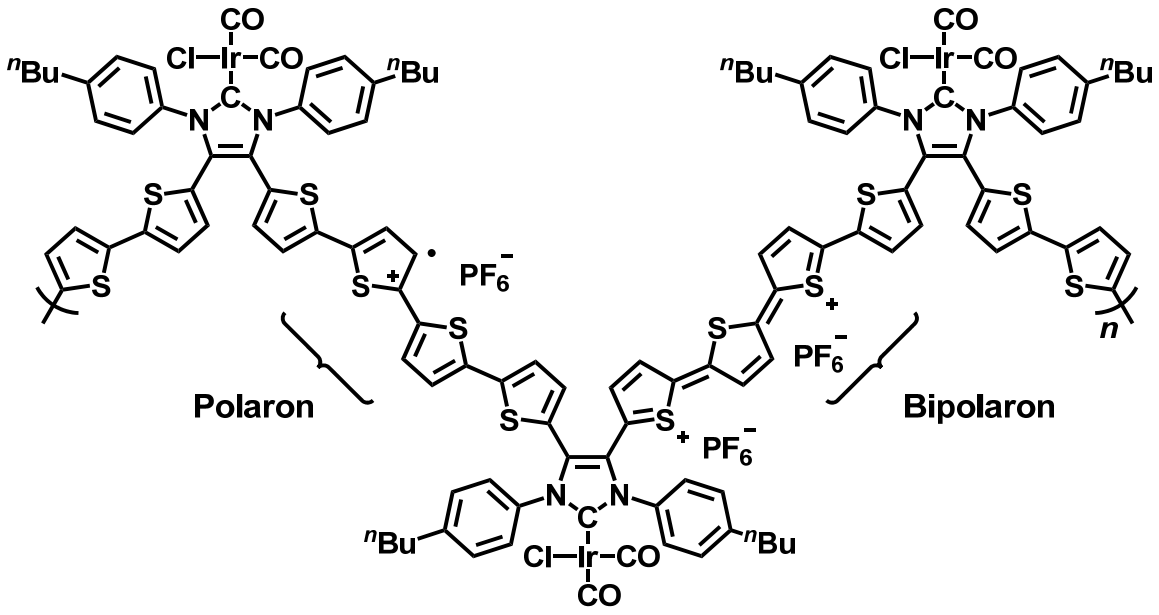

Figure 1.4. Formation of polaron and bipolaron excitations along the main-chain of a metallopolymer containing an NHC supported $Ir(CO)_2Cl$ complex.

Chapter 2: Thiophene-substituted 1,4-Diazabutadiene (α-diimine) Ligands, Electrochemical Analyses and Their Conversion to Phosphenium Triiodide Salts

2.1 Introduction

The 1,4-diaza-1,3-butadiene (α-diimine) ligand class is employed widely in main-group, transition metal, and lanthanide chemistry.[1] One facet of interest in such ligands is their ability to undergo redox chemistry, which is dependent on the nature of the chelated moiety (See Scheme 2.1). For example, in the context of lanthanide chemistry, it has been found that the Eu oxidation state of decamethyleuropocene diazabutadiene complexes can be either +2 or +3 depending on the nature of the substituents on the diazabutadiene ligand.[2]

Scheme 2.1. Reaction of diimines with various metals and main-group reagents.

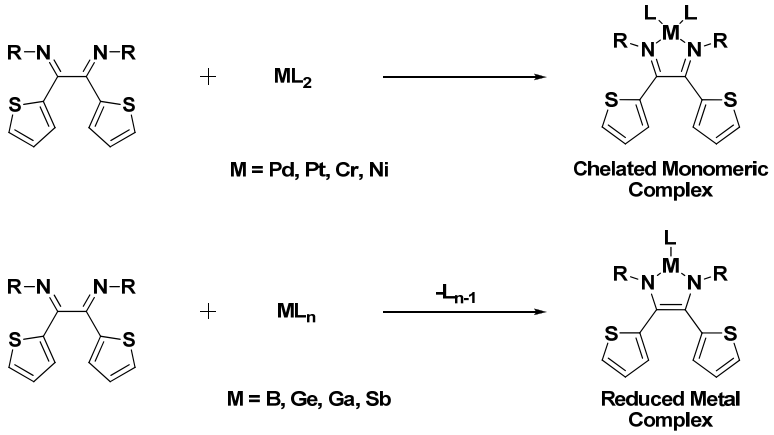

The monomeric behavior of such systems is well understood. A logical next in this area of chemistry would be to incorporate 1,4-diazabutadiene complexes into oligomers and polymers with a view to assessing their physical and photophysical

properties. Inspired by the work of Holliday *et al.*[3] on the assembly of a photoluminescent Eu-containing polymer by electropolymerization of a 3,4-(ethylenedioxy)thiophene (EDOT)-substituted monomer, an attempt was made to synthesize analogous thiophene-substituted diazabutadiene monomers. However, it was not possible to effect the attachment of the thiophene moieties to the imine carbons of the diazabutadiene scaffold. In fact, the literature contains only one reference to a compound of this type.[4] Furthermore, the yield was low (28%) and no characterization data were provided. Unfortunately, attempts to repeat this synthesis were unsuccessful. A more reliable and general synthetic pathway was therefore needed. Recent research by Miller *et al.*[5] has demonstrated that phenyl analogues of the desired molecule can be synthesized by means of symmetrical aldimine coupling. Accordingly, this relatively unexplored methodology was employed for the syntheses of ligands **5-8** and **12**. As a second way of avoiding the use of thiophene-substituted primary amines, the first example of a diazabutadiene ligand that features phenyl spacers between the thiophene moieties and the diazabutadiene nitrogen atoms has been prepared (**12**).

The profound impact of N-heterocyclic carbenes (NHCs) on catalysis[6], synthetic chemistry[7] and materials science[8] has stimulated interest in a quest for analogous systems that feature an element other than carbon. Since phosphenium ions (R_2P^+) are, like carbenic carbon, six-electron species, interest has emerged in so-called N-heterocyclic phosphenium ions (NHPs).[9] Such species might be expected to be strong π-acceptor ligands as opposed to NHCs which function primarily as strong σ-donors. As noted by Miller *et al.*, 4,5-diaryl-substituted heterocyclic imidazolylidene carbenes and their precursor diazabutadienes are relatively rare.[5] The use of phosphenium cations as ligands for transition-metal catalysts has inspired further exploration into the synthesis of novel

scaffolds capable of supporting potentially promising cations of this type.[10] Following chelation with a phosphorus cation it was hoped that these interesting heterocycles heterocycles could be electropolymerized under oxidative potential. The first examples of thiophene-substituted NHPs are described in the present work.

2.2 Synthesis of thiophene-substituted diimines

Preliminary attempts to prepare the desired ligands **5-8** focused on the traditional synthetic approach to diazabutadienes, namely the reaction of a diketone with a primary amine (Scheme 2.2).

Scheme 2.2. Attempted arylamine condensation reactions.

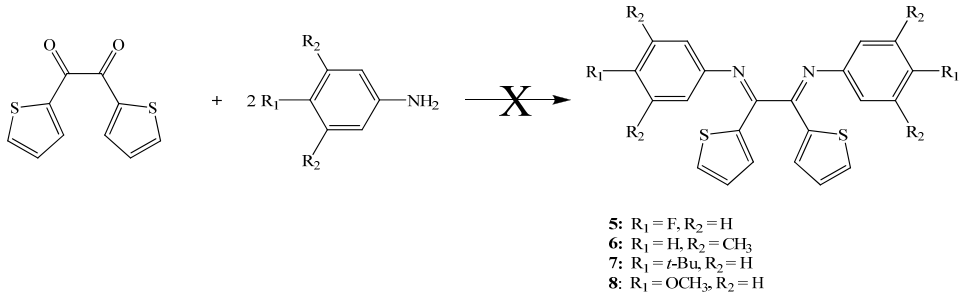

5: $R_1 = F, R_2 = H$
6: $R_1 = H, R_2 = CH_3$
7: $R_1 = t\text{-Bu}, R_2 = H$
8: $R_1 = OCH_3, R_2 = H$

However, even under Dean-Stark conditions or in the presence of an acid catalyst, it was only possible to isolate the ketoimines rather than the desired α-diimines. The condensation of diketones with arylamines is known to occur only rarely for diketones with bulky substituents such as phenyl or thiophene. In the present work, the desired diazabutadienes were prepared by cyanide ion-catalyzed intermolecular coupling of the appropriate aromatic aldimines **1-4** as shown below in Scheme 2.3.

Scheme 2.3. Synthesis of N-aryl-2-thienyl substituted 1,4-diazabutadiene ligands **5-8**.

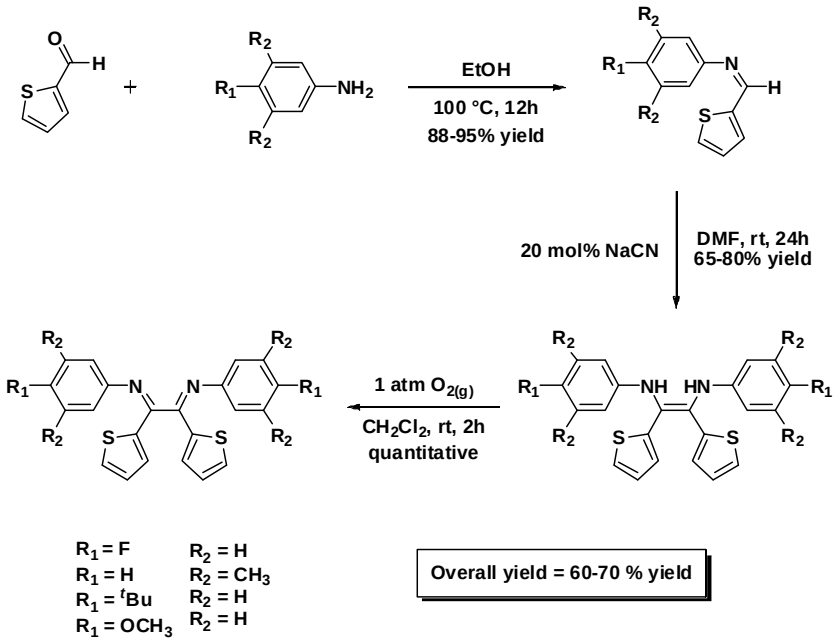

The initial step in the process involves the formation of 2-thiophene-substituted aldimines **1-4** *via* a condensation reaction of 2-thiophene carboxaldehyde with the appropriate arylamine. The less polar monoimine products are easily separated from the starting materials by flash column chromatography in each case. The cyanide-catalyzed coupling of the aldimines to form the corresponding diamines is best carried out in polar aprotic solvents such as DMF or DMSO because of the ability of these solvents to dissolve sodium cyanide. An atmosphere of dry nitrogen or argon was required. Furthermore, it was important that the DMF or DMSO was dried and distilled prior to use. The ene-diamine was formed in solution and in each case the limited solubility of this intermediate provided an additional driving force for the C-C coupling reaction. The aldimine coupling is similar to the benzoin condensation in the sense that each step in the

reaction pathway is reversible. This reversiblity prevents the complete conversion of benzoin and thus limits the yields of the diimines presented herein. The ene-diamines **5**-**8** can be isolated by filtration following heating of the crude reaction mixture in MeOH. Higher yields were obtained, however, by isolation of the ene-diamine using flash column chromatography (FCC). The product collected comprised a mixture of the ene-diamine and the diimine in each case. The oxidation of the diamines to the corresponding diazabutadienes took place autogenously upon column chromatographic separation of the product mixtures. However, in order to complete the oxidation reactions, it was necessary to bubble oxygen through the initially-formed solutions of the products. Chemical oxidation using 1,4-benzoquinone also represented an effective method. The progress of this oxidation process can be monitored conveniently by ^{1}H NMR.

The cyanide coupling method is apparently only effective for the synthesis of aryl-substituted diazabutadienes. Alkyl-substituted aldimines have not been shown to react, possibly owing to their failure to stabilize the carbanion intermediate as suggested in previous work.[11] The aryl substituents can range from electron withdrawing to electron donating. However, in the present work, it was found that the use of a *para*-nitro substituted aldimine in the dimerization reaction resulted in an inseparable mixture of intermediates. A further limitation is that aryl-substituted aldimines with sterically demanding groups such as 2,6-diisopropylphenyl or 2,4,6-trimethylphenyl fail to undergo the coupling process. Steric and electronic limitations clearly exist and further exploration into this area is warranted.

It was surmised that the phenyl ring between thiophene and the nitrogen in compound **12** would lower the oxidation potential of the thiophene proton at the 2-position thus stabilizing the radical cation that is necessary to initiate polymerization.[12]

The synthetic route to the targeted α-diimine **12** comprises two novel steps and is outlined in Scheme 2.4.

Scheme 2.4. Synthesis of the "phenyl spacer" α-diimine ligand **12**.

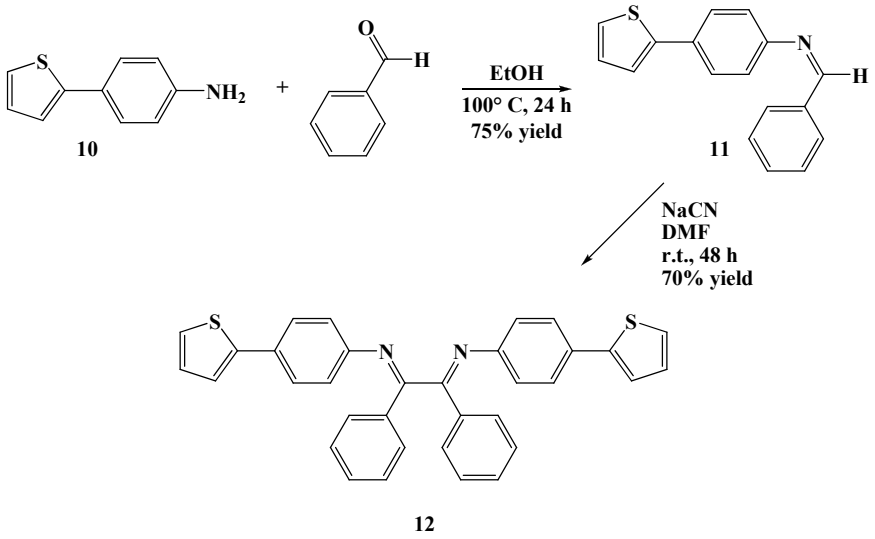

The first step in the procedure involves the reduction of 4-thienyl-nitrobenzene **9** to form the primary amine 4-thienylaniline **10**. Absolute EtOH is needed for this reduction as well as an inert atmosphere. The aldimine intermediate **11** is then synthesized by treatment of 4-thienylaniline with benzaldehyde. This step is followed by cyanide coupling of the aldimine to form the desired 1,2-diimine ligand **12**. In contrast to the syntheses of **5-8**, complete oxidation of the diamine to the diimine took place spontaneously in air following chromatographic separation of the unreacted monoimine. The superior electron-withdrawing ability of thiophene compared with a phenyl group may explain the greater stability of the ene-diamines **5-8**. The alkylated analogue of **12** shown below in Scheme 2.5 was constructed using 4-butylbenzaldehyde instead of

benzaldehyde. It was thought that the presence of *n*-butyl substituents would allow for greater solubility of the resulting ligand and metal complexes.

Scheme 2.5. Synthesis of alkylated 4-thienylphenyl diimine.

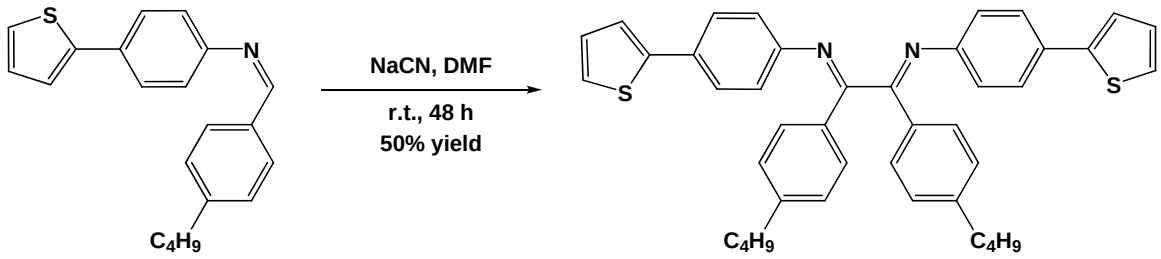

2.3 Electrochemical analysis of diazabutadiene ligands

CV data were obtained for dichloromethane solutions of each of the five new ligands. The cyclic voltammogram for the diimine **5** is shown in Figure 2.1. The oxidation of the thiophene occurred at 1.50 V. Diimine **7**, which contains a *t*-butyl group instead of a fluorine atom at the 4-position of the phenyl ring, exhibited a lower oxidation potential of 1.43 V as illustrated in Figure 2.2. The presence of a methoxy group at the *para* position of the phenyl ring lowered the oxidation potential even further than in the case of **7** (Figure 2.3). Conversely, in the case of diimine **12**, in which a thiophene moiety is attached to a phenyl ring, the thiophene oxidation potential is suppressed as evident in Figure 2.4.

Collectively, these observations indicate a high degree of electronic communication in the diimines **5**-**8** and **12**. It was speculated that electron-donating groups such as methoxy would lower the oxidation potential of thiophene sufficiently to facilitate polymerization. Unfortunately, no film formation or other evidence of

polymerization was observed for **5**-**8**, **12**, even in the case of alkylated **12** (Scheme 2.5). It is possible that oxidative coupling of the pendant thiophene moieties could have occurred in a similar fashion to that described by Swager *et al.*[13] thus precluding electropolymerization. On the other hand, diimine **12**, which features thiophene units on opposite sides of the molecule, seemed like a good candidate for avoiding the coupling reaction reported by Swager and co-workers. Repeated cycling of a solution of **12** within the appropriate window resulted in the deposition of a very thin film. Unfortuantely, the film did not exhibit electroactivity in monomer-free solution.

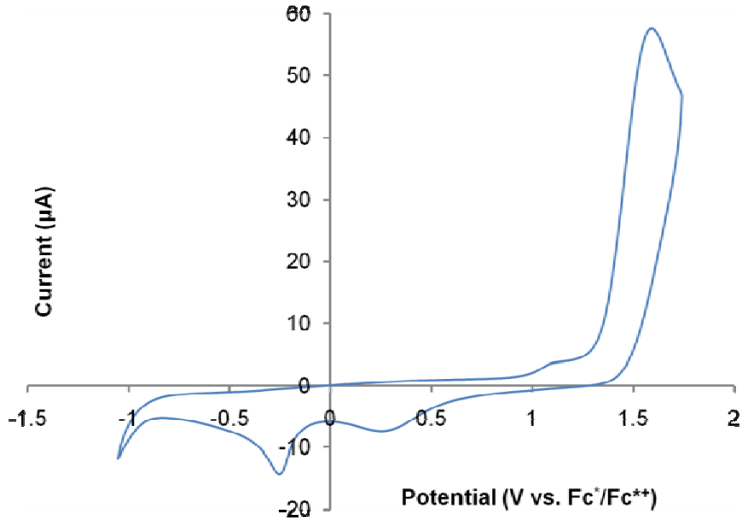

Figure 2.1. Cyclic voltammogram of diimine **5**.

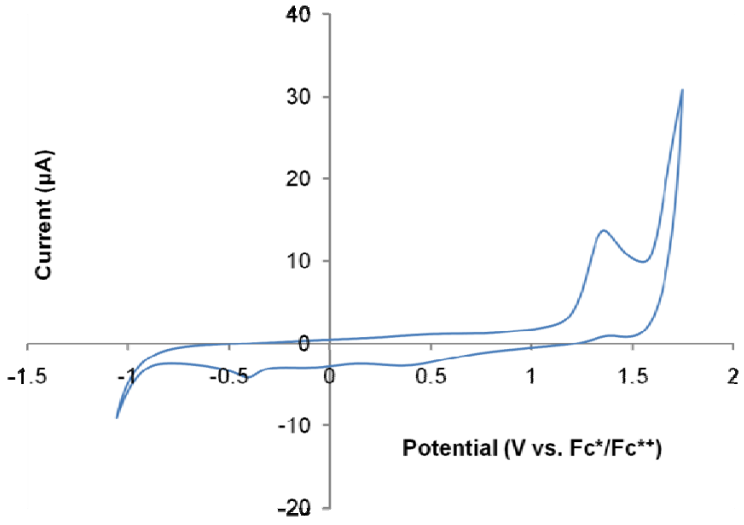

Figure 2.2. Cyclic voltammogram of diimine **7**.

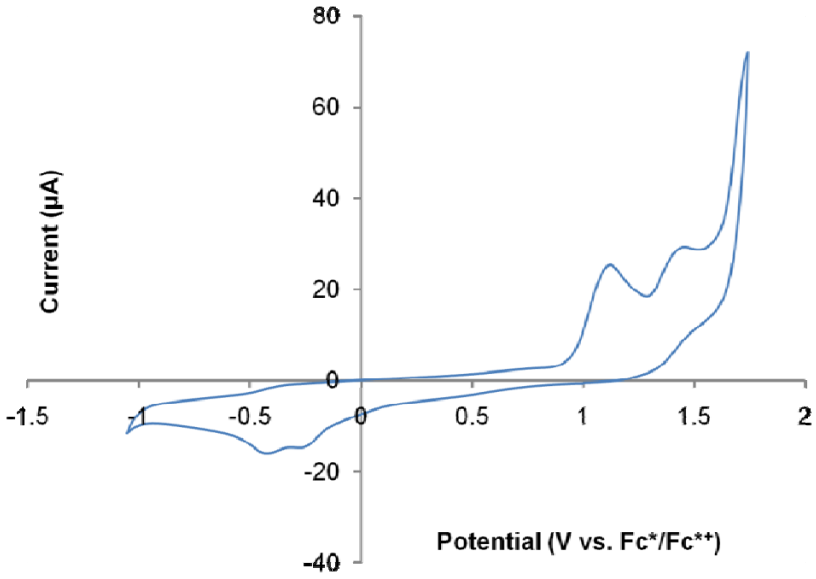

Figure 2.3. Cyclic voltammogram of diimine **8**.

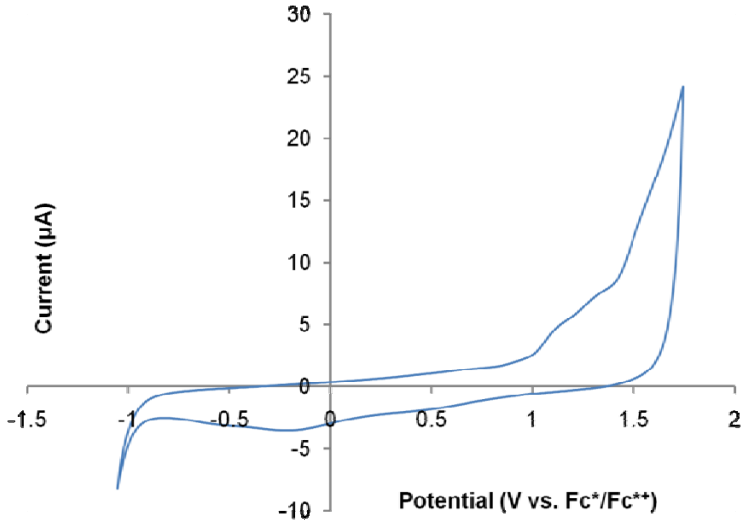

Figure 2.4. Cyclic voltammogram of diimine **12**.

2.4 Synthesis of phosphenium cations

Recently, Macdonald *et al.*[14] and our group[15] demonstrated that NHPs can be prepared by a simple high-yielding redox reaction between PI_3 or $PCl_3/SnCl_2$ and diazabutadienes. It was therefore of interest to explore the reactions of the new thiophene-substituted diazabutadiene ligands with PI_3. Each of the four thiophene-substituted diazabutadiene ligands reacted readily with PI_3 in CH_2Cl_2 solution to afford the air-sensitive triiodide salts of the corresponding phosphenium cations. The reaction failed, however, when a solution of PI_3 in CH_2Cl_2 was added to a solution of the diimine. The light-sensitivity of PI_3, especially when in solution, caused the reagent to decompose before it could be added to the diimine solution. Interestingly, this was only the case for dilute solutions.

Previous reports by our group did not note this behavior because the PI_3 solutions were more than ten-fold more concentrated. An improved procedure was therefore developed which involves the addition of both reagents to one flask under an inert

atmosphere, followed by the addition of the dry solvent. Clearly, the outcomes of these redox reactions are not sensitive to the electron withdrawing or electron donating character of the aryl substituents. The reactions take place within a couple of hours as evidenced by ^{31}P NMR and a color change of the reaction mixture from yellow to reddish brown.

Scheme 2.6. Reactions of diimines **5**-**8** with phosphorus triiodide.

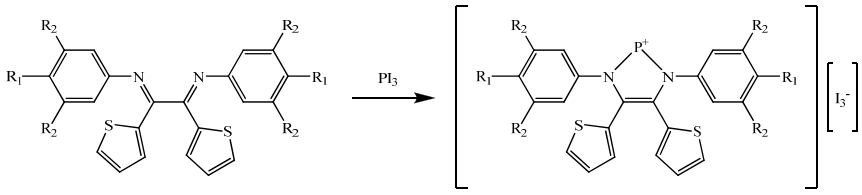

5: $R_1 = F, R_2 = H$
6: $R_1 = H, R_2 = CH_3$
7: $R_1 = t\text{-Bu}, R_2 = H$
8: $R_1 = OCH_3, R_2 = H$

13: $R_1 = F, R_2 = H$
14: $R_1 = H, R_2 = CH_3$
15: $R_1 = t\text{-Bu}, R_2 = H$
16: $R_1 = OCH_3, R_2 = H$

Phosphenium salts **13**-**16** were prepared by a one-step procedure as outlined in Scheme 2.6. As in the case of previously reported phosphenium triiodide salts,[14,15] a ^{31}P NMR singlet is observed in the δ 190-200 ppm region for complexes **13**-**16**. The ^{19}F NMR chemical shift of **13** is ~ δ 10 ppm downfield compared with that of the precursor diimine ligand **5**, which suggests the donation of electron density from the *para*-fluorine substituent to the cationic phosphorus center some six bonds away. In the case of diimine **12**, a color change from yellow to dark brown was observed. However, it was only possible to isolate an insoluble solid **17** that was not identified. It is likely that alkylated analogues of **12** represent more promising candidates for phosphenium salt formation.

2.5 Crystallography of diimines and phosphenium cations

Single-crystal X-ray diffraction data were acquired for diimines **5**, **6**, **7**, **12**, and phosphenium salt **15**. However, discussion is restricted to the structures of **7**, **12**, and **15**. The structural data for **5** and **6** are available from the CCDC by citing numbers 707513 and 707514, respectively. Details of the data collection and structure refinements are provided in Table 2.1, and a listing of pertinent metrical parameters is presented in Table 2.2

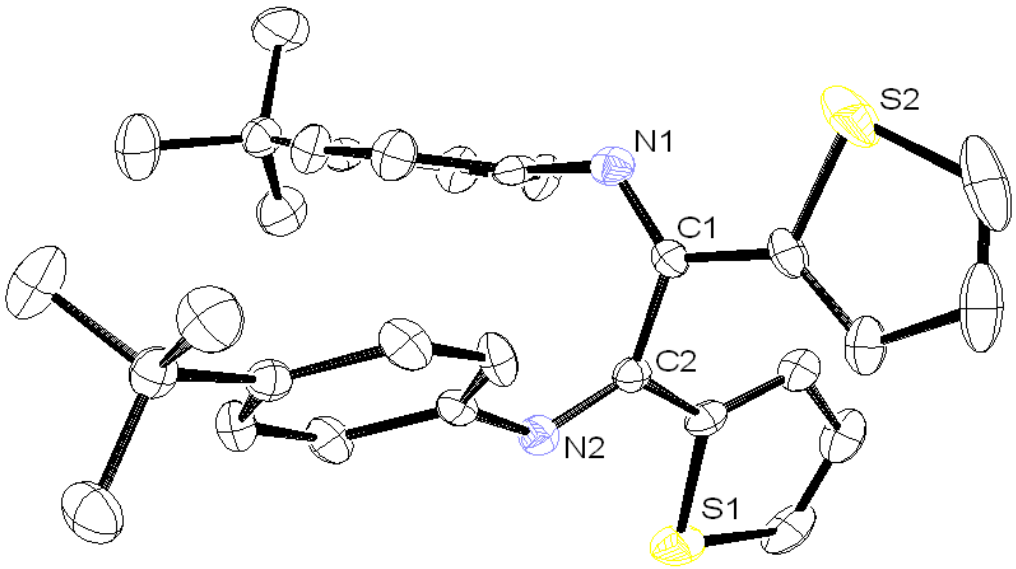

Figure 2.5. ORTEP diagram of **7** showing thermal ellipsoids at 30% probability with H atoms omitted for clarity.

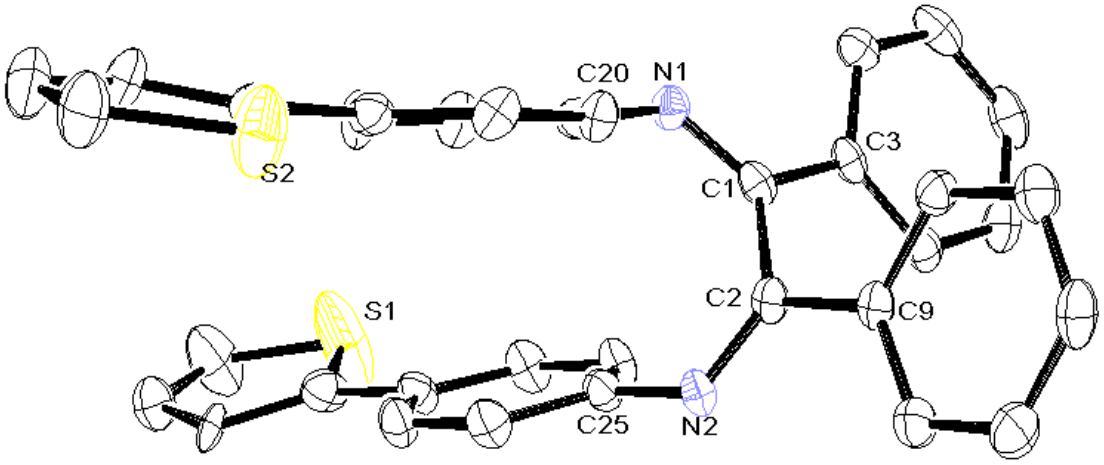

Figure 2.6. ORTEP diagram of **12** showing thermal ellipsoids at 30% probability with H atoms omitted for clarity.

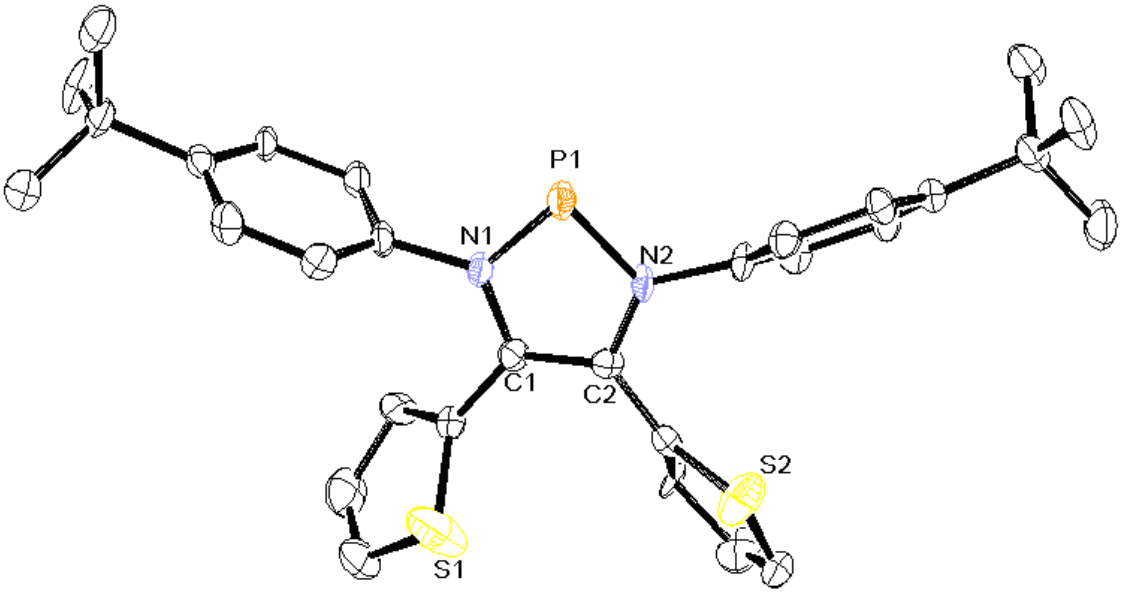

Figure 2.7. ORTEP diagram of phosphenium cation **15** at 30% probability with H atoms omitted for clarity.

The X-ray crystal structures of diimines **7** and **12** and the phosphenium triiodide salt **15** are illustrated in Figures 2.5, 2.6, and 2.7, respectively. None of the structures

shows evidence of any unusually short contacts. Diimines **7** and **12** adopt the s-*cis* conformation and the metrical parameters for the diimine fragments are in line with expectation. Akin to other phosphenium cation structures,[14,15] the C(1)-C(2) bond distance of 1.366(8) Å for **15** is markedly shorter than the C(1)-C(2) bond distance for the free diimine **7**. This shortening is due to a two-electron reduction of the diimine by PI_3 resulting in a C(1)-C(2) bond order of approximately two. The bond distance data in Table 2.2 also indicate a lengthening of the C-N double bond such that it corresponds to a bond order of approximately one. The C(1)-N(1) and C(2)-N(2) bond distances listed in Table 2.2 for **15** fall within the range reported for other phosphenium complexes that have been structurally characterized. These bond distances, however, appear to be slightly longer than those of typical α-diimine phosphenium complexes.[15,16] The steric bulk introduced at the C(1) and C(2) positions provides a rational explanation for this observation. The mechanism of the reaction of diimines with PI_3 has not been established. However, it is plausible that the first step involves the formation of I_2, and a donor-acceptor complex between the α-diimine and PI, from which I^- is abstracted by I_2, thereby forming an I_3^- anion. Completion of the process is achieved by the subsequent or concomitant transfer of two electrons from the P^+ moiety into the LUMO of the α-diimine.[15]

Table 2.1. Selected data collection and refinement parameters for **7**, **12**, and **15**.

	7	**12**	**15**
Formula	$C_{30}H_{32}N_2S_2$	$C_{35}H_{26}Cl_2N_2S_2$	$C_{30}H_{32}N_2PS_2I_3$
Formula weight	484.72	609.62	896.37
Crystal system	Triclinic	Triclinic	Orthorhombic
Space Group	*P*-1	*P*-1	$P2_12_12_1$
a/Å	9.7281(19)	9.5726(19)	11.682(2)
b/Å	12.001(2)	10.449(2)	16.724(3)
c/Å	12.295(3)	15.535(3)	17.083(3)

Table 2.1 (continued). Selected data collection and refinement parameters for **7**, **12**, and **15**.

α/°	110.01(3)	100.09(3)	90
β/°	98.25(3)	103.56(3)	90
γ/°	96.87(3)	95.64(3)	90
V/Å^3	1312.6(5)	1471.3(5)	3337.4(11)
Z	2	2	4
P_{calcd}/g cm^{-3}	1.226	1.376	1.784
F(000)	516	632	1728
Crystal size/mm	0.24 x 0.16 x 0.13	0.18 x 0.15 x 0.12	0.16 x 0.14 x 0.09
θ *range* /°	2.05 to 27.47	2.00 to 27.49	2.11 to 27.48
No. of reflns. collected	8618	10484	7608
No. of indep. reflns.	5933	6669	7608
$R_1[I > 2\sigma(I)]$	0.0524	0.0709	0.0417
wR_2 (all data)	0.1465	0.1649	0.0954
Peak and hole /e Å^3	0.324 and -0.376	0.427 and -0.452	0.825 and -0.812

Table 2.2. Selected bond distances (Å) and bond angles (deg) for diimines **7** and **12** and phosphenium cation **15**.

parameter	**7**	**12**	**15**
C(1)-C(2)	1.514(3)	1.516(6)	1.366(8)
N(1)-C(1)	1.277(3)	1.282(4)	1.394(7)
N(2)-C(2)	1.287(2)	1.275(4)	1.389(7)
N(1)-P(1)			1.659(5)
N(2)-P(1)			1.663(5)
N(1)-P(1)-N(2)			89.5(2)
N(1)-C(1)-C(2)	124.49(18)	124.1(3)	110.8(5)
N(2)-C(2)-C(1)	125.96(17)	124.1(3)	110.1(5)

2.6 Conclusions

A relatively unexplored transformation has been employed for the synthesis of a new class of thiophene-substituted diimine ligands. These ligands have been fully characterized and their behavior appears to mirror that of conventional 1,2-diimine systems. The first structurally characterized example of a ligand with a phenyl spacer between a thiophene carbon atom and an imino nitrogen atom has also been prepared. Diimines **5**-**8** failed to undergo electropolymerization, but diimine **12** did deposit a very thin film that displayed no electroactivity in monomer-free solution. The thiophene-substituted diimines undergo redox reactions with PI_3 to produce the corresponding phosphenium triiodide salts. These complexes are the first examples of NHP analogues of 4,5-diaryl-substituted heterocyclic carbenes. Investigation of the reactivity of these phosphenium salts with transition metal moieties is currently underway.

2.7 Experimental

General procedures. All air-sensitive manipulations and reactions were performed under a dry, oxygen-free, catalyst-scrubbed argon atmosphere using a combination of standard Schlenk techniques or in a Vacuum Atmospheres drybox. All glassware was oven-dried and vacuum- and argon-flow degassed before use. All solvents were distilled over sodium benzophenone ketyl, except dichloromethane, which was distilled over calcium hydride and degassed prior to use. Phosphorus triiodide was obtained from a commercial source and used without further purification.

Physical Measurements. Low-resolution chemical ionization mass spectral data (MS-CI) were collected on a Finnigan MATTSQ-700 mass spectrometer, and high-resolution CI-MS spectra were recorded on a VG Analytical ZAB-VE sector instrument. All MS analyses were performed on samples that had been sealed in glass capillaries under an argon atmosphere. Solution-phase NMR spectra were recorded at 298 K on Varian Inova instrument (^{1}H NMR, 300.14 MHz; ^{13}C NMR, 75.48 MHz; ^{31}P NMR, 121.52 MHz and ^{19}F NMR, 282.41 MHz) using $CDCl_3$ as an internal reference unless otherwise stated. The data for the phosphenium salts were recorded immediately following removal of the sample from the drybox. The ^{31}P NMR chemical shift values are reported relative to an external 85% H_3PO_4 reference. The ^{19}F NMR chemical shift values are reported relative to Freon-11.

Electrochemistry. Electrochemical syntheses and studies were performed in a drybox under a dry nitrogen atmosphere using a CH Instruments Electrochemical Workstation (series 700B). All the electrochemical experiments were carried out in a three-electrode cell containing a silver wire reference electrode. The supporting electrolyte was 0.1 M [(*n*-Bu)$_4$N$^+$][PF$_6^-$] ($TBAPF_6$) that had been purified by recrystallization three times from hot ethanol before being dried for 3 days at 100–150 °C

under dynamic vacuum. Electrosyntheses of the films were performed from 1 x 10^{-3} M monomer solutions by continuous cycling between –1.00 V and 1.70 V at v = 100 mV s^{-1}. The resulting films were then washed with excess CH_2Cl_2. Decamethylferrocene was used as an external reference (0.0 V) for all electrochemical measurements.

X-Ray Crystallography. A suitable crystal of **5**, **6**, **7**, **12** or **15** was removed from a vial sealed inside a Schlenk tube, placed on a glass slide, covered with degassed hydrocarbon oil, and mounted on a thin nylon loop. The X-ray diffraction data were collected at 153 K on a Nonius Kappa CCD area detector diffractometer equipped with an Oxford Cryostream low-temperature device and a graphite-monochromated Mo Kα radiation source (λ = 0.71073 Å). In each case, corrections were applied for Lorentz and polarization effects. The structures were solved by direct methods and refined by full-matrix least-squares cycles on F^2.[17] All non-hydrogen atoms were refined with anisotropic thermal parameters, and all hydrogen atoms were placed in fixed, calculated positions using a riding model (C-H 0.96 Å). The pertinent experimental data are listed in Table 2.

Preparation of thiophene monoimines 1-4. A round-bottom flask was charged with thiophene carboxaldehyde (2.244 g, 20 mmol), and the appropriate arylamine (22 mmol) along with 200 mL of absolute EtOH. The reaction mixture was heated at reflux for 12 h following which it was cooled to room temperature and the EtOH was removed under reduced pressure. Purification of the crude products was effected by flash chromatography (SiO_2) using 80% hexanes and 20% ethyl acetate.

4-fluoro-*N*-[thiophen-2-ylmethylidene]aniline (1). Yellow oil (90%). ^{1}H NMR (300.14 MHz, $CDCl_3$): δ 8.52 (s, 1H), 7.46 (m, 2H), 7.18 (m, 2H), 7.11 (dd, 1H, J = 5.4, 3.6 Hz), 7.04 (t, 2H, J = 9.0 Hz). ^{13}C{^{1}H} NMR (75.48 MHz, $CDCl_3$): δ 160.96 [J(^{19}F-^{13}C) = 972 Hz], 152.63 (J(^{19}F-^{13}C) = 4.2 Hz), 147.13 [J(^{19}F-^{13}C) = 12.9 Hz], 142.35, 132.25, 130.19,

127.62, 122.22 (J(^{19}F-^{13}C) = 32.7 Hz), 115.63 (J(^{19}F-^{13}C) = 89.7 Hz). ^{19}F{^{1}H} NMR (282.41 MHz, $CDCl_3$): δ -116.78 (m). IR (cm^{-1}) 1615 (C=N), 1498 (C-C_{arom}), 1428 (C-C_{arom}), 1230, 1188, 819.

3,5-dimethyl-*N*-[thiophen-2-ylmethylidene]aniline (2). Yellow oil (88%). ^{1}H NMR (300.14 MHz, $CDCl_3$): δ 8.56 (s, 1H) 7.46 (m, 2H), 7.12 (t, 1H J = 5.4 Hz), 6.86 (s, 1H), 6.84 (s, 2H), 2.40 (s 6H). ^{13}C{^{1}H} NMR (75.48 MHz, $CDCl_3$): δ 152.07, 150.96, 142.66, 138.24, 131.70, 129.67, 127.42, 127.35, 118.48, 20.95. IR (cm^{-1}) 1616 (C=N), 1600 (C-C_{arom}), 1584 (C-C_{arom}), 1425 (C-C_{arom}), 1237, 1217, 1143, 1044, 945, 926, 846.

4-*t*-butyl-*N*-[thiophen-2-ylmethylidene]aniline (3). Yellow solid (95%). ^{1}H NMR (300.14 MHz, $CDCl_3$, TMS): δ 8.50 (s, 1H), 7.39 (m, 2H), 7.32 (d, 2H, J = 4.5 Hz), 7.08 (d, 2H J = 4.5 Hz), 7.04 (t, 1H J = 3.6 Hz), 1.35 (s, 9H). ^{13}C{^{1}H} NMR (75.48 MHz, $CDCl_3$): δ 152.23, 149.02, 148.60, 142.94, 131.82, 129.89, 127.58, 125.90, 120.56, 34.38, 31.32. IR (cm^{-1}) 1616 (C=N), 1498 (C-C_{arom}), 1428 (C-C_{arom}), 1230, 1189, 914.

4-methoxy-*N*-[(*E*)-thiophen-2-ylmethylidene]aniline (4). Yellow solid (92%). ^{1}H NMR (300.14 MHz, $CDCl_3$): δ 8.58 (s, 1H), 7.46 (m, 2H), 7.24 (d, 2H, J = 6.6 Hz), 7.12 (dd, 1H, J = 1.8, 1.5 Hz), 6.92 (d, 2H, J = 6.6 Hz), 3.78 (s, 3H). ^{13}C{^{1}H} NMR (75.48 MHz, $CDCl_3$): δ 158.13, 150.97, 144.22, 142.99, 131.53, 129.66, 127.59, 122.51, 114.21, 55.32. IR (cm^{-1}) 1615 (C=N), 1500 (C-C_{arom}), 1463 (C-C_{arom}), 1429 (C-C_{arom}), 1292, 1246, 1193, 1163, 1107, 1032, 959, 832.

Preparation of diimines 5-8. Each of the imines **1-4** was added to a Schlenk flask along with an equimolar amount of NaCN. The reaction vessel was degassed and dry DMF (15 mL) was added *via* cannula. The reaction mixture was stirred at room temperature for 3 days under argon, following which it was diluted with 20 mL of DI water. The solid product was extracted with diethyl ether (100 mL), washed with DI water (5 x 50 mL) and back-extracted with 50 mL of diethyl ether. The organic layers

were combined, dried with $MgSO_4$, filtered and concentrated to yield the crude product. In each case purification of the crude product was carried out by flash chromatography (SiO_2) with hexanes and ethyl acetate resulting in a mixture of the diamine and the diimine. The latter mixture was then dissolved in 50 mL of DCM and oxygen gas was bubbled through the solution until the conversion was deemed complete (4 hours).

4-fluoro-*N*-2-[(4-fluorophenyl)imino]-1,2-di(thiophen-2-yl)ethylidene]aniline (5). The reaction of **1** (2.63 g, 12.80 mmol) with NaCN (0.63 g, 12.80 mmol) resulted in the formation of a yellow-green solid. The fully oxidized product was purified by flash chromatography (SiO_2) with 80% hexanes and 20% ethyl acetate to yield **5** as a yellow solid (69%). ^{1}H NMR (300.14 MHz, $CDCl_3$, TMS): δ 7.46 (d, 2H, J = 5.4 Hz), 7.26 (d, 2H, J = 5.1 Hz), 6.99 (dd, 2H, J = 5.7, 4.5 Hz), 6.74 (t, 4H, J = 6.9 Hz), 6.48 (m, 4H). ^{13}C{^{1}H} NMR (75.48 MHz, $CDCl_3$): δ 160.44 [J(^{19}F-^{13}C) = 972.0 Hz], 157.34, 157.33, 144.39 [J(^{19}F-^{13}C = 10.8 Hz), 144.20, 131.54 [J(^{19}F-^{13}C) = 266.4 Hz], 128.17, 122.22 [J(^{19}F-^{13}C) = 32.7 Hz], 115.25 [J(^{19}F-^{13}C) = 89.4 Hz). ^{19}F{^{1}H} NMR (282.41 MHz, $CDCl_3$): δ -117.23 (m). LRMS (CI^+, *m/z*): 409 (100% M + H^+). IR (cm^{-1}) 1601 (C=N), 1495 (C-C_{arom}), 1422 (C-C_{arom}), 1216, 1195, 1184, 881, 850, 821.

3,5-dimethyl-*N*-[2-[(3,5-dimethylphenyl)imino]-1,2-di(thiophen-2-yl)ethylidene]aniline (6). The reaction of **2** (2.00 g, 8.57 mmol) with NaCN (0.428 g, 8.57 mmol) resulted in the formation of a yellow solid. Following oxidation, the yellow solid was purified by flash chromatography (SiO_2) with 80% hexanes and 20% ethyl acetate to yield **6** as a yellow solid (45%). ^{1}H NMR (300.14 MHz , $CDCl_3$): δ 7.46 (d, 2H, J = 5.4 Hz), 7.23 (d, 2H, J = 5.4 Hz), 7.04 (t, 2H, 4.8 Hz), 6.65 (s, 2H), 6.15 (s, 4H) 2.08 (s, 12H). ^{13}C{^{1}H} NMR (75.48 MHz, $CDCl_3$): δ 157.26, 148.55, 144.87, 137.69, 131.56, 130.42, 127.89, 126.57, 118.19, 21.18. LRMS (CI^+, *m/z*): 429 (100% M + H^+).

IR (cm^{-1}) 3064 (methyl C-H), 1617 (C=N), 1581 (C-C_{arom}), 1419 (C-C_{arom}), 1290, 1234, 1145, 1055, 1047, 851, 843.

4-*t*-butyl-*N*-[2-[(4-*t*-butylphenyl)imino]-1,2-di(thiophen-2-yl)ethylidene]aniline (7). The reaction of **3** (1.79 g, 7.35 mmol) and NaCN (0.360 g, 7.35 mmol) resulted in the formation of a yellow solid. Following oxidation, the yellow solid was purified by flash chromatography (SiO_2) with 80% hexanes and 20% ethyl acetate to yield **7** as a yellow solid (53%). ^{1}H NMR (300.14 MHz , $CDCl_3$, TMS): δ 7.40 (d, 2H, J = 5.4 Hz), 7.23 (d, 2H, J = 5.2 Hz), 6.97 (m, 6H), 6.42 (d, 4H, J = 6.6 Hz), 1.19 (s 18H). ^{13}C{^{1}H} NMR (75.48 MHz, $CDCl_3$): δ 156.63, 148.15, 145.70, 144.81, 131.40, 130.21, 127.96, 125.16, 120.33, 34.32, 31.33. LRMS (CI^+, *m/z*) 485 (100% M + H^+). IR (cm^{-1}) 2959 (^{t}Bu C-H), 1591 (C=N), 1498(C-C_{arom}), 1460(C-C_{arom}), 1421(C-C_{arom}), 1360, 1268, 1202, 1176, 894, 850.

4-methoxy-*N*-[2-[(4-methoxyphenyl)imino]-1,2-di(thiophen-2-yl)ethylidene]aniline (8). The reaction of **4** (2.50 g, 11.51 mmol) and NaCN (0.56 g, 11.51 mmol) resulted in the formation of a yellow solid. Following oxidation, the yellow solid was purified by flash chromatography (SiO_2) with 60% hexanes and 40% ethyl acetate to yield **8** as a yellow solid (52%). ^{1}H NMR (300.14 MHz , $CDCl_3$, TMS): δ 7.38 (d, 2H, J = 5.4 Hz), 7.17 (d, 2H, J = 5.6 Hz), 6.92 (dd, 2H, J = 5.4, 4.5 Hz), 6.69 (d, 4H, J = 6.6 Hz), 6.60 (d, 4H, J = 6.6 Hz), 3.65 (s 6H). ^{13}C{^{1}H} NMR (75.48 MHz, $CDCl_3$): δ 157.53, 156.49, 144.19, 141.40, 131.09, 130.24, 127.96, 122.75, 113.75, 55.28. (CI^+, *m/z*) 433 (100% M + H^+). IR (cm^{-1}) 2922 (methyl C-H), 1602 (C=N), 1587 (C-C_{arom}), 1500 (C-C_{arom}), 1462 (C-C_{arom}), 1422 (C-C_{arom}), 1357, 1301, 1283, 1243, 1192, 1106, 1056, 1028, 925, 890.

4-thienylnitrobenzene (9). Palladium (II) acetate (0.073, 0.325 mmol) was added to a 250 mL Schlenk flask under a nitrogen atmosphere, following which degassed DMF (65 mL) was added *via* cannula. Next, 1-Iodo-4-nitrobenzene (2.70 g, 10.83 mmol), DABCO

(0.070 g, 0.649 mmol), and K_2CO_3 (4.50 g, 32.50 mmol) were then added against an argon backflow. Next, 2-thiophene boronic acid (2.08 g, 16.25 mmol) was added and the reaction was monitored until deemed complete by TLC (24 h). The reaction mixture was then diluted with diethyl ether (100 mL), washed with DI water (4 x 50 mL) and back-extracted with diethyl ether (100 mL). The combined layers were dried with $MgSO_4$, filtered and concentrated to afford **9** as a yellow solid (86%). ^{1}H NMR (300.14 MHz, $CDCl_3$, TMS): δ 8.17 (d, 2H, J = 6.4 Hz), 7.68 (d, 2H, J = 6.4 Hz), 7.41 (d, 1H, J = 4.8 Hz), 7.37 (d, 1H, J = 4.7 Hz), 7.09 (dd, 1H, J = 4.8, 4.2 Hz). LRMS (CI^+, *m/z*): 206 (100% M + H^+).

4-thienylaniline 10. $SnCl_2$ (8.78 g, 46.29 mmol) and **9** (1.90 g, 9.26 mmol) were added under an inert atmosphere to a three-neck round-bottom flask equipped with a condenser. Degassed absolute EtOH (15 mL) was then added *via* cannula and the reaction mixture was heated to reflux. Following this, a suspension of $NaBH_4$ (0.175 g, in EtOH (15 mL) was added dropwise to the solution and the reaction mixture was heated at reflux overnight. The reaction mixture was then cooled to 0 ºC and quenched with 50 mL of DI water. After adding sufficient 1 M NaOH to render the solution strongly basic, the product was extracted into diethyl ether (50 mL) and washed with DI water (3 x 50 mL). The aqueous layer was then back-extracted with diethyl ether (50 mL). The combined organic layers were dried with $MgSO_4$, filtered and concentrated to afford a yellow-green solid **10** (90%). ^{1}H NMR (300.14 MHz, $CDCl_3$, TMS): δ 7.34 (d, 2H, J = 8.4 Hz), 7.09 (m, 2H), 6.96 (t, 1H, J = 4.8 Hz), 6.61 (d, 2H, J = 8.4 Hz), 3.70 (b, 2H). ^{13}C{^{1}H} NMR (75.48 MHz, $CDCl_3$): δ 145.93, 144.90, 127.75, 127.02, 124.95, 122.96, 121.15, 115.18.

***N*-[phenylmethylidene]-4-(thiophen-2-yl)aniline (11).** 3 Å Molecular sieves (6.00 g) and **10** (1.30 g, 7.42 mmol) were added to a 100 mL Schlenk flask equipped with a condenser and the mixture was degassed. Absolute EtOH (40 mL) was then added *via*

cannula. The reaction mixture was heated to reflux and benzaldehyde (0.71 g, 6.74 mmol) was added dropwise. The reaction mixture was then heated at reflux under argon for 24 h. Next, the molecular sieves were filtered off and the EtOH was removed under reduced pressure to yield green solid **11**. Purification of the crude product by flash chromatography (SiO_2) with 90% hexanes and 10% ethyl acetate afforded the pure product as a yellow powder (75%). ^{1}H NMR (300.14 MHz, $CDCl_3$, TMS): δ 8.42 (s, 1H), 7.84 (m, 2H), 7.57 (d, 2H, J = 8.4 Hz), 7.40 (m, 3H) 7.24 (d, 1H, J = 4.8 Hz), 7.17 (m, 2H), 7.01 (t, 1H, J = 4.8 Hz). {^{1}H} NMR (75.48 MHz, $CDCl_3$): δ 160.02, 151.07, 143.98, 136.11, 132.26, 131.42, 128.81, 128.75, 128.05, 126.63, 124.64, 122.85, 121.50. IR (cm^{-1}) 1623 (C=N), 1574 (C-C_{arom}), 1491 (C-C_{arom}), 1449 (C-C_{arom}), 1314, 1260, 1199, 1168, 1113, 846, 815.

4-thienyl-*N*-[2-[(4-thienylphenyl)imino]-1,2-diphenyl ethylidene]aniline (12). Compound **11** (0.36 g, 1.37 mmol) and NaCN (0.07 g, 1.37 mmol) were added to a 50 mL Schlenk flask and the mixture was degassed. Dry DMF (10 mL) was added *via* cannula into the reaction vessel and the resulting mixture was stirred under argon at 25 ºC for 48 hours. The reaction mixture was then quenched with DI water (20 mL), following which it was extracted into diethyl ether (50 mL) and washed with DI water (3 x 50 mL). The aqueous layer was then back-extracted with diethyl ether (50 mL). The combined organic layers were dried with $MgSO_4$, filtered and concentrated to yield **12** as a yellow powder. Purification of the crude product by flash chromatography (SiO_2) with 90% hexanes and 10% ethyl acetate afforded the pure product as a yellow powder (70%). ^{1}H NMR (300.14 MHz, $CDCl_3$, TMS): δ 7.84 (d, 4H, J = 6.4 Hz), 7.37 (m, 6H), 7.28 (d, 4H, J = 6.2 Hz), 7.18 (d, 4H, J = 6.2 Hz), 6.98 (t, 2H, J = 4.8 Hz), 6.51 (d, 4H, J = 6.4 Hz). ^{13}C{^{1}H} NMR (75.48 MHz, $CDCl_3$, TMS): δ 163.87, 148.54, 144.14, 137.39, 131.26, 131.14, 128.83, 128.32, 127.99, 125.88, 124.40, 122.57, 120.80. LRMS (CI^+, *m/z*): 525

(100% M + H^+). IR (cm^{-1}) 1601 (C=N), 1593 (C-C_{arom}), 1576 (C-C_{arom}), 1494 (C-C_{arom}), 1448 (C-C_{arom}), 1259, 1212, 1196, 1167, 1020, 959, 934, 848.

Preparation of phosphenium triiodide salts 13-17. Each of the diimines **5-8** and **12** was added to a 50 mL Schlenk flask along with an equimolar amount of PI_3 under an inert atmosphere. The reaction vessel was covered with aluminum foil and 20 mL of dry, degassed DCM was added *via* cannula. The reaction mixture was allowed to stir for 24 hours under argon. Removal of volatiles under reduced pressure resulted in the isolation of powdery products, each of which was recrystallized from a 4:1 dichloromethane/hexanes mixture at -40 ºC under an argon atmosphere to form dark red crystalline **13-17**.

Fluorodiimine phosphenium salt 13. The reaction of **5** (0.100 g, 0.245 mmol) with PI_3 (0.101 g, 0.245 mmol) resulted in the formation of 0.140 g (70%) of a dark red powder. ^{1}H NMR (300.14 MHz, CD_2Cl_2): δ 7.64 (m, 4H), 7.41 (d, 2H, J = 5.4 Hz), 7.18 (t, 4H, J = 6.6 Hz), 7.04 (d, 2H J = 5.4 Hz), 6.93 (t, 2H, J = 5.2 Hz). ^{13}C{^{1}H} NMR (75.48 MHz, CD_2Cl_2): δ 158.41 [J(^{19}F-^{13}C) = 965.0 Hz], 156.32, 156.15, 146.48, 133.16, 130.43, 129.64 (dd, 2C, J = 21.9, 13.2 Hz), 127.56, 116.94 [J(^{19}F-^{13}C) = 93.9 Hz). ^{31}P{^{1}H} NMR (121.52 MHz, CD_2Cl_2): δ 191.57. ^{19}F{^{1}H} NMR (282.41 MHz, $CDCl_3$): δ -107.70 (m). LRMS (CI^+, *m/z*): 439 (100% **5** + P^+). HRMS (CI^+, CH_4): Calculated for $C_{22}H_{14}N_2F_2S_2P^+$, 439.0304; found 439.0298.

Dimethyldiimine phosphenium salt 14. The reaction of **6** (0.100 g, 0.233 mmol) with PI_3 (0.096 g, 0.233 mmol) resulted in the formation of 0.110 g (56%) of a dark red powder. ^{1}H NMR (300.14 MHz, CD_2Cl_2): δ 7.35 (d, 2H, J = 5.7 Hz), 7.29 (s, 4H), 7.08 (s, 2H), 7.07 (d, 2H, J = 5.4 Hz), 6.91 (dd, 2H, J = 6.0, 5.4 Hz), 2.25 (s, 12H). ^{31}P{^{1}H} NMR (121.52 MHz, CD_2Cl_2): δ 194.03. LRMS (CI^+, *m/z*): 460 (100% **6** + P^+). HRMS (CI^+, CH_4) Calculated for ($C_{26}H_{24}N_2S_2P^+$), 459.1119 found 459.1111.

Tert-butyldiimine phosphenium salt 15. The reaction of **7** (0.100 g, 0.206 mmol) with PI_3 (0.084 g, 0.206 mmol) resulted in the formation of 0.130 g (70%) of a dark red powder. ^1H NMR (300.14 MHz, CD_2Cl_2): δ 7.51 (m, 8H), 7.38 (d, 2H, J = 5.4 Hz), 7.02 (d, 2H J = 5.2 Hz), 6.89 (t, 2H, J = 5.4 Hz), 1.35 (s, 18H). $^{13}C\{^1H\}$ NMR (75.48 MHz, CD_2Cl_2): δ 154.35, 151.73, 138.60, 136.85, 133.40, 131.16, 130.56, 127.02, 126.53, 35.18, 31.30. $^{31}P\{^1H\}$ NMR (121.52 MHz, CD_2Cl_2): δ 188.21 LRMS (CI^+, *m/z*): 515 (100% **7** + P^+). HRMS (CI^+, CH_4): Calculated for $C_{30}H_{32}N_2S_2P^+$), 515.1745, found 515.1744.

Methoxydiimine phosophenium salt 16. The reaction of **8** (0.100 g, 0.232 mmol) with PI_3 (0.095 g, 0.232 mmol) resulted in the formation of 0.135 g (69%) of a dark red powder. ^1H NMR (300.14 MHz, $CDCl_3$): δ 7.58 (d, 4H, J = 6.9 Hz), 7.34 (d, 2H, J = 5.2 Hz), 7.05 (d, 2H, J = 5.1 Hz), 6.90 (m, 6H), 3.82 (s, 6H). $^{13}C\{^1H\}$ NMR (75.48 MHz, CD_2Cl_2): δ 161.32, 159.92, 144.82, 136.79, 133.32, 130.56, 128.99, 127.48, 115.02, 56.03. $^{31}P\{^1H\}$ NMR (121.52 MHz, $CDCl_3$): δ 192.06 LRMS (CI^+, *m/z*): 313 (100%, **8** – 4-OMe anil), 463 (20%, **8** + P^+). HRMS (CI^+, CH_4): Calculated for ($C_{24}H_{20}N_2O_2S_2P^+$), 463.0704, found 463.0703.

Thienylphenyldiimine phosphenium salt 17. The reaction of **12** (0.100 g, 0.19 mmol) with PI_3 (0.078 g, 0.19 mmol) resulted in the formation of 0.140 g (79%) of an insoluble brown solid which could not be characterized by NMR spectroscopy or mass spectrometry.

Chapter 3: Investigation of Steric and Electronic Limitations of Cyanide-catalyzed Aldimine Coupling

3.1 Introduction

Substituted diimine ligands have been utilized extensively in transition metal and main-group chemistry.[1] The simplest synthetic approach to such ligands involves the reaction of glyoxal with an alkyl or arylamine and can be carried out at room temperature.[2] However, the analogous reactions of amines with 2,3-butadione require more rigorous conditions.[3] Such diimine scaffolds have been well-studied, but the tetraaryldiimine-type structure shown in Scheme 3.01 remains rare. Ligands of this class are useful due to facile substitution of the phenyl rings attached to the imine carbon and the phenyl ring attached to the imine nitrogen. Recent applications of such ligands include the hydrogenation of acetophenone with high-turnover efficiency and metal-mediated electrochromism.[4] Reliable methods for the synthesis of these tetraaryldiimines, however, have lagged far behind their glyoxal or 2,3-butadione-derived analogues.

Scheme 3.01. Various routes to the formation of a phenyl-substituted 1,2-diimine

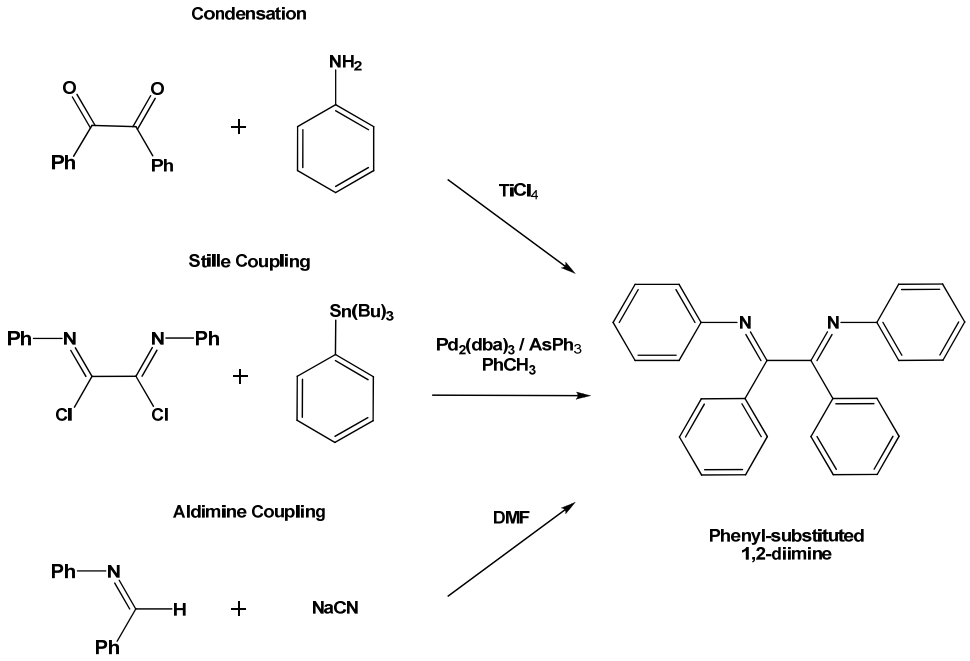

Three possible routes have been reported for the synthesis of benzil dianil (Scheme 3.01). The first method involves the use of a titanium[5] or aluminum reagent[6] that reacts initially with an amine to form an air-sensitive cluster product. The latter complex is then allowed to react with benzil at high temperature to form the desired compound in moderate yield. The instability of the aforementioned cluster intermediate is the likely reason that this route has been used infrequently. A second synthetic route involves the Stille-coupling of tin-substituted phenyl reagents with imidoyl halides[7] as illustrated in Scheme 3.02. However, several problems plague this particular method. For example, the imidoyl chloride derivative is extremely sticky and too unstable for purification by column chromatography. Moreover, the double-Stille coupling method is typically very low-yielding and the mono-coupled intermediate is virtually impossible to separate from the di-coupled product. It was clear that a more general and atomically-

efficient method would be necessary if a variety of highly-substituted 1,2-diimines were to be synthesized and used for subsequent reactions.

Scheme 3.02. Synthetic pathway for tetraaryldiimine.

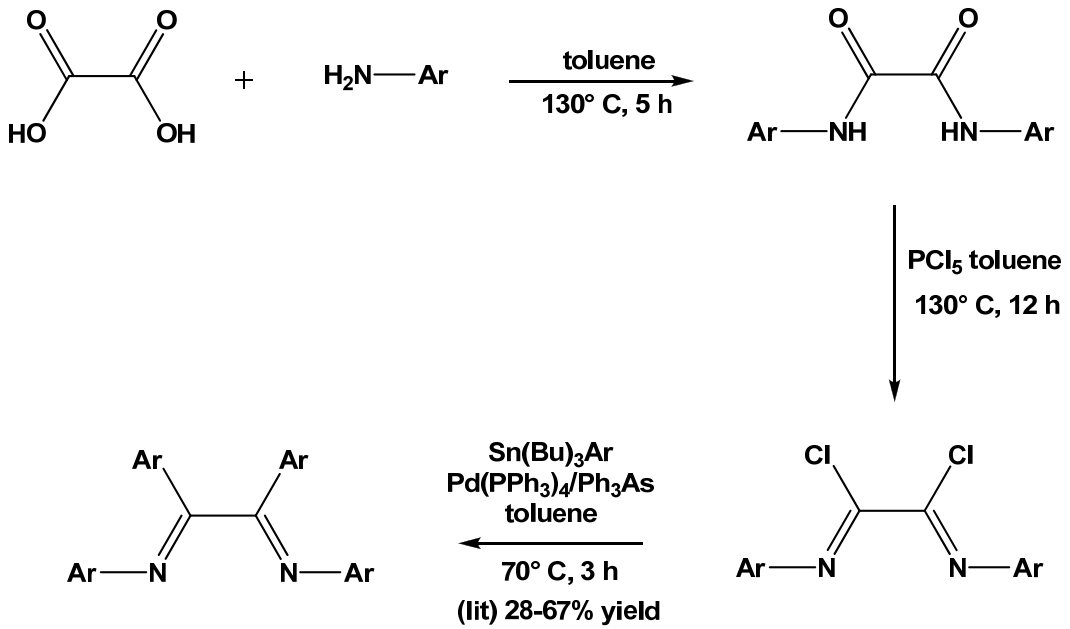

The aldimine coupling method (Scheme 3.01), which consists of the dimerization of aryl-containing monoimines, was first studied in detail in the late 1960s by Satyanarayana and co-workers.[8] These authors reported that aldimines of the general structure shown in Scheme 3.01 could be dimerized to form the corresponding diimines provided that dry DMSO was employed as the solvent. It was also noted that the reaction was concentration dependent in the sense that the use of higher concentrations of reagent and catalyst resulted in higher product yields. On the other hand, heating of the reaction mixture was found to have a deleterious effect on product yield. Interestingly however, a detailed study of these various effects was not undertaken.

The mechanism is thought to mirror closely that of the well-known benzoin condensation, outlined in Scheme 3.03.[9] Initially the cyanide in solution attacks the

carbonyl carbon of the benzaldehyde molecule. Proton-transfer in water or alcoholic solvent then results in a the formation of a resonance-stabilized carbanion. In turn, this carbanion reacts with another equivalent of benzaldehyde, followed by elimination of cyanide to liberate the desired benzoin product. The resulting alpha-hydroxy ketone is stable in air for extended periods of time and requires chemical oxidation for benzil to be obtained.

Scheme 3.03. Mechanism of benzoin condensation.

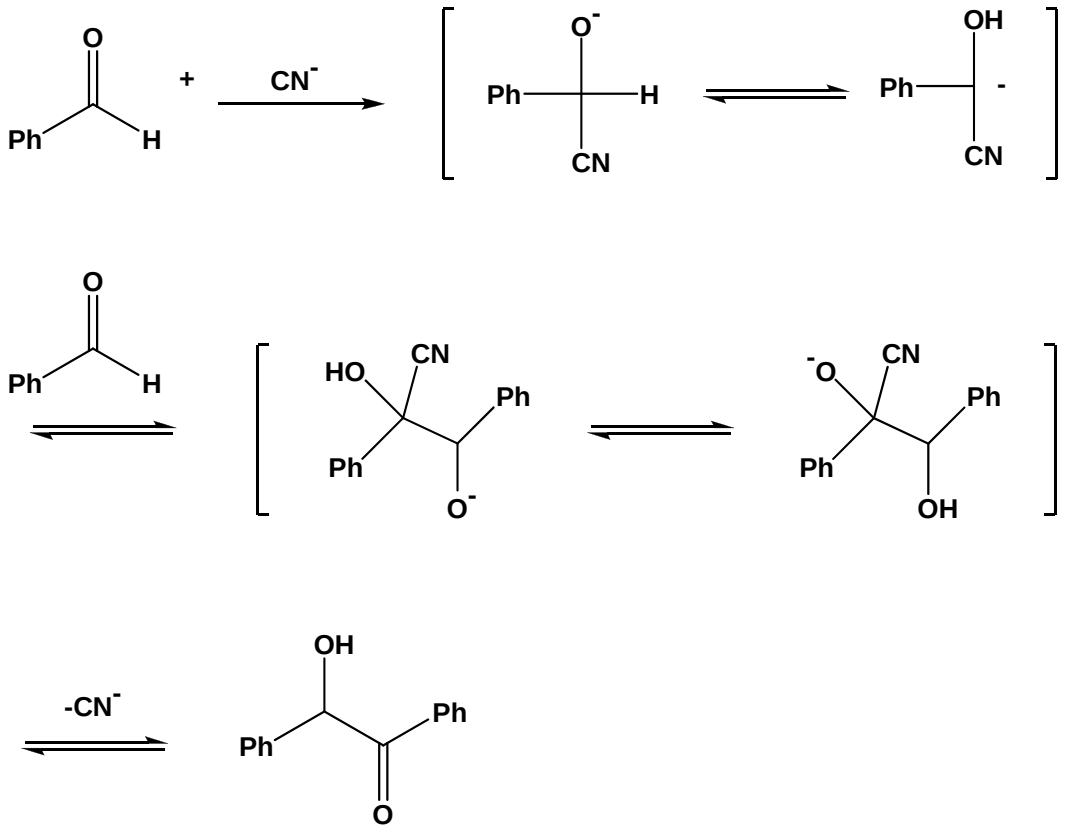

Mechanistic studies of the aldimine coupling were initiated in 1970 by Becker and co-workers.[10] In this study it was found that aldimines could be dimerized in good yields with catalyst loadings of as low as 10 mol%. A deuterium labeling study proved that the

dimerization of aldimines in DMF or DMSO solution took place to form the corresponding ene-diamine as shown in Scheme 3.04. In turn, the latter is auto-oxidized by air to produce the desired benzil dianil. In contrast to the benzoin condensation, which preferentially forms an α-hydroxy ketone, no coupled iminoamine was detected using this procedure. The authors also employed DMSO as the solvent due to its potential ability to oxidize the ene-diamine product *in-situ*. The ene-diamine was found to be stable in neutral methanol solution. However, it was readily oxidized to the diimine following the addition of a small amount of hydrochloric acid.[10] Some ene-diamines were reported to be easier to oxidize than others, but no explanation was offered for this behavior.

Scheme 3.04. Reaction pathway for aldimine dimerization.

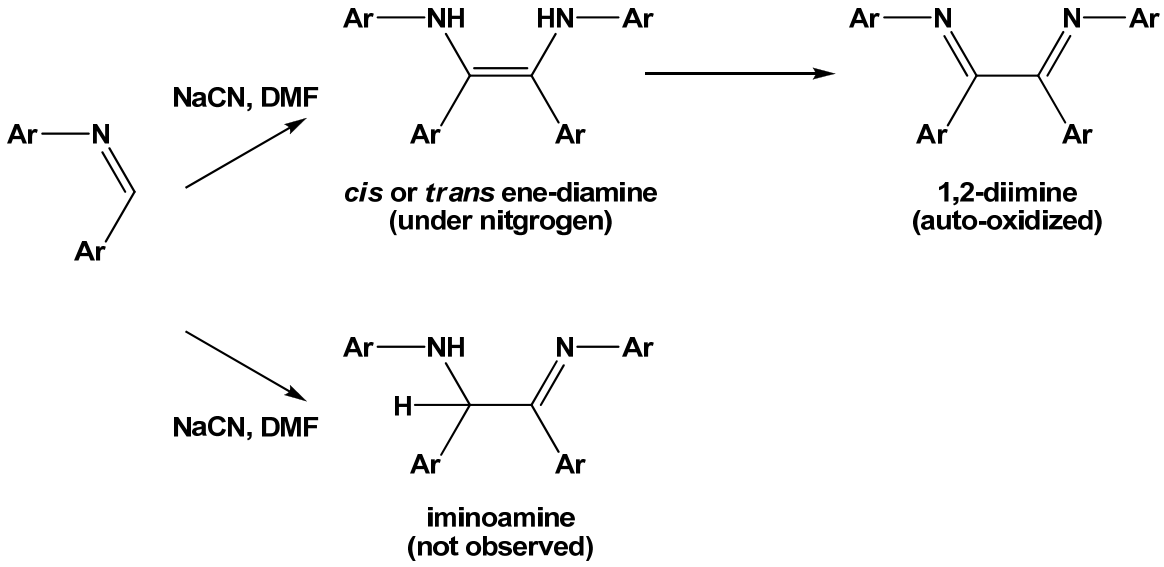

The dimerization of aldimines is thought to occur by initial nucleophillic attack of the imine carbon by a cyanide anion.[11] A proton transfer takes place next. However, this transformation will not occur readily in alcoholic solvents, which in turn results in long reaction times. The proton transfer reaction results in the formation of a resonance-

stabilized carbanion, which attacks a neighboring aldimine to afford the alpha-cyano diamine. Finally, the elimination of cyanide and protonation of the second nitrogen atom produces the ene-diamine. Three canonical structures for the ene-diamine fall within 0.8 kcal/mol of each other. However, the most commonly observed isomer is the ene-diamine structure shown at the bottom center of Scheme 3.05.[12]

Scheme 3.05. Proposed mechanism for intermolecular aldimine dimerization.

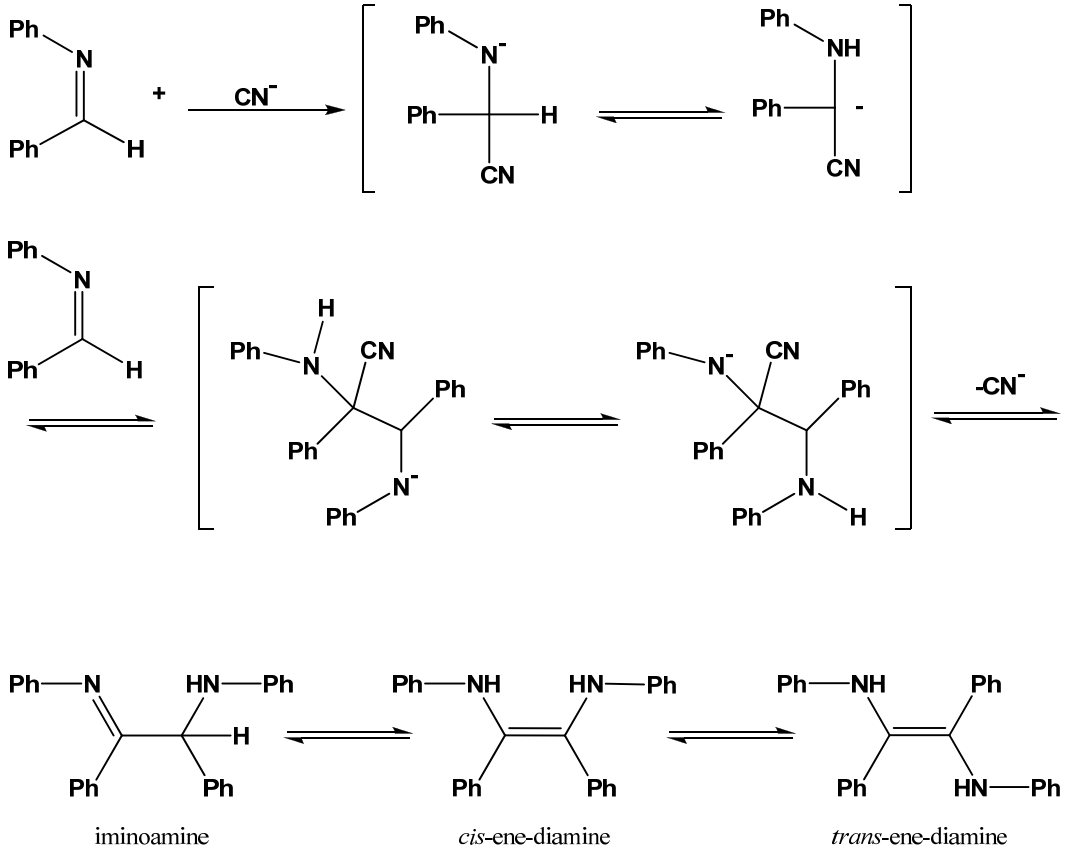

In contrast to the benzoin condensation, the aldimine coupling will not take place in the presence of water or strong bases such as the hydroxide anion. Alcoholic solvents have also been found to prevent the dimerization reaction. The air-sensitive nature of the aldimine coupling reaction represents another important distinctive feature.

Recent research by Miller et al.[13] has demonstrated the electronic limitations of the aldimine coupling reaction and is illustrated in Table 3.1. In this study, a variety of substituents were attached to the aldimines ranging from dimethylamino to nitro. However, dimerization could not be accomplished with any of these functional groups. The mechanism outlined in Scheme 3.05 reveals that the starting material must act as both a nucleophile and electrophile. Thus a substrate with extremely electon-donating groups such as dimethylamino group prevents the aldimine from acting as a carbanion nucleophile toward another equivalent of aldimine. Substrates with nitro groups do not undergo dimerization either as shown in Scheme 3.05. A range of aldimines with electronic properties between the two extremes was therefore determined to react with cyanide. Attempts were made to form the desired diimine in a one-pot reaction. However, this approach failed due to reaction of the 1,4-benzoquinone oxidizing agent with the cyanide catalyst.

Table 3.1. Cyanide-catalyzed aldimine coupling reactions used for the preparation of symmetrical α-diimines.

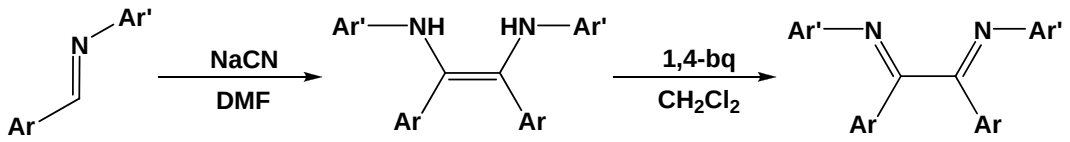

entry	Ar	Ar'	temp (°C)	time (h)	yield (%)
1	Ph	Ph	25	24	54
2	4-MeC_6H_4	Ph	25	40	78
3	4-FC_6H_4	Ph	25	20	67
4	4-CF_3C_6H4	Ph	25	20	65
5	4-$MeOC_6H_4$	Ph	25	24	57
6	Ph	4-FC_6H_4	25	22	51
7	4-MeC_6H_4	4-MeC_6H_4	80	36	40

Table 3.1 (continued). Cyanide-catalyzed aldimine coupling reactions used for the preparation of symmetrical α-diimines.

8	**Ph**	**4-$MeOC_6H_4$**	**80**	**24**	**28**
9	**4-$NO_2C_6H_4$**	**Ph**	**25**	**24**	**-**
10	**4-$NMe_2C_6H_4$**	**Ph**	**80**	**120**	**-**
11	**4-$CF_3C_6H_4$**	**4-MeC_6H_4**	**25**	**18**	**31**
12	**4-$CF_3C_6H_4$**	**4-$MeOC_6H_4$**	**25**	**24**	**55**
13	**4-MeC_6H_4**	**4-$NO_2C_6H_4$**	**80**	**48**	**-**
14	**1-naphthyl**	**Ph**	**25**	**24**	**9**
15	**2-OH, 3-$MeOC_6H_3$**	**4-MeC_6H_4**	**25**	**24**	**-**
16	**Ph**	**2,4,6-$Me_3C_6H_2$**	**25**	**24**	**0**

Steric effects appeared to prevent dimerization in the case of entry 16. However, no study was undertaken to elucidate the steric limitations of this transformation. Almost every entry in Table 3.1 featured the inclusion of substituents in the *para* position of both phenyl rings. Furthermore, the authors performed these reactions on multi-gram scales so that recrystallization of the resulting products could be accomplished in respectable yields. The work described herein is focused on the optimization of the aldimine coupling reaction in conjunction with an investigation of the steric and electronic limitations of cyanide-catalyzed aldimine process.

3.2 Exploration of aldimine coupling conditions

Table 3.2 details the conditions that were employed in an effort to increase the aldimine coupling yield above the range of 50-70% that is typically reported. Quantitative conversion has not been reported in the literature, presumably because each step in the mechanism is expected to be reversible. A darkening of the color of the reaction mixture following the addition of DMF is indicative of aldimine dimerization. The progress of the reaction can be followed by ^{1}H NMR monitoring of the

disappearance of the imine proton around 8.5 ppm. An additional diagnostic is the emergence of a somewhat broad singlet at 5.4 ppm that is characteristic of the N-H proton. Following an aqueous workup for each entry, the product was isolated as a mixture of ene-diamine and 1,2-diimine. Subjection of the product to flash column chromatography (FCC) resulted in the oxidation of the ene-diamine and isolation of the pure 1,2-diimine. To gain more insight into the nature of this transformation the amount of catalyst was varied systematically. Comparable yields were obtained with catalyst loadings between 20 and 300 mol%. The isolated yields dropped from 60% to 45% when the amount of catalyst was lowered to 5 mol%. As anticipated, replacement of the sodium counteranion with potassium had no discernible effect.

Table 3.2. Exploration of the aldimine coupling reaction under various conditions.

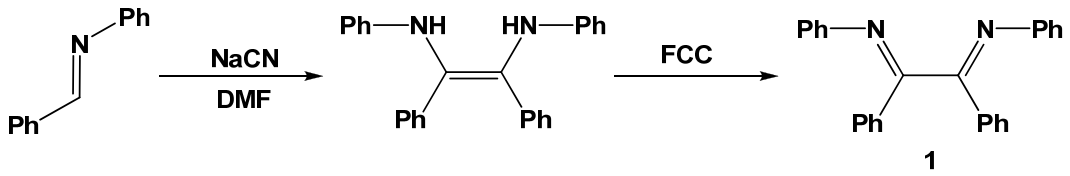

1

entry	catalyst	mol (%)	solvent	vol (mL)	temp (°C)	time (h)[a]	yield (%)[b]
1	NaCN	300	DMF	20	25	24	55
2	NaCN	100	DMF	20	25	24	55
3	NaCN	50	DMF	20	25	24	57
4	NaCN	20	DMF	20	25	24	60
5	NaCN	5	DMF	20	25	24	43
6	NaCN	20	DMF	2	25	24	75
7	NaCN	20	DMF	10	25	24	70
8	NaCN	20	DMF	40	25	24	53
9	NaCN	20	DMF	80	25	24	45
10	1:3 $NaCN/K_2CO_3$	100	DMF	20	25	24	60
11	1:3 thiamine HCl/K_2CO_3	100	DMF	20	25	24	0
12	Kühn Carbene	100	DCM	20	25	24	0

Table 3.2 (continued). Exploration of the aldimine coupling reaction under various conditions.

13	**I-Mes DAD salt + DBU**	**100**	**DMF**	**5**	**25**	**24**	**0**
14	**benzimid. salt + DBU**	**100**	**DMF**	**5**	**25**	**24**	**0**
15	**DMAP**	**100**	**DMF**	**20**	**25**	**24**	**0**
16	**NaN_3**	**100**	**DMF**	**20**	**25**	**24**	**0**
17	**KCN**	**100**	**DMF**	**20**	**25**	**24**	**55**
18	**NaCN**	**100**	**DMF**	**20**	**50**	**24**	**23**
19	**NaCN**	**100**	**no solvent**	**0**	**70**	**24**	**0**
20	**NaCN**	**100**	**DMSO**	**20**	**25**	**24**	**43**
21	**$(Bu)_4NCN$**	**100**	**H_3CCN**	**20**	**25**	**24**	**70**
22	**$(Bu)_4NCN$**	**100**	**CH_2Cl_2**	**20**	**25**	**24**	**30**
23	**$(Bu)_4NCN$**	**100**	**toluene**	**20**	**25**	**24**	**65**
24	**$(Bu)_4NCN$**	**100**	**hexanes**	**20**	**25**	**24**	**45**

[a] Reaction monitored by NMR at hourly intervals; deemed complete after 12 h

[b] Isolated yield (2.21 mmol starting material used)

A large number of catalysts, including several that are active in the benzoin condensation reaction, were evaluated. However, only cyanide sources were found to be effective for carrying out the desired transformation. The catalytic system in entry 14 of Table 3.2 is the most potent N-heterocyclic carbene (Scheme 3.06) in terms of dimerizing benzaldehyde to benzoin.[14] Given the similarities in the mechanism between these two reactions it was thought that the conditions outlined in entry 14 had a reasonable chance of dimerizing the aldimine. In this process the non-nucleophilic base 1,8-Diazabicyclo[5.4.0]undec-7-ene (DBU) was used to deprotonate the imidazolium salts listed in Table 3.2. Unfortunately, the non-cyanide source employed in this study showed no reactivity and only starting material was obtained for entries 11-17.

Scheme 3.06. Reaction of benzaldehyde with an imidazolium halide.

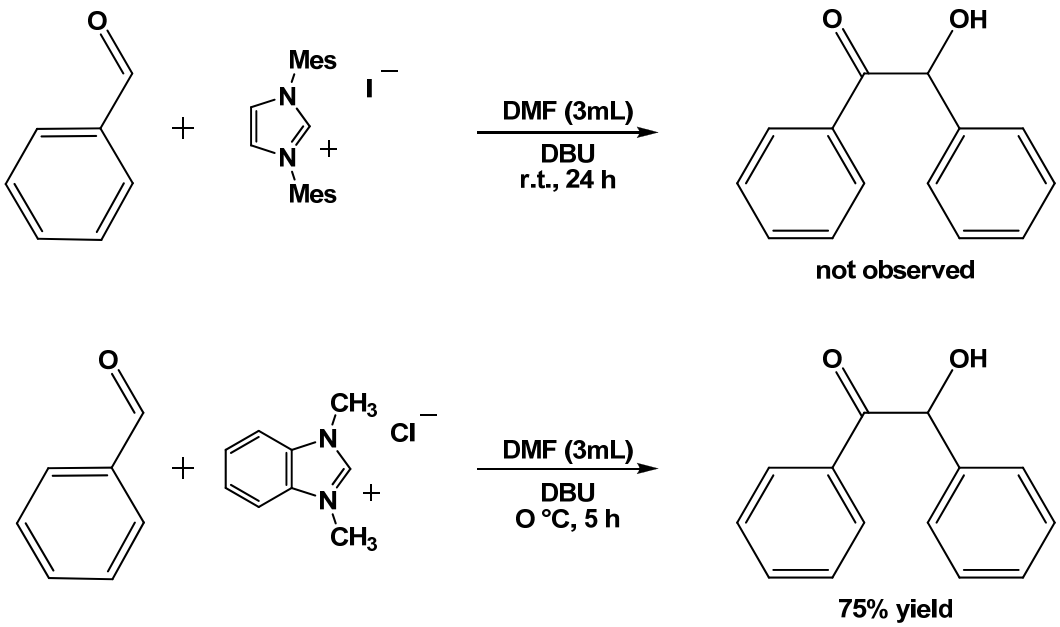

DBU = 1,8-Diazabicycloundec-7-ene

Surprisingly, concentration turned out to be a critical factor in terms of optimizing the conversion to product. Interestingly, decreasing the volume of dry DMF from 80 mL to 2 mL increased the product yield from 45% to 75%. This observation prompted an investigation of the possibility of running the reaction without a solvent. In order to test this hypothesis, a mixture of the substrate and sodium cyanide was heated at 70° C under an argon atmosphere, which caused the substrate to melt in the reaction flask. However, carrying out the reaction at elevated temperature in the presence of sodium cyanide resulted only in the recovery of starting material, which in turn underscored the importance of a mediating solvent. Table 3.2 entry 18 also illustrates the deleterious effect increased temperature has on the aldimine coupling reaction in DMF solvent.

Aldimine coupling was accomplished for the first time in a variety of solvents by employing a cyanide source with a tetrabutylammonium counteranion. Using this particular cyanide source the desired diimine can be produced in H_3CCN, CH_2Cl_2,

toluene and even hexanes. All previously reported examples of intermolecular aldimine coupling required either dry DMF or dry DMSO as the solvent. It should be noted however, that DMF is not normally used in industry due to long-term health risks and the fact that DMSO is difficult to remove by aqueous workup. Even though an array of green solvents were found to affect aldimine coupling the best yields were obtained using a small volume of DMF. Accordingly, DMF was chosen as the best solvent for carrying out dimerization reactions involving cyanide.

3.3 Electronic tuning to form assymetric diimines

Previous reports by Miller and coworkers,[13] as well as experiments carried out in our laboratory, demonstrated that aldimines with strongly electron-donating or withdrawing functional groups fail to undergo dimerization. A logical next step, therefore, was to determine if electron-rich aldimines would react with electron-poor aldimines, thus forming asymmetric diimines. The reactions that were explored are summarized in Scheme 3.07.

Scheme 3.07. Combination of electronically-diverse aldimines.

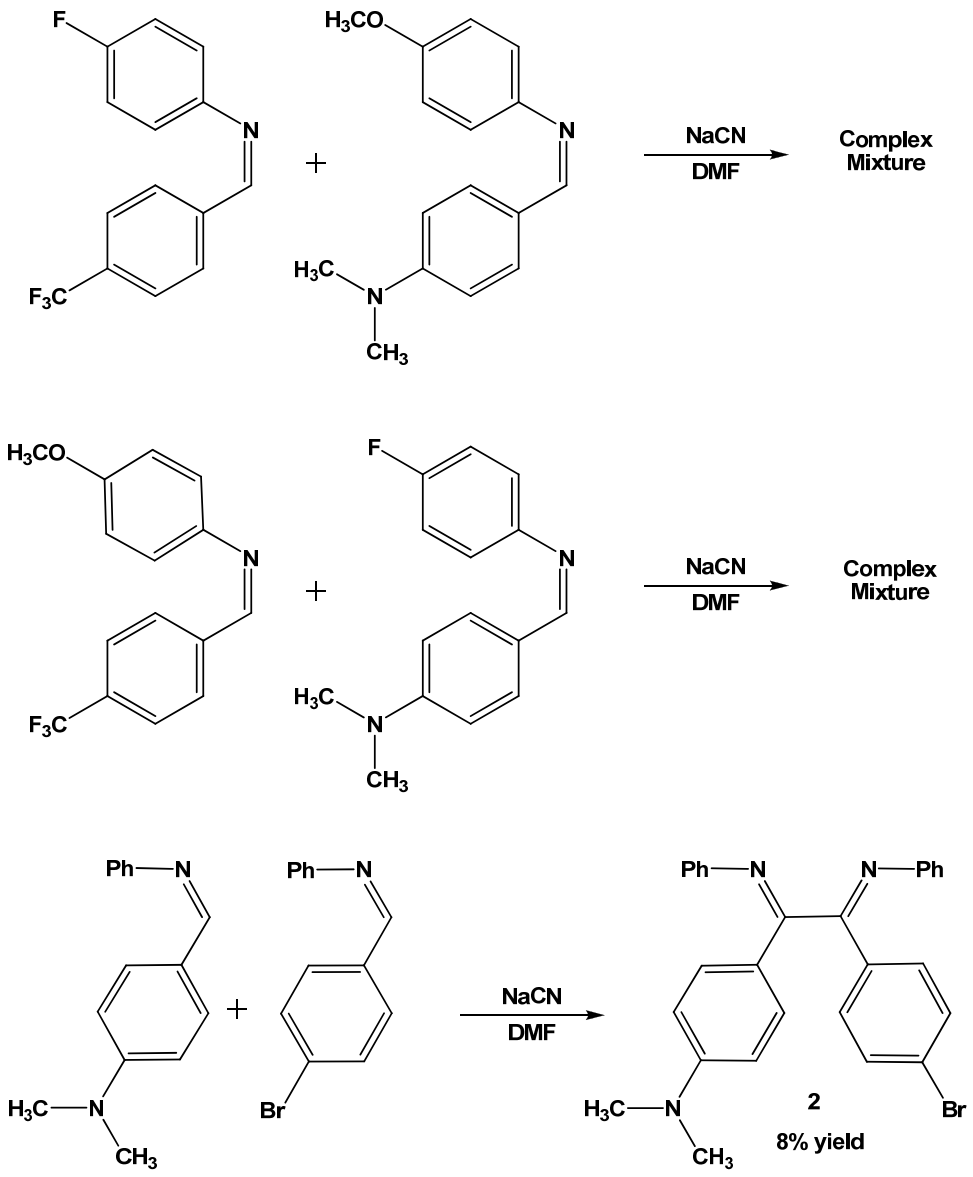

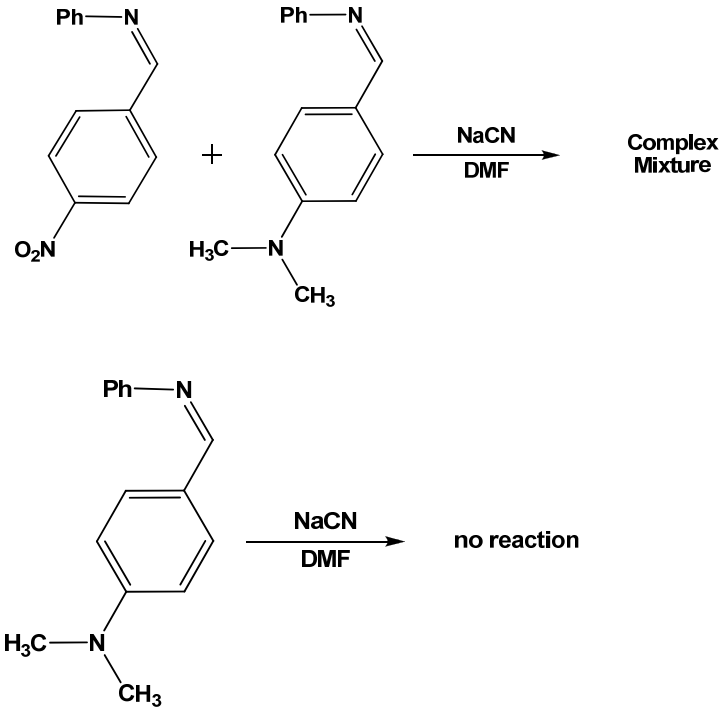

In order for the coupling reaction to occur, it is necessary for one molecule of an aldimine to act as a nucleophile and the other molecule of aldimine to serve as an electrophile. The first two attempts each resulted in a complex mixture of products that did not include the desired cross-coupled diimine. This result indicated that electronic effects alone could not be used to facilitate the synthesis of asymmetric diimines. Interestingly, the reaction of a brominated aldimine with the dimethylamino-subsituted aldimine did result in the formation of asymmetric diimine **2** in 8% yield. However, the very low yield implies that the presence of two aldimines complicates the production of diimines and interferes with the catalytic cyanide process. In order to limit the number of possible products, the next step was to explore the reaction of the nitro and dimethylamino aldimines because neither aldimine dimerizes with itself. However, once again a complex reaction mixture was obtained that comprised mostly unreacted starting

materials. The low yields and the presence of many side-products rendered this an unattractive route for the synthesis of the desired diimines.

3.4 Steric aspects of aldimine coupling

The work of Miller et al.[13] revealed that mesityl-substituted aldimines failed to undergo dimerization. A study of the several aldimines prepared and tested (Table 3.1) illustrates the severe steric limitations of this transformation. A review of the literature revealed that while *para*-substituted substrates are common, the corresponding but *ortho* examples are extremely rare and only formed in low yields. Examination of Table 3.3 (entry 2) reveals that the difluoro substrate is recovered in only about 30% yield and is accompanied by many side-products. Entry 3 shows that the dimerization of an aldimine with a methyl group in the *ortho* position of the Ar' (diimine **3**) ring decreases the yield significantly in comparison with the optimum substrate. The presence of an ethyl group (diimine **4**) essentially prevents any conversion to the desired product within the specified reaction time. Furthermore, the use of the analogous isopropyl compound results in the exclusive isolation of starting material.

Other aryl derivatives were found to be even more sensitive to the nature of the substituents. For example, substitution of a methyl group on the 2-position of the other aryl ring prevents any dimerization from occurring at all as shown in entries 6-7. This observation is logical because the aryl ring is closer to the imine carbon, which is the site of the dimerization. In order to explore the limitations of the steric properties, mixtures of the aldimine from entry 1 and other aldimines listed in Table 3.3 were treated with cyanide in an attempt to construct asymmetric diimines (see Scheme 3.08).

Table 3.3. Steric limitations of aldimine coupling.

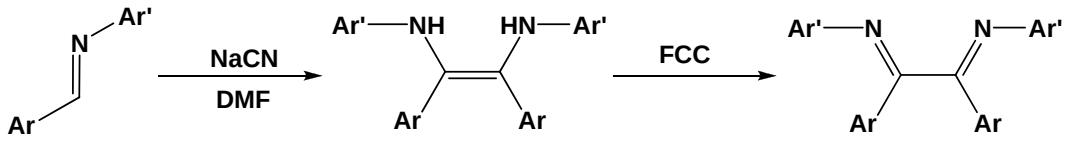

entry	Ar	Ar'	solvent (2 mL)	temp (°C)	time (h)	yield (%)
1	Ph	Ph	DMF	25	24	75
2	Ph	2,6-FC_6H_3	DMF	25	24	30
3	Ph	2-MeC_6H_4	DMF	25	24	45
4	Ph	2-ethylC_6H_4	DMF	25	24	10
5	Ph	2-^{i}prC_6H_3	DMF	25	24	0
6	2,5-$(CH_3)_2C_6H_3$	Ph	DMF	25	24	0
7	2,5-$(CH_3)_2C_6H_4$	3,5$(CH_3)_2C_6H_3$	DMF	25	24	0
8	Ph	2,4,6-$Me_3C_6H_2$	DMF	25	24	0
9	Ph	2,6-^{i}pr$_3C_6H_2$	DMF	25	24	0

Six different attempts were made to prepare asymmetric diimines as summarized in Scheme 3.08. However, in each case the homo-coupled tetraphenyldiimine was the exclusive diimine product recovered. The sterically bulky aldimines were found to be unreactive and most of the starting material was recovered by FCC. Surprisingly, however, the yield of the tetraphenyldiimine was found to decrease in the presence of another aldimine. This observation implies that some reaction of the two substrates had taken place to form a series of intermediates. However, in no case could an asymmetric diimine be prepared by this method.

For aldimine coupling to become used more estensively it was clear that a wider array of possible products need to be synthesized. With the aforementioned thought in mind, attempts were made to synthesize a wider variety of substrates that could be utilized in fields other than metal chelation.

Scheme 3.08. Reaction of sterically-constrained aldimines with phenyl aldimine.

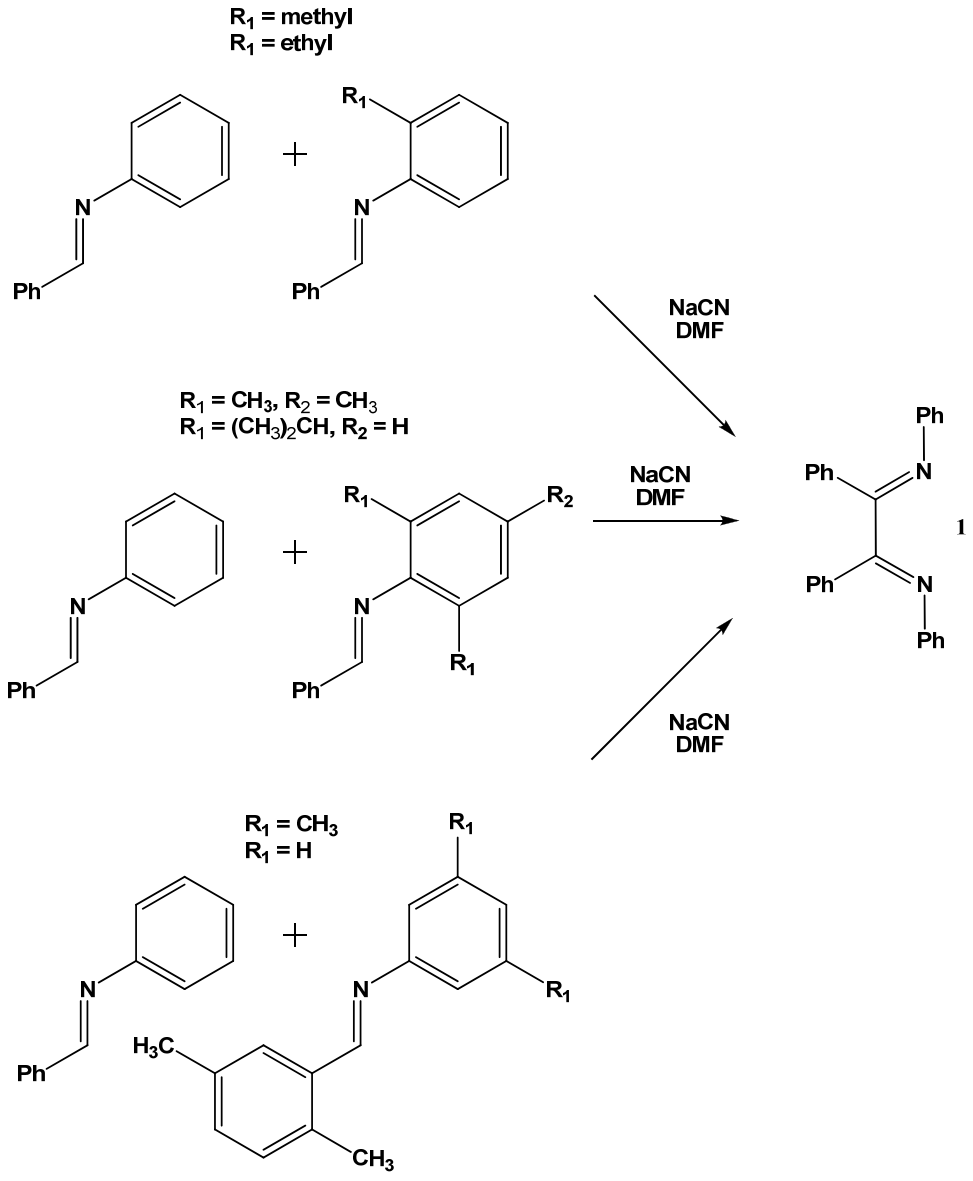

3.5 Survey of unexplored aldimines

Previous work in our lab has shown that thiophene diimines can be prepared by the cyanide-catalyzed dimerization process outlined in Table 3.4. Entry 1 (structure **5**)

had not been reported in the literature previously. Moderate yields of each dimeric product were isolated, but in contrast to the phenyl diimines, the compounds listed in Table 3.4 were isolated as the ene-diamines. Thiophene possesses a more electron-withdrawing capability than a phenyl group, which may explain the ability of thiophene diimines to resist auto-oxidation in air. Thus, several hours of exposure to pure oxygen or chemical oxidation with 1,4-benzoquinone was required for quantitative conversion of the aforementioned ene-diamine to the 1,2-diimine.

Table 3.4. Dimerization of thiophene diimines.

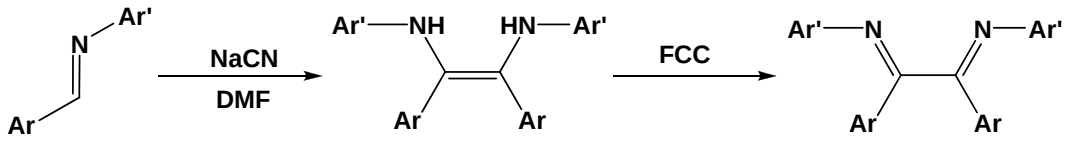

entry	Ar	Ar'	yield (%)
1	Thiophene	C_6H_5	75
2	Thiophene	4-F(C_6H_4)	69
3	Thiophene	4-(^{t}Bu)C_6H_4	65
4	Thiophene	4-(OCH$_3$)C_6H_4	60
5	Thiophene	3,5(CH$_3$)$_2C_6H_4$	56

Knowing that the heterocycles in Table 3.4 can be prepared, attention was turned next to the synthesis of the pyrrole and benzyl derviatives instead of phenyl derivatives. Even though it is known that protonated solvents impede dimerization, these reactions were conducted to determine if substrates with acidic hydrogens could be dimerized. As summarized in Scheme 3.09, these protonated substrates failed to react and only starting material was recovered. The location of the acidic hydrogen atom was found to have no effect on the reactivities of the substrates. It was surmised that the cyanide anion would

deprotonate the acidic hydrogen on the substrates hence the catalyst load was increased to 300 mol%. However, in each case, no dimerized product could be detected. The anionic substrates that resulted from the deprotonation reactions may be too electron-rich to undergo the delicate dimerization transformation. The benzyl analogue was found to be unreactive, presumably due to the break in conjugation that occurs in close proximity to the imine carbon atom of the aldimine.

Two tosyl hydrazones were also tested for reactivity with cyanide. However, only complex product mixtures were obtained. The product mixtures were separated by FCC, but no evidence of dimerized product could be detected by ^{1}H NMR or MS-CI. Differences in the electronic characters of the functional groups (nitro versus dimethylamino) did not affect the ability of the dimerization to occur.

Scheme 3.09. Attempted dimerization with aldimine analogues.

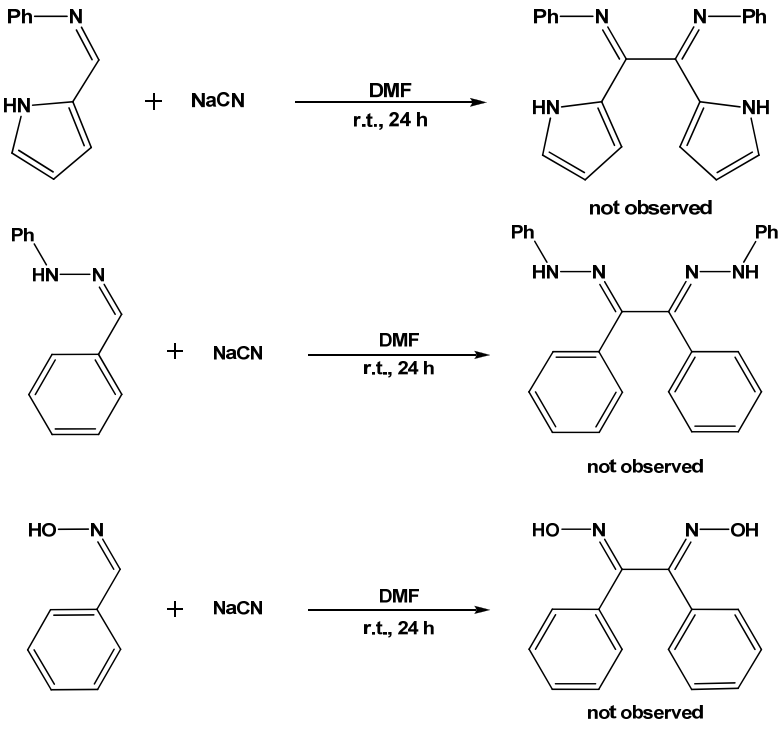

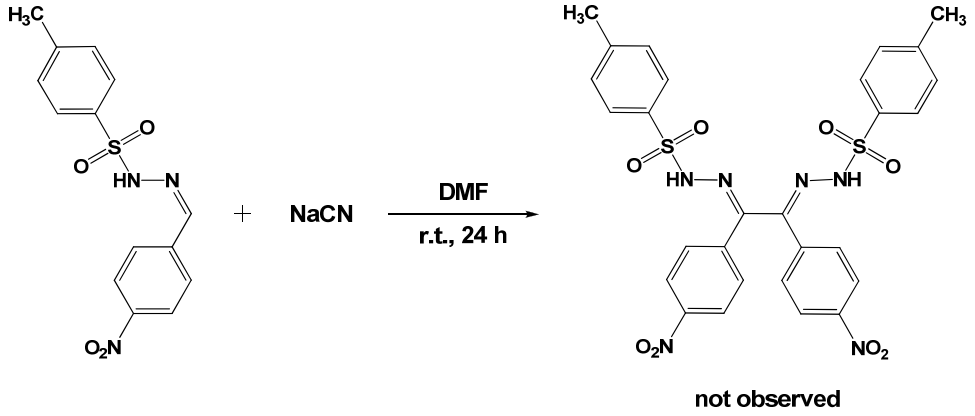

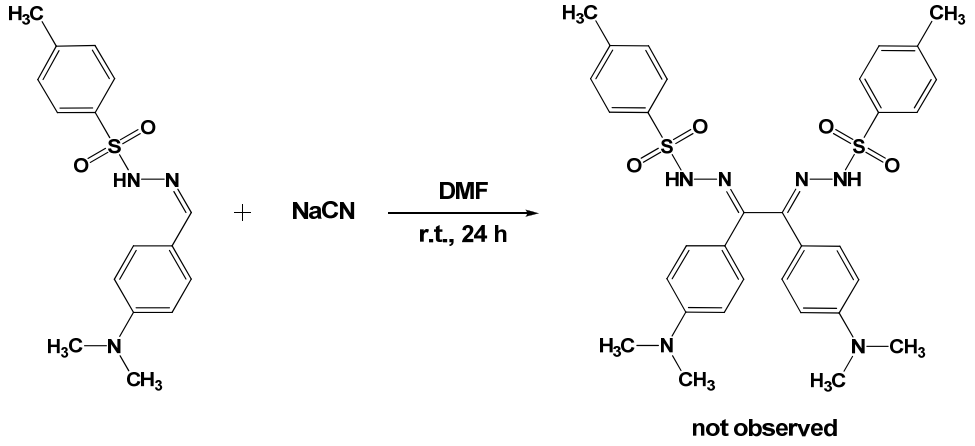

Previous work in our laboratory demonstrated that thiophene diimines cannot be polymerized by means of cyclic voltammetry.[15] Subsequent attempts were therefore made to prepare diimines with other polymerizable functionalities such as bromide or vinyl groups (see Scheme 3.10). It seemed likely that the bis(brominated) diimine **6** could be polymerized either by Suzuki polymerization with a bis(boronic acid)[16] or by polymerization using Grubbs Metathesis (GRIM)[17]. The requisite aldimines were prepared in good yields *via* condensation reactions and purified by FCC, but these dimerization attempts did not result in appreciable quantities of the desired products.

Despite the fact that only minimal quantities of starting material remained following the reaction of the bis(brominated) aldimine, unusually large quantities of side-products were produced concomitantly. In contrast, a bis(fluorinated) diimine had been synthesized previously in a respectable yield (Table 3.4, entry 2). The modest yield of the brominated aldimine in the attempt to form **6** is attributable to the higher reactivity of the brominated carbon atom with the cyanide anion. This low yield discouraged any further use of this method for the synthesis of polymerizable brominated monomers.

Scheme 3.10. Preparation of polymerizable diimines.

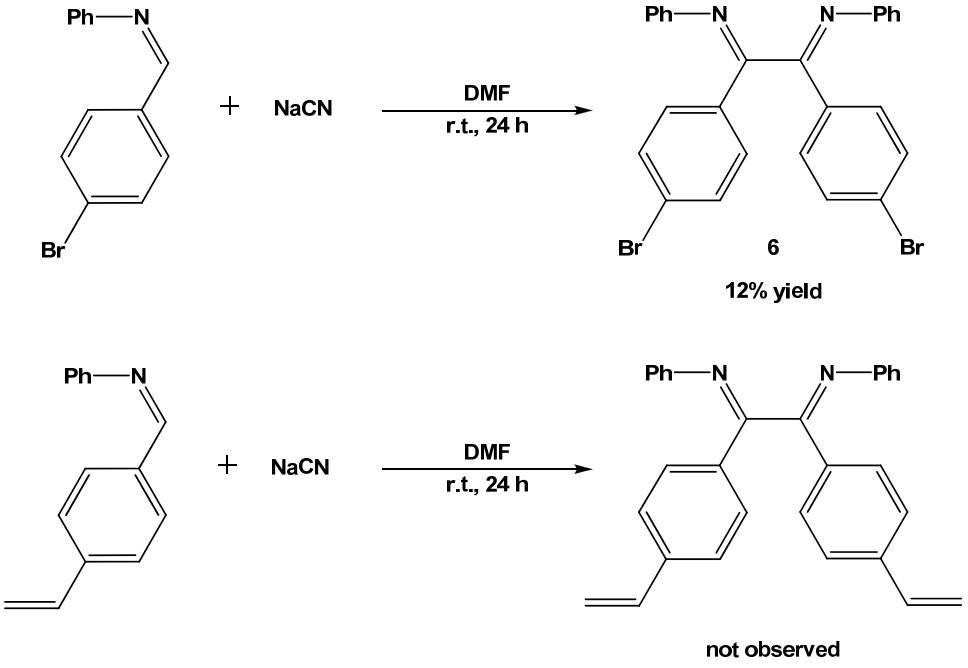

It is well-known that vinyl groups can be readily polymerized using commercially-available Grubbs catalysts. However, in the case of the vinyl-substituted substrate, no starting material could be identified in the crude reaction mixture, and desired product was not formed. Presumably the carbanion that is formed in the catalytic cycle reacts with the terminal vinyl group, which precludes the assembly of the desired

product. If a bis(vinyl)diimine is to be prepared the diketone should be prepared first, and this step should be followed by a titanium-mediated condensation to form the desired 1,2-diimine.

3.6 Conclusions

A comprehensive investigation of the aldimine coupling transformation has revealed several important aspects. First, it has been found that green solvents such as acetonitrile and hexanes can affect the desired dimerization when the cyanide counteranion was changed from sodium to tetrabutylammonium. The steric limitations of aldimine coupling have been systematically identified and a series of possible substrates have been eliminated as viable candidates for dimerization. Substrates with acidic protons were found to be unreactive despite the use of excess quantities of sodium cyanide. Diimines with bromine or vinyl polymerizable functionalities and those with asymmetric units could not be prepared by this method. The foregoing information should prove to be valuable for the future assembly of diimine systems that possess useful catalytic or polymer properties.

3.7 Experimental

General procedures. All dimerization reactions were performed under a dry, oxygen-free, catalyst-scrubbed argon atmosphere using a combination of standard Schlenk techniques or in a Vacuum Atmospheres drybox. All glassware was oven-dried and vacuum- and argon-flow degassed before use. All solvents were distilled over sodium benzophenone ketyl, except dichloromethane, which was distilled over calcium hydride and degassed prior to use.

Physical Measurements. Low-resolution chemical ionization mass spectral data (MS-CI) were collected on a Finnigan MATTSQ-700 mass spectrometer, and high-resolution CI-MS spectra were recorded on a VG Analytical ZAB-VE sector instrument. All MS analyses were performed on samples that had been sealed in glass capillaries under an argon atmosphere. Solution-phase NMR spectra were recorded at 298 K on Varian Inova instrument (^{1}H NMR, 400.27 MHz; ^{13}C NMR, 100.65 MHz) using $CDCl_3$ the an internal reference unless otherwise stated.

Optimization Table. Specific conditions for each trial are displayed in Table 3.2. A 50 mL Schlenk flask was charged with monoimine **1** (0.40 g, 2.21 mmol) and various catalysts. The flask was de-gassed and dry, de-gassed solvent was added *via* cannula transfer. The resulting solution was stirred at ambient temperature for various times and temperatures under an atmosphere of argon. After the specified time, the reaction mixture was extracted into ethyl acetate (50 mL), washed with brine (3 x 100 mL) and back-extracted with 50 mL of ethyl acetate. The organic layers were combined, dried over $MgSO_4$, filtered and then concentrated to yield a yellow oil in each case. The crude product was purified *via* FCC using hexanes (hx) and ethyl acetate (EA), which resulted in a pure cream-colored solid. (95:5 hx:EA) $R_f = 0.38$. ^{1}H NMR (400.27 MHz, $CDCl_3$, TMS): δ 7.89 (d, 4H, J = 8.0 Hz), 7.40 (m, 6H), 7.10-6.99 (m, 6H), 6.52 (d, 4H, J = 7.2 Hz) ^{13}C{^{1}H} NMR (100.65 MHz, $CDCl_3$): δ 163.85, 149.28, 137.59, 131.08, 128.71, 128.35, 128.29, 124.85, 120.03.

Mixing of Electronically-Diverse Aldimines. A 50 mL flask was charged with equimolar amounts of the two different aldimines (4.0 mmol of each aldimine) along with 4.0 mmol of NaCN. The reaction flask was de-gassed and dry, de-gassed DMF (5 mL)

was added *via* cannula transfer. The resulting solution was stirred at ambient temperature for 24 h under an atmosphere of argon. Following this, the reaction mixture was extracted into ethyl acetate (50 mL), washed with brine (3 x 100 mL) and back-extracted with 50 mL of ethyl acetate. The organic layers were combined, dried over $MgSO_4$, filtered and then concentrated to yield a yellow oil in each case. The crude product was purified *via* FCC. Two of the products listed in Scheme 3.07 were isolated and characterized.

Asymmetric diimine. Compound **2**. Orange solid. Solvent system (80:20 hx: EA). R_f = 0.57. ^{1}H NMR (400.27 MHz, $CDCl_3$, TMS): δ 7.71 (d, 2H, *J* = 8.4 Hz), 7.45 (d, 2H, *J* = 8.4 Hz), 7.02 (t, 2H, *J* = 7.6 Hz), 6.96 (m, 3H), 6.59 (d, 2H, *J* = 9.2 Hz), 6.50 (d, 2H, *J* = 7.2 Hz), 2.97 (s, 6H). LRMS (CI^+, *m/z*): 482 (100% M^+)

Steric Limitations Table. The specific conditions employed for each trial are displayed in Table 3.3. A 50 mL Schlenk flask was charged with each monoimine (0.40 g, 2.21 mmol) and an equimolar amount of NaCN. The reaction flask was de-gassed and dry, de-gassed DMF (5 mL) was added *via* cannula transfer. The resulting solution was stirred at ambient temperature for 24 h under an atmosphere of argon. After 24 h the reaction mixture was extracted into ethyl acetate (50 mL), washed with brine (3 x 100 mL) and back-extracted with 50 mL of ethyl acetate. The organic layers were combined, dried over $MgSO_4$, filtered and then concentrated to yield a yellow oil in each case. The crude products were purified *via* FCC.

Benz-2-methanil-diimine. Compound **3**. Yellow solid. Solvent system (95:5 hx: EA). R_f = 0.65. ^{1}H NMR (400.27 MHz, $CDCl_3$, TMS): δ 7.95 (d, 4H, *J* = 8.0 Hz), 7.43 (m, 6H), 6.91 (m, 4H), 6.78 (t, 2H, *J* = 5.6 Hz), 6.49 (d, 2H, *J* = 7.6 Hz), 1.28 (s, 6H, *J* = 8.0 Hz). LRMS (CI^+, *m/z*): 389 (100% M + H^+).

Benz-2-ethanil-diimine. Compound **4**. Yellow solid. Solvent system (95:5 hx: EA). R_f = 0.58 ^{1}H NMR (400.27 MHz, $CDCl_3$, TMS): δ 7.98 (d, 4H, *J* = 6.4 Hz), 7.46 (m, 6H), 6.98 (d, 4H, *J* = 4.4 Hz), 6.83 (p, 2H, *J* = 4.0 Hz), 6.56 (d, 2H, *J* = 8.0 Hz), 1.37 (quart, 4H, *J* = 7.6 Hz) 0.93 (t, 6H, *J* = 8.0 Hz). LRMS (CI^+, *m/z*): 417 (100% M + H^+).

Dimerization with Aldimine Analogues. A 50 mL flask was charged with the monoimine and an equimolar amount of NaCN. The reaction flask was de-gassed and dry, de-gassed DMF (10 mL) was added *via* cannula transfer. The resulting solution was stirred at ambient temperature for 24 h under an atmosphere of argon. After 24 h, the reaction mixture was extracted into ethyl acetate (50 mL), washed with brine (3 x 100 mL) and back-extracted with 50 mL of ethyl acetate. The organic layers were combined, dried over $MgSO_4$, filtered and then concentrated to a yield dark solid in each case. The crude product was purified *via* FCC. Unfortunately, none of the products were successfully synthesized and isolated.

Dimerization with Aldimine Analogues. A 50 mL flask was charged with the requisite monoimine (2.0 mmol) and an equimolar amount of NaCN. The flask was de-gassed and dry, de-gassed DMF (10 mL) was added *via* cannula transfer. The resulting solution was stirred at ambient temperature for 24 h under an atmosphere of argon. After 24 h, the reaction mixture was extracted into ethyl acetate (50 mL), washed with brine (3 x 100 mL) and back-extracted with 50 mL of ethyl acetate. The organic layers were combined, dried over $MgSO_4$, filtered and then concentrated to yield a dark solid in each case. Each crude product was purified *via* FCC. The dibromophenyl diimine shown in Scheme 3.09 was isolated and characterized.

Phenyl-substituted thiophene diimine. Light-yellow solid. Compound **5**.

Dibromophenyl diimine. Bright-yellow solid. Compound **6**. Solvent system (90:10 hx: EA). $R_f = 0.47$. ^1H NMR (400.27 MHz, $CDCl_3$, TMS): δ 7.65 (d, 4H, $J = 8.4$ Hz) 7.46 (d, 4H, $J = 8.7$ Hz), 7.15-6.90 (m, 6H), 6.42 (d, 4H, $J = 6.9$ Hz). LRMS (CI^+, *m/z*): 519 (100% $M + H^+$). Two isotopes of **6** were detected, each with 55% abundance at 517 and 521 amu.

Chapter 4: Electropolymerization of an N-Heterocyclic Carbene Gold (I) Complex

4.1 Introduction

In contrast to the large number of useful polymeric materials which contain tethered N-heterocyclic carbenes (NHCs),[1] there are relatively few examples of polymers in which the NHCs are integral components of the main chain.[2] Moreover, several of these polymeric NHCs exhibit sensitivity to air and moisture, thus severely limiting their usefulness.[3] Furthermore, in all of these examples, the carbene functionalities are essential to maintain the polymer structure hence they are not available for ligation or further reactivity.

It was envisioned that electrochemical polymerization of an appropriately substituted thiophene-based monomer would constitute a new and promising approach to a polymer which contains an NHC orthogonally positioned with respect to its main chain. Arrangements of this type are of considerable interest for their ability to attach readily-accessible entities with catalytic or biological properties, or to enable electronically tunable features to these systems. Furthermore, because NHCs are so prevalent in the literature, such an approach should be general and readily extended to incorporate a wide variety of NHC-metal complexes into polymeric materials. Given the rapidly expanding interest in both the catalytic[4] and the medicinal applications of gold,[5] the initial efforts described below focused on the polymerization of an NHC-AuCl complex.

Scheme 4.1. Synthesis of Gold NHC Metallopolymer **6**.

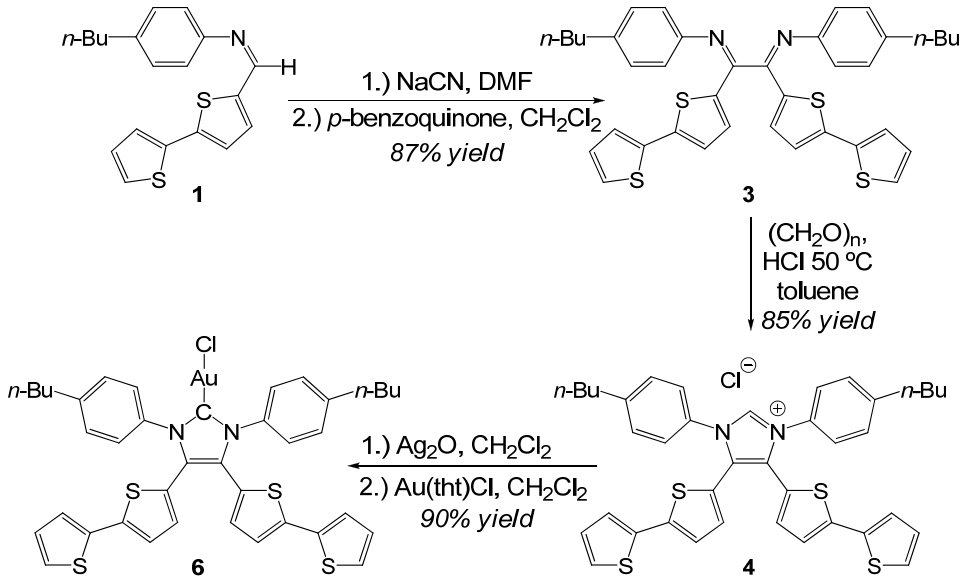

4.2 Synthesis of polymerizable gold NHC metallpolymer

As summarized in Scheme 4.1, gold NHC **6** was synthesized using a five-step procedure in an overall yield of approximately 60%. The bithiophene aldimine **1**, which was prepared by condensing bithiophene carboxaldehyde with 4-*n*-butylaniline (92% yield), was dimerized to the corresponding *ene*-diamine **2** (structure not shown) *via* a NaCN catalyzed aldimine coupling reaction.[6] The ene-diamine could be isolated in air without auto-oxidation unlike the phenyl-substituted ene-diamines synthesized previously. Subsequent oxidation of **2** with *p*-benzoquinone afforded the desired diimine **3**. Freshly sublimed *p*-benzoquinone was required to oxidize **2** to the diimine **3**. When treated with paraformaldehyde and anhydrous HCl, the diimine was cyclized resulting in the formation of **4**. Treatment of the latter with the Ag_2O afforded AgCl complex **5** (structure not shown). Finally, transmetallation of **5** with Au(tht)Cl (tht =

tetrahydrothiophene) afforded the desired AuCl complex **6** (diagnostic ^{13}C NMR signal: δ = 172 ppm in CD_2Cl_2).[7] The NMR spectra of **5** and **6** were found to be nearly identical, but the phenyl resonances for silver NHC **5** were much more broad than those observed for **6**. High-resolution mass spectrometry was used to distinguish between **5** and **6**. Further confirmation of this structural assignment was obtained via X-ray diffraction analysis (see Figure 4.1, left). Although the key bond lengths and angles are similar to those of known NHC-Au complexes,[7] the packing diagram revealed a one-dimensional series of Au···Au contacts (3.2262(4) Å) between neighboring units of **6** that are arranged in a head-to-head fashion (see Figure 4.1, right).

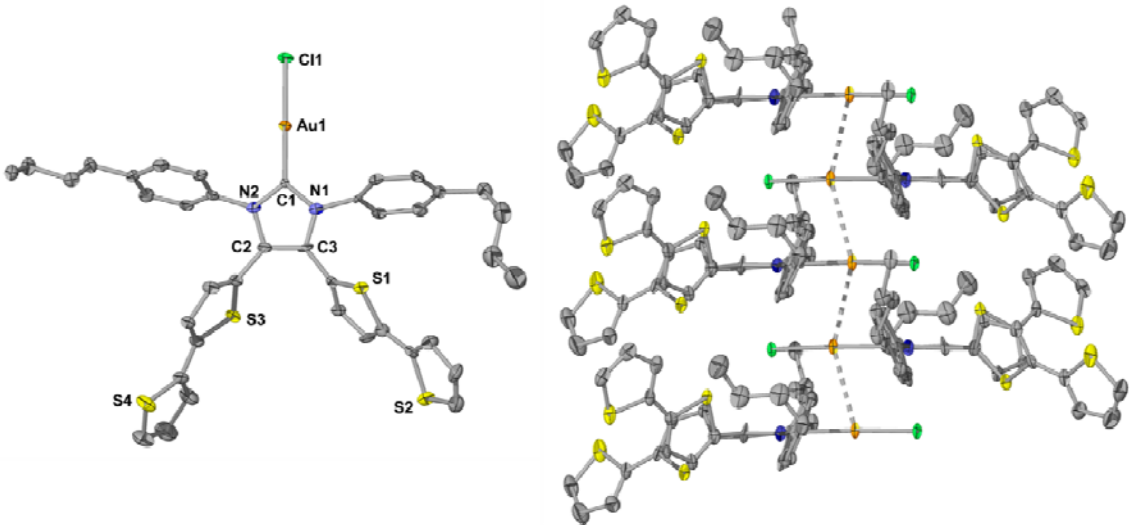

Figure 4.1. (left) ORTEP diagram showing 50% probability thermal ellipsoids and selected atom labels for **6**. (right) Packing diagram of **6** showing Au···Au contacts. Hydrogen atoms have been omitted for clarity.

Scheme 4.2. Electrochemical Polymerization of Bithiophene-substituted Gold (I) Carbene Monomer **6**.

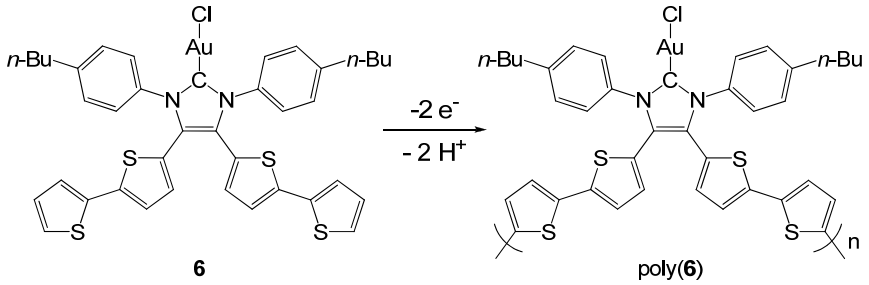

4.3 Electrochemical characterization of gold NHC polymer

Electropolymerization of a 1 mM solution of **6** (in CH_2Cl_2) onto a platinum disk or an ITO glass slide afforded poly(**6**) as illustrated in Scheme 4.2.[8] The reaction was performed in a drybox using a three-electrode cell containing a silver wire quasi-reference electrode and $[(n\text{-Bu})_4N^+][PF_6^-]$ as the supporting electrolyte.[8] Films prepared outside of the drybox were marginally less active than those formed under an inert atmosphere. As shown in Figure 4.2 (top), the polymerization proceeded cleanly and in the anticipated fashion within a window of –0.2 to 1.5 V.[9] The polymer film oxidation wave grew with subsequent scans at 1.1 V and continued to increase for over 20 cycles, indicating good conductivity through the film. The observed shift to higher peak potentials with additional scans is typical and may originate from polymer growth on the elctrode.[8] Similar to other thiophene-based polymerizations, the reduction peak (0.9 V) shifted cathodically with increasing scans.[10] Subsequent oxidation or reduction of the deposited film (in monomer-free solutions) resulted in no decrease in peak height, reflecting the high-stability of the polymer.[11] Examination of the scan rate dependence

(see Figure 4.2, bottom) revealed that the peak current for the electrodeposited film of poly(**6**) in a solution of CH_2Cl_2/[(*n*-Bu)$_4$N$^+$][PF_6^-] increased with scan rate as expected on the basis of the Cottrell equation for spherical electrodes and was in accord with related examples in the literature.[10] Scan rates above 100 mV/s resulted in distortion of the electrochemical profiles. The fast scan rate deprives the film of sufficient time for the removal of the counter anions from the matrix of the thin film.

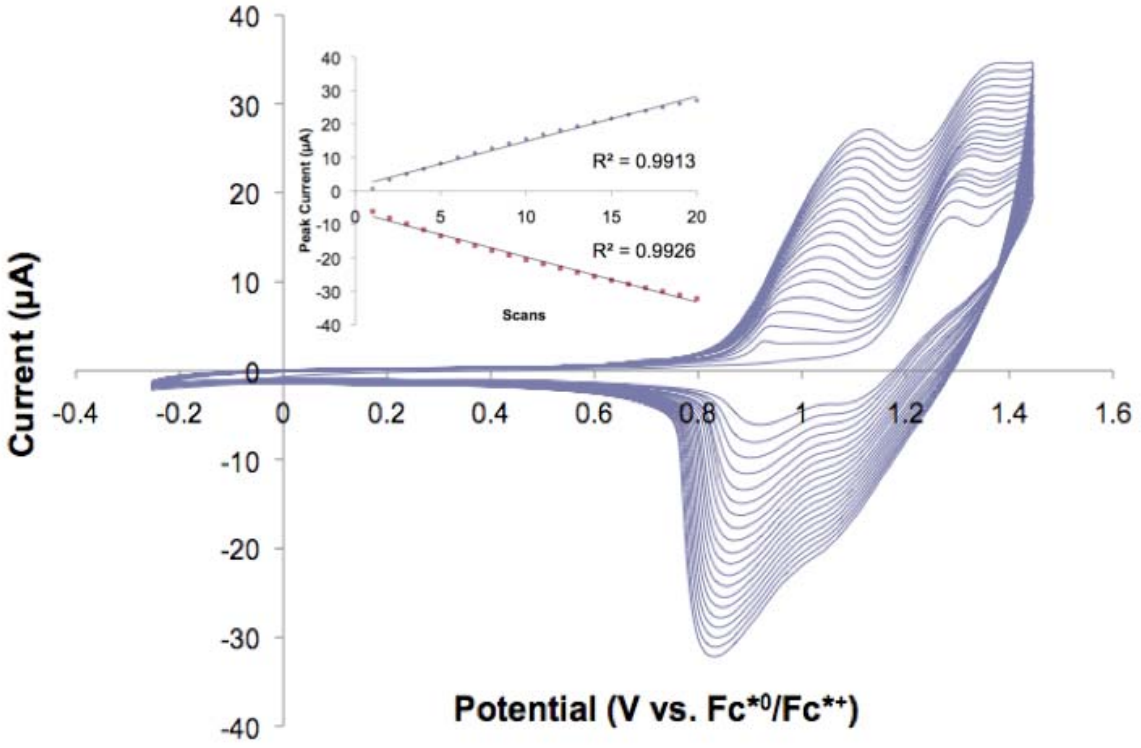

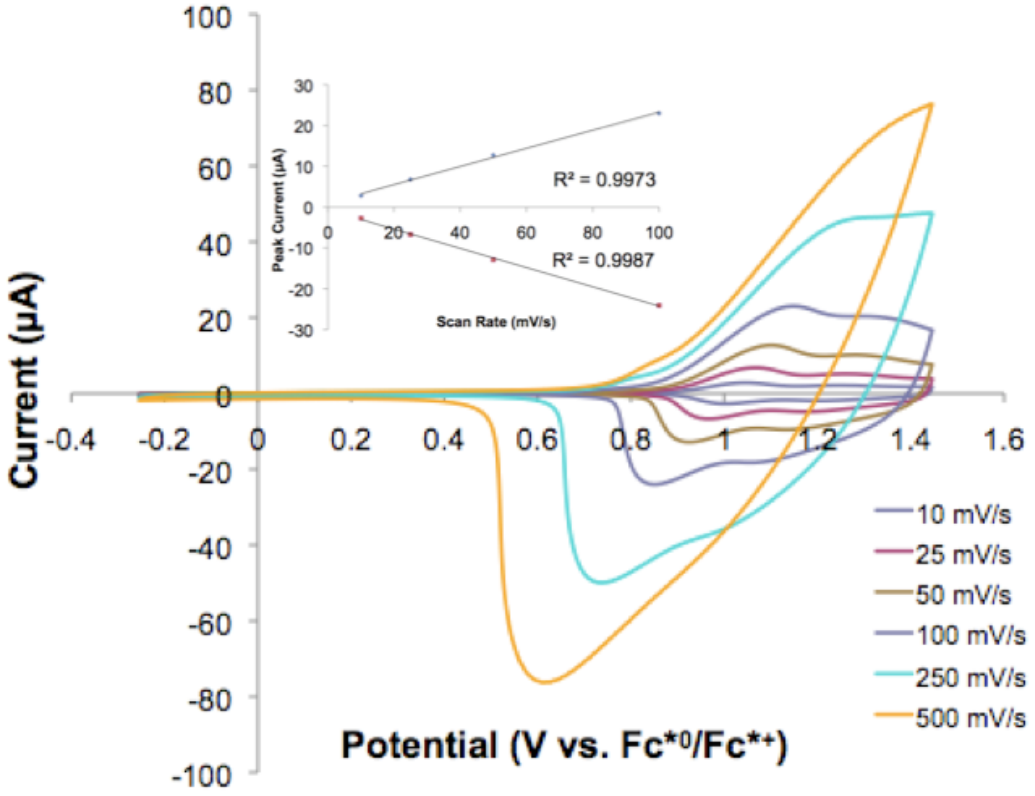

Figure 4.2. (top) Electropolymerization of **6**. Inset: plot of linear current increase vs. number of scans. (bottom) Poly(**6**) scan rate dependence. Inset: plot of linear current increase vs. scan rate.

4.4 Spectroscopic studies of gold NHC polymer

Films of poly(**6**) were also examined by X-ray photoelectron spectroscopy, which is capable of simultaneously probing the atomic ratios of the metallopolymer poly(**6**). The N 1s, S 2p and Au 4f signals were observed at 401.5, 165, and 87 eV respectively. The integrated ratios of N:Au (2.08) and S:Au (4.17) were within experimental error[12] of the values anticipated for the structure of poly(**6**) shown in Scheme 4.2. The S 2p signal featured a shoulder that was assigned to sulfur atoms in slightly different chemical

environments. Scheme 4.2 illustrates these different locations where the sulfurs on the thiophenes reside. Because the monomer contains distinct thiophene units, such splitting was anticipated. A small amount of metallic gold deposition may be present in the samples that were analyzed since the Au 4f signals revealed small shoulders at lower binding energies.

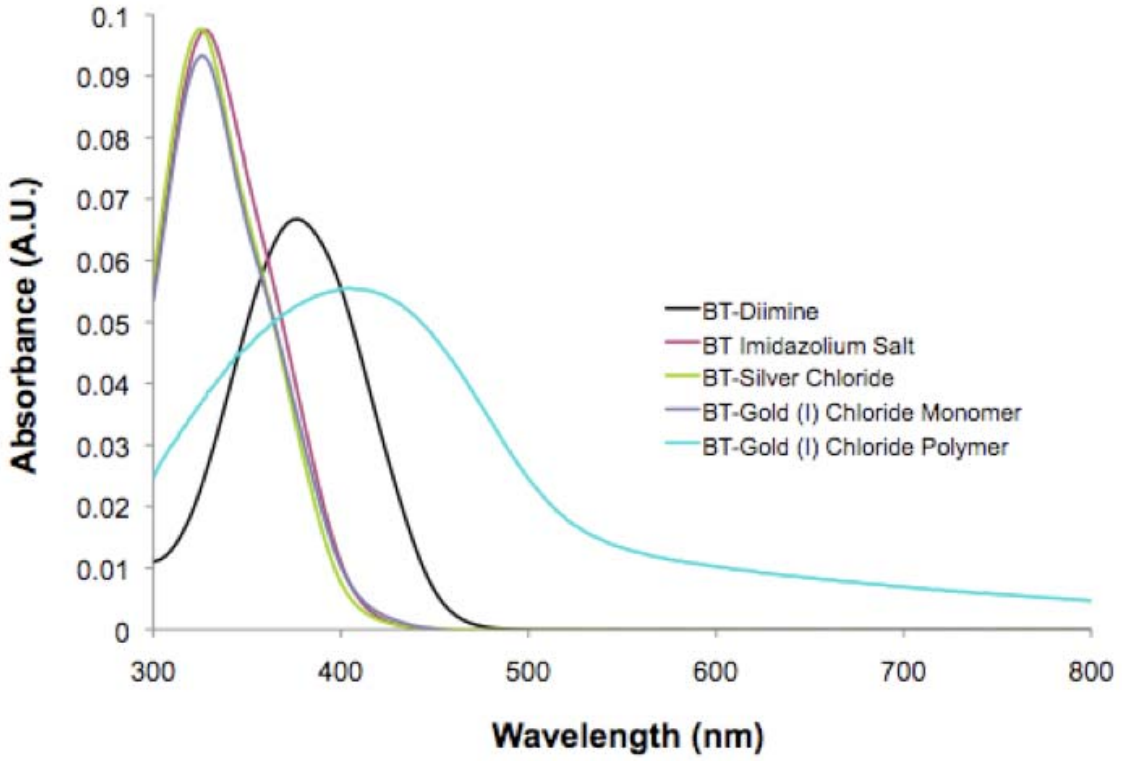

Figure 4.3. UV-vis spectra of monomers **3** – **6** and poly(**6**) in CH_2Cl_2. The concentration of **3** – **6** was 2.0 x 10^{-6} M.

Finally, the photophysical properties of poly(**6**) were investigated and compared with those of compounds **3** – **6**. As shown in Figure 4.3, the λ_{max} for **3** was found at 376 nm and attributed to the π-π^* transitions of the diimine moiety. This seemed logical given

that the conjugation persists thoroughout the entire molecule with the exception of the butyl fragments. Upon cyclization to the imidazolium chloride **4**, the λ_{max} hypsochromically shifted to 326 nm, an observation which is consistent with an increase of charge on the complex. Metallation of **4** to form silver NHC **5** and transmetallation to gold NHC **6** resulted in nearly identical UV-vis profiles. This indicates that the spectroscopic properties of these compounds are largely ligand-based. Upon polymerization of **6**, however, the λ_{max} shifted bathochromically to 406 nm and the absorption signature broadened as anticipated for a polymeric system. Based on these results, it was concluded that the spectroscopic character of **3** – **6** is dominated by ligand π-π^* transitions. The electrochemical, XPS and UV-vis spectroscopic studies collectively support the structural assignment of poly(**6**).

4.5 Conclusions

In summary, the first example of a polymer containing an NHC orthogonally connected to its main chain has been synthesized and characterized. Due to this structural arrangement, the carbene moiety in this material is poised to ligate transition metals or to facilitate other carbene-based reactivities. Using the numerous reports of NHC metal complexes in the literature, the methodology presented herein may be readily extended to access a variety of materials containing NHC-metal complexes connected directly to the main chains of polymers.

4.6 Experimental

General Procedures: All air-sensitive reactions were performed under a dry, oxygen-free, catalyst-scrubbed argon atmosphere using a combination of standard Schlenk techniques or in a Vacuum Atmospheres drybox. The glassware used air-sensitive reactions was oven-dried and degassed before use. All solvents and reagents

were used as received from commercial sources unless other stated. Bithiophene carboxaldehyde was synthesized according to a literature procedure.[13] DMF was distilled over $MgSO_4$ under reduced pressure and stored over 3 Å molecular sieves prior to use. Toluene was distilled over sodium benzophenone ketyl prior to use. The methylene chloride used in the silver carbene synthesis was distilled over calcium hydride prior to use. NMR spectra were recorded at 298 K on a Varian Inova instrument (^{1}H NMR, 400.27 MHz; ^{13}C NMR, 100.65 MHz) using $CDCl_3$ as an internal reference unless stated otherwise. Low-resolution chemical ionization mass spectral data (MS-CI) were collected on a Thermo Scientific TSQ Quantum GC mass spectrometer. High-resolution CI-MS spectra were recorded on a magnetic sector Waters Autospec Ultima instrument and reported as *m/z* (relative intensity). Infrared spectra were recorded using a Nicolet Avatar 260 FT-IR spectrometer and analyzed in the solid state (KBr). Absorption spectra were recorded on a Varian Cary 5000 UV-vis-NIR Spectrophotometer using Starna Quartz Fluorometer Cells with a pathlength of 10 mm for monomers **1** – **6** and 0.1 mm for poly(**6**).

Electrochemistry: Electrochemical syntheses and studies were performed in a drybox under a dry nitrogen atmosphere using a CH Instruments Electrochemical Workstation (series 700B). All the electrochemical experiments were carried out in a three-electrode cell containing a silver wire reference electrode. The supporting electrolyte was 0.1 M $[(n\text{-Bu})_4N^+][PF_6^-]$ ($TBAPF_6$) that had been purified by recrystallization three times from hot ethanol before being dried for 3 days at 100–150 °C under dynamic vacuum. Electrosyntheses of the films were performed from 1 x 10^{-3} M monomer solutions by continuous cycling between –0.20 V and 1.50 V at v = 100 mV s^{-1}. The resulting films were then washed with excess CH_2Cl_2. Decamethylferrocene was used as an external reference (0.0 V) for all electrochemical measurements.

X-Ray Photoelectron Spectroscopy. XPS spectra were recorded on a Kratos Axis Ultra X-ray photoelectron spectrometer utilizing a monochromated Al-Kα X-ray source (hυ = 1486.5 eV), hydrid optics (employing a magnetic and electrostatic lens simultaneously) and a multi-channel plate and delay line detector coupled to a hemispherical analyzer. The photoelectron take off angle was 0° (measured from the surface normal). All spectra were recorded using an aperture slot of 300 x 700 microns, and the high resolution spectra were collected with pass energy of 20 eV. The pressure in the analysis chamber was typically maintained at 2 x 10^{-9} Torr during data acquisition. Kratos XPS analysis software was used to determine the stoichiometry of samples from corrected peak areas and employing appropriate sensitivity factors for each element of interest.

X-Ray Crystallography. Crystals suitable for data collection were covered with hydrocarbon oil and mounted on a thin nylon loop. The X-ray diffraction data were collected at 153 K on a Rigaku AFC-12 with Saturn 724 + CCD and area detector diffractometer equipped with an Oxford Cryostream low-temperature device and a graphite-monochromated Mo Kα radiation source (λ = 0.71073 Å). Corrections were applied for Lorentz and polarization effects. The structure was solved by direct methods and refined by full-matrix least-squares cycles on F^2.[14] All non-hydrogen atoms except C1 were refined with anisotropic thermal parameters, and all hydrogen atoms were placed in fixed, calculated positions using a riding model (C-H 0.96 Å). The refinement of C1 was problematic in that the atom could not be refined anisotropically without going non-positive definite due to the value for U22 going negative. However, the identity of C1 is known from other methods such as ^{13}C NMR and HRMS. Numerous attempts were undertaken to solve the structure and the CIF provided reflects the best structure obtainable.

Bithiophene Monoimine (1). A round-bottomed flask was charged with bithiophene carboxaldehyde (11.0 mmol, 2.14 g), 4-*n*-butylaniline (13.2 mmol, 1.97 g) and 100 mL of absolute ethanol. The reaction mixture was stirred at reflux for 12 h, following which it was cooled and the ethanol was removed under vacuum. Purification of the crude product by flash chromatography using 90% hexanes and 10% ethyl acetate afforded **1** as a yellow solid (92% yield). ^{1}H NMR (400.27 MHz, $CDCl_3$): δ 8.51 (s, 1H), 7.33 (d, 1H *J* = 4.0 Hz), 7.28 (t, 2H, *J* = 3.6 Hz), 7.19-7.13 (m, 5H), 7.03 (dd, 1H, *J* = 5.2, 1.6 Hz), 2.60 (t, 2H, *J* = 7.6 Hz), 1.57 (p, 2H, *J* = 8.0 Hz), 1.35 (sextet, 2H, *J* = 7.6 Hz), 0.92 (t, 3H, *J* = 7.2 Hz). ^{13}C{^{1}H} NMR (100.65 MHz, $CDCl_3$): δ 151.56, 148.69, 141.55, 141.36, 140.96, 136.92, 132.57, 129.01, 128.02, 125.50, 124.76, 123.79, 120.88, 35.11, 33.55, 22.27, 13.90. LRMS (CI^+, *m/z*): 326 (100% M + H^+). IR (cm^{-1}): 2948, 2925, 2854, 1612, (C=N), 1589 (C-C_{arom}), 1457 (C-C_{arom}), 1423, 1193, 1059, 859, 840, 800, 691. λ_{max} = 377 nm. ε = 3.0 x 10^4 M^{-1} cm^{-1}.

Bithiophene-Substituted ene-Diamine (2). A 50 mL Schlenk flask was charged with monoimine **1** (9.52 mmol, 3.10 g) and an equimolar amount of NaCN. The reaction flask was de-gassed and dry DMF (10 mL) was added *via* cannula transfer. The resulting solution was stirred at ambient temperature for 24 h under an atmosphere of argon. The reaction mixture was then diluted with a 1:1 mixture of THF and ethyl acetate (200 mL), washed with brine (5 x 100 mL) and extracted with 100 mL of ethyl acetate. The organic layers were combined, dried over $MgSO_4$, filtered and then concentrated to yield the crude product an orange solid. The crude product was heated in methanol while stirring for 30 minutes, cooled, then placed in the freezer (–40 °C) overnight. The resulting precipitated orange solid was collected by vacuum filtration (75% yield). ^{1}H NMR

(300.14 MHz, THF-d_8, TMS): δ 7.12 (d, 2H, J = 5.1 Hz), 6.94 (m, 4H), 6.82 (m, 8H), 6.75 (s, 2H), 6.58 (d, 4H, J = 8.7 Hz), 2.38 (t, 4H, J = 8.1 Hz), 1.43 (p, 4H, J = 7.8 Hz), 1.24 (sextet, 4H, J = 7.2), 0.79 (t, 6H, J = 7.5). $^{13}C\{^1H\}$ NMR (75.48 MHz, $CDCl_3$): δ 145.26, 140.37, 139.38, 138.60, 133.19, 129.72, 129.39, 128.87, 128.50, 125.05, 124.01, 123.64, 115.18, 35.73, 34.93, 23.27, 14.34. LRMS (CI^+ *m/z*): 651 (30% $M + H^+$). IR (cm^{-1}): 3324 (N-H), 2926, 2855, 1612 (C=C), 1512 (C-C_{arom}), 1464 (C-C_{arom}), 1297, 1250, 1132, 1044, 822, 794, 700. λ_{max} = 442 nm. ε = 3.6 x 10^4 M^{-1} cm^{-1}.

Bithiophene-Substituted Diimine (3). The ene-diamine **2** (3.84 mmol, 2.50 g) was dissolved in dichloromethane (250 mL) and an equimolar amount of freshly sublimed 1,4-benzoquinone was added. The resulting orange reaction mixture was stirred at ambient temperature for 12 h and then extracted with deionized water (3 x 100 mL). The aqueous layer was extracted with dichloromethane. The organic layers were combined, dried with $MgSO_4$, filtered and concentrated to yield a sticky yellow solid (98% yield). ^1H NMR (400.27 MHz, $CDCl_3$, TMS): δ 7.23 (t, 4H, J = 3.6 Hz), 7.14 (d, 2H, J = 3.6 Hz), 7.03 (d, 2H, J = 4.4 Hz), 6.98 (dd, 2H, J = 5.2, 1.6 Hz), 6.84 (d, 4H, J = 8.4 Hz), 6.53 (d, 4H, J = 8.0 Hz), 2.45 (t, 4H, J = 7.6 Hz), 1.45, (p, 4H, J = 7.2 Hz), 1.23 (sextet, 4H, J = 7.6 Hz), 0.84 (t, 6H, J = 7.6 Hz). $^{13}C\{^1H\}$ NMR (100.65 MHz, $CDCl_3$): δ 156.26, 145.90, 142.68, 142.09, 140.17, 136.86, 132.19, 128.45, 128.10, 125.71, 124.92, 124.13, 120.90, 35.04, 33.51, 22.11, 13.92. LRMS (CI^+ *m/z*): 649 (100% $M + H^+$). IR (cm^{-1}): 3068, 2953, 2926, 2855, 1579 (C-C_{arom}), 1444 (C-C_{arom}), 1259, 1193, 1045, 875, 801, 700. λ_{max} = 376 nm. ε = 3.4 x 10^4 M^{-1} cm^{-1}.

Bithiophene-Substituted Imidazolium Chloride (4). The diimine **3** (1.23 mmol, 0.80 g) was de-gassed in a 100 mL three-neck flask equipped with a condenser using three

consecutive vacuum and argon cycles (10 min vacuum per cycle) Next, a previously prepared solution of paraformaldehyde (3.70 mmol, 0.11 g) in toluene (60 mL) was added *via* cannula transfer to the reaction mixture at 40 °C under an atmosphere of argon. After 5 minutes of stirring, HCl in dioxane (3.70 mmol, 4.00 M) was added via syringe. The yellow solution immediately turned dark red and subsequently to an orange-red color after 1 h. The reaction mixture was stirred at 40 °C for 2 days under argon. The toluene was then removed under reduced pressure. Purification of the dark sticky solid by flash chromatography using 94% CH_2Cl_2 and 6% MeOH afforded the desired product as a yellow solid (87% yield). ^{1}H NMR (400.27 MHz, CD_2Cl_2, TMS): δ 10.41 (s, 1H), 7.63 (d, 4H, J = 8.0 Hz), 7.20 (d, 4H, J = 8.4 Hz), 7.14, (dd, 2H, J = 5.2, 1.2 Hz), 6.98 (dd, 2H, J = 4.0, 1.2 Hz), 6.91 (s, 4H), 6.85 (dd, 2H, J = 5.2, 1.2 Hz), 2.54 (t, 4H, J = 7.6 Hz), 1.48 (p, 4H, J = 7.6 Hz), 1.22 (sextet, 4H, J = 7.6 Hz), 0.79 (t, 6H, J = 7.6 Hz). ^{13}C{^{1}H} NMR (100.65 MHz, CD_2Cl_2): δ 146.42, 142.43, 138.38, 135.64, 133.77, 130.91, 129.78, 128.13, 127.21, 126.62, 125.94, 125.00, 123.74, 122.32, 35.34, 33.25, 22.40, 13.79. LRMS (CI^+ *m/z*): 661 (10% M-Cl). IR (cm^{-1}): 3040, 2954, 2926, 2855, 1619 (C=N), 1527 (C-C_{arom}), 1490 (C-C_{arom}), 1320, 1222, 1201, 1044, 1021, 838, 802, 690. λ_{max} = 328 nm. ε = 4.9 x 10^4 M^{-1} cm^{-1}.

Bithiophene-Substituted Silver (I) Carbene (5). The imidazolium chloride **4** (0.90 mmol, 0.63 g) and silver (I) oxide (0.45 mmol, 0.11 g) were added to a round-bottomed flask along with dry CH_2Cl_2 (15 mL). The reaction flask was covered with aluminum foil and the reaction mixture was stirred at ambient temperature for 24 h. The reaction mixture was then filtered through Celite and the CH_2Cl_2 was removed under reduced pressure to afford the desired product as a brown solid (95% yield). Numerous attempts to crystallize **5** were unsuccessful. ^{1}H NMR (300.14 MHz, CD_2Cl_2, TMS): δ 7.27 – 7.18

(m, 8H), 7.12 (dd, 2H, J = 5.1, 0.9 Hz), 6.98 (dd, 2H, J = 3.6, 0.9 Hz), 6.89 – 6.85 (m, 4H), 6.67 (d, 2H, J = 3.6 Hz), 2.59 (t, 4H, J = 7.5 Hz), 1.54 (p, 4H, J = 7.8 Hz), 1.26 (sextet, 4H, J = 6.9 Hz), 0.83 (t, 6H, J = 7.2 Hz). $^{13}C\{^{1}H\}$ NMR (75.48 MHz, CD_2Cl_2): δ 145.28, 141.20, 136.31, 136.16, 132.13, 129.75, 128.28, 127.46, 127.36, 125.89, 125.72, 124.77, 123.75, 35.34, 33.55, 22.68, 14.05. LRMS (CI^+ *m/z*): 804 (10% M^+ + H^+). As observed for similar complexes, the carbene carbon could not be detected by ^{13}C NMR spectroscopy.[15] HRMS (CI^+, CH_4): Calculated for $C_{39}H_{36}N_2S_4Ag^{107}$, 767.0812; found 767.0822. Calculated for $C_{39}H_{36}N_2S_4Ag^{109}$, 769.0809, found 769.0813. IR (cm^{-1}): 3060, 2954, 2926, 2856, 1628 (C-C_{arom}), 1510 (C-C_{arom}), 1388, 1229, 1048, 1019, 838, 800, 696. λ_{max} = 325 nm. ε = 4.9 x 10^4 M^{-1} cm^{-1}.

Bithiophene-Substituted Gold (I) Carbene (6). The bithiophene-substituted silver (I) carbene **5** (0.28 mmol, 0.222 g) and tetrahydrothiophene gold (I) chloride (0.262 mmol, 0.084 g) were added to a round-bottomed flask containing dry CH_2Cl_2 (15 mL) and the flask was covered with aluminum foil. The reaction mixture was stirred at ambient temperature for 24 h, following which it was filtered through Celite and the CH_2Cl_2 was removed under reduced pressure to afford the desired product as a yellow powder (95% yield). Crystals suitable for X-ray diffraction data collection were obtained by slow vapor diffusion of a THF solution of **6** into hexanes (1 : 2.75 THF : hexanes) at ambient temperature and in the absence of light. ^{1}H NMR (300.14 MHz, CD_2Cl_2, TMS): δ 7.34 (d, 4H, J = 8.1 Hz), 7.23 (d, 4H, J = 8.4 Hz), 7.15 (dd, 2H, J = 5.1, 1.5 Hz), 7.00 (dd, 2H, J = 3.6, 1.5 Hz), 6.89 (m, 4H), 6.68 (d, 2H, J = 3.9, 1.2 Hz), 2.61 (t, 4H, J = 7.5 Hz), 1.57 (p, 4H, J = 7.8 Hz), 1.29 (sextet, 4H, J = 7.5 Hz), 0.84 (t, 6H, J = 7.5 Hz). $^{13}C\{^{1}H\}$ NMR (100.65 MHz, $CDCl_3$): δ 172.26, 144.43, 140.81, 135.81, 134.70, 131.58, 129.17, 127.73, 127.28, 126.38, 125.12, 125.06, 124.25, 123.20, 35.11, 32.86, 22.16, 13.78.

LRMS (CI^+ *m/z*): 857 (100% M^+ - Cl, 20% M + H^+), HRMS (CI^+, CH_4): Calculated for $C_{39}H_{36}N_2S_4AuCl$, 892.1115; found 892.1116. IR (cm^{-1}): 3068, 2953, 2922, 2855, 1629, 1510 (C-C_{arom}), 1415 (C-C_{arom}), 1341, 1228, 1200, 1047, 836, 798, 696, 688. λ_{max} = 326 nm. $\varepsilon = 4.7 \times 10^4\ M^{-1}\ cm^{-1}$.

Table 4.1. Crystal data and structure refinement for **6**.

Empirical formula	C39 H36 Au Cl N2 S4	
Formula weight	893.35	
Temperature	100(2) K	
Wavelength	0.71075 Å	
Crystal system	Monoclinic	
Space group	I2/a	
Unit cell dimensions	a = 32.529(4) Å	α = 90°.
	b = 6.2720(8) Å	β = 95.816(12)°.
	c = 36.401(5) Å	γ = 90°.
Volume	7388.5(16) $Å^3$	
Z	8	
Density (calculated)	1.606 Mg/m^3	
Absorption coefficient	4.311 mm^{-1}	
F(000)	3552	
Crystal size	0.20 x 0.02 x 0.02 mm^3	
Theta range for data collection	3.20 to 25.00°.	
Index ranges	-38<=h<=38, -7<=k<=7, -42<=l<=43	
Reflections collected	22818	
Independent reflections	6492 [R(int) = 0.0921]	
Completeness to theta = 25.00°	99.6 %	

Table 4.1 (continued). Crystal data and structure refinement for **6**.

Absorption correction	Semi-empirical from equivalents
Max. and min. transmission	0.920 and 0.450
Refinement method	Full-matrix least-squares on F^2
Data / restraints / parameters	6492 / 276 / 421
Goodness-of-fit on F^2	1.224
Final R indices [I>2sigma(I)]	R1 = 0.0686, wR2 = 0.1440
R indices (all data)	R1 = 0.1038, wR2 = 0.1610
Largest diff. peak and hole	2.849 and -2.709 e.$Å^{-3}$

Table 4.2. Selected bond lengths (Å) and angles (°) for **6**.

Bond lengths (Å)	
Au(1)-C(1)	1.950(8)
Au(1)-Cl(1)	2.319(2)
N(1)-C(3)	1.370(12)
N(1)-C(1)	1.381(11)
N(2)-C(1)	1.361(11)
N(2)-C(2)	1.415(12)
C(2)-C(3)	1.381(13)
Bond angles (°)	
C(1)-Au(1)-Cl(1)	177.8(2)
N(2)-C(1)-Au(1)	128.1(6)
N(1)-C(1)-Au(1)	129.5(6)
C(3)-N(1)-C(1)	113.9(8)
C(1)-N(2)-C(2)	112.0(8)
N(1)-C(3)-C(2)	105.3(8)
N(2)-C(1)-N(1)	102.3(7)
C(3)-C(2)-N(2)	105.8(8)

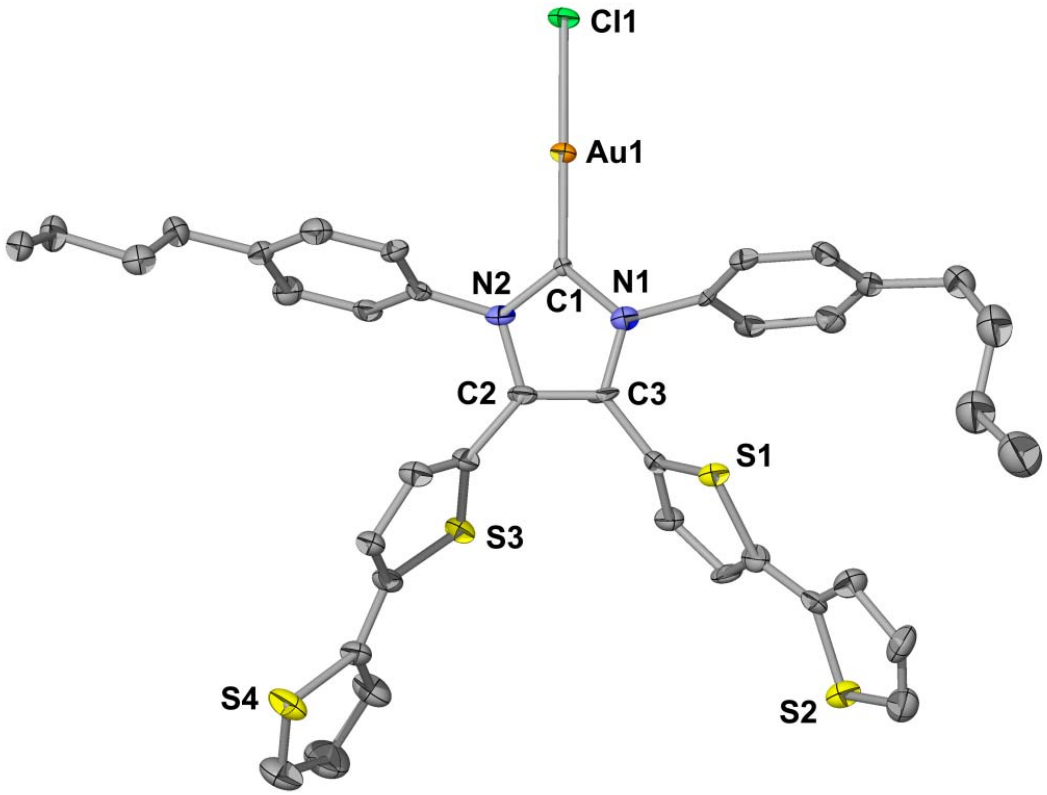

Figure 4.4. POV-Ray diagram of gold (I) carbene **6** drawn at 50% probability. Hydrogen atoms have been omitted for clarity.

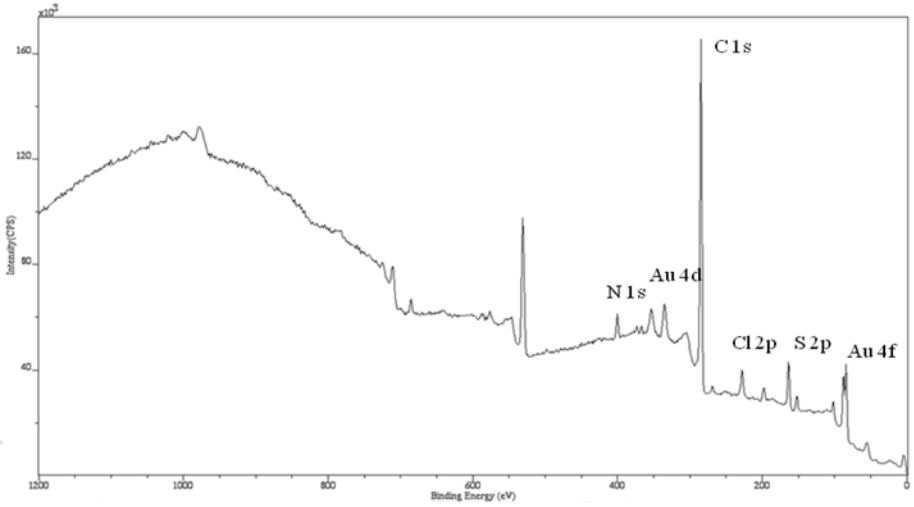

Figure 4.5. Survey XPS data for poly(**6**).

(a)

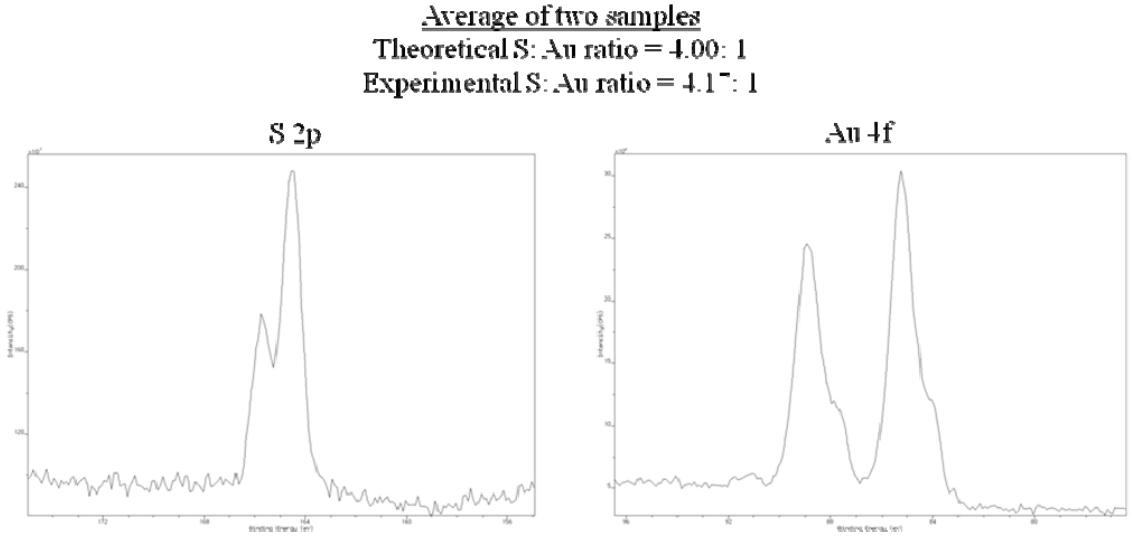

(b)

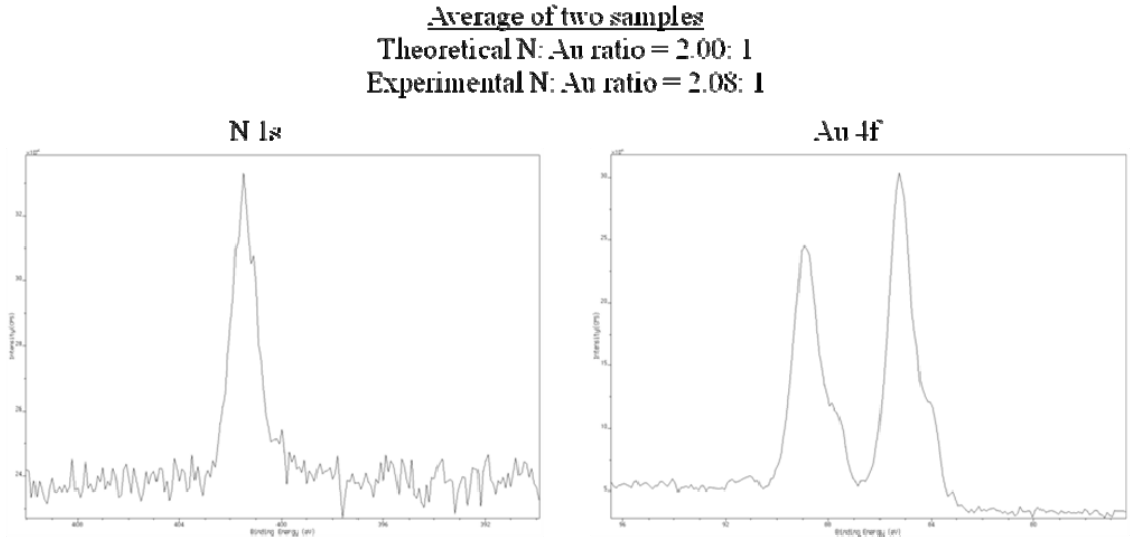

Figure 4.6. XPS data for poly(**6**) (a) S 2p vs. Au $4f_{7/2}$ and Au $4f_{5/2}$. (b) N 1s vs. Au $4f_{7/2}$ and Au $4f_{5/2}$.

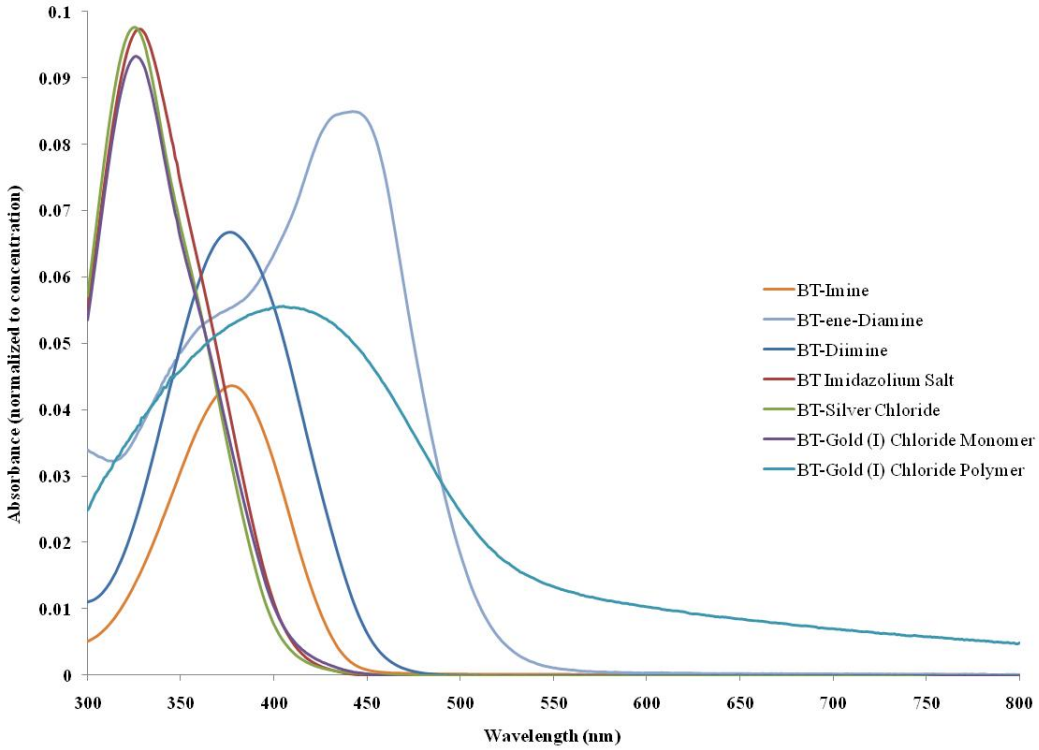

Figure 4.7. UV-vis profiles for compounds **1** - **6** and poly(**6**). The concentrations of **1** – **6** were 2.0 x 10^{-6} M.

Chapter 5: Design, Synthesis, and Study of Main Chain Poly(N–Heterocyclic Carbene) Complexes

5.1 Introduction

Electroconducting polymers (ECPs) have become an area of intense research following the discovery of polyacetylene by Shirakawa and co-workers in 1977.[1] Organic ECPs, in particular, have been studied extensively and have found utility in many photovoltaic,[2] sensing,[3] and medicinal applications, among others.[4] Such materials are polymerized by electrochemical methods, which offer a number of advantages including synthetic ease and the ability to deposit the polymer directly onto the conducting substrate of choice.[5] Thiophene is commonly used as an appended moiety for accessing ECPs due to its high functional group tolerance. However, ethylenedioxythiophene (EDOT) and bithiophene-based monomers are often employed in its place due to their abilities to decrease the electrochemical potentials required for polymerization.[6]

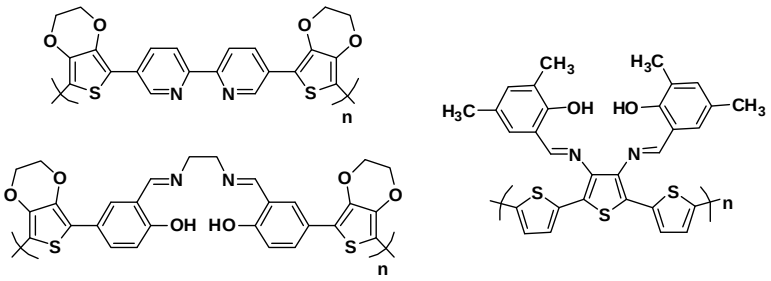

Figure 5.01. Examples of polymers synthesized via electropolymerization.

The incorporation of transition metal and main-group atoms into ECPs has been shown to effect significant increases in conductivity, thus greatly expanding their utility.[7] For example, the polymerizable scaffolds shown in Figure 5.01 have been used for the

support of elements which span the periodic table.[8] Of the various electropolymerizable scaffolds depicted in Figure 1, the most widely employed are those derived from the *N,N′*–ethylenebis(salicylimine) (Salen) ligand framework, mainly because this system can be prepared via simple condensation of ethylene diamine and salicylaldehyde. However, a notable disadvantage of Salen and related ligands is that the attachment of electroactive, polymerizable substituents such as thiophene or bithiophene is challenging due to the coupling chemistry required.[9] Moreover, the rigid geometry of the resulting Salen ligand constrains the coordinated metal to a tight, four-coordinate environment which can complicate further derivatization.

Given the widespread use of α-diimines for the support of a significant variety of p, d and f-block functionalities, in both our laboratory and others, we were prompted to develop a new electropolymerizable ligand class via the attachment of flanking thiophene substituents to an α-diimine. Such a system was envisioned to create a more open site for metal coordination and also to avoid the use of challenging coupling reactions. Although the initially synthesized diimine ligand, 1,2(bis)-thiophene diazadiene, met these requirements, it failed to undergo electropolymerization under reasonable conditions.[10,11] To overcome this limitation, the aforementioned thiophene moieties were replaced with bithiophenes and the ligand was incorporated into the well-established N-heterocyclic carbene (NHC) scaffold.

NHCs have attracted considerable attention over the last two decades due to their unsurpassed ability to stabilize many transition metal and main-group complexes under a wide range of conditions.[12] Furthermore, polymeric systems have been shown to possess superior stabilities[13] and enhanced electrocatalytic kinetics[14,15] when compared with their monomeric analogues. Although many examples are known[16] in which NHCs have been incorporated into the backbones of polymeric materials, no examples existed until very

recently of a polymer in which the NHC was positioned orthogonally with respect to the main chain and thus was available for ligation to other functionalities.[17] As summarized in Scheme 5.1, the requisite monomer for accessing such main-chain poly(NHC)s was synthesized by cyclization of diimine **1** to form the corresponding imidazolium chloride **2**. Subsequent metallation of **2** with Ag_2O (to form **3**), followed by transmetallatation with tetrahydrothiophene (tht)AuCl, afforded **4** which was subsequently electropolymerized and characterized using standard techniques.[17]

Scheme 5.1. Synthesis of the Gold (I) Carbene Complex **4**.

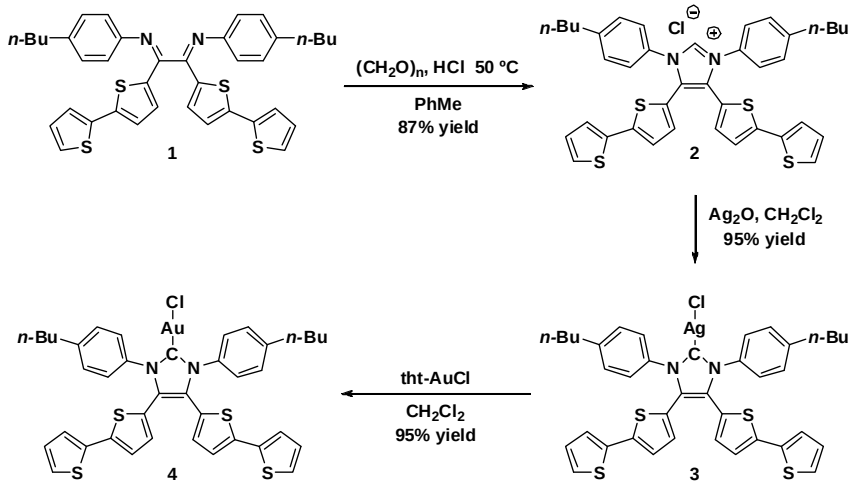

Inspired by a recent account which demonstrated the impact of different coordinated metals on the electronic behavior of ECPs,[18] a comprehensive investigation of the influence of the ligated metal centers on the electronic properties of the aforementioned poly(NHC)s was undertaken. The methodology outlined in Scheme 1 was expanded to include polymers containing other transition metal and main-group element moieties (see Scheme 5.2), which were characterized using a suite of

electrochemical, X-ray photoelectron and UV-vis spectroscopy, profilometry and four-point probe conductivity measurements.

Scheme 5.2. Electrochemical Polymerization of Bithiophene–Substituted NHC-Metal Complexes **3** – **8**.

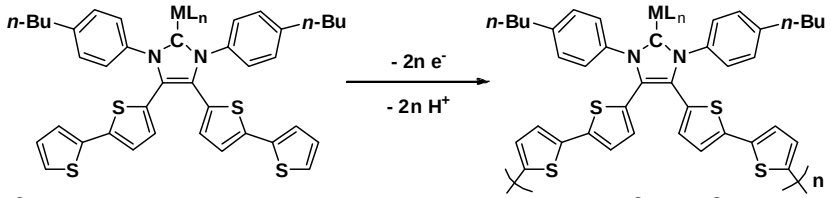

3: ML_n = AgCl **6**: ML_n = S
4: ML_n = AuCl **7**: ML_n = Ir(cod)Cl
5: ML_n = AgOAc **8**: ML_n = $Ir(CO)_2Cl$

During the course of these studies, a noticeable color change was observed when the gold NHC complex **4** was electropolymerized on an indium tin oxide (ITO) slide. It was surmised that this color change originated from the development of polarons along the polymer main chain, which manifested itself as electrochromism. In general, polymers such as poly(3,4-ethylenedioxythiophene) (PEDOT) are well known to exhibit such behavior, but examples of organometallic-based ECPs are scarce.[18] Electrochromism is a useful property that has found commercial applications in electrochromic mirrors,[19] polymer light-emitting diodes[20] and near infrared (NIR) devices.[21] Moreover, there is a current demand for organic materials that exhibit excellent color efficiencies and fast switching capabilities.[22] Electrochromic studies are also useful for analysis of the electronic structures of *p*-doped conjugated polymers in both the oxidized (cationic) and reduced (neutral) states.[23] The metallopolymer scaffolds shown in Scheme 5.2 are well suited for use in electrochromic devices since they possess the following advantages: (1) a broad range of transition and main-group metals may be

incorporated, each of which may display different characteristics and (2) they feature orthogonally – positioned carbene groups in direct electronic contact with the polymerizable scaffold, which may be further derivatized to tailor the electronic properties exhibited by the materials in which they are contained.

5.2 Monomer synthesis and characterization

Poly(**3**) and poly(**5**) – poly(**8**) were synthesized as summarized in Scheme 5.3; poly(**4**) was prepared as previously described.[17] The precursor bithiophene – substituted diimine **1** was synthesized by sodium cyanide – catalyzed coupling of the requisite aldimine in DMF solution. Optimum yields of diimine **1** were prepared by using a minimum amount of DMF since the aldimine coupling procedure has been found to be concentration–dependent. Oxidation of the ene-diamine to the diimine **1** can be accomplished with pure oxygen or by chemical oxidation with *p*-benzoquinone. Cyclization of the diimine with paraformaldedyde afforded the anticipated imidazolium chloride **2** in 87% yield. The sticky crude reaction mixture was most easily isolated by column chromatography with 15:1 CH_2Cl_2/MeOH as the solvent system. The imidazolium proton was identified as a singlet at δ = 10.41 ppm in CD_2Cl_2 solution. Access to silver NHC **3**, which has been utilized as a carbene transfer reagent previously,[17] was obtained by metallation of the requisite imidazolium chloride with Ag_2O. The metallation had a long reaction time (40 h) and protection from light was important for complete conversion to silver NHC **5**. The ^{1}H NMR spectrum revealed the presence of somewhat broad resonances for the phenyl protons of **5**, possibly indicating a fluxional behavior in solution. As reported for other silver NHC complexes,[26] an equilibrium exists in solution between **3** and its dimeric analogue (see Scheme 5.4). As a consequence, the carbene nucleus of **3** could not be detected by ^{13}C NMR spectroscopy in CD_2Cl_2 solution. However, it was observed as a broad singlet at δ = 181 ppm when the

NMR spectrum was recorded in $CDCl_3$ solution. In turn, this broad singlet resolved into two sets of doublets (in $CDCl_3$) at –50 °C, due to coupling of the ^{13}C nucleus to the ^{107}Ag and ^{109}Ag isotopes with coupling constants of approximately 260 Hz. Related examples of this phenomenon have been reported previously for both silver phosphine and silver carbene complexes.[27] Silver NHC **3** was also detectable by double – sector high-resolution mass spectroscopy, and the presence of a cationic complex consisting of the aforementioned complex of a Ag atom bound to two NHC ligands was evident from electrospray ionization mass spectrometry.

As shown in Figure 5.02 (left), a single – crystal X-ray diffraction experiment confirmed the monomeric structure of **3**. Interestingly, the packing diagram for **3** comprises a 1D array of metal atoms connected by short Ag-Ag contacts (Figure 5.02, right) analogous to that previous observed for the gold NHC **4**. The presence of these argentophilic interactions in silver carbene structures has been shown to be highly dependent upon the extent of steric crowding proximal to the metal center. For example, phenyl-substituted silver carbenes analogous to **3** exhibit comparable 1-D arrays of Ag-Ag contacts.[28] However, silver carbene analogues with bulky 2,4,6-trimethylphenyl or 2,6-diisopropylphenyl (DIPP) groups fail to align in the solid state.[29] The distance between the carbene nucleus and the Ag atoms of **3** was measured to be 2.087(3) Å. This value is significantly longer than the 1.950(8) Å distance previously observed[17] for the gold NHC **4** as anticipated on the basis of relativistic effects.[30] The longer bond distance for **3** helps to explain the lability of these types of complexes toward *trans*-metallation by gold, copper, iridium or rhodium complexes.

Scheme 5.3. Syntheses of Monomers **3** and **5** – **8**.

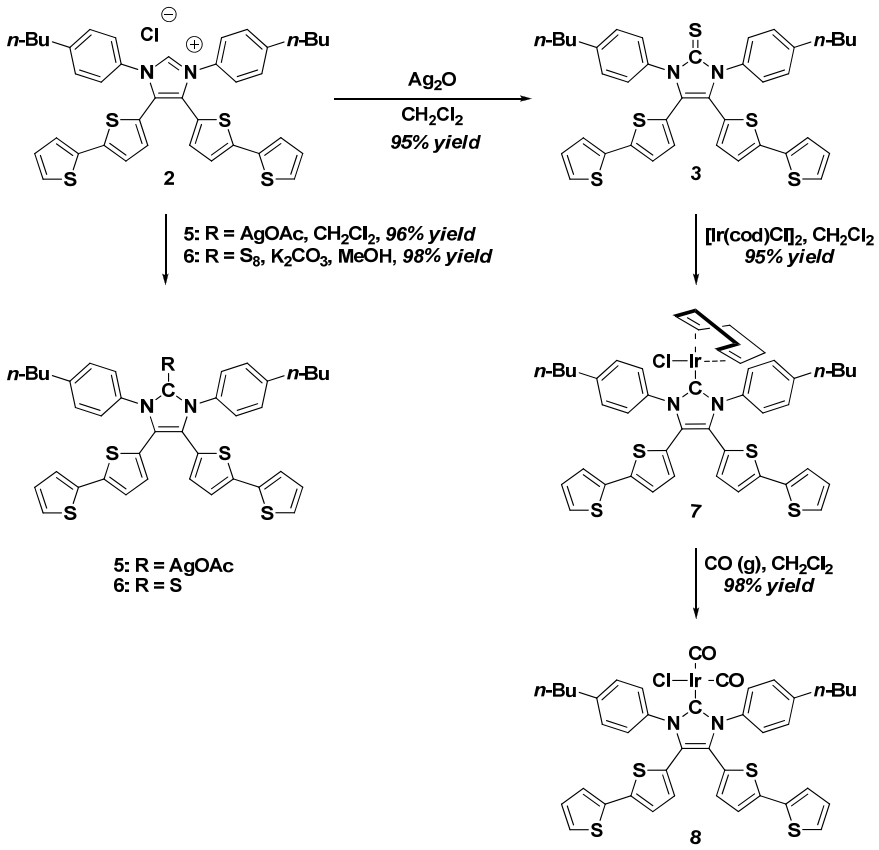

Scheme 5.4. Equilibrium between **3** and a dimeric analogue

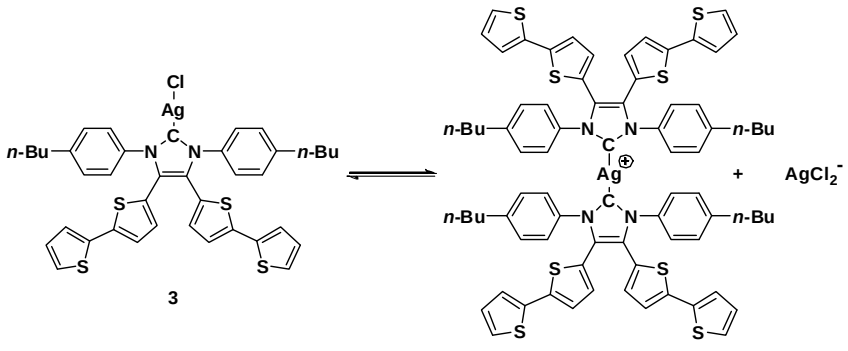

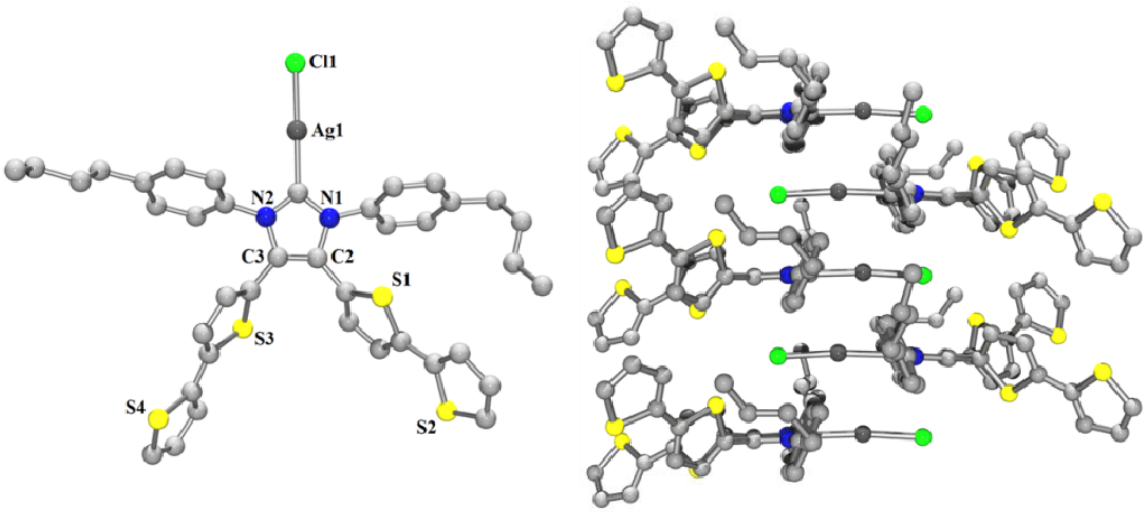

Figure 5.02. (left) POV-Ray view of **3** showing 50% probability thermal ellipsoids and selected atom labels. (right) Packing diagram for **3** showing Ag· · ·Ag contacts. Hydrogen atoms have been omitted for clarity.

Attention was paid next to the synthesis of the more sterically demanding silver carbene acetate **5** in order to discern whether the differences in solid state structure would affect the stabilities of the resulting polymers (see below). Complex **5** was formed in nearly quantitative yield by metallation of the precursor imidazolium chloride **2** with silver (I) acetate in CH_2Cl_2. ^1H NMR spectroscopic analysis revealed broad resonances for the phenyl groups, which suggested that this complex may exist in equilibrium with its dimeric counterpart, as observed in the case of **3**. Indeed, analysis by electrospray ionization (ESI) mass spectrometry revealed the presence of the di-ligated silver cation as shown in Scheme 5.4. Decomposition of **5** in solution was observed over the course of a few days, but could be slowed at lower temperatures. In contrast, **5** was found to be remarkably robust in the solid-state and was stored for several months under atmospheric conditions without noticeable decomposition. X-ray crystallographic analysis revealed that **5** could be isolated as the monomeric silver carbene (Figure 5.03, left), replete with

dimeric argentophilic interactions (Figure 5.03, right),[31] presumably due to the increased steric demands of the acetate ligand (as compared with that of the chloride ligand in **3**).

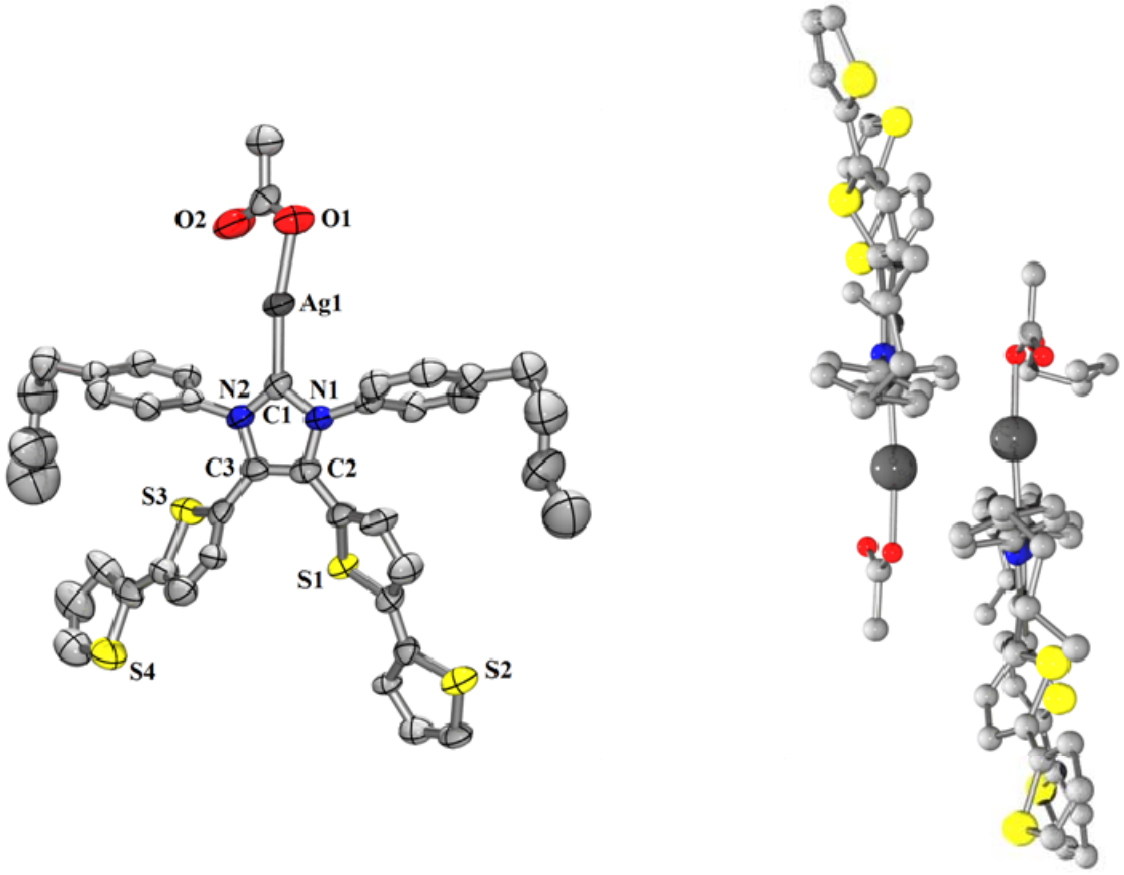

Figure 5.03. (left) POV-Ray view of **5** showing 50% probability thermal ellipsoids and selected atom labels. (right) Packing diagram for **5** showing Ag· · ·Ag contacts. Hydrogen atoms have been omitted for clarity.

Bithiophene–substituted iridium NHC complex **7** was synthesized by transmetallation of **3** with $[Ir(cod)Cl]_2$ (cod = 1,5-cyclooctadiene) in CH_2Cl_2 solution. In comparison with those of the starting material, the *ortho*-phenyl protons of **7** were shifted significantly downfield (δ = 7.27 to 7.57 ppm) as the reaction proceeded. Furthermore, the vinyl protons of the cod ligand were split into two separate resonances, one at δ 2.50

(assigned to the olefin *cis* to the NHC) and the other at δ 4.15 (assigned to the olefin *trans* to the NHC) due to the significantly stronger *trans* effect of the NHC compared with that of a chloride ligand.[32] The iridium NHC complex **8** was synthesized by exposure of **7** to an atmosphere of carbon monoxide at ambient temperature for 12 h. Although solutions of **8** were unstable to prolonged storage, as previously reported for other iridium NHC carbonyl complexes,[33] two IR absorptions were detected at υ_{CO} = 2058 and 1974 cm^{-1} corresponding to the symmetric and assymetric stretches of the CO ligand.[34] The carbene ^{13}C NMR signal for **8** was detected at δ = 180 ppm (CD_2Cl_2) as a sharp singlet which is a similar value to that observed for **7** (δ = 183 ppm; CD_2Cl_2).

In parallel with the aformentioned metallation reactions, efforts were also directed toward the synthesis of a monomer that contained a main-group element in lieu of a transition metal. As shown in Scheme 5.03, thione **6** was prepared via treatment of imidazolium chloride **2** with a mixture of S_8 and K_2CO_3 in methanol. The ^{13}C NMR resonance assigned to the thione carbon was observed at δ = 167 ppm (CD_2Cl_2) and the expected composition was confirmed by ESI mass spectrometry. Analysis of **6** via single-crystal X-ray diffraction confirmed the anticipated structure (see Figure 5.04).[35]

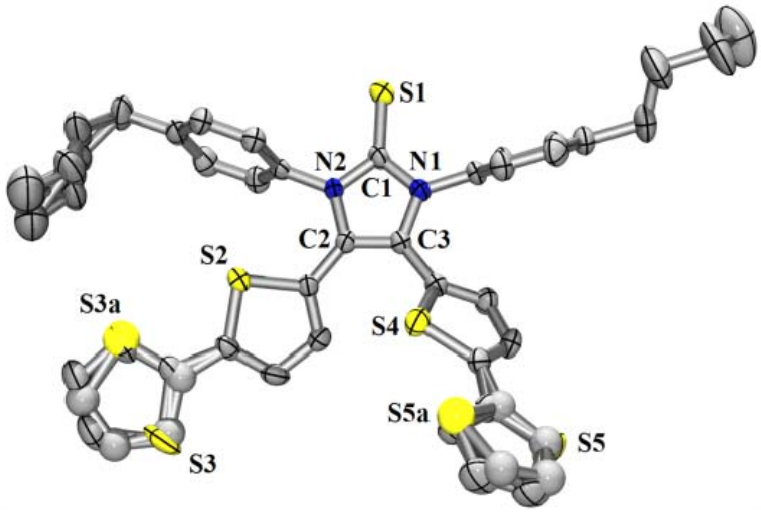

Figure 5.04. POV-Ray view of **6** showing 50% probability thermal ellipsoids and selected atom labels.

5.3 Electropolymerization studies

In general, the aforementioned complexes were independently electropolymerized in a three-electrode cell using a platinum button as the working electrode. The polymers synthesized from these reactions were obtained as thin films and were characterized using a suite of electrochemical,[36] XPS,[37] UV-vis spectroscopy, profilometry and four-point probe conductivity measurements.

The first monomer studied, the bithiophene–substituted diimine **1**, was successfully electropolymerized by continuous electrochemical cycling between –0.2 and +1.7 V. Although the current from the generated thin film of poly(**1**) was found to increase linearly with respect to the scan rate, as expected,[38] the pertinent cyclic voltammogram of **1** revealed a reduction process near 0.0 V (see Supporting Information). As a result of this low potential, **1** was deemed unsuitable as a

polymerizable ligand that could be used to coordinate various transition metals and thereby form metallopolymers. As described above, **1** was cyclized to form the imidazolium salt **2**, which was envisioned as a stable NHC precursor. Unfortunately, attempts to electropolymerize **2** were unsuccessful,[39] a likely consequence of the high oxidation potential of the monomer.

In contrast, the silver NHC complex **3**[17] was successfully electropolymerized under the aforementioned conditions. As shown in Figure 5.05 (top), multiple oxidation and reduction waves overlapped and the current measured increased in a linear fashion over ten cycles. Cyclic voltammetry experiments conducted on a thin film of poly(**3**) revealed that the current generated was directly proportional to the applied scan rate of the potentiostat, as expected (see Figure 5.05, bottom).

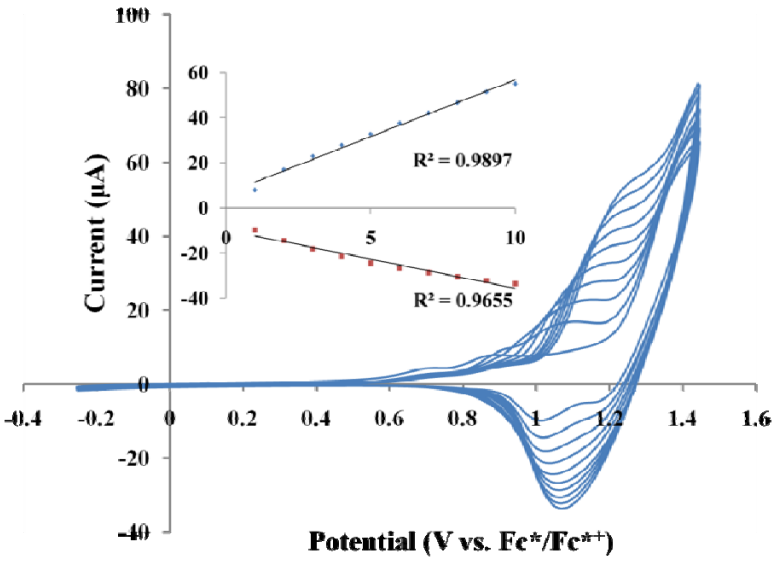

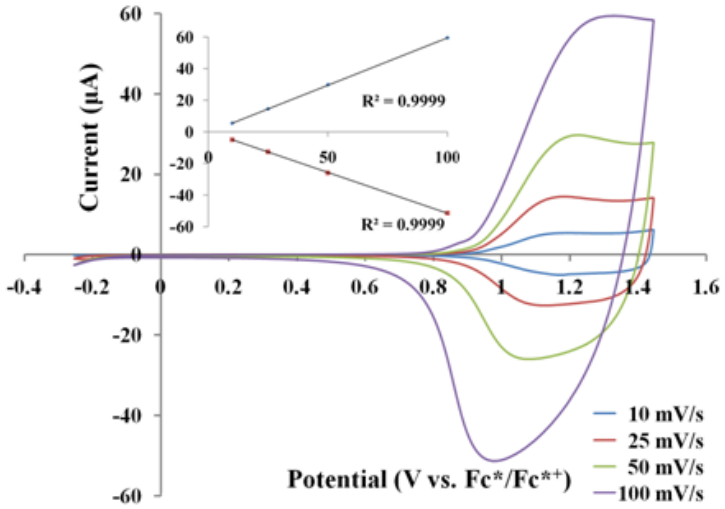

Figure 5.05. (top) Overlay of continuous cyclic voltammograms for silver NHC **3** over time. Inset: plot of current maxima vs. number of cycles. (bottom) Cyclic voltammogram of thin film poly(**3**) at different scan rates. Inset: plot of current vs. scan rate.

To further characterize poly(**3**), its respective monomer was also electropolymerized onto stainless steel. Two distinct phases resulted, both of which were analyzed by XPS to determine their chemical compositions. One phase, which was visibly white in color, featured of a 1:1 molar ratio of silver to chlorine atoms. The lack of sulfur or nitrogen signals suggested that the bithiophene–substituted NHC moiety was absent. By inference, the silver chloride that was formed was presumed to originate from the electrochemical oxidation of the $AgCl_2^-$ anion which is typically present in solutions of silver NHC complexes.[40] Analysis of the other phase, which was visibly yellow in color, revealed a S : Ag ratio of 3.70 and an N : Ag ratio of 1.83 (Table 5.1), values which are in agreement with the anticipated canonical structure of poly(**3**).[41] Moreover when poly(**3**) was deposited onto an ITO slide, the yellow film exhibited a λ_{max} = 399

nm, a value that is red-shifted by 74 nm with respect to that measured for its monomer, and consistent with the formation of an electronically-delocalized polymeric structure.

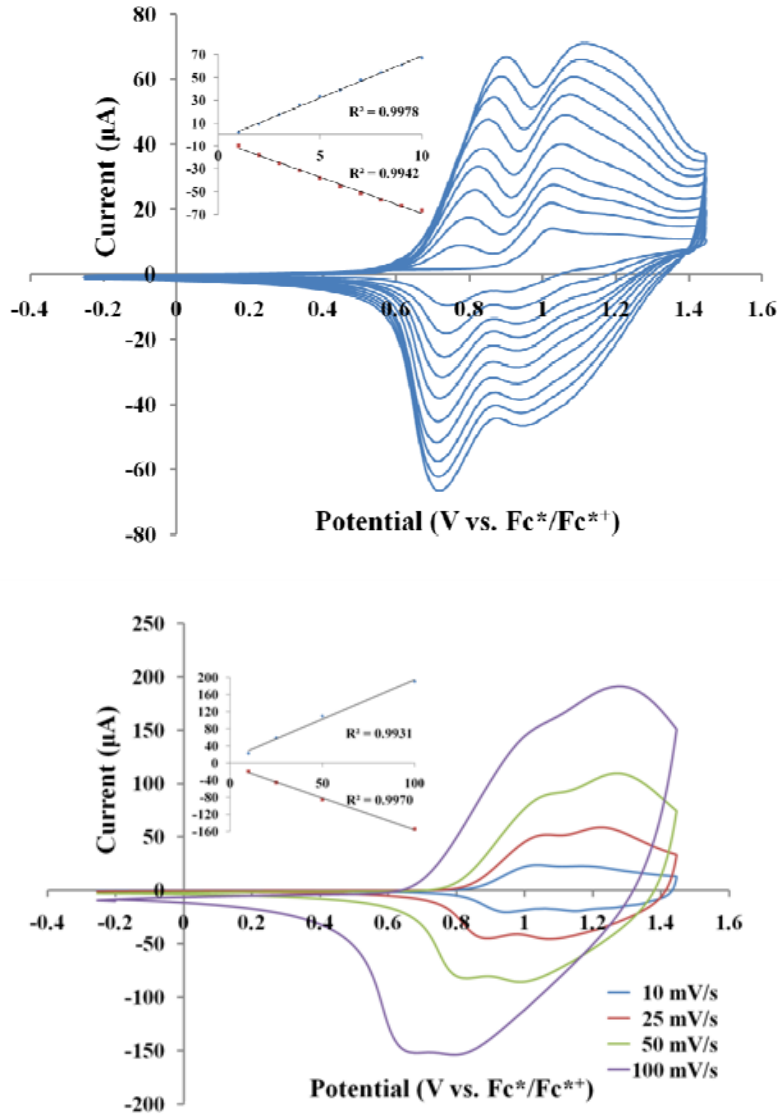

Figure 5.06. (top) Overlay of continuous cyclic voltammograms for silver NHC **5** over time. Inset: plot of current maxima vs. number of cycles. (bottom) Cyclic voltammogram of thin film poly(**5**) at different scan rates. Inset: plot of current vs. scan rate.

Although poly(**3**) was successfully synthesized, subsequent efforts focused on the silver NHC acetate complex **5**, a monomer for which the electropolymerization characteristics were predicted to not entail competitive deleterious processes.[42] Using the method described above, electropolymerization of **5** afforded a thin film that was measured to be 1000 nm thick by profilometry. As shown in Figure 5.06 (top), cyclic voltammetry revealed that the oxidation current observed at 0.8 V increased along with the anticipated potential shifts with each subsequent cycle. The oxidation and reduction waves assigned to the polymer were clearly delineated from those of the monomer. Moreover, the current generated by cycling the potential of poly(**5**) was directly related to the scan rate up to 100 mV/s (Figure 5.06, bottom).

XPS examination of a thin film of poly(**5**) revealed that the atomic ratios of the Ag, N, and S atoms were in accord with the anticipated structure of this material. As predicted,[43] the silver 3d core electrons of poly(**5**) possess a binding energy of 368.6 eV, which is significantly higher than that measured for poly(**3**) (367.4 eV). The UV-vis spectrum of poly(**5**) also exhibits a strong bathocromic shift of 69 nm when compared with that measured for its respective monomer. As noted above, this observation is consistent with the formation of an electronically–delocalized polymeric structure.

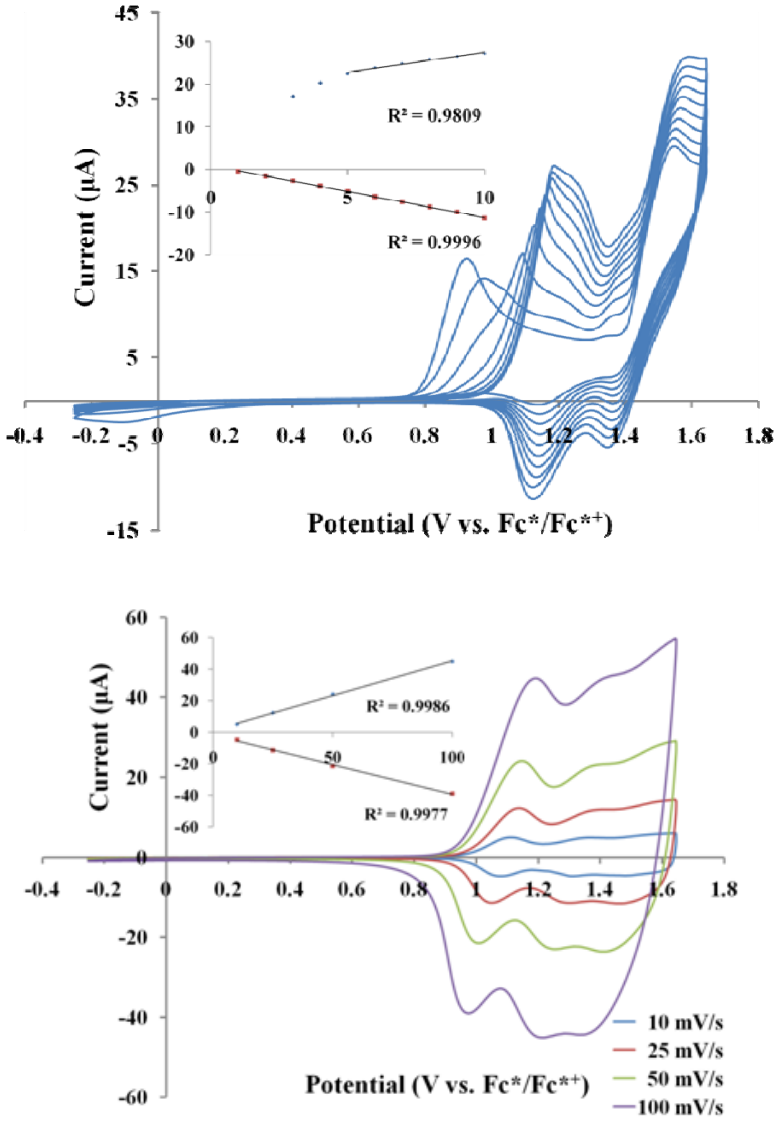

Figure 5.07. (top) Overlay of continuous cyclic voltammograms for thione **6** over time. Inset: plot of current maxima vs. number of cycles. (bottom) Cyclic voltammogram of poly(**6**) at different scan rates. Inset: plot of current vs. scan rate.

Electropolymerization of the thione **6** was accomplished in a similar fashion to that described above. As shown in Figure 5.07 (top), the maximum oxidation current was

observed at 1.15 V, which is a higher potential than that observed for the other polymers analyzed thus far. In the first three electrochemical cycles, an oxidation peak was also detected at 0.9 V. Previous reports have suggested that this feature represents the oxidative attachment of the thione sulfur onto the platinum button[44] and that the accompanying reduction wave (-0.1 V) reflects detachment. After the first three cycles, however, poly(**6**) was observed to coat the surface of the electrode, which in turn prevented any further thione attachment.[45] As shown in Figure 5.07 (bottom), the current generated by poly(**6**) was also found to increase linearly with the scan rate up to 100 mV/s.

XPS analysis of poly(**6**) on a stainless steel substrate revealed a S : N ratio of 2.52, which is in close agreement with the expected value of 2.50. This observation provided additional evidence that **6** did not decompose during polymerization and that the structure of the polymer was formed as expected. Examination of the UV-vis spectrum of this material revealed a λ_{max} = 367 nm, a value which is bathochromically shifted by 43 nm in comparison with that of the corresponding monomer.

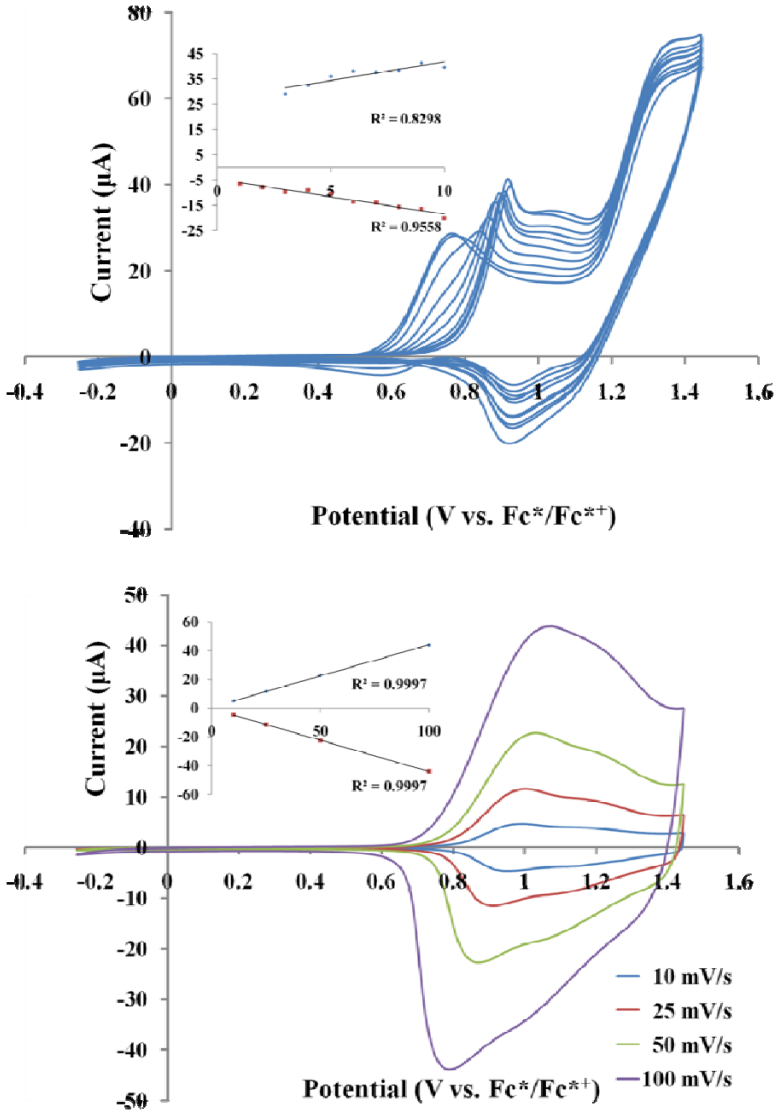

Figure 5.08. (top) Overlay of continuous cyclic voltammograms for iridium NHC **7** over time. Inset: plot of current maxima vs. number of cycles. (bottom) Cyclic voltammogram of thin film poly(**7**) at different scan rates. Inset: plot of current vs. scan rate.

The bithiophene–substituted iridium NHC **7** was electropolymerized next and the plot of current versus potential is displayed in Figure 5.08 (top). Oxidation of the metal

center occurred at a potential of 0.75 V and was pseudo–reversible in accord with related systems.[46] The corresponding reduction peak was observed at 0.60 V. Both peaks decreased rapidly in intensity with repeated cycling and were no longer present after five cycles. Since a similar observation was made for the thin film poly(**6**), it was concluded that the coating of the electrode by poly(**7**) was responsible for this phenomenon. A linear relationship between current increase and the number of consecutive cycles was not evident due to the concurrent oxidation of the coordinated iridium metal. Moreover, the metal oxidation process could not be detected by electrochemical cycling of poly(**7**) (Figure 5.08, bottom) in monomer–free solution, thus suggesting that the metal may not be present in the polymeric thin film. Related iridium-containing polymers, however, have been shown to lack a metal-centered oxidation process.[47] Hence, to gain additional insight into the composition of poly(**7**), the material was analyzed by XPS which revealed that the iridium, sulfur and nitrogen atoms were present in the expected ratios. Surprisingly, the λ_{max} of the polymer was found to be only slightly red-shifted (9 nm) with respect to the corresponding monomer, which suggested that the film consisted primarily of oligomers.

To minimize the concurrent oxidation of the metal center during electropolymerization, the cod ligand of **7** was displaced with carbon monoxide since the latter is known to anodically shift the oxidation potential of iridium NHC complexes. During the electropolymerization of iridium NHC **8** (Figure 5.09, top), metal oxidation was observed to increase from 0.75 V to 1.20 V. As a result, and in contrast to **7**, a linear relationship between the increase in polymer current and the number of electrochemical cycles was observed. Poly(**8**) also exhibited a λ_{max} = 374 nm, a value that is bathochromically shifted by 48 nm compared with its monomer, which represents a significantly larger shift than that oberved for iridium NHC **7**. The electrodeposited thin

film poly(**8**) was therefore expected to consist of polymeric chains and not oligomers. Electrochemical cycling at different scan rates revealed a significant cathodic shift of the reduction wave of poly(**8**) and a broadening of its oxidation feature above scan rates of 25 mV/s (Figure 5.09, bottom). Such distortions at these low scan rates are consistent with a lower degree of ion mobility for poly(**8**), particularly when compared with poly(**4**) – poly(**7**).

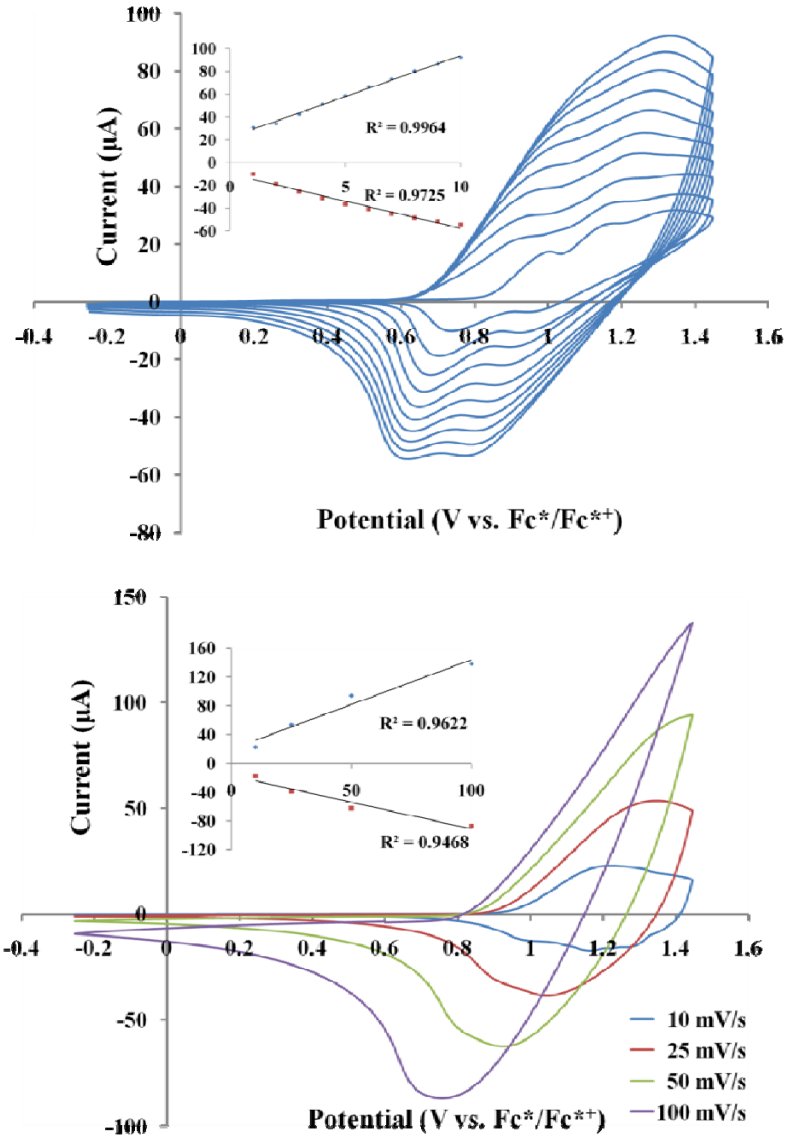

Figure 5.09. (top) Overlay of continuous cyclic voltammograms for iridium NHC **8** over time. Inset: plot of current maxima vs. number of cycles. (bottom) Cyclic voltammogram of thin film poly(**8**) at different scan rates. Inset: plot of current vs. scan rate.

Table 5.1. Selected Properties of the Thin Films Prepared.[a]

Poly.	ML_n	λ_{red}[a] (nm)	λ_{ox}[b] (nm)	stability[c] (cycles)	thickness[d] (nm)
poly(**3**)	AgCl	399	--	--	558
poly(**4**)	AuCl	392	702	35	348
poly(**5**)	AgOAc	395	677	12	1173
poly(**6**)	S	367	687	20	126
poly(**7**)	Ir(cod)Cl	333	704	30	294
poly(**8**)	$Ir(CO)_2Cl$	374	692[e]	50	750

[a] Absorbance maxima at 0.0 V. [b] Absorbance maxima for polaron peak under oxidative potentials. [c] Stability was defined as the number of cycles (listed) observed until half of the absorbance peak near 700 nm was depleted. [d] Determined by profilometry. [e] A bipolaron excitation was observed at 1092 nm.

5.4 Electrochromism of Metallopolymers

It is well-established that electrochemical oxidation of polythiophene-type systems increases the degree of planarity along the main chain. As a result, an absorption

feature typically appears near 700 nm and has been assigned to polaron–induced $\pi \rightarrow \pi^*$ transitions that occur along the backbone of the polymer.[23] Further oxidation of these materials gives rise to new absorption features in the NIR region that have been attributed to $\pi \rightarrow \pi^*$ bipolaron excitations.[48] In the case of the polymers described herein, metal-ligated imidazole moieties are infused into the main chain and connected through quarterthiophene linkages. It was envisioned that polaron and bipolaron excitations would likewise occur at the oligothiophene linkages of poly(**4**) – poly(**8**), and hence these polymers were subsequently analyzed for their abilities to exhibit electrochromic characteristics.

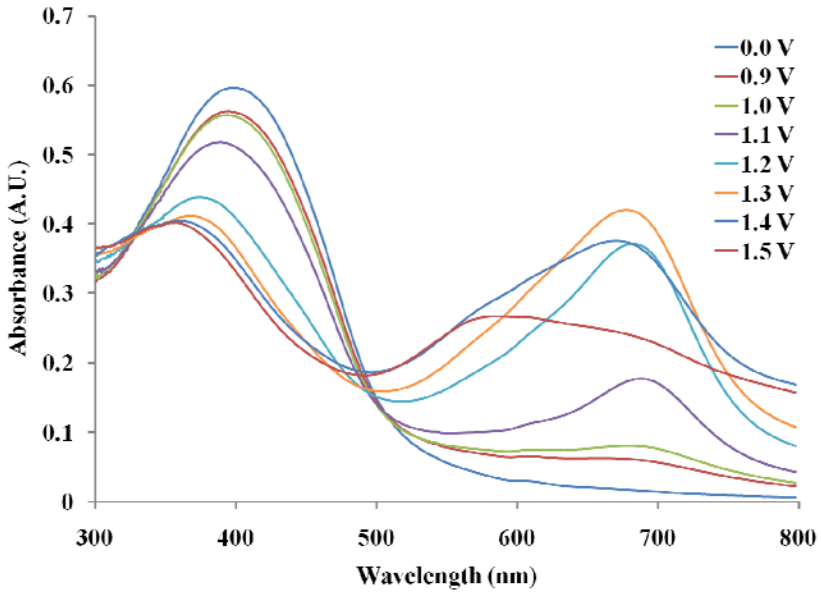

Figure 5.10. UV-vis profile for silver NHC thin film poly(**5**) at different potentials. The film was deposited on ITO and used as the working electrode of a three – electrode cell assembled in a quartz cuvette.

Spectroelectrochemical measurements were carried out on poly(**4**) – poly(**8**) by increasing the potential from 0.0 V to 1.5 V in 0.1 V increments in conjunction with the acquisition of UV-vis-NIR spectral data. An absorption peak near 700 nm was observed upon oxidation of a film of poly(**4**) at 1.2 V and the thin film was stable for 35 cycles. Moreover, the material underwent a drastic color change from yellow (reduced state) to dark blue (oxidized state) during this process. Although similar results were obtained for poly(**5**) (Figure 5.10), this material was found to be stable for only 12 cycles, which is in accord with the labile nature of **5** in solution. To underscore the importance of a coordinated transition metal, the thione thin film poly(**6**), was also examined and found to exhibit diminished electrochromic behavior in comparison with poly(**4**) and poly(**5**). This observation implies the existence of a cooperative effect on the part of the coordinated metal in terms of the appearance of the new absorption feature near 700 nm.

Based on the data presented, combined with the well-known electrochromic properties of oligothiophenes, a proposed mechanism for the observed electrochromic activity is outlined in Scheme 5.5. At high potentials, the quarterthiophene moieties undergo oxidation to generate polaron excitations which causes the thiophenes to orient in a planar arrangement. In turn, this results in the appearance of the new absorbances near 700 nm.[49] Since no significant NIR activity was observed, it is unlikely that bipolarons are being formed in the aforementioned materials. Nevertheless, in all cases studied, the polaron absorbance near 700 nm shifted hypsochromically above potentials of 1.2 – 1.3 V, which is likely due to over-oxidation (which breaks planarity).[50]

Poly(**7**), which contains a coordinated iridium metal and a cod ligand, exhibits only a weak UV–vis absorption near 700 nm under oxidative conditions. However, a thin film of poly(**8**) exhibited significant absorption at 692 and 1092 nm at 1.2 V (see Figure 11). The absorbance at 1092 nm was attributed to the formation of bipolarons along the

quarterthiophene chains of poly(**8**) (see Figures 5.10 and 5.11). In this respect, poly(**8**) is unique in that the incorporation of CO ligands on the monomer resulted in the formation of polaron (692 nm) and bipolaron (1092 nm) excitations in the resulting polymer. (Figure 5.11). As a result, thin films of poly(**8**) were found to be relatively robust as evidenced by the high degree of electrochromic reversibility that was observed (> 50 cycles).

Scheme 5.5. Proposed Mechanism of Polaron and Bipolaron Formation For Thin Films Poly(**4**) – Poly(**8**) in $TBAPF_6/CH_2Cl_2$ Solution Under Oxidative Conditions.

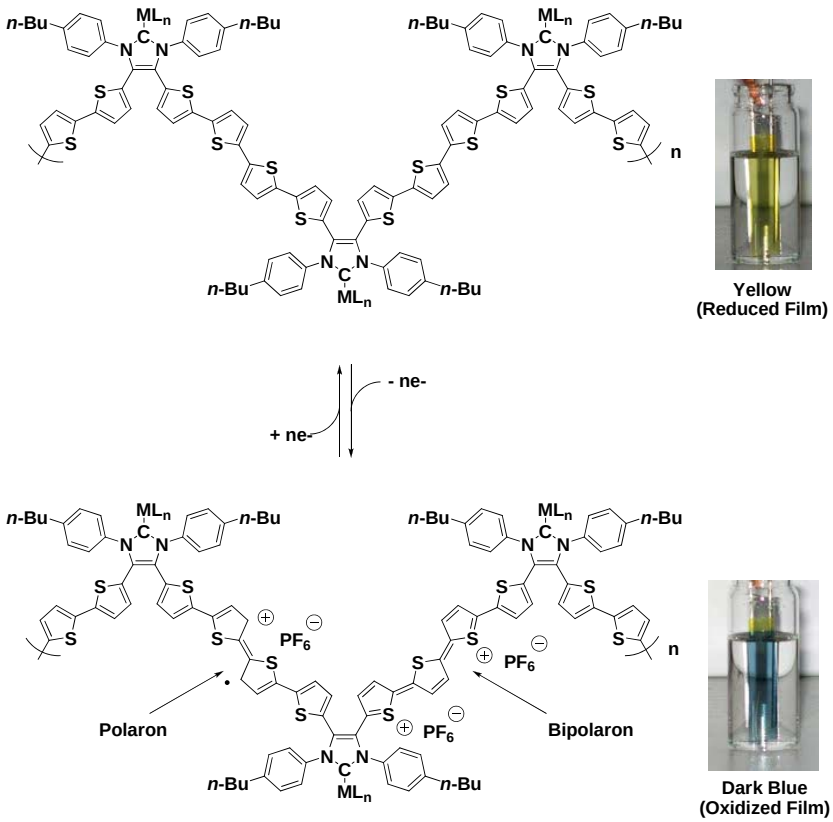

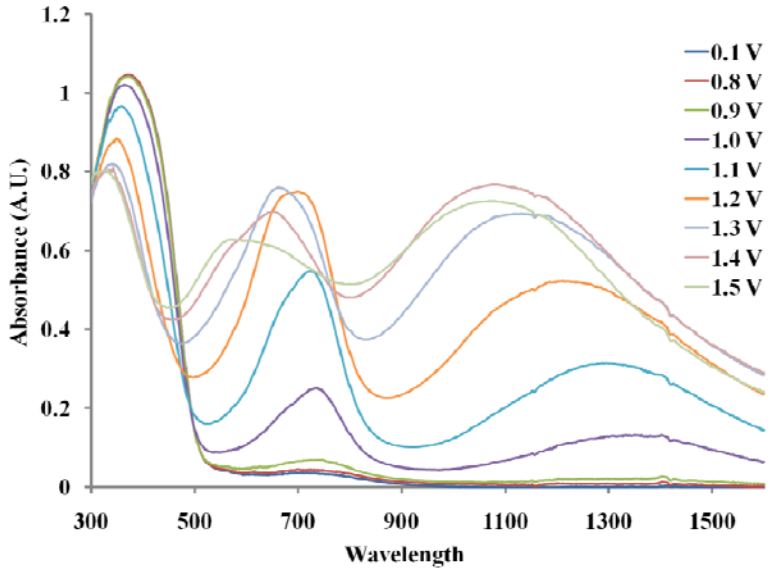

Figure 5.11. UV-vis-NIR profile for iridium NHC thin film poly(**8**) at different potentials. The film was deposited onto ITO and used as the working electrode of a three – electrode cell assembled in a quartz cuvette.

5.5 Conclusions

In summary, high-yielding syntheses of various silver, gold, iridium, and sulfur – substituted NHCs with bis(bithiophene) moieties have been developed. The resulting NHC metal complexes were successfully polymerized under oxidative conditions to afford stable thin films. The polymeric materials obtained, which were characterized using a range of electrochemical, XPS, and UV-vis spectroscopic techniques, were found to be consistent with their canonical structures. A unique feature of these materials is that the ligated main group or transition metals are orthogonally-positioned with respect to the main-chain of the polymer.

In addition, most of the new polymers exhibit electrochromic characteristics that are dependent on the nature of the incorporated metal. These results highlight the pivotal

role that both the NHC-metal moieties and the ancillary ligands play in optimizing the electrochromic behavior and other electronic properties exhibited by NHC-based polymeric materials.

5.6 Experimental

General Procedures. All solvents and reagents were used as received from commercial sources unless stated otherwise. The synthesis of the bithiophene-substituted diimine **1** and imidazolium chloride **2** are reported elsewhere.[17] Methylene chloride was distilled over calcium hydride prior to use. All NMR spectra were recorded at 298 K on a Varian Inova instrument (^{1}H NMR, 499.40 MHz; ^{13}C NMR, 125.57 MHz) using residual protio solvent or tetramethylsilane (TMS) as an internal reference unless stated otherwise. Low-resolution chemical ionization mass spectral data (MS-CI) were collected on a Thermo Scientific TSQ Quantum GC mass spectrometer. High-resolution CI-MS spectra were recorded on a magnetic sector Waters Autospec Ultima instrument or on an IonSpec 9.4T FT Mass Spectrometer equipped with an ESI source and data are reported as *m/z* (relative intensity). Infrared spectra were recorded in the solid state (KBr) using a Nicolet Avatar 260 FT-IR spectrometer. The spectroelectrochemical and absorbance measurements were recorded on a Varian Cary 5000 UV-vis-NIR spectrophotometer using Starna Quartz fluorometer cells with a pathlength of 10 mm for **3** and **5** – **8** and a 0.1 mm pathlength for poly(**3**) – poly(**8**).

Electrochemistry. Electrochemical syntheses and studies were performed in a glovebox under a nitrogen atmosphere using a CH Instruments Electrochemical Workstation (series 700B). All electrochemical experiments were carried out in a three-electrode cell consisting of a platinum button working electrode, a tungsten counter-

electrode and a silver wire pseudo-reference electrode. A 0.1 M solution of [(*n*-Bu)$_4$N$^+$][PF$_6^-$] (TBAPF$_6$) was used as the supporting electrolyte. The TBAPF$_6$ was purified via recrystallization three times from hot ethanol before being dried for 3 days at >100 °C under a dynamic vacuum. Electrosyntheses of the films onto a platinum button were performed from 1×10^{-3} M monomer solutions by continuous cycling between –0.20 V and 1.50 V (upper limit of 1.70 V for **6**) at v = 100 mVs^{-1}. Analogous continuous cycling was performed between –0.20 V and +1.70 V for deposition of the polymers onto either stainless steel or ITO slides. The resulting films were then washed with copious amounts of CH_2Cl_2 and stored in the absence of light. All potentials listed in the manuscript and supplementary information were referenced to SCE by shifting Fc*^{0}/Fc*$^+$ to -0.057 V.[24]

Spectroelectrochemistry. Spectroelectrochemical data were recorded on a Varian Cary 5000 UV-vis-NIR spectrophotometer using Starna Quartz fluorometer cells. A three-electrode cell was constructed in which polymer had been previously deposited on the ITO working electrode. The counter-electrode and pseudo-reference electrode consisted of tungsten and silver wires, respectively. A solution of 0.1 M TBAPF$_6$ in CH_2Cl_2 solution was used as the electrolyte. An Eco Chemie Autolab PGSTAT30 equipped with GPES software was used to adjust the potential of the three-electrode cell in the UV-vis spectrophotometer. The polymers that were deposited on ITO electrodes were analyzed by UV-vis-NIR spectroscopy (1600 nm – 300 nm) while increasing the voltage in stepwise intervals of 0.10 V, from 0.0 V to 1.5 V. The stability of each film was determined by continuous cycling at 0.10 V/s until the electrochromic signal observed at approximately 700 nm decreased to 50% of its initial absorbance.

X-Ray Photoelectron Spectroscopy. All XPS spectra were recorded on a Kratos Axis Ultra X-ray photoelectron spectrometer utilizing a monochromated Al-Kα X-ray

source ($h\upsilon$ = 1486.5 eV), hybrid optics (employing a magnetic and electrostatic lens simultaneously) and a multi-channel plate and delay line detector coupled to a hemispherical analyzer. The photoelectron take-off angle of 0° (measured from the surface normal) was used in all experiments. All spectra were recorded using an aperture slot of 300 × 700 microns, and the high resolution spectra were collected with a pass energy of 20 eV. The pressure in the analysis chamber was typically held at 2 x 10^{-9} Torr during data acquisition. Kratos XPS analysis software was used to determine the stoichiometries of the samples from the corrected peak areas by applying the appropriate sensitivity factors for each element of interest. All reported ratios represent the average of two independent sample acquisitions and all binding energies are reported with respect to the carbon 1s signal at 286.1 eV.

X-Ray Crystallography. All crystals were allowed to grow in the absence of light. Crystals suitable for data collection were covered with hydrocarbon oil and mounted on thin nylon loops. The X-ray diffraction data were collected at 153K on a Rigaku AFC-12 diffractometer equipped with a Saturn 724 and CCD area detector, an Oxford Cryostream low-temperature device and a graphite-monochromated Mo Kα radiation source (λ = 0.71073 Å). Corrections were applied for Lorentz and polarization effects. The structures were solved by direct methods and refined by full-matrix least-squares cycles on F^2.[25] All non-hydrogen atoms were refined with anisotropic thermal parameters, and all hydrogen atoms were placed in fixed, calculated positions using a riding model (C–H, 0.96 Å).

Profilometry and Conductivity. Profilometry measurements for **3 - 8** were performed on a Dektak 6M Stylus Profilometer in a clean-room facility. The average thickness of the polymers were based on an average of 12 data acquisitions on two

different samples. The samples were prepared by electropolymerizaton of the polymers on ITO slides using cyclic voltammetry (50 cycles) between –0.2 V and +1.7 V.

Bithiophene-Substituted Silver NHC Complex 3. The imidazolium chloride **2**[17] (0.115 mmol, 0.080 g) and silver (I) oxide (0.069 mmol, 0.016 g) were added to a round-bottomed flask containing dry CH_2Cl_2 (15 mL) and the flask was covered with aluminum foil. The reaction mixture was stirred at ambient temperature for 48 h, after which it was filtered through Celite. The residual solvent was removed under reduced pressure to afford the desired product **3** as a yellow solid (95% yield). Single crystals suitable for X-ray data collection were obtained by slow vapor diffusion of hexanes into a solution of **3** in THF (1 : 3.00 THF : hexanes) over a period of 5 d at ambient temperature. ^{1}H NMR (499.40 MHz, CD_2Cl_2, TMS): δ 7.28 (d, 4H, *J* = 8.0 Hz), 7.22 (d, 4H, *J* = 8.0 Hz) 7.15 (dd, 2H, *J* = 5.0, 1.0 Hz), 7.00 (dd, 2H, *J* = 3.5, 1.0 Hz), 6.90 – 6.88 (m, 4H), 6.69 (d, 2H, *J* = 3.5 Hz), 2.60 (t, 4H, *J* = 7.5 Hz), 1.55 (p, 4H, *J* = 7.0 Hz), 1.29 (sextet, 4H, *J* = 7.5 Hz), 0.85 (t, 6H, *J* = 7.0 Hz). ^{13}C{^{1}H} NMR (125.57 MHz, CD_2Cl_2): δ 145.38, 141.22, 136.40, 136.22, 132.15, 129.81, 128.32, 127.50, 127.43, 126.01, 125.73, 124.81, 123.80, 35.39, 33.60, 22.73, 14.06. The carbenic was detected when $CDCl_3$ was used as the solvent: ^{13}C{^{1}H} NMR (150.83 MHz, $CDCl_3$): δ 181.21(br). LRMS (CI^+ *m/z*): 804 (100% M + H^+). HRMS (CI^+, CH_4): Calcd for $C_{39}H_{36}N_2S_4{}^{107}AgCl$, 802.0504; found 802.0501. Calcd for $C_{39}H_{36}N_2S_4{}^{109}AgCl$, 804.0493; found 804.0497. The bis-ligated silver cation was also detected. HRMS (ESI): Calcd for $C_{78}H_{72}N_4S_8{}^{107}Ag$, 1427.25681, found 1427.25317. IR (cm^{-1}): 3060, 2954, 2926, 2856, 1628 (C-C_{arom}), 1510 (C-C_{arom}), 1388, 1229, 1048, 1019, 838, 800, 696. λ_{max} = 325 nm. ε = 4.9 × 10^4 M^{-1} cm^{-1}.

Bithiophene-Substituted Silver Carbene Complex 5. The imidazolium chloride **2**[17] (0.057 mmol, 0.040 g) and silver (I) acetate (0.143 mmol, 0.024 g) were added to a round-bottomed flask containing 3 Å sieves and dry CH_2Cl_2 (15 mL). The reaction vessel

was then covered with aluminum foil and the reaction mixture was stirred at ambient temperature for 48 h in the absence of light. The reaction mixture was then filtered through Celite and the residual solvent was removed under reduced pressure to afford the desired product **5** as a yellow solid (96% yield). Single crystals suitable for X-ray data collection were obtained by layering a THF solution of **5** with hexanes at –40 °C for one week (1 : 3 THF : hexanes v/v). ^{1}H NMR (400.27 MHz, $CDCl_3$, TMS): δ 7.29 – 7.20 (m, 8H), 7.16 (d, 2H, *J* = 5.2 Hz) 7.00 (d, 2H, *J* = 4.0 Hz), 6.91-6.88 (m, 4H), 6.68 (d, 2H, *J* = 3.2 Hz), 2.61 (t, 4H, *J* = 7.6 Hz), 1.81 (s, 3H), 1.56 (p, 4H, *J* = 8.4 Hz), 1.30 (sextet, 4H, *J* = 7.2 Hz), 0.86 (t, 6H, *J* = 7.2 Hz). ^{13}C{^{1}H} NMR (125.57 MHz, CD_2Cl_2): δ 175.86, 144.06, 140.07, 135.30, 135.20, 131.01, 128.63, 127.19, 126.40, 126.27, 124.98, 124.58, 123.67, 122.66, 34.45, 32.48, 21.59, 21.47, 12.94. As in the cases of similar complexes, the carbenic carbon could not be detected by ^{13}C NMR spectroscopy.[26] LRMS (CI^+ *m/z*): 661 (100% $M^+ + H^+ - AgC_2H_3O_2$), 828 (20% $M + H^+$). The bis-ligated silver cation was also detected. HRMS (ESI): Calcd for $C_{78}H_{72}N_4S_8{}^{107}Ag$, 1427.25681; found 1427.25771. IR (cm^{-1}): 3067, 2954, 2927, 2858, 1578 (C-C_{arom}), 1510 (C-C_{arom}), 1382, 1327, 1018, 838, 804, 696. λ_{max} = 325 nm. ε = 3.0 × 10^4 M^{-1} cm^{-1}.

Bithiophene-Substituted Thione 6. The imidazolium chloride **2**[17] (0.143 mmol, 0.100 g), elemental sulfur (0.179 mmol, 0.006 g) and (0.179 mmol, 0.025 g) K_2CO_3 were added to a Schlenk flask. Degassed MeOH (25 mL) was then added *via* cannula to the reaction mixture, which was stirred subsequently at ambient temperature for 24 h. The product was then extracted into CH_2Cl_2 (50 mL) and washed with water (3 × 25 mL). Finally, the organic layer was then separated, dried with $MgSO_4$, filtered and concentrated to afford the desired product **6** as an orange solid (98% yield). Single crystals suitable for X-ray data collection were obtained by slow vapor diffusion of hexanes into a solution of **6** in THF (1 : 2.5 THF : hexanes v/v) at ambient temperature. ^{1}H NMR (499.40 MHz, CD_2Cl_2,

TMS): δ 7.24 (d ,4H, *J* = 8.5 Hz), 7.21 (d, 4H, *J* = 8.5 Hz) 7.12 (dd, 2H, *J* = 5.5, 1.0 Hz), 6.96 (dd, 2H, *J* = 3.5, 1.0 Hz), 6.96 (dd, 2H, *J* = 5.0, 1.5 Hz), 6.83 (d, 2H, *J* = 3.5 Hz), 6.62 (d, 2H, *J* = 4.0 Hz), 2.58 (t, 4H, *J* = 7.5 Hz), 1.55 (p, 4H, *J* = Hz), 1.27 (sextet, 4H, *J* = 7.5 Hz), 0.84 (t, 6H, *J* = 7.0 Hz). $^{13}C\{^{1}H\}$ NMR (125.57 MHz, CD_2Cl_2): δ 167.11, 144.67, 140.27, 136.63, 134.71, 131.50, 129.45, 129.17, 128.24, 127.14, 125.42, 124.52, 123.58, 123.36, 35.35, 33.66, 22.70, 14.07. LRMS (CI^- *m/z*): 692 (100% M^+). HRMS (CI^+, CH_4): Calcd for $C_{39}H_{36}N_2S_5$, 693.15548; found 693.15543. IR (cm^{-1}): 3067, 2956, 2928, 2857, 1510 (C-C_{arom}), 1385 (C-C_{arom}), 1344, 1229, 1048, 1019, 838, 800, 696. λ_{max} = 324 nm. ε = 4.3 × 10^4 M^{-1} cm^{-1}.

Bithiophene-Substituted Iridium NHC Complex 7. The bithiophene-substituted silver carbene **3** (0.137 mmol, 0.110 g) and the chloro(1,5-cyclooctadiene)iridium(I) dimer (0.075 mmol, 0.051 g) were added to a round-bottomed flask containing dry CH_2Cl_2 (15 mL) and the reaction vessel was covered with aluminum foil. The reaction mixture was stirred at ambient temperature for 72 h, after which it was filtered through Celite and the residual solvent was removed under reduced pressure to afford the desired product **7** as a brown powder (95% yield). ^{1}H NMR (499.40 MHz, CD_2Cl_2, TMS): δ 7.57 (d ,4H, *J* = 8.0 Hz), 7.16 (d, 4H, *J* = 8.5 Hz), 7.12 (dd, 2H, *J* = 5.0, 1.0 Hz), 6.98 (dd, 2H, *J* = 3.5, 1.0 Hz), 6.87 (m, 4H), 6.71 (d, 2H, *J* = 3.5 Hz), 4.13 (m, 2H), 2.59 (t, 4H, *J* = 7.0), 2.50 (m, 2H), 1.56 (p, 6H, *J* = 7.5 Hz), 1.27 (sextet, 8H, *J* = 7.5 Hz), 1.11 (m, 2H), 0.83 (t, 6H, *J* = 7.5 Hz). $^{13}C\{^{1}H\}$ NMR (125.57 MHz, CD_2Cl_2, TMS): δ 182.62, 142.87, 139.38, 135.54, 134.86, 130.83, 128.04, 127.41, 127.11, 125.94, 125.90, 124.31, 123.47, 122.51, 82.14, 50.75, 34.50, 32.75, 32.06, 28.09, 21.35, 12.94. LRMS (CI^+ *m/z*): 996 (100% $M^+ + H^+$), 959 (55% M - Cl). HRMS (CI^+, CH_4): Calcd for $C_{47}H_{48}N_2ClS_4{}^{193}Ir$, 996.2024; found 996.2018. IR (cm^{-1}): 3067, 2954, 2924, 2858, 1509 (C-C_{arom}), 1420 (C-C_{arom}), 1375, 1327, 1262, 1019, 837, 799, 689. λ_{max} = 324 nm. ε = 4.2 × 10^4 M^{-1} cm^{-1}.

Bithiophene-Substituted Iridium NHC Complex 8. Complex **7** was added to a round-bottomed flask containing dry CH_2Cl_2 (5 mL). The reaction vessel was then fitted with a rubber septum and the resulting solution was stirred under an atmosphere of carbon monoxide for 12 h, after which it was filtered through Celite and the residual solvent was removed under reduced pressure to afford the desired product **8** as a brown powder (98% yield). ^{1}H NMR (499.40 MHz, CD_2Cl_2, TMS): δ 7.36 (d, 4H, *J* = 8.5 Hz), 7.20 (d, 4H, *J* = 8.5 Hz), 7.12 (dd, 2H, *J* = 5.0, 1.0 Hz), 6.97 (dd, 2H, *J* = 4.0, 1.5 Hz), 6.86 (m, 4H), 6.65 (d, 2H, *J* = 4.0 Hz), 2.61 (t, 4H, *J* = 5.0 Hz), 1.57 (p, 4H, *J* = 8.0 Hz), 1.28 (sextet, 4H, *J* = 8.0 Hz), 0.85 (t, 6H, *J* = 7.5 Hz). ^{13}C{^{1}H} NMR (125.57 MHz, CD_2Cl_2, TMS): δ 180.33, 174.44, 167.45, 144.14, 140.07, 135.28, 134.00, 130.94, 128.12, 127.98, 127.16, 126.84, 124.69, 124.55, 123.64, 122.62, 34.51, 32.39, 21.55, 12.97. LRMS (CI^+ *m/z*): 944 (20% M^+), 909 (100% M – Cl). HRMS (CI^+, CH_4): Calcd for $C_{41}H_{36}N_2ClO_2S_4{}^{193}Ir$, 944.0978; found 944.0974. IR (cm^{-1}): 2953, 2926, 2856, 2058 (C≡O), 1974 (C≡O), 1658, 1510 (C-C_{arom}), 1398 (C-C_{arom}), 1334, 1261, 1202, 1020. λ_{max} = 326 nm. ε = 1.8×10^4 M^{-1} cm^{-1}.

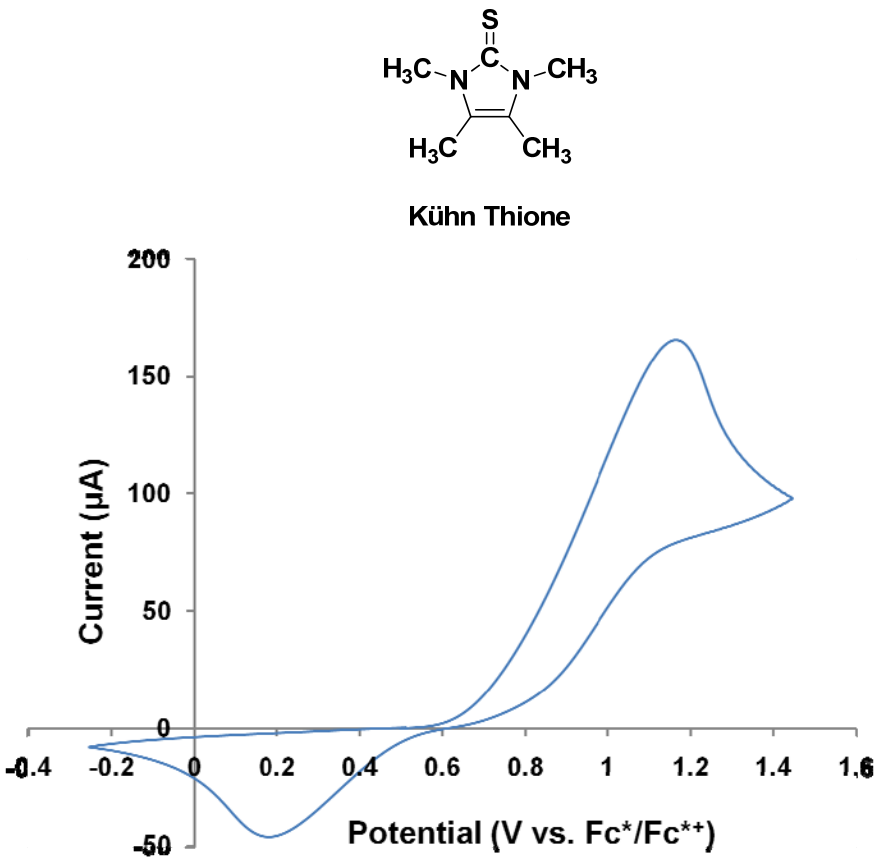

Figure 5.12. Cyclic Voltammogram of a 1.0 mM solution of the Kühn thione in CH_2Cl_2.

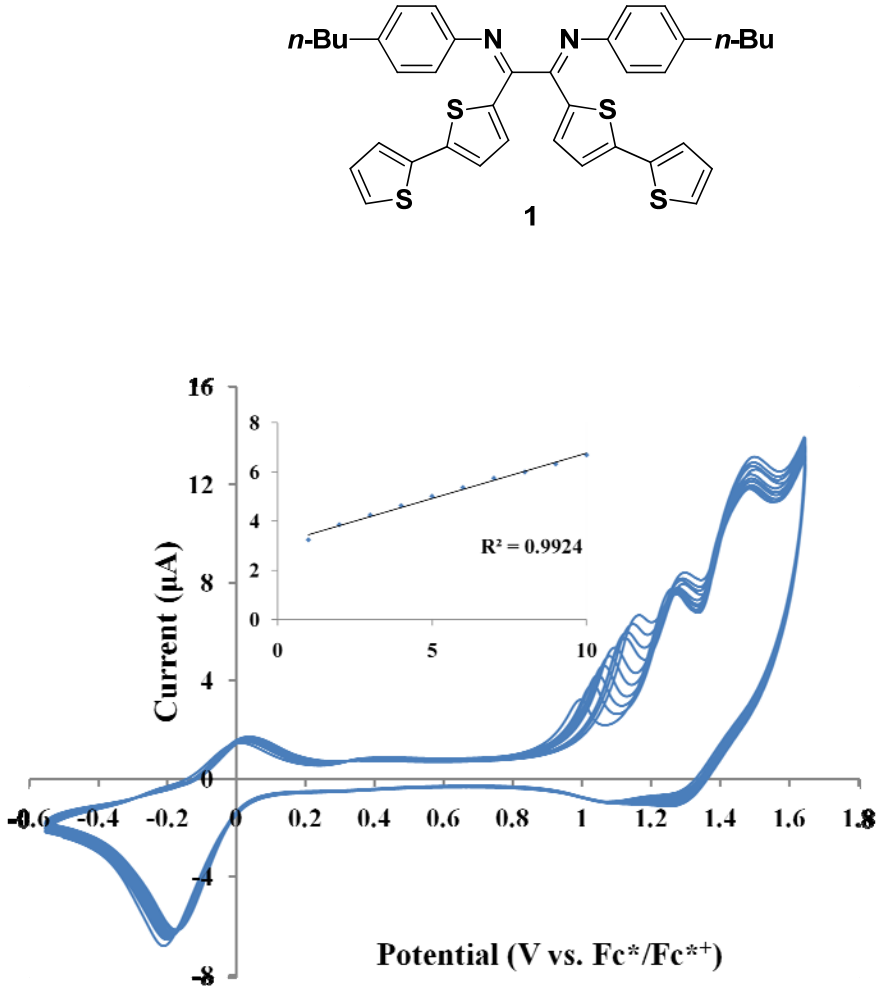

Figure 5.13. (a) Overlay of continuous cyclic voltammograms of diimine **1** over time. Inset: plot of oxidation current vs. number of cycles. The concentration of **1** was 1.0 mM in 0.1 M $TBAPF_6/CH_2Cl_2$.

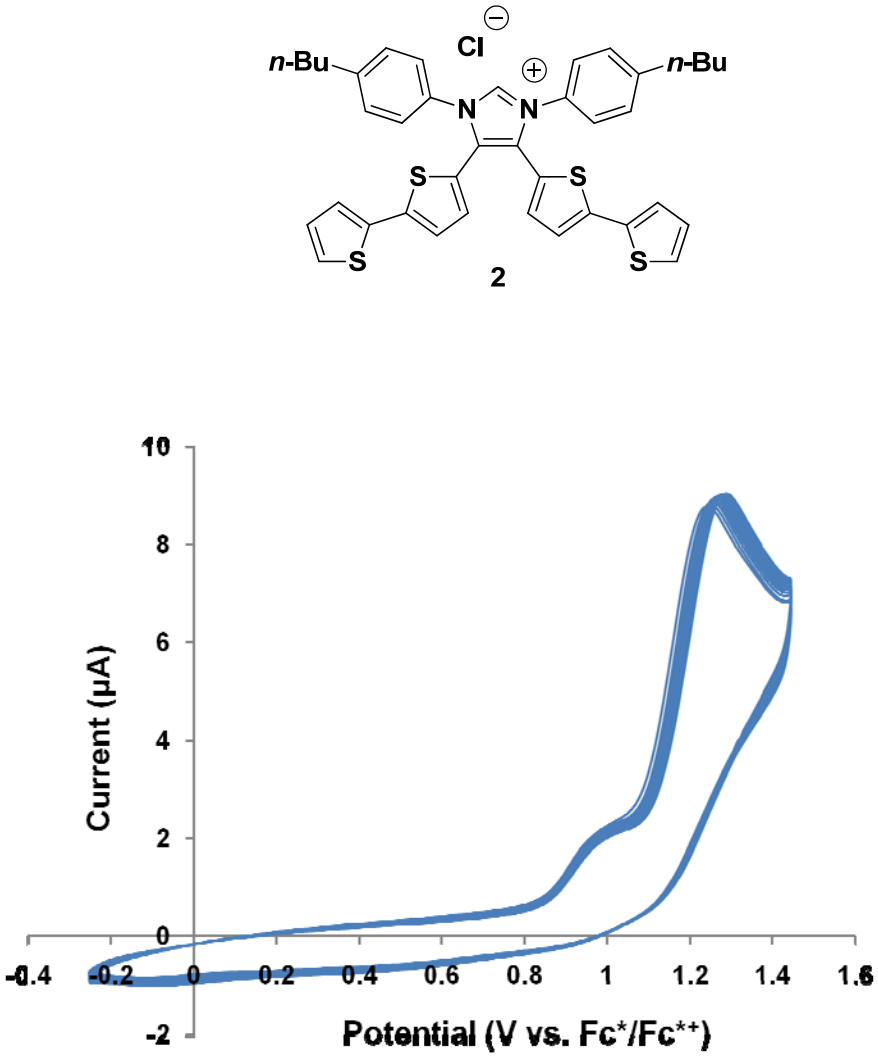

Figure 5.14. Cyclic voltammogram of bithiophene–substituted imidazolium chloride **2**. The concentration of **2** was 1.0 mM in 0.1 M $TBAPF_6/CH_2Cl_2$.

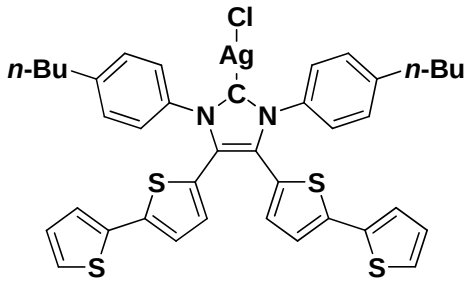

3

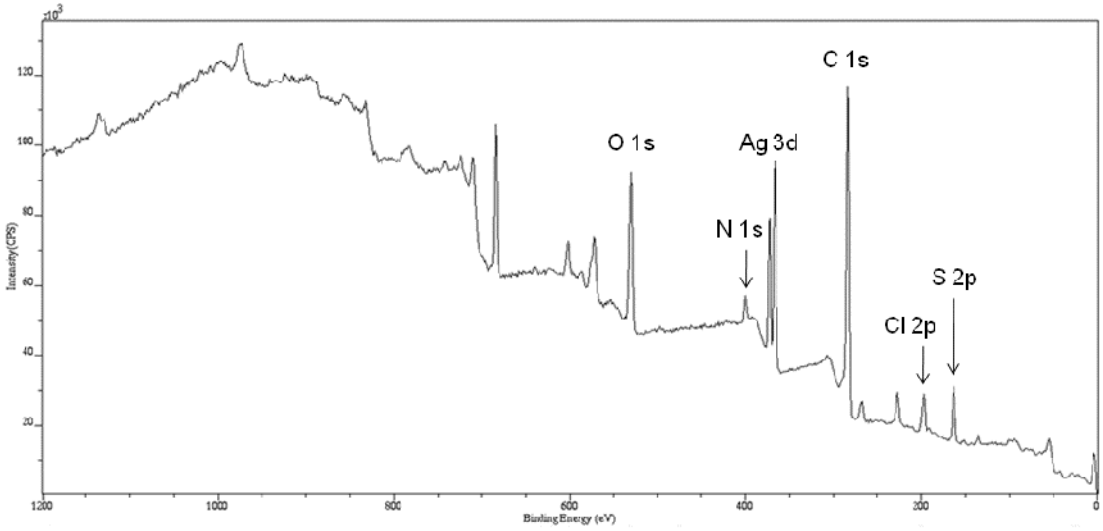

Figure 5.15. Survey XPS of bithiophene-substituted silver NHC yellow film poly(**3**).

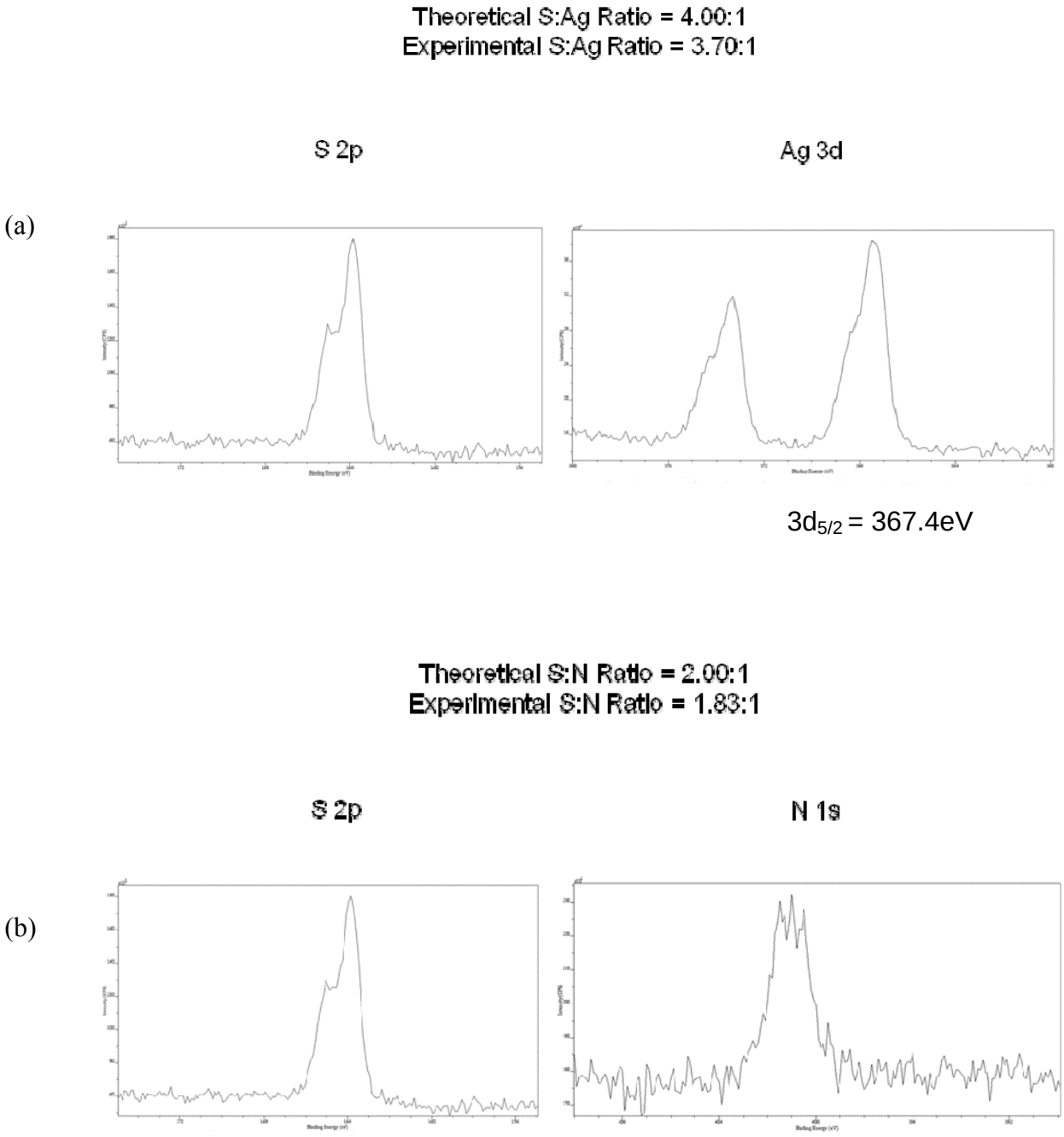

Figure 5.16. High-resolution XPS of bithiophene-substituted silver NHC yellow film poly(**3**). (a) Ratio of sulfur 2p to silver 3d. (b) Ratio of sulfur 2p to nitrogen 1s.

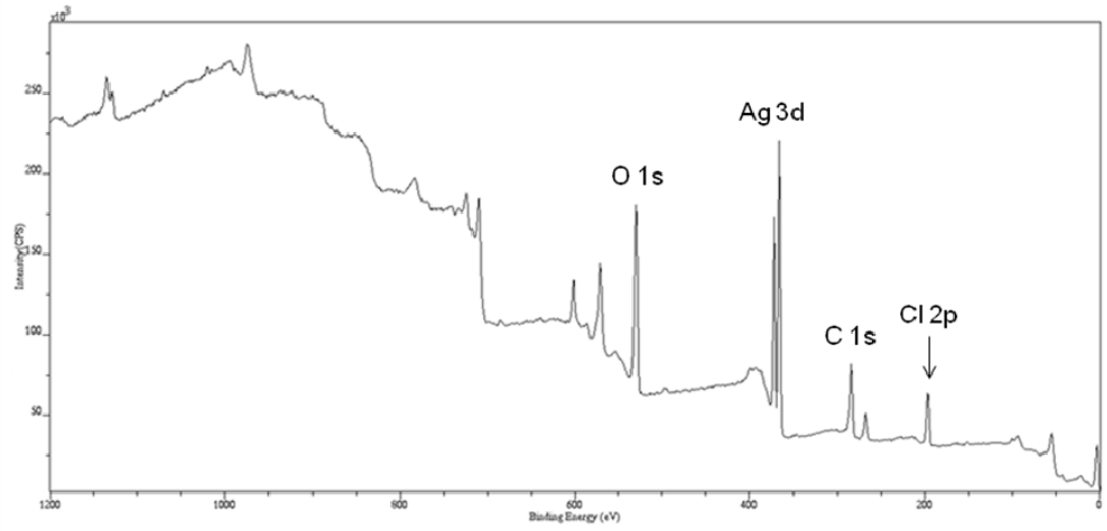

Figure 5.17. Survey XPS of bithiophene-substituted silver NHC white film poly(**3**).

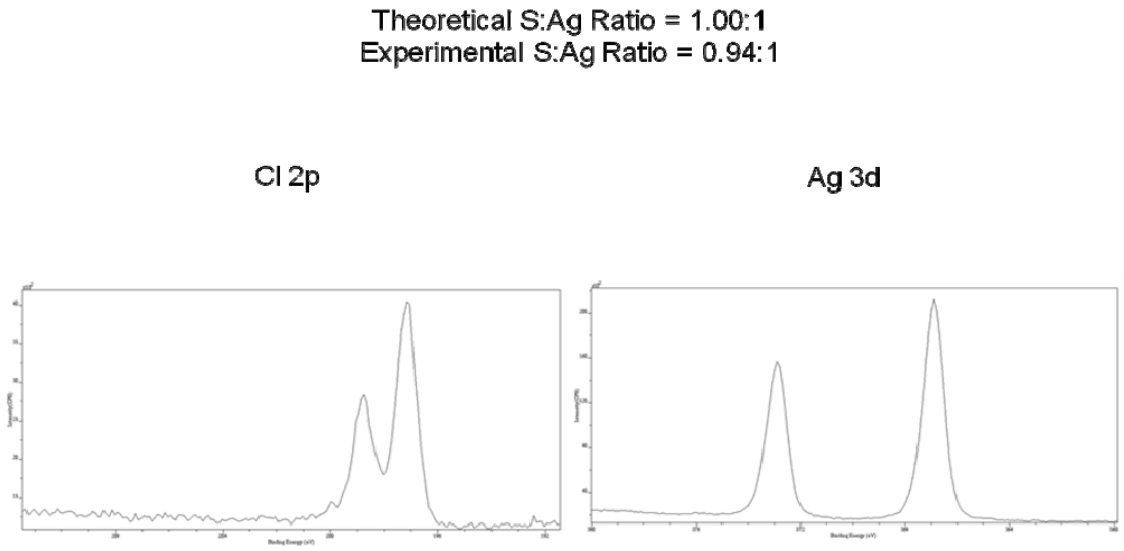

Figure 5.18. High-resolution XPS of bithiophene-substituted silver NHC white film poly(**3**). Ratio of chlorine 2p to silver 3d.

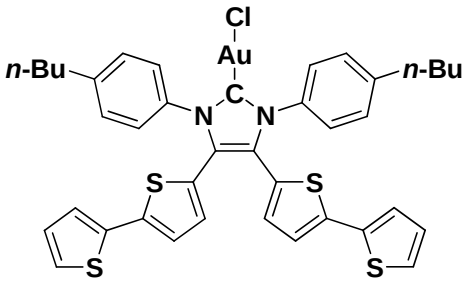

4

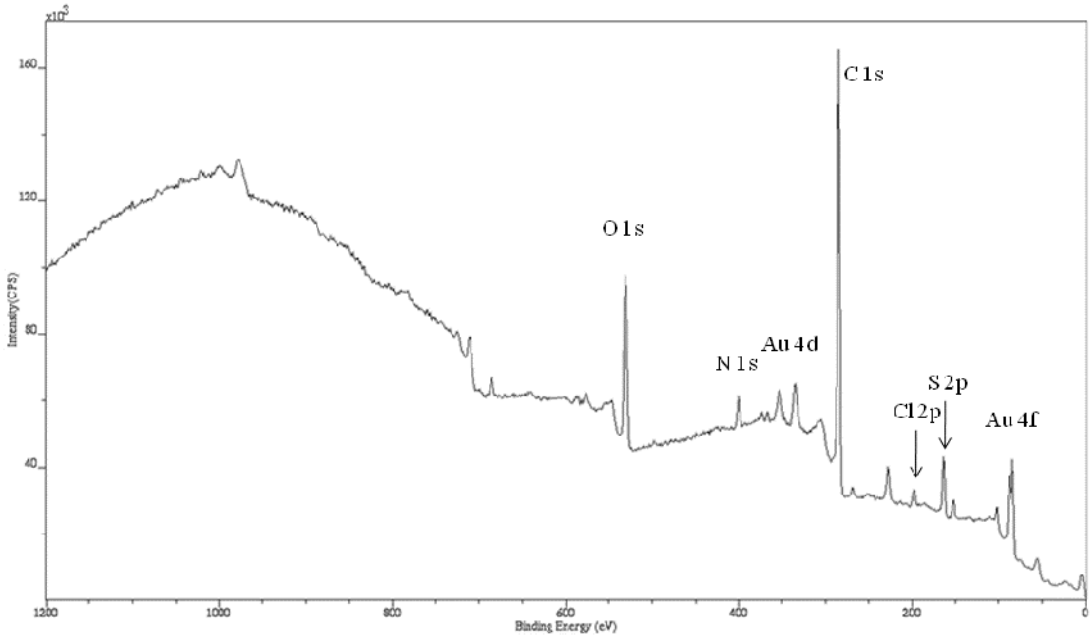

Figure 5.19. Survey XPS of bithiophene-substituted gold NHC thin film poly(**4**).

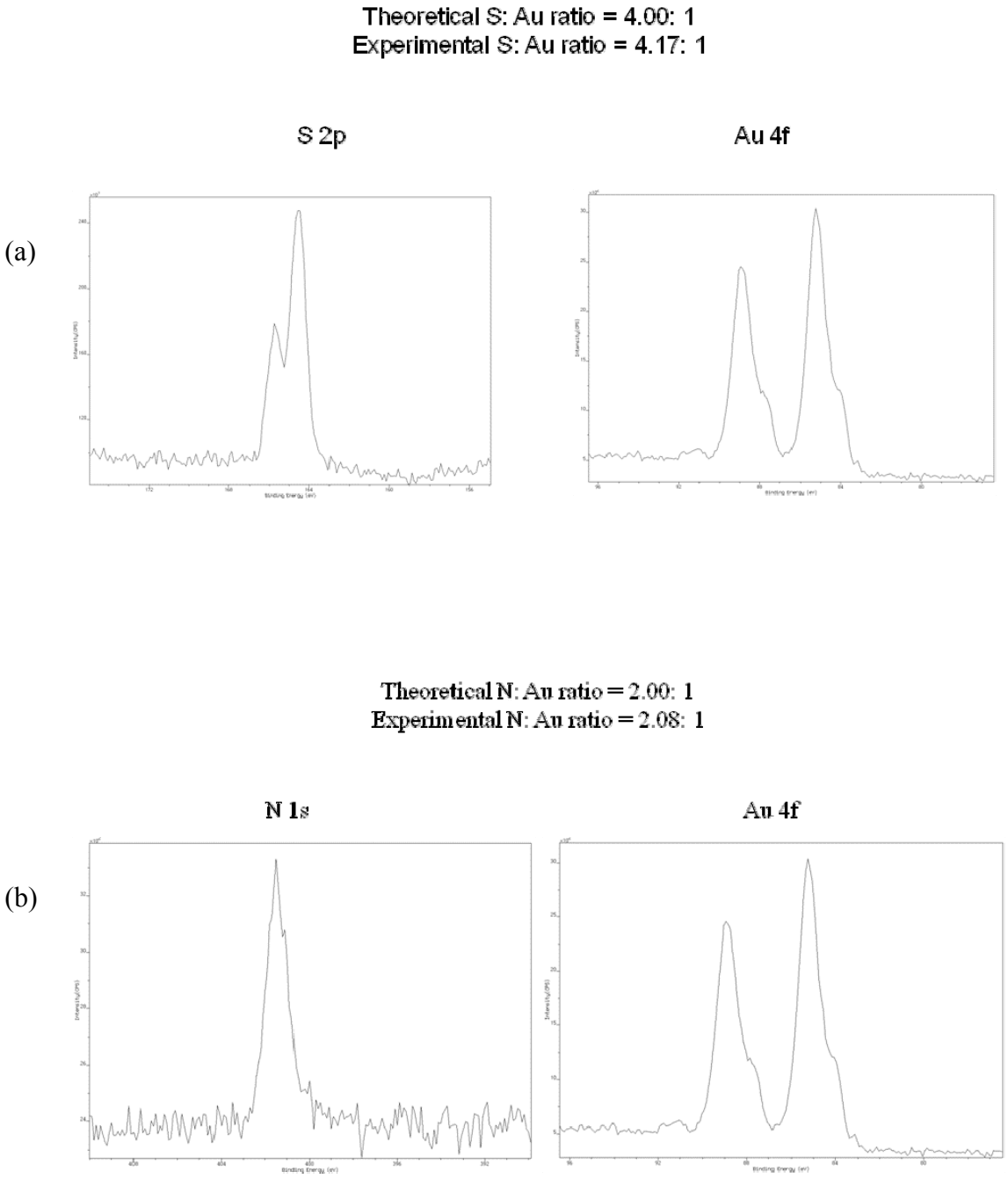

Figure 5.20. High-resolution XPS of bithiophene-substituted gold NHC thin film poly(**4**). (a) Ratio of sulfur 2p to gold 4f. (b) Ratio of nitrogen 1s to gold 4f.

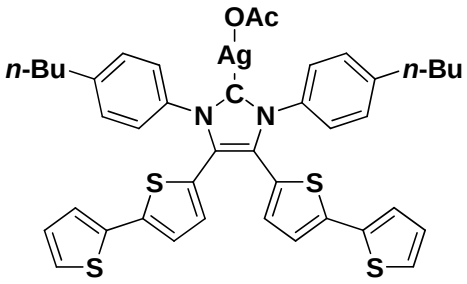

5

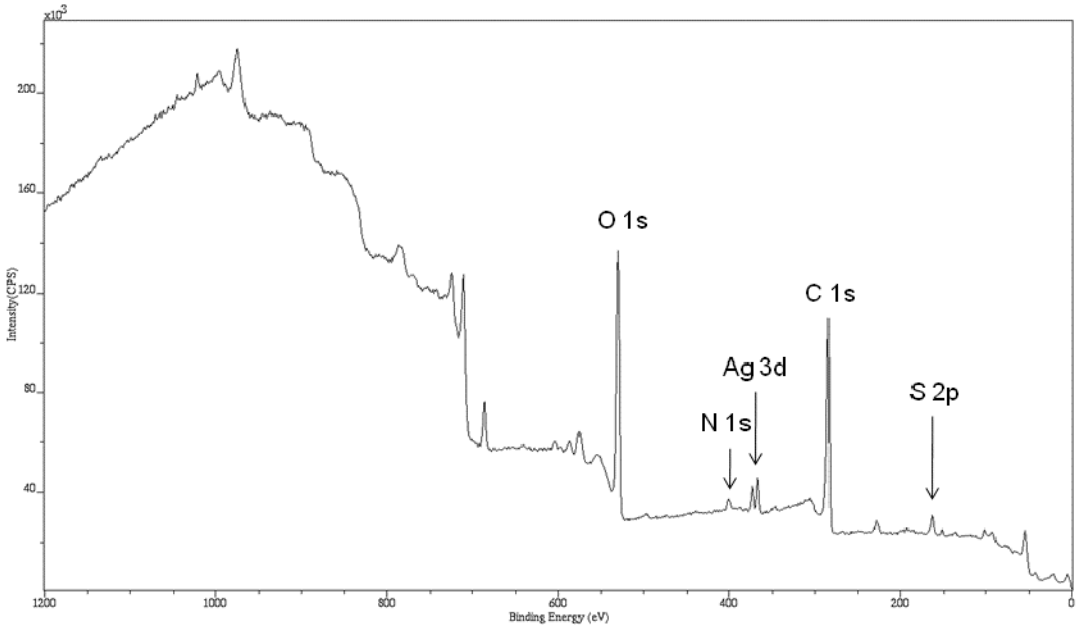

Figure 5.21. Survey XPS of bithiophene-substituted silver NHC thin film poly(**5**).

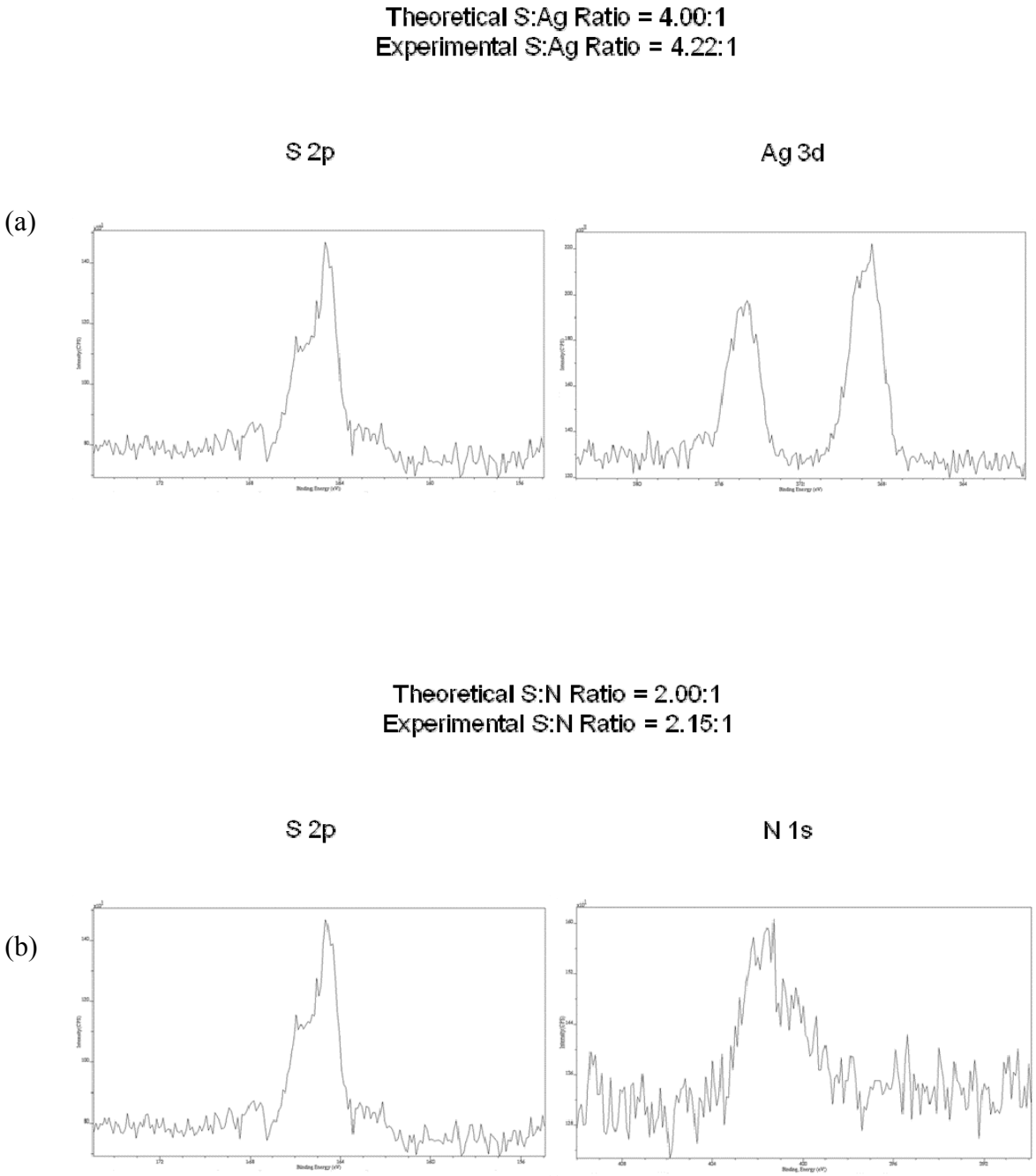

Figure 5.22. High-resolution XPS of bithiophene-substituted silver NHC thin film poly(**5**). (a) Ratio of sulfur 2p to silver 3d. (b) Ratio of sulfur 2p to nitrogen 1s.

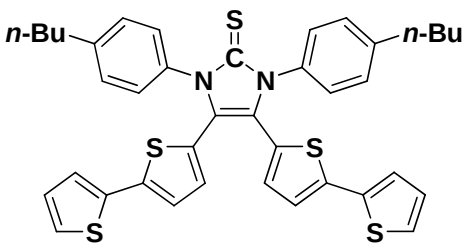

6

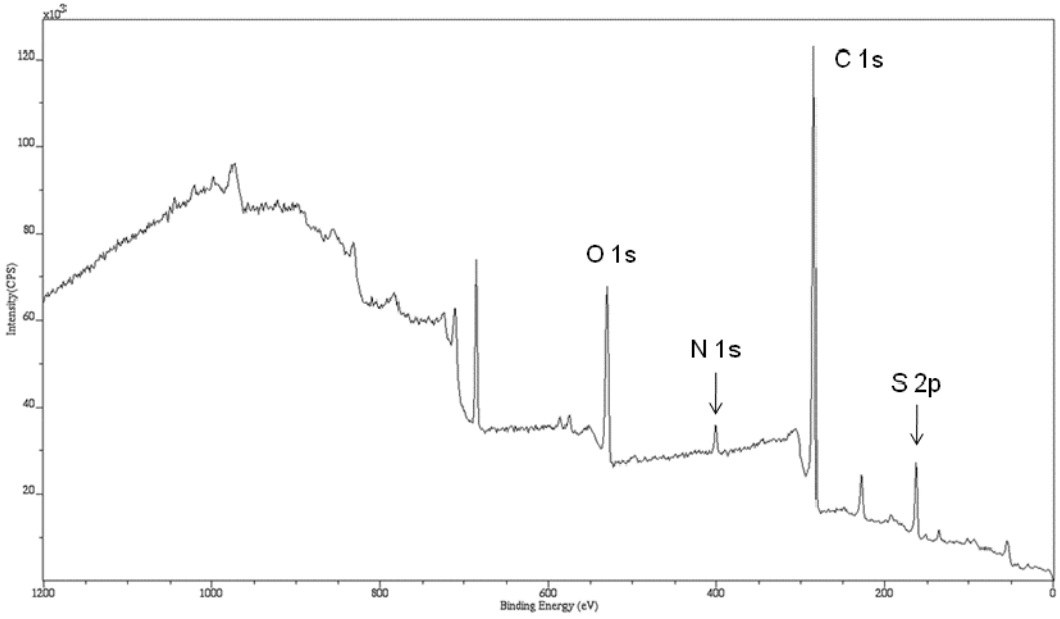

Figure 5.23. Survey XPS of bithiophene-substituted thione thin film poly(**6**).

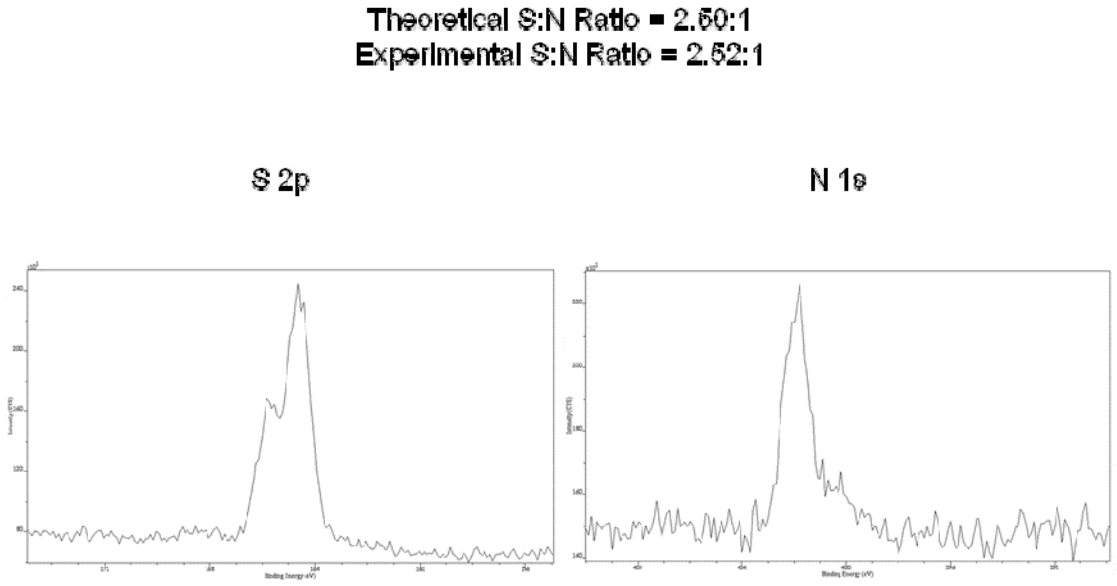

Figure 5.24. High-resolution XPS of bithiophene-substituted thione thin film poly(**6**). Ratio of sulfur 2p to nitrogen 1s.

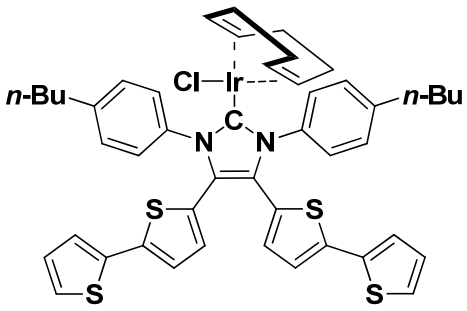

7

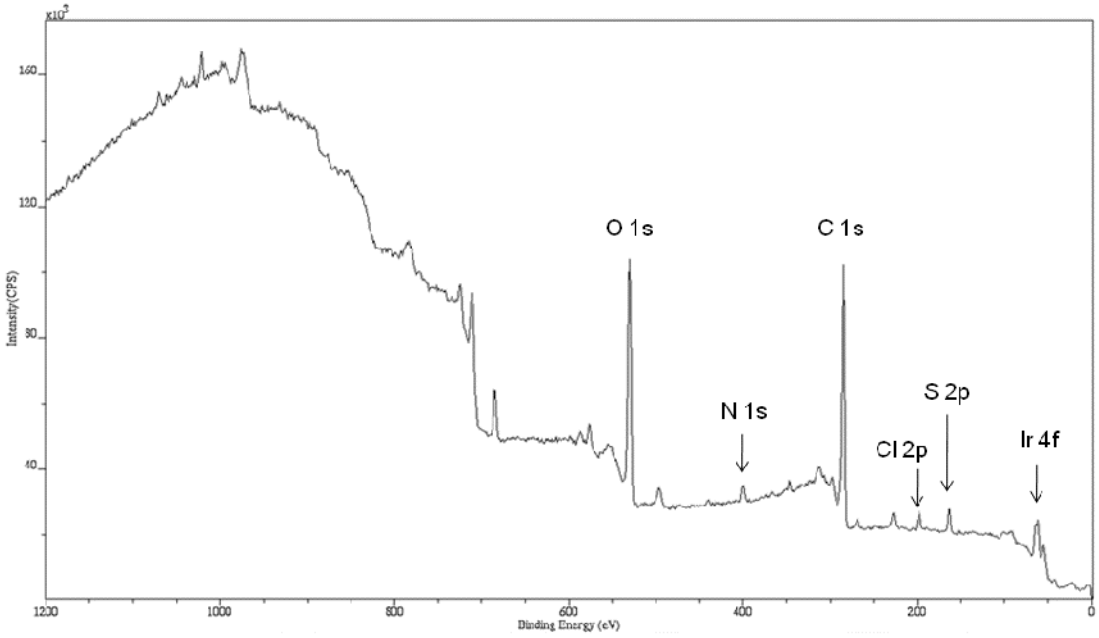

Figure 5.25. Survey XPS of bithiophene-substituted iridium NHC thin film poly(**7**).

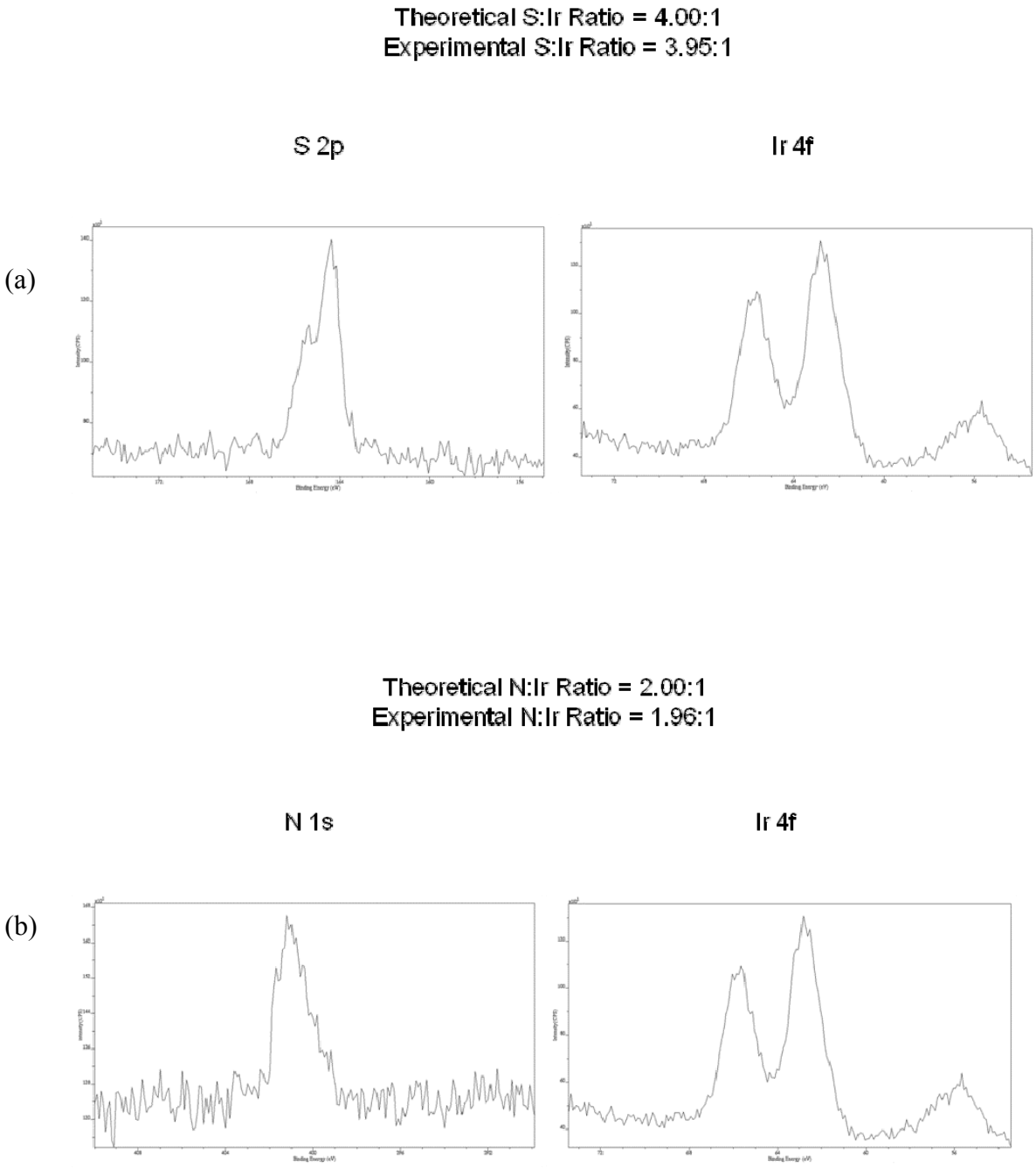

Figure 5.26. High-resolution XPS of bithiophene-substituted iridium NHC thin film poly(**7**). (a) Ratio of sulfur 2p to iridium 4f. (b) Ratio of nitrogen 1s to iridium 4f.

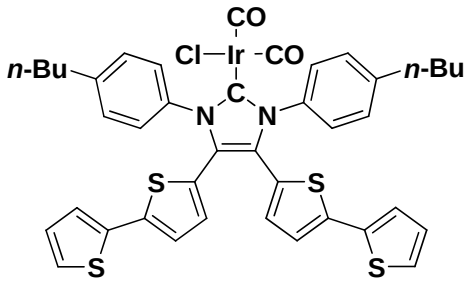

8

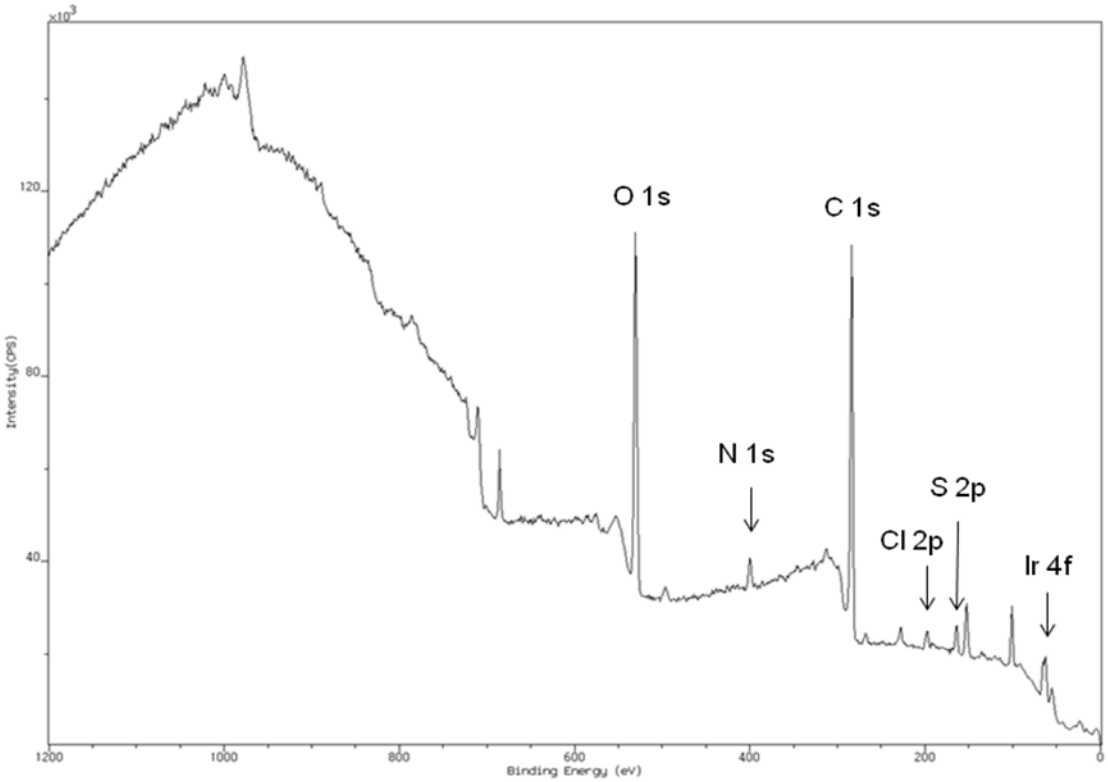

Figure 5.27. Survey XPS of bithiophene-substituted iridium NHC thin film poly(**8**).

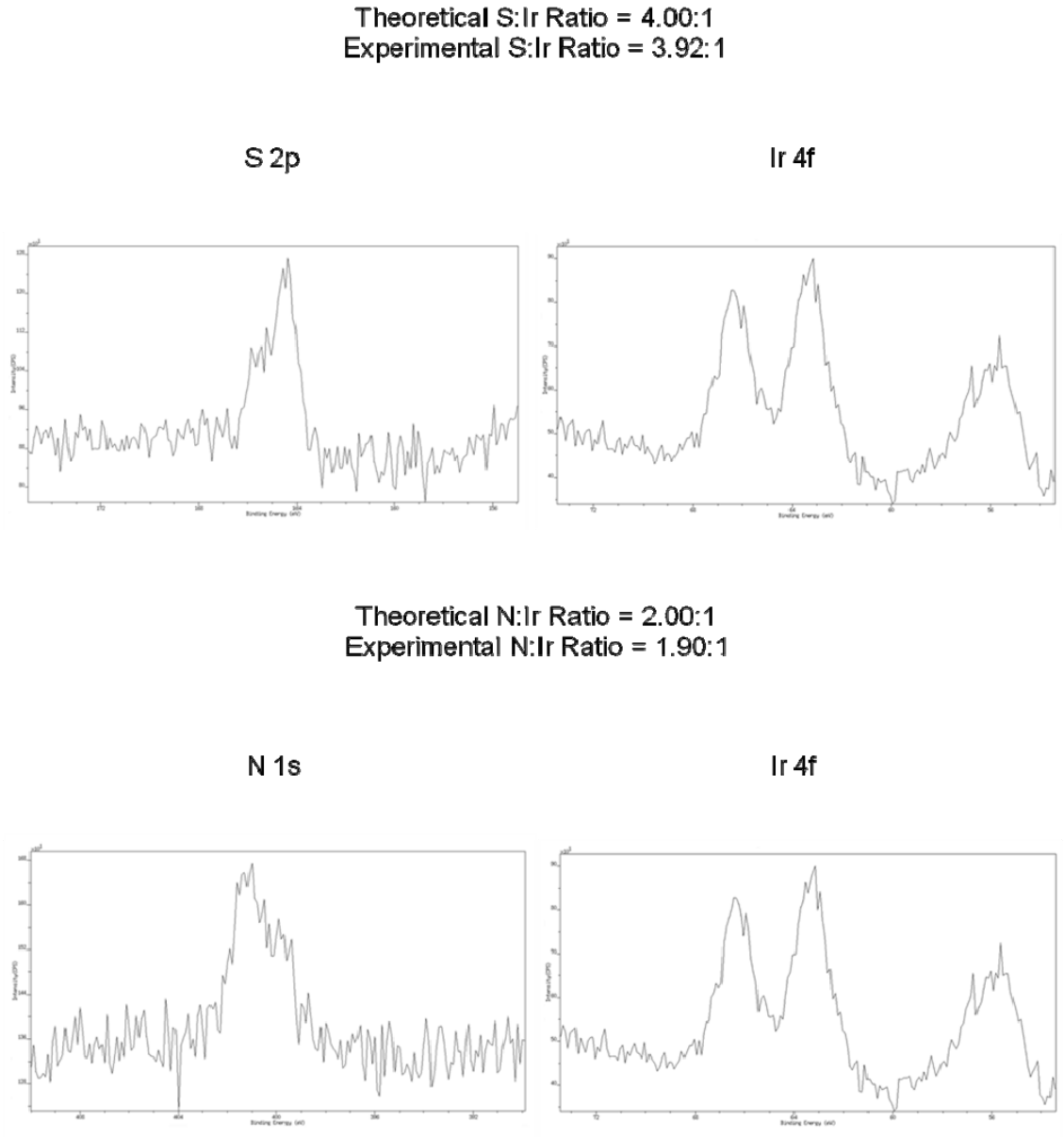

Figure 5.28. High-resolution XPS of bithiophene-substituted iridium NHC thin film poly(**8**). (a) Ratio of sulfur 2p to iridium 4f. (b) Ratio of nitrogen 1s to iridium 4f.

(a)

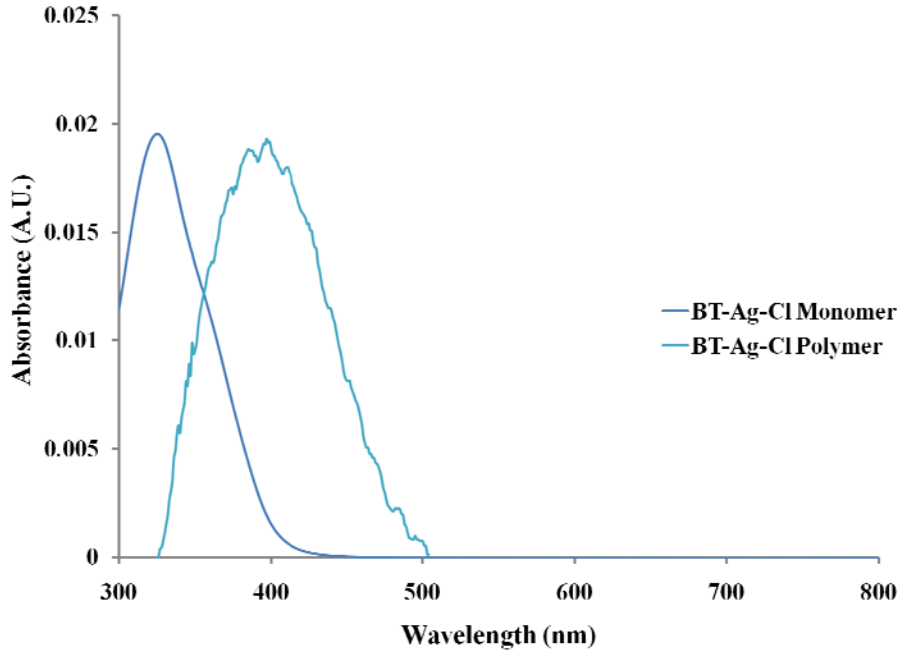

(b)

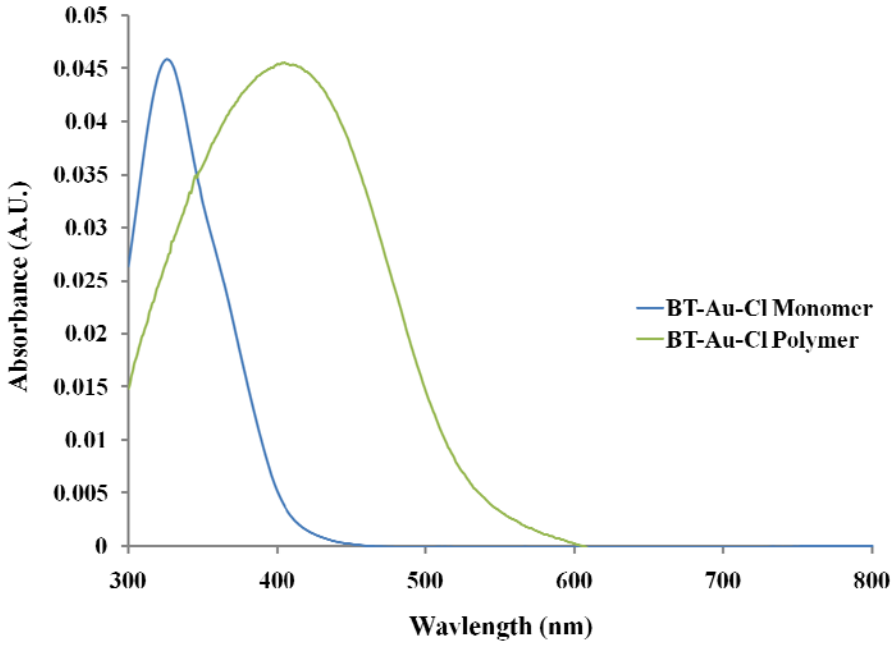

Figure 5.29. UV-vis profiles for compounds (a) **3** and poly(**3**) and (b) **4** and poly(**4**). The concentration of both monomers was 2 x 10^{-6} M in CH_2Cl_2 and the absorbance maxima were adjusted to the same absorbance as that of the corresponding thin film.

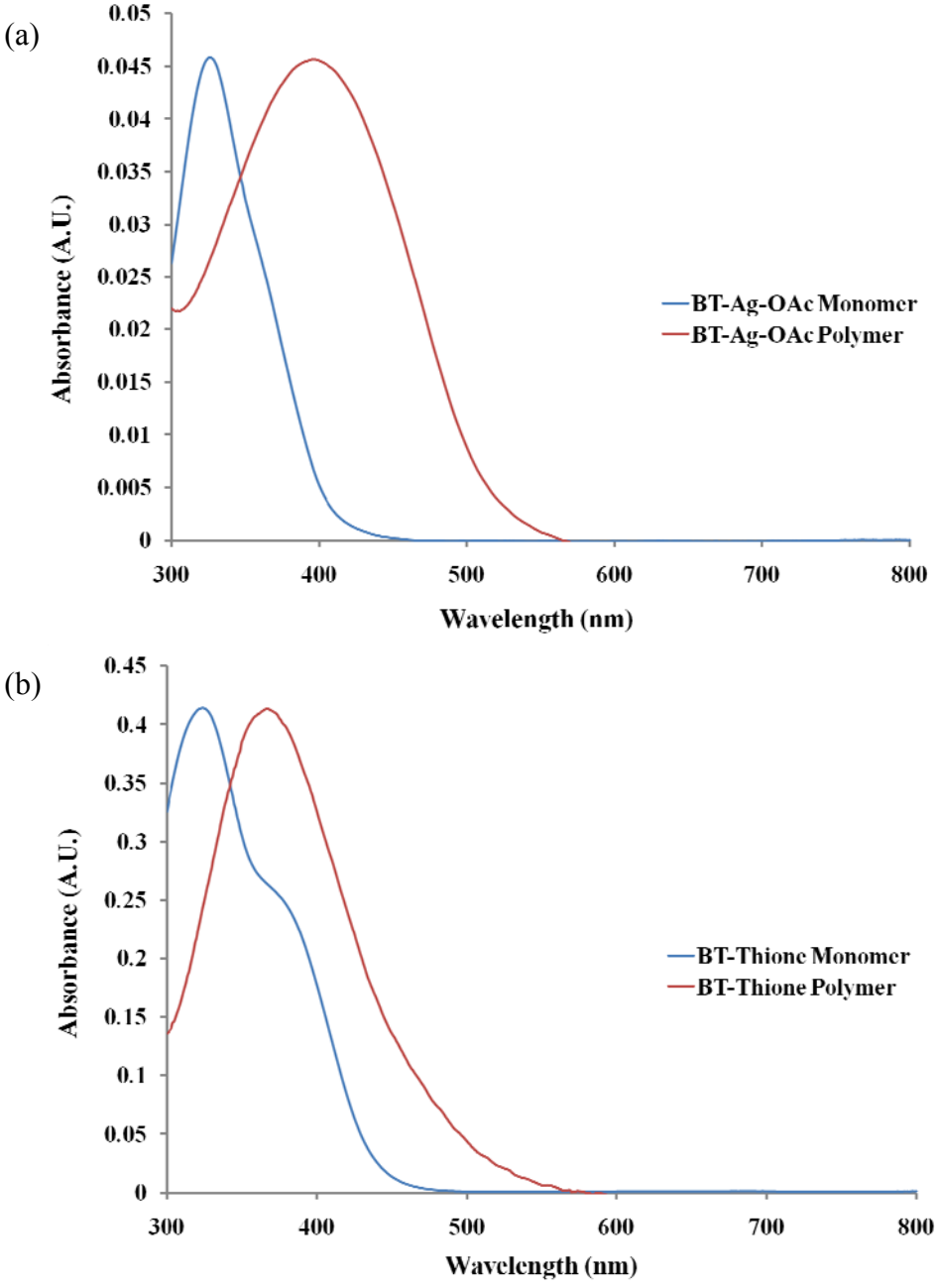

Figure 5.30. UV-vis profiles for compounds (a) **5** and poly(**5**) and (b) **6** and poly(**6**). The concentration of both monomers was 2 x 10^{-6} M in CH_2Cl_2 and the absorbance maxima were adjusted to the same absorbance as that of the corresponding thin film.

(a)

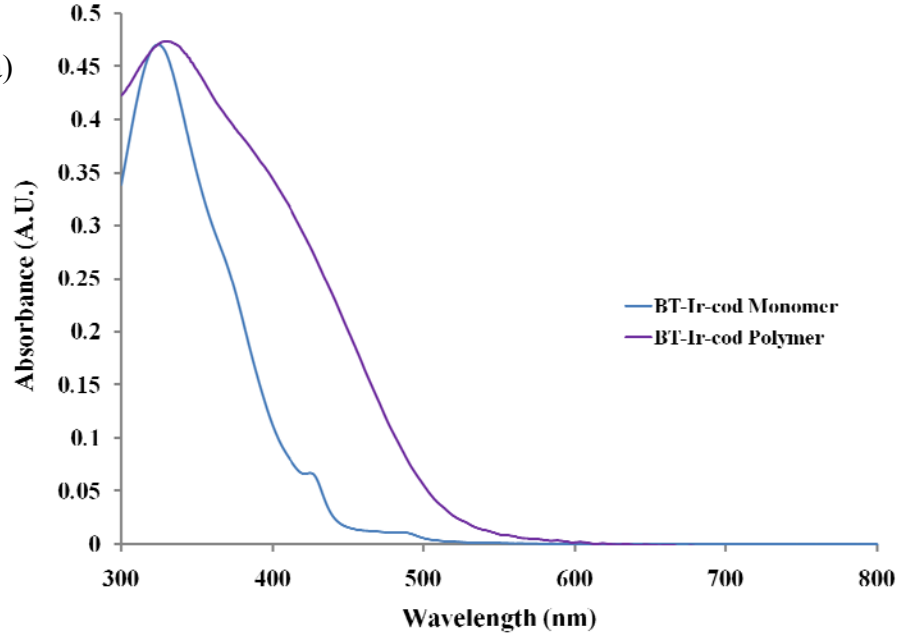

(b)

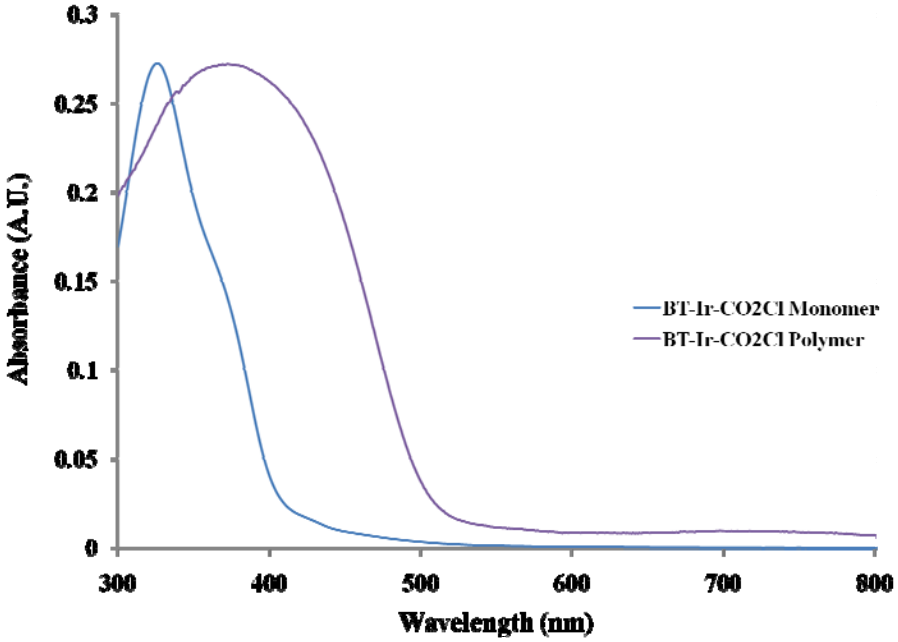

Figure 5.31. UV-vis profiles for compounds **7** and poly(**7**) and (b) **8** and poly(**8**). The concentration of both monomers was 2 x 10^{-6} M in CH_2Cl_2 and the absorbance maxima were adjusted to the same absorbance as that of the corresponding thin film.

(a)

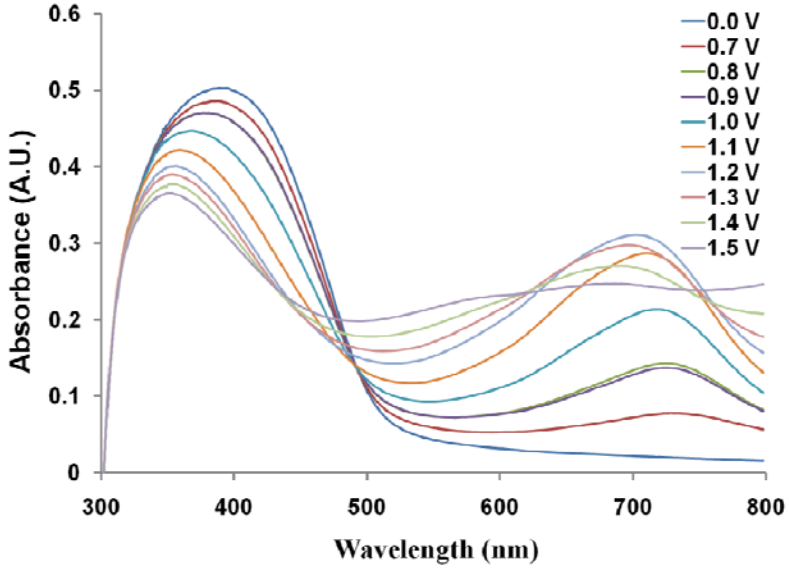

(b)

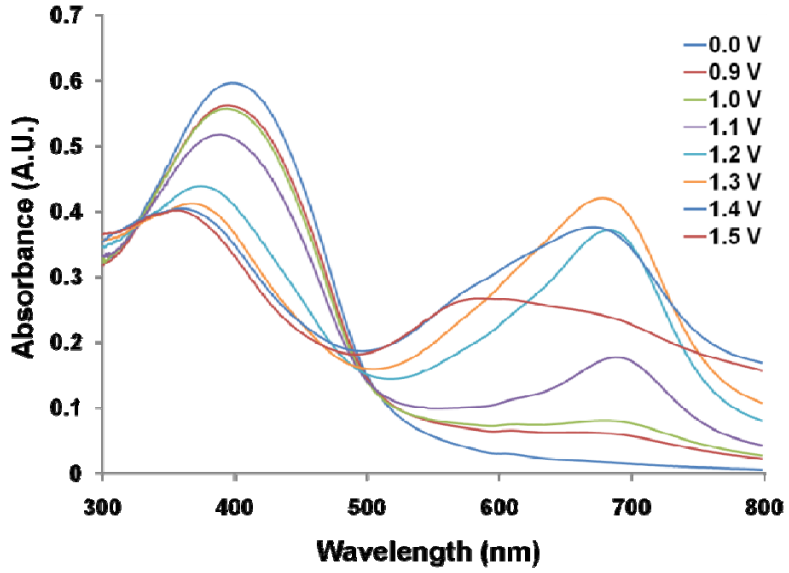

Figure 5.32. UV-vis overlay at different potentials of (a) Bithiophene-substituted gold NHC thin film poly(**4**). (b) Bithiophene-substituted silver NHC thin film poly(**5**). The spectra were acquired by depositing the thin film on an ITO slide, then assembling a three-electrode cell (0.1 M $TBAPF_6/CH_2Cl_2$) with the ITO slide serving as the working electrode. The potential was varied from 0.0 to 1.5 V.

(a)

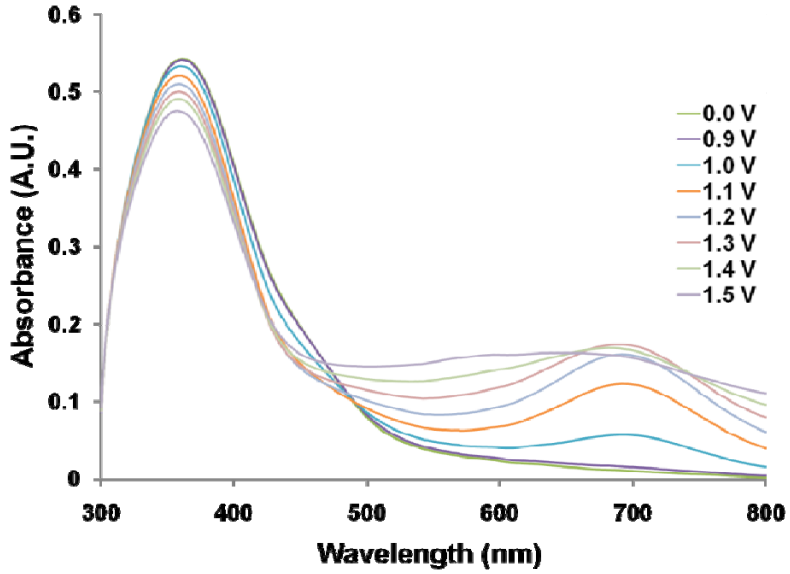

(b)

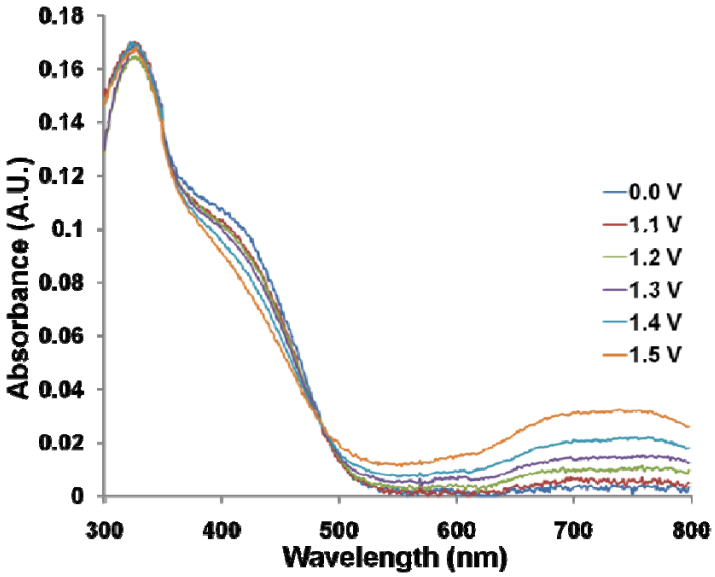

Figure 5.33. UV-vis overlay at different potentials of (a) Bithiophene-substituted thione poly(**6**). (b) Bithiophene-substituted iridium NHC thin film poly(**7**). The spectra were acquired by depositing the thin film on an ITO slide, then assembling a three-electrode cell (0.1 M $TBAPF_6/CH_2Cl_2$) with the ITO slide serving as the working electrode. The potential was varied from 0.0 to 1.5 V.

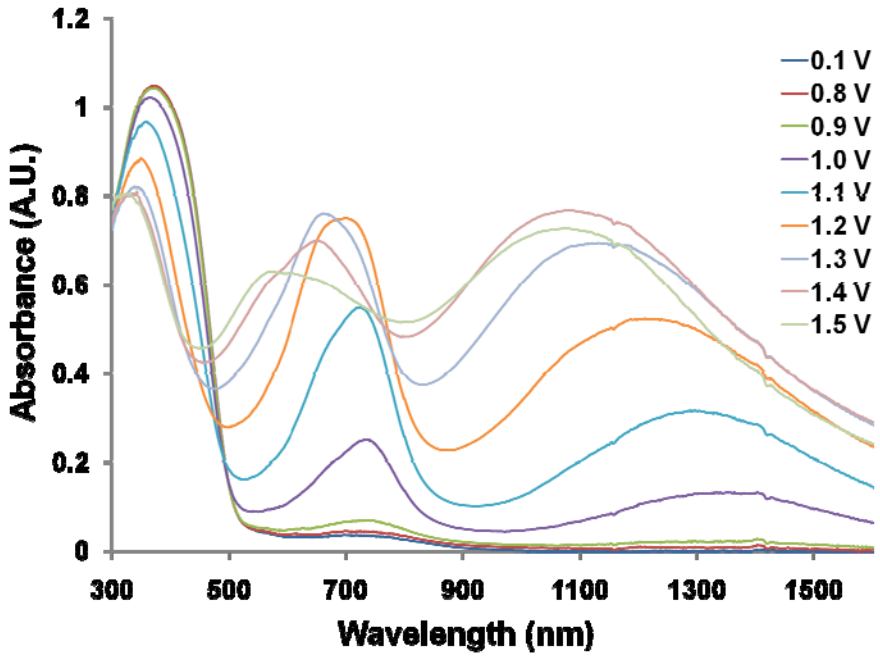

Figure 5.34. UV-vis overlay at different potentials of bithiophene-substituted iridium NHC thin film poly(**8**). The spectra were acquired by depositing the thin film on an ITO slide, then assembling a three-electrode cell (0.1 M $TBAPF_6/CH_2Cl_2$) with the ITO slide serving as the working electrode. The potential was varied from 0.0 to 1.5 V.

Table 5.2. Crystal data and structure refinement for **3**.

Empirical formula	C39 H36 Ag Cl N2 S4	
Formula weight	804.26	
Temperature	153(2) K	
Wavelength	0.71069 Å	
Crystal system	Monoclinic	
Space group	I2/a	
Unit cell dimensions	a = 32.472(2) Å	α= 90°.
	b = 6.2695(7) Å	β= 95.889(2)°.
	c = 36.429(2) Å	γ = 90°.
Volume	7377.2(10) $Å^3$	
Z	8	
Density (calculated)	1.448 Mg/m^3	
Absorption coefficient	0.876 mm^{-1}	
F(000)	3296	
Crystal size	0.32 x 0.16 x 0.04 mm	
Theta range for data collection	1.8 to 27.5°.	
Index ranges	-37<=h<=42, -8<=k<=6, -47<=l<=47	
Reflections collected	23951	
Independent reflections	8425 [R(int) = 0.0734]	
Completeness to theta = 27.49°	99.5 %	

Table 5.2 (continued). Crystal data and structure refinement for **3**.

Absorption correction	Semi-empirical from equivalents
Max. and min. transmission	0.966 and 0.806
Refinement method	Full-matrix least-squares on F^2
Data / restraints / parameters	8425 / 282 / 426
Goodness-of-fit on F^2	1.226
Final R indices [I>2sigma(I)]	R1 = 0.0593, wR2 = 0.1258
R indices (all data)	R1 = 0.1067, wR2 = 0.1431
Largest diff. peak and hole	1.362 and -1.060 e.$Å^{-3}$

Table 5.3. Selected bond lengths (Å) and angles (°) for **3**.

Bond Lengths (Å)	
Ag(1)-C(1)	2.087(3)
Ag(1)-Cl(1)	2.3470(10)
N(1)-C(2)	1.402(5)
N(1)-C(1)	1.351(5)
N(2)-C(3)	1.390(5)
N(2)-C(1)	1.357(5)
C(2)-C(3)	1.334(6)
Bond angles (°)	
C(1)-Ag(1)-Cl(1)	175.26(10)
N(1)-C(1)-Ag(1)	128.7(3)
N(2)-C(1)-Ag(1)	126.9(3)
C(1)-N(1)-C(2)	111.0(3)
C(2)-N(2)-C(3)	111.3(3)
N(1)-C(1)-N(2)	104.3(3)
C(3)-C(2)-N(1)	106.6(3)
C(2)-C(3)-N(2)	106.9(3)

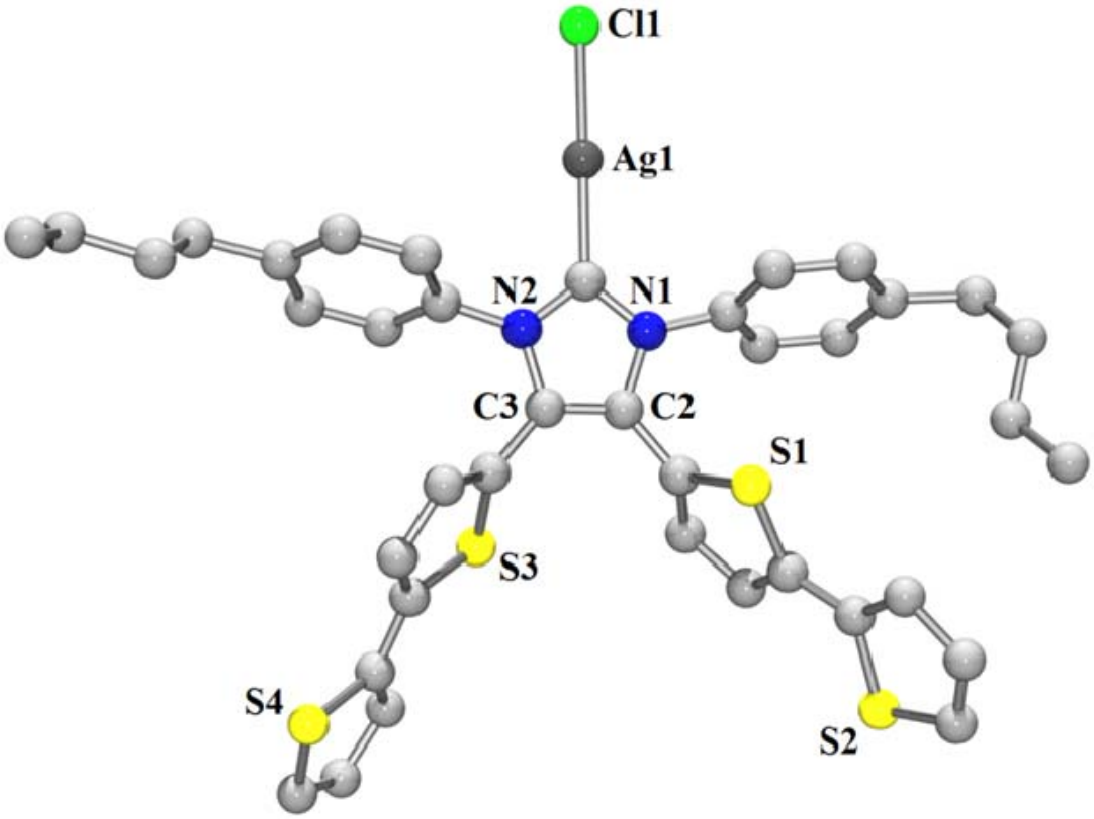

Figure 5.35. POV-Ray diagram of bithiophene-substituted silver NHC **3** drawn at 50% probability. All hydrogen atoms have been omitted for clarity.

Table 5.4. Crystal data and structure refinement for **5**.

Empirical formula	C45 H47 Ag N2 O3 S4	
Formula weight	899.96	
Temperature	233(2) K	
Wavelength	0.71069 Å	
Crystal system	Triclinic	
Space group	P-1	
Unit cell dimensions	a = 11.495(3) Å	α= 103.717(5)°.
	b = 13.381(3) Å	β= 92.327(6)°.
	c = 14.703(4) Å	γ = 101.007°.
Volume	2147.9(9) $Å^3$	
Z	2	
Density (calculated)	1.392 Mg/m^3	
Absorption coefficient	0.705 mm^{-1}	
F(000)	932	
Crystal size	0.24 x 0.13 x 0.09 mm	
Theta range for data collection	3.02 to 25.00°.	
Index ranges	-16<=h<=16, -31<=k<=31, -11<=l<=11	
Reflections collected	13683	
Independent reflections	7422 [R(int) = 0.0412]	
Completeness to theta = 25.00°	98.1 %	

Table 5.4 (continued). Crystal data and structure refinement for **5**.

Absorption correction	Semi-empirical from equivalents
Max. and min. transmission	0.940 and 0.600
Refinement method	Full-matrix least-squares on F^2
Data / restraints / parameters	7422 / 0 / 454
Goodness-of-fit on F^2	1.160
Final R indices [I>2sigma(I)]	R1 = 0.0756, wR2 = 0.0983
R indices (all data)	R1 = 0.1838, wR2 = 0.1986
Largest diff. peak and hole	1.182 and -0.568 e.$Å^{-3}$

Table 5.5. Selected bond lengths (Å) and angles (°) for **5**.

Bond Lengths (Å)	
Ag(1)-C(1)	2.085(6)
Ag(1)-O1(1)	2.196(5)
N(1)-C(2)	1.413(8)
N(1)-C(1)	1.366(7)
N(2)-C(3)	1.404(7)
N(2)-C(1)	1.350(8)
C(2)-C(3)	1.381(9)
Bond angles (°)	
C(1)-Ag(1)-O(1)	170.8(2)
N(1)-C(1)-Ag(1)	125.6(5)
N(2)-C(1)-Ag(1)	129.8(4)
C(1)-N(1)-C(2)	111.4(5)
C(1)-N(2)-C(3)	112.3(5)
N(1)-C(1)-N(2)	104.6(5)
C(3)-C(2)-N(1)	105.8(5)
C(2)-C(3)-N(2)	105.9(5)

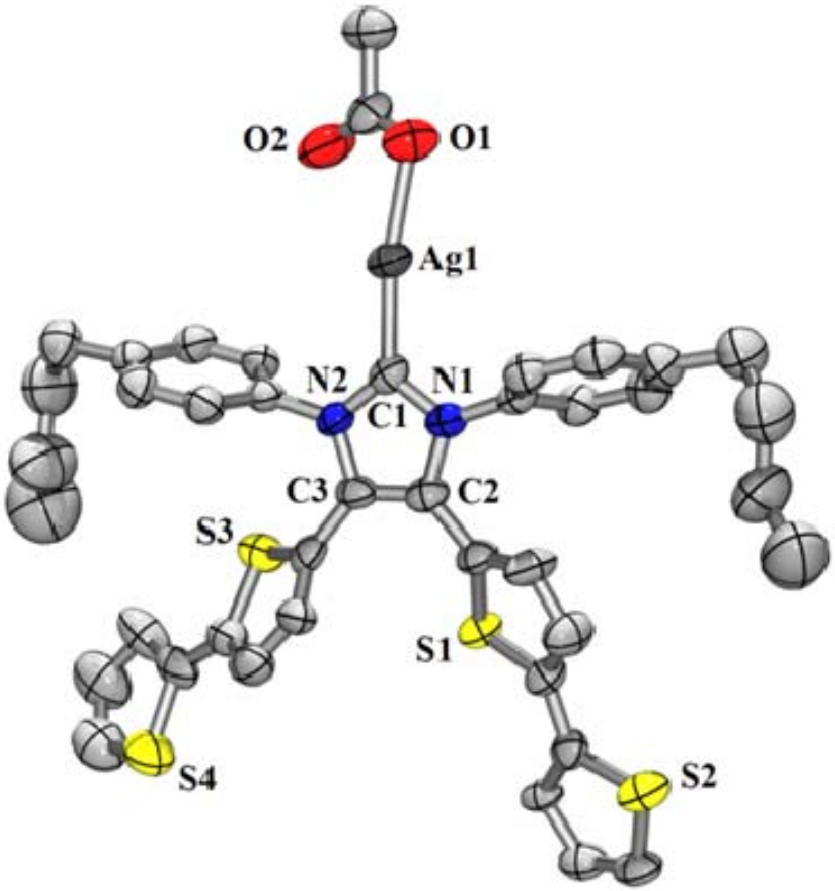

Figure 5.36. POV-Ray diagram of bithiophene-substituted silver NHC **5** drawn at 50% probability. One THF molecule was removed using SQUEEZE and all hydrogen atoms have been omitted for clarity.

Table 5.6. Crystal data and structure refinement for **6**.

Empirical formula	C39 H36 N2 S5	
Formula weight	693.00	
Temperature	233(2) K	
Wavelength	0.71069 Å	
Crystal system	Monoclinic	
Space group	P21/c	
Unit cell dimensions	a = 14.114(3) Å	α= 90°.
	b = 26.755(6) Å	β= 107.286(6)°.
	c = 10.005(2) Å	γ = 90°.
Volume	3607.4(13) $Å^3$	
Z	4	
Density (calculated)	1.276 Mg/m^3	
Absorption coefficient	0.352 mm^{-1}	
F(000)	1456	
Crystal size	0.46 x 0.06 x 0.02 mm	
Theta range for data collection	3.02 to 25.00°.	
Index ranges	-16<=h<=16, -31<=k<=31, -11<=l<=11	
Reflections collected	27560	
Independent reflections	6338 [R(int) = 0.1108]	
Completeness to theta = 25.00°	99.9 %	

Table 5.6 (continued). Crystal data and structure refinement for **6**.

Absorption correction	Semi-empirical from equivalents
Max. and min. transmission	0.990 and 0.531
Refinement method	Full-matrix least-squares on F^2
Data / restraints / parameters	6338 / 492 / 487
Goodness-of-fit on F^2	1.098
Final R indices [I>2sigma(I)]	R1 = 0.0678, wR2 = 0.1364
R indices (all data)	R1 = 0.1361, wR2 = 0.1622
Largest diff. peak and hole	0.340 and -0.362 e.$Å^{-3}$

Table 5.7. Selected bond lengths (Å) and angles (°) for **6**.

Bond Lengths (Å)	
S(1)-C(1)	1.665(4)
N(1)-C(3)	1.405(5)
N(1)-C(1)	1.374(5)
N(2)-C(2)	1.411(5)
N(2)-C(1)	1.379(5)
C(2)-C(3)	1.376(5)
Bond angles (°)	
N(1)-C(1)-(S)1	128.7(3)
N(2)-C(1)-(S)1	126.7(3)
N(1)-C(1)-N(2)	104.6(3)
C(1)-N(2)-C(2)	111.1(3)
C(1)-N(1)-C(3)	111.2(3)
C(3)-C(2)-N(2)	106.2(3)
C(2)-C(3)-N(1)	106.9(3)

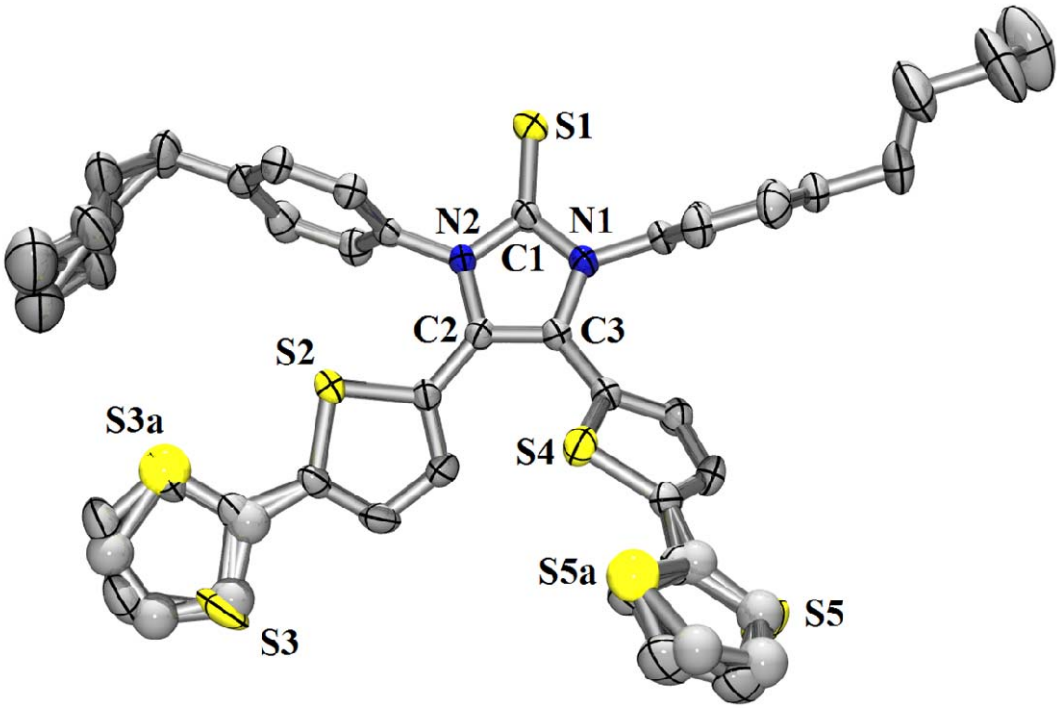

Figure 5.37. POV-Ray diagram of bithiophene-substituted thione **6** drawn at 50% probability. All hydrogen atoms have been omitted for clarity.

Chapter 6: Boron Di- and Tri-cations

6.1 Introduction

Neutral boron compounds have seen widespread application in the fields of asymmetric catalysis, olefin polymerization, and hydride anion abstraction.[1] The chemistry of the boron-group elements is dominated by their Lewis acidic properties and intrinsic electronic deficiency.[2] Boron cations have been shown to be even more reactive than their neutral boron analogues. Most of the boron cations that permeate the literature can be categorized into the three classes shown below in Figure 6.1. The boron cations investigated herein constitute a different class in which four ligands are bound to boron, but the charge on the complex is greater than +1.

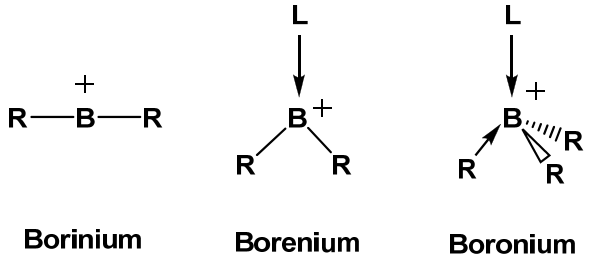

Figure 6.1. Nomenclature for reported boron monocations.

Boron di- and tri-cations were first reported in the literature over fifty years ago, but very little characterization data was provided at the time.[3] A more detailed study in this field was undertaken by Prasad and Singh,[4] who reported a complex consistent with the formula $[L_3BCl]Cl_2$ (L = amine). However, crystallographic data were not presented. Several publications appeared in the late 1960's that described monomeric boron di-cations,[5] including the informative study by Ryschkewitsch and co-workers that is detailed below.

Scheme 6.1. Reaction of amine-borane complex in various pyridine solvents.

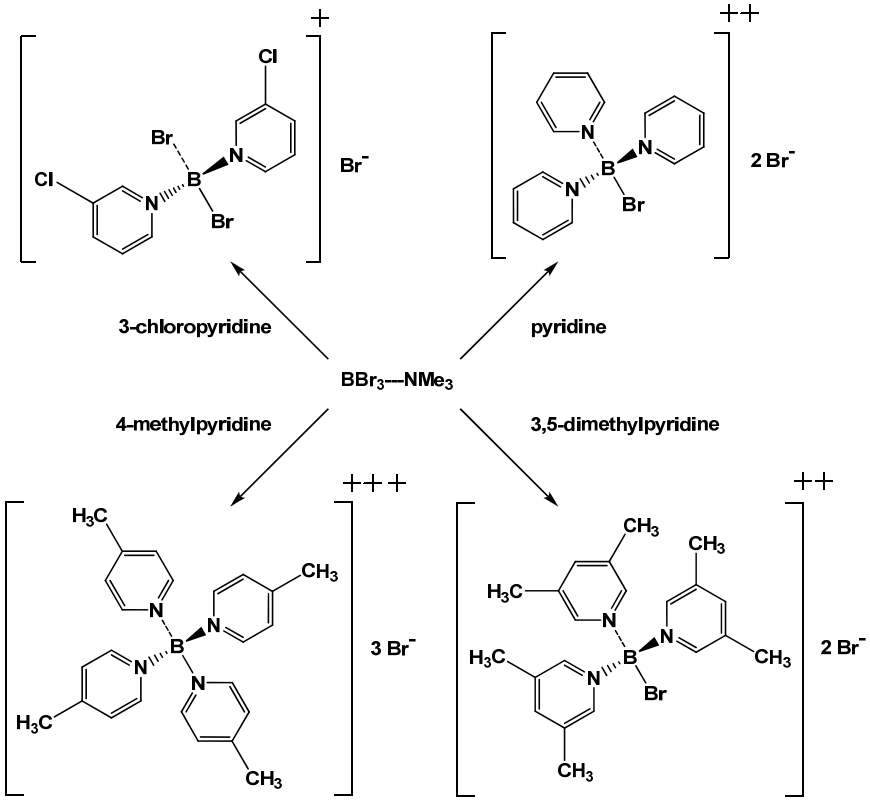

Scheme 6.1 shown above represents a summary of the boron cations that result from the displacement of the amine and bromides from the amine-borane complex Me_3NBBr_3. The labile trimethylamine is substituted first, followed by the bromide ligands. The most electron-donating pyridine, 4-methylpyridine (4-picoline), replaces all four ligands to form the first boron trication. Analogues such as 3,5-dimethylpyridine and pyridine displace only three out of four ligands thereby forming a boron dication in each case. Pyridine is slightly less nucleophillic than 4-picoline and this behavior underscores the delicate electronic effects in this system. The dimethylpyridine likely suffers from steric hindrance thereby precluding substitution at all four possible sites. The attachment of a chlorine atom at the 3-position of pyridine resulted in the binding of only two pyridines to the boron cation, which furnished a boron monocation. Anion exchange of

bromide with both PF_6^- and AsF_6^- was accomplished in quantitative yield. The compounds described by Ryschkewitsch and co-workers were characterized on the basis of elemental and titrimetric analysis. These methods of characterization however only averages of the atomic abundance and charge and therefore do not provide definitive prove the existence of the polycations reported. Since no structural characterization of data are available for any of the compounds listed in Scheme 6.1, this became the focus of the work detailed below.

6.2 Synthesis of boron cations

The synthesis of the trication tetrakis(4-methylpyridine)boron (III) bromide was successful and followed literature procedure detailed by Ryschkewitsch et al. that is illustrated in Scheme 6.2.[5] The reaction of boron tribromide with excess trimethylamine afforded the mildly air-sensitive donor-acceptor complex $Me_3N \rightarrow BBr_3$ in 56 % yield. The observed ^{11}B chemical shift of δ -4 ppm falls in the range anticipated for four-coordinate boron complexes.[6] Refluxing the donor-acceptor complex $Me_3N \rightarrow BBr_3$ in 4-methylpyridine (16 equivalents) for 4 hours in the presence of air, followed by work-up of the reaction mixture, afforded the air-stable, hygroscopic boron trication salt tetrakis(4-methylpyridine)boron (III) bromide in 83% yield. The boron trication salt was characterized on the basis of ^1H NMR, MS-CI and single crystal X-ray analysis.

Scheme 6.2. Synthesis of (4-methylpyridine)boron (III) bromide (**1**).

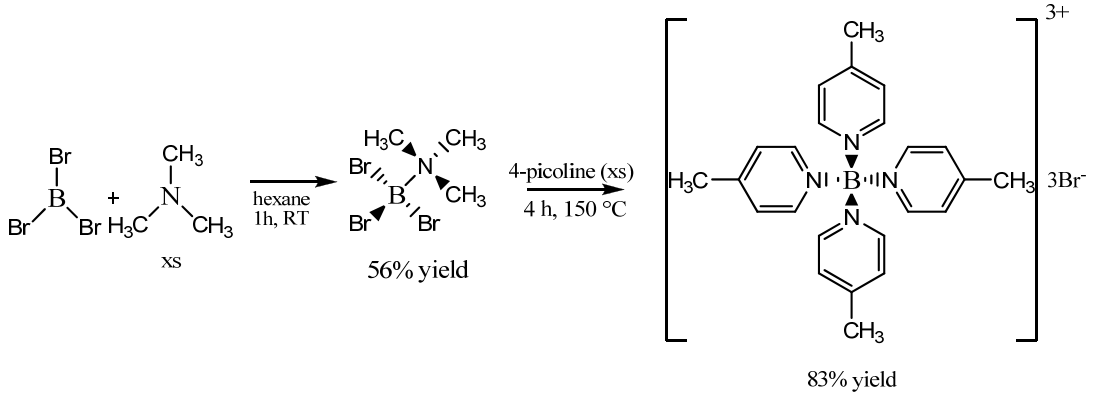

The synthesis of the dication salt bromotris(pyridine)boron (III) bromide was attempted next. An attractive feature of this dication is the presence of a potentially good leaving group as shown in Scheme 6.3. The donor-acceptor complex $Me_3N \rightarrow BBr_3$, the synthesis of which was described above, was then refluxed with 20 equivalents of pyridine for 4 hours as indicated in the literature.[5] These conditions resulted in the isolation of mostly starting material (confirmed by ^{11}B NMR) along with several unidentified products. Optimization of the reaction conditions showed that heating the reaction mixture for 16 hours affords two products with ^{11}B resonances at δ 9.5 ppm and 19 ppm. It was discovered that the resonance at δ 19 ppm corresponds to tetrakis(pyridine)boron (III) bromide, and that δ 9.5 ppm resonance is assignable to the desired dication. Recrystallizion of the latter compound was attempted by layering an ethanol solution of the product with pentane to yield the pure dication. However, the pure product could not be obtained in this fashion. Like the previously synthesized cation, the product is air stable but hygroscopic. The MS-CI spectrum of the product was somewhat convoluted and the molecular ion was not the base peak as would be expected for an ionic species. Furthermore, the assignment of peaks was further complicated by the fact that bromine and pyridine have similar formula weights. The assignment of peaks on the

basis of isotopic abundance was not possible due to the presence of several bromines and several pyridines. However, the identity of the cationic complex was established on the basis of high-resolution mass spectrometry. Salt metathesis of the resulting dication with three equivalents of $KBAr_f$ (BAr_f = tetrakis(pentaflurophenyl)borate) was attempted in an effort to produce a three-coordinate trication. However, only starting material could be recovered from the reaction mixture.

Scheme 6.3. Synthesis of bromotris(pyridine)boron (III) bromide (**2**).

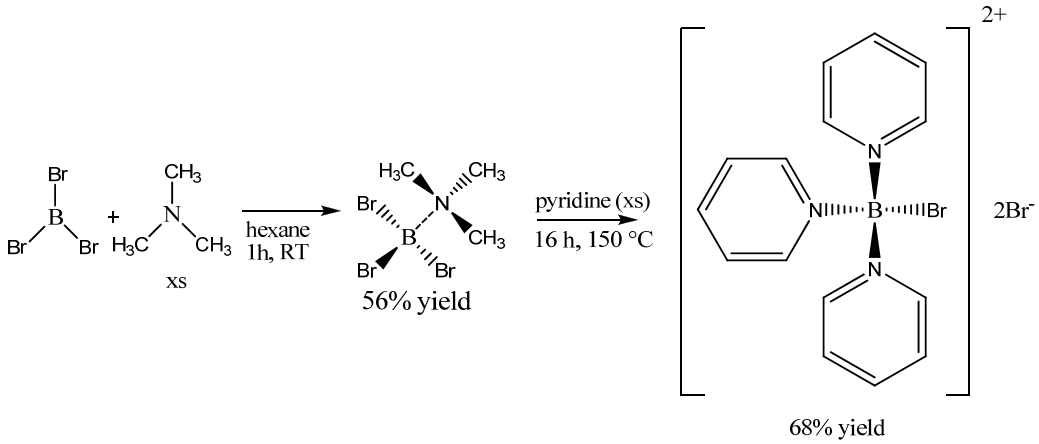

N-Heterocyclic carbenes (NHCs) represent an interesting class of compounds and the reactivity of carbenes with boron compounds is relatively unexplored. The reaction of four equivalents of the Kühn carbene,[7] 1,3,4,5-tetramethylimidazol-2-ylidene, with $Me_3N \rightarrow BBr_3$ was attempted by refluxing a toluene solution of these reagents. However, only starting materials were recovered. The Kühn carbene is significantly more nucleophilic than either of the pyridyl ligands used previously. The decision was made to use only four equivalents of carbene unlike previous reactions where 20 equivalents of pyridine or 4-methylpyridine had been employed. The smaller mass action effect could have contributed to the lack of reaction in the case of the Kühn carbene. Interaction of the

carbene with the bromide counteranions may have prevented coordination to the boron atom. Another factor is that the reactions that are performed with the pyridine analogues can be run at a much higher temperatures. Furthermore, the Kühn carbene might be too sterically demanding for nucleophilic attack at the small boron center.

6.3 Crystallography of boron cations

As stated in the introduction, none of the di- or tri-cations previously reported had been structurally authenticated. The trication shown below (Figure 6.2) represents the first crystallographic-characterized boron trication. The X-ray data collection and refinement details for the boron cations are displayed in Table 6.1 and a tabulation of the metrical parameters is provided in Table 6.2. The unit cell volume for **2** is much larger than those observed for other reported boron cation structures,[8] which in turn complicated the refinement of the data collection.

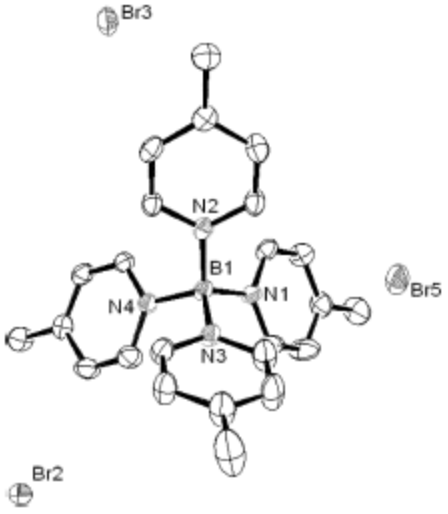

Figure 6.2. ORTEP diagram of **1** with 40% probability thermal ellipsoids. Hydrogen atoms have been omitted for clarity.

The precursor molecule **1** adopts a classical staggered geometry, which is the favored conformation for Lewis acid-base complexes of this type. The N → B donor-acceptor bond distances are consistent with those reported in the CCDC. The boron trication **2** possesses S_4 symmetry and the closest B-Br distance is 4.395 Å, which exceeds the sum of the van der Waals radii (3.52 Å).[9] Such a long distance between the two atoms indicates the absence of covalent interactions between boron and any of the bromide atoms, therefore confirming the tricationic nature of compound **2**.

Table 6.1. Selected crystal data, data collection and refinement parameters for BBr_3-NH_3 (**1**) and $[(4\text{-Mepy})_4B]Br_3$ (**2**).

	1	**2**
Formula	$C_3H_9BBr_3N$	$C_{24}H_{28}BBr_3N_4$
Formula weight	309.65	623.04
Crystal system	Monoclinic	Monoclinic
Space group	$P2_1/m$	$P2_1/c$
***a*/Å**	6.626(5)	17.704(4)
***b*/Å**	10.493(5)	17.664(4)
***c*/Å**	6.810(5)	18.891(4)
α/°	90.000(5)	90.0
β/°	115.211(5)	99.60(3)
γ/°	90.000(5)	90.0
Z	2	8
D_c/g cm^{-3}	2.401	1.421
***F*(000)**	288	2480
Crystal size/ nm	0.11 x 0.10 x 0.05	0.04 x 0.25 x 0.20
θ range/ °	3.31-27.38	1.86-27.50
Collected reflections	1631	23 787
Independent	1023	13 255
R_1 [$I > 2\sigma(I)$]	0.0364	0.0608
wR_2 (all data)	0.0925	0.169

Table 6.2. Metrical parameters for BBr_3-NH_3 (1) and $[(4\text{-Mepy})_4B]Br_3$ (2).

1		2	
Distances/ Å			
B(1)-N(1)	1.594(8)	B(1)-N(1)	1.564(6)
B(1)-Br(1)	2.002(7)	B(1)-N(2)	1.567(7)
B(1)-Br(2)	2.021(4)	B(1)-N(3)	1.562(6)
N(1)-C(1)	1.509(5)	B(1)-N(4)	1.564(6)
N(1)-C(2)	1.498(7)		
Bond angles/ °			
Br(1)-B(1)-Br(2)	109.2(2)	N(1)-B(1)-N(2)	111.1(4)
N(1)-B(1)-Br(1)	110.4(4)	N(1)-B(1)-N(3)	113.6(4)
N(1)-B(1)-Br(2)	110.3(2)	N(1)-B(1)-N(4)	104.3(4)
C(1)-N(1)-B(1)	110.9(3)	N(2)-B(1)-N(3)	105.1(4)
C(2)-N(1)-B(1)	112.3(5)	N(2)-B(1)-N(6)	113.2(4)
C(1)-N(1)-C(2)	107.5(3)	N(2)-B(1)-N(4)	109.8(4)

6.4 Conclusions

The structures of **1** and **2** proposed earlier by Ryschkewitsch on the basis of elemental and titrimetric analysis have been confirmed by X-ray crystallography. These structures are of interest due to the large charge buildup on boron and the potential use of highly charged boron compounds in asymmetric catalysis and olefin polymerization. Cationic structures are expected to be more reactive than their neutral analogues. Unfortunately, attempts to construct boron cations with labile leaving groups using the compounds described by Ryschkewitsch et al. were unsuccessful.

6.5 Experimental

General Considerations. Unless stated otherwise, all synthetic manipulations were carried out using standard Schlenk techniques under an argon atmosphere or in a Vacuum Atmospheres glove box under an atmosphere of purified argon. All reactions

were carried out in oven-dried glassware that had been cooled under vacuum. All solvents were purified under a nitrogen atmosphere from sodium benzophenone ketyl (toluene, hexane) and degassed prior to use. All non-dried solvents were reagent grade or better.

All NMR samples were prepared in a glove box under an atmosphere of purified argon. ^{1}H NMR spectra were recorded on a Varian 300 MHz instrument with chemical shifts reported relative to the residual solvent peak. ^{13}C NMR spectra were recorded on a Varian 300 MHz instrument with chemical shifts reported relative to the residual solvent peak. ^{11}B NMR spectra were recorded on a Varian 300 MHz instrument with shifts referenced to BF_3-OEt as the external standard. The starting materials BBr_3 in hexane solution (Aldrich), pyridine (Aldrich), and 4-methylpyridine (Acros) were used as received. The Kühn carbene 1,3,4,5-tetramethylimidazol-2-ylidene was prepared according to the literature procedure.[7]

Trimethylamine-boron tribromide (1). A 1.0 M solution of BBr_3 in hexane (20.0 mL, 20.0 mmol) was cannulated into a degassed Schlenk flask equipped with a magnetic stir bar. Trimethylamine gas was bubbled into the solution and the addition was continued until no more white solid formation was observed (approximately 1 hour). The hexanes were removed under reduced pressure, and the resulting white solid was collected under an inert atmosphere (3.45 g, 56% yield). The solid product was mildly air-sensitive. ^{1}H NMR ($CDCl_3$ 299.89 MHz) δ 3.18 (m 3H). ^{11}B NMR (BF_3-OEt_2, 96.22 MHz) δ -4.0.

Tetrakis(4-methylpyridine)boron(III) bromide (2). Trimethylamine-boron tribromide (1.53 g, 4.9 mmol) was added to a Schlenk flask equipped with a magnetic stir bar and a condenser. Degassed 4-methylpyridine (7.35 g, 79.0 mmol) was cannulated into the reaction vessel and the reaction mixture was refluxed under a constant argon flow for 4 hours. After filtration, the resulting solid was washed with benzene (50 mL) and diethyl

ether (50 mL) (83% yield). Recrystallization from EtOH at -40° C for 5 days produced purple crystals that were suitable for X-ray data collection. ^{1}H NMR. ^{1}H NMR (D_2O 299.89 MHz) δ 8.42 (b, 2H), δ 7.98 (d, 2H), δ 2.66 (s, 3H). MS-CI *m/z* (%) 620 (1) [M^+], 437 (44) [M^+-184], 357 (100) [M^+-264].

Bromotris(pyridine)boron(III) bromide (3). Trimethylamine-boron tribromide (0.60 g, 19.0 mmol) was added to a 100 mL Schlenk flask. Degassed pyridine was cannulated into the flask and the reaction mixture was refluxed for 16 hours under a constant argon flow. The reaction mixture was then cooled to room temperature, filtered and washed with dry pentane. The crude product was recrystallized from an ethanol solution that had been layered with pentane. (0.63 g, 68%) ^{1}H NMR (CD_3OD 299.89 MHz) δ 9.06 (b, 2H), δ 8.85 (m, 1H), δ 8.26 (t, 2H). ^{11}B NMR (BF_3-OEt_2, 96.22 MHz) δ 8.5. MS-CI *m/z* (%) 487 (46) [M^+], 408 (100) [M^+- Br], 328 (68) [M^+- 2Br].

Summary and Future Directions

The early work described in this dissertation was focused on advancing the diimine chemistry which has been studied extensively in our lab. The specific aim was to develop polymeric versions of this ligand class. A polymerizable thiophene-substituted diimine was successfully synthesized, but found to be unsuitable for metal chelation and polymerization. An investigation was undertaken to examine the aldimine coupling, which was the key transformation responsible for the construction of the desired thiophene diimine scaffold. This study revealed the importance of using a highly-concentrated reaction mixture. Also, it was found that replacement of the cation of the catalyst resulted in the dimerization of aldimines in green solvents.

Modification of the diimine scaffold resulted in the first polymerizable NHC metal complex in which the carbene functionality is orthogonal to the polymer main-chain. This reaction pathway results in an overall yield of about 60%, which represents a vast improvement over most polymerizable scaffolds that have been described in the literature. A series of these metal complexes was synthesized and successfully polymerized. The identity of the metal and ancillary ligand were found to affect the stability and electrochromic properties of the resulting thin films.

The placement of the carbene functionalities in an orthogonal direction with respect to the polymer main chain resulted in spectroscopic properties unprecadented for this class of polycarbenes. It is anticipated that future work will focus on the construction of orthogonally-directed NHCs that can be synthesized in bulk quantities. Monomeric NHCs with similar architectures have been shown to catalyze a variety of substrates. It is plausible that the proposed new poly(NHCs) will also possess catalytic activity. The extent of the catalytic activity could then be compared to the monomer and investigated for other advantages it might possess in comparison with monomeric systems.

Appendix

NMR spectra for compounds of interest.

4-f-thiodiimine
CDCl3, TMS
Adam Powell
abp_46a

Pulse Sequence: s2pul
Solvent: CDCl3
Ambient temperature
UNITYplus-300 "nmr2"

Relax. delay 1.000 sec
Pulse 15.0 degrees
Acq. time 3.813 sec
Width 4196.4 Hz
28 repetitions
OBSERVE H1, 300.1390526 MHz
DATA PROCESSING
Line broadening 0.1 Hz
FT size 32768
Total time 2 min, 34 sec

Chapter 2

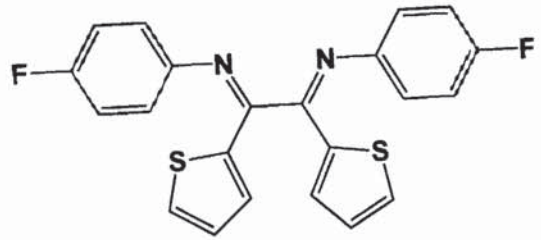

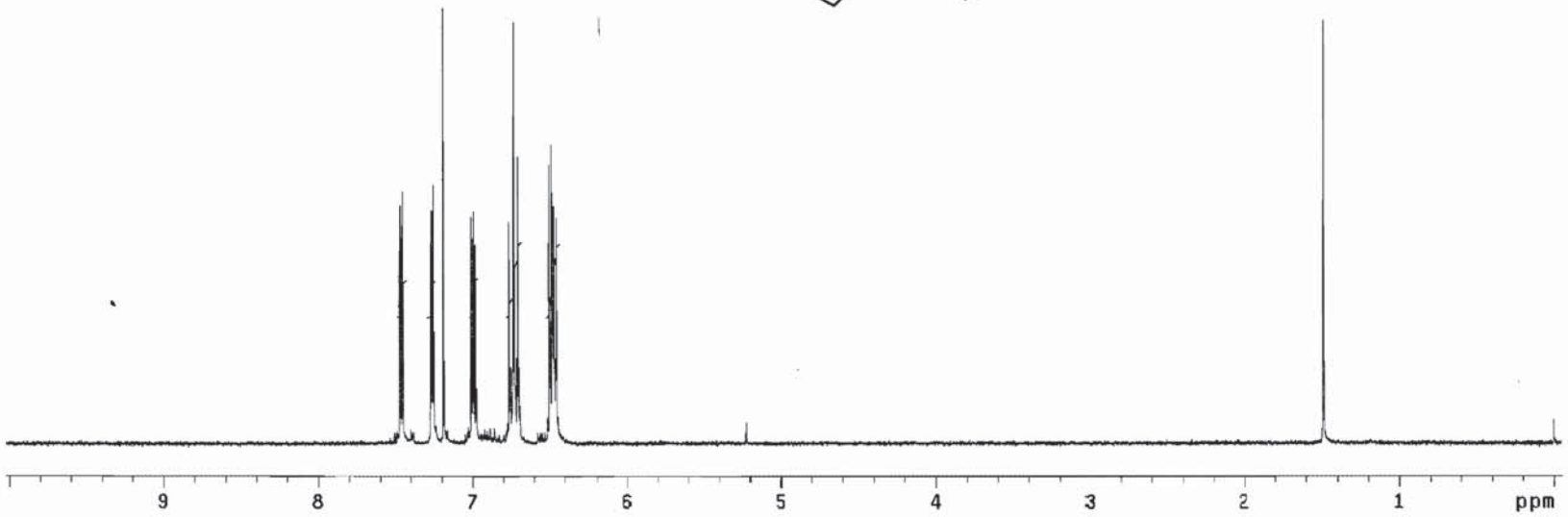

p-F diimine
CDCl3
Adam Powell
abp_49a

Pulse Sequence: s2pul

Solvent: CDCl3
Ambient temperature
File: abp_49a
INOVA-500 "u5b"

Relax. delay 2.000 sec
Pulse 36.0 degrees
Acq. time 1.777 sec
Width 18009.9 Hz
96 repetitions
OBSERVE C13, 75.4700236 MHz
DECOUPLE H1, 300.1409259 MHz
Power 40 dB
continuously on
WALTZ-16 modulated
Single precision data
DATA PROCESSING
Line broadening 1.0 Hz
FT size 65536
Total time 1 hr, 4 min, 36 sec

INDEX	FREQUENCY	PPM	HEIGHT
1	12230.189	162.054	18.7
2	11985.608	158.813	16.8
3	11871.837	157.305	24.3
4	11873.486	157.327	24.5
5	10897.363	144.393	33.1
6	10894.615	144.357	28.2
7	10882.524	144.197	42.6
8	9959.714	131.969	111.2
9	9892.660	131.081	111.4
10	9671.714	128.153	114.4
11	9227.072	122.261	108.3
12	9218.828	122.152	108.3
13	8708.232	115.387	115.8
14	8685.698	115.088	112.5
15	5843.070	77.422	86.5
16	5811.192	77.000	86.6
17	5778.764	76.570	82.7

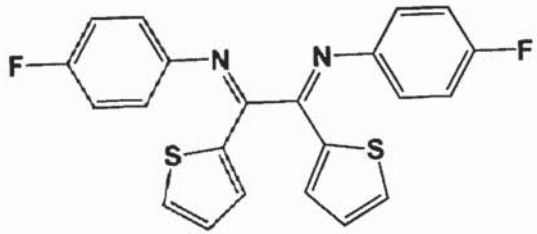

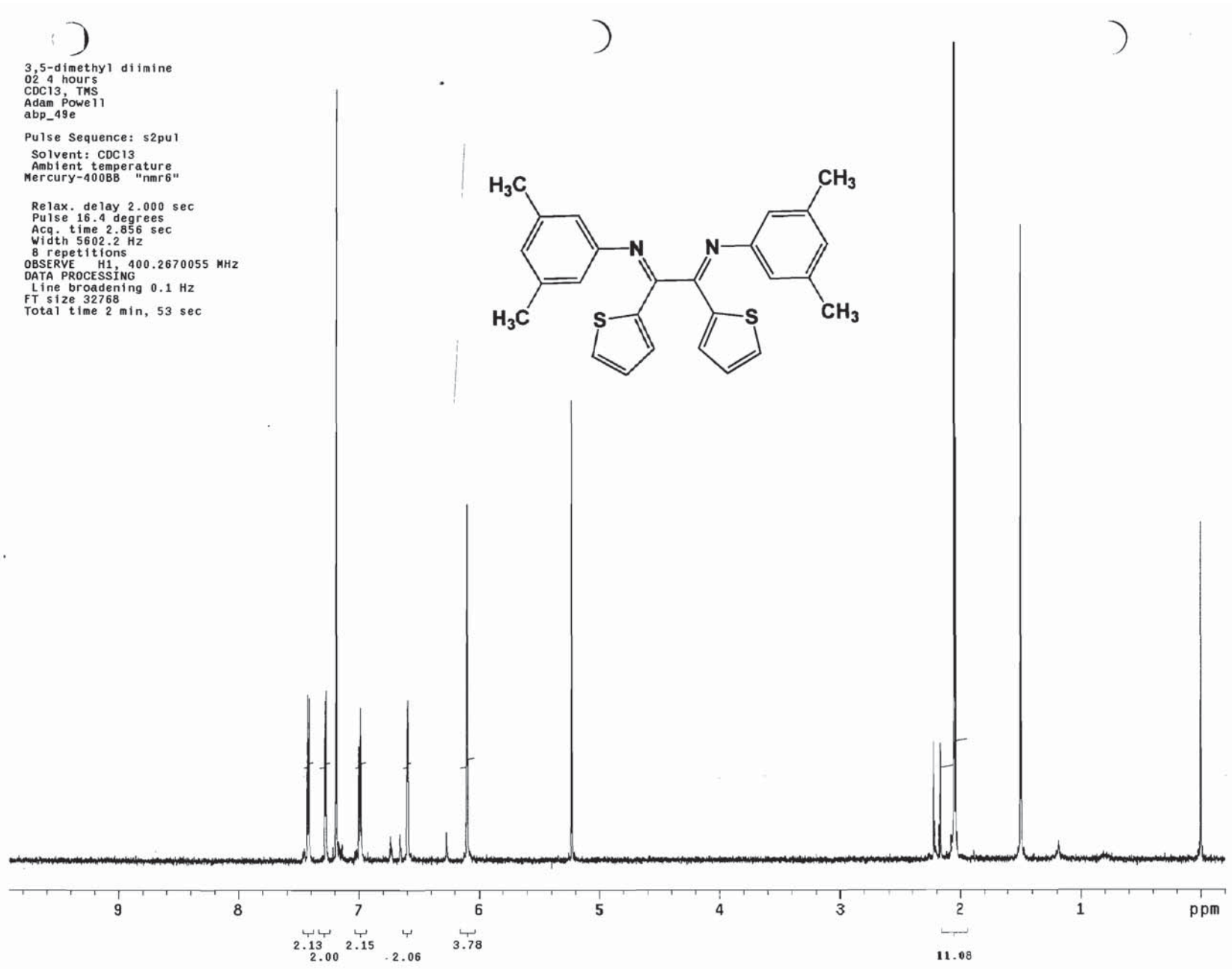
3,5-dimethyl diimine
02 4 hours
CDCl3, TMS
Adam Powell
abp_49e
Pulse Sequence: s2pul
Solvent: CDCl3
Ambient temperature
Mercury-400BB "nmr6"
Relax. delay 2.000 sec
Pulse 16.4 degrees
Acq. time 2.856 sec
Width 5602.2 Hz
8 repetitions
OBSERVE H1, 400.2670055 MHz
DATA PROCESSING
Line broadening 0.1 Hz
FT size 32768
Total time 2 min, 53 sec
H3C
CH3
N
N
S
S
H3C
CH3
9
8
7
6
5
4
3
2
1
ppm
2.13
2.00
2.15
2.06
3.78
11.08

3,5-dimethyl Ligand
CDCl3
Adam Powell
abp_49e

Pulse Sequence: s2pul
Solvent: CDCl3
Ambient temperature
UNITYplus-300 "nmr2"

Relax. delay 2.000 sec
Pulse 36.0 degrees
Acq. time 1.777 sec
Width 18009.9 Hz
96 repetitions
OBSERVE C13, 75.4700222 MHz
DECOUPLE H1, 300.1409259 MHz
Power 40 dB
continuously on
WALTZ-16 modulated
Single precision data
DATA PROCESSING
Line broadening 1.0 Hz
FT size 65536
Total time 1 hr, 4 min, 38 sec

INDEX	FREQUENCY	PPM	HEIGHT
1	11868.175	157.257	37.0
2	11211.360	148.554	50.2
3	10933.245	144.869	39.0
4	10391.304	137.688	121.0
5	9928.511	131.556	87.1
6	9842.768	130.420	82.0
7	9651.495	127.885	95.5
8	9552.011	126.567	83.7
9	8919.930	118.192	166.8
10	5843.071	77.422	222.2
11	5811.192	77.000	230.9
12	5779.313	76.578	224.1
13	1598.236	21.177	162.5

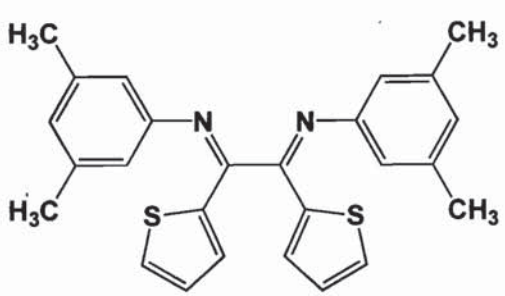

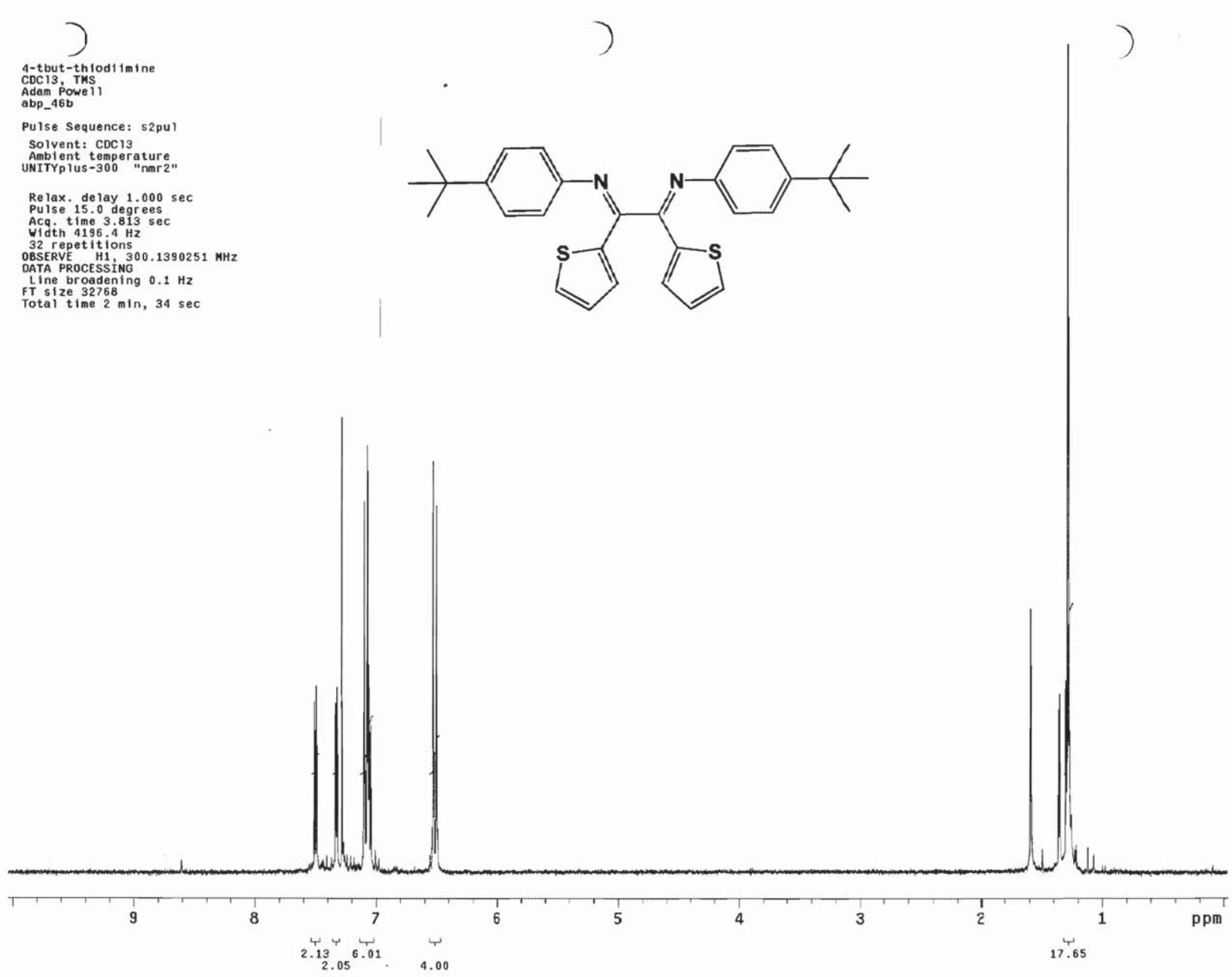
4-tbut-thiodiimine
CDCl3, TMS
Adam Powell
abp_46b
Pulse Sequence: s2pul
Solvent: CDCl3
Ambient temperature
UNITYplus-300 "nmr2"
Relax. delay 1.000 sec
Pulse 15.0 degrees
Acq. time 3.813 sec
Width 4196.4 Hz
32 repetitions
OBSERVE H1, 300.1390251 MHz
DATA PROCESSING
Line broadening 0.1 Hz
FT size 32768
Total time 2 min, 34 sec
N
N
S
S
9
8
7
6
5
4
3
2
1
ppm
2.13
2.05
6.01
4.00
17.65

t-butyl Ligand
CDCl3
Adam Powell
abp_49b

Pulse Sequence: s2pul
 Solvent: CDCl3
 Ambient temperature
File: abp_49b
INOVA-500 "nmrfred"

 Relax. delay 2.000 sec
 Pulse 36.0 degrees
 Acq. time 1.777 sec
 Width 18009.9 Hz
 96 repetitions
OBSERVE C13, 75.4700216 MHz
DECOUPLE H1, 300.1409259 MHz
 Power 40 dB
 continuously on
 WALTZ-16 modulated
Single precision data
DATA PROCESSING
 Line broadening 1.0 Hz
FT size 65536
Total time 1 hr, 4 min, 36 sec

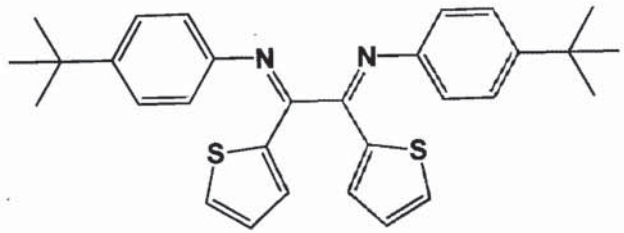

INDEX	FREQUENCY	PPM	HEIGHT
1	11821.068	156.633	16.0
2	11180.762	148.148	24.1
3	10996.090	145.701	22.2
4	10929.037	144.813	19.8
5	9916.639	131.398	35.6
6	9827.051	130.211	34.5
7	9657.219	127.961	36.3
8	9446.166	125.164	74.7
9	9081.219	120.329	70.2
10	5843.415	77.427	76.8
11	5811.537	77.005	76.4
12	5779.659	76.582	75.5
13	2590.222	34.321	25.7
14	2364.329	31.328	115.8

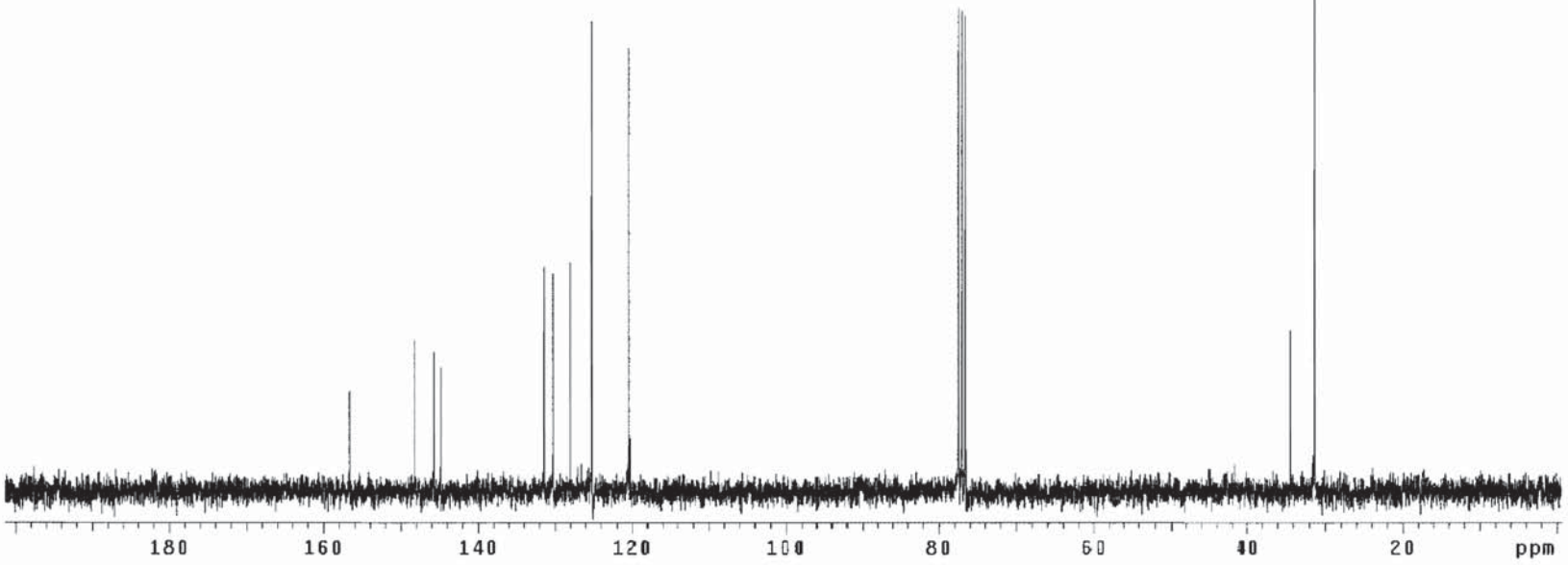

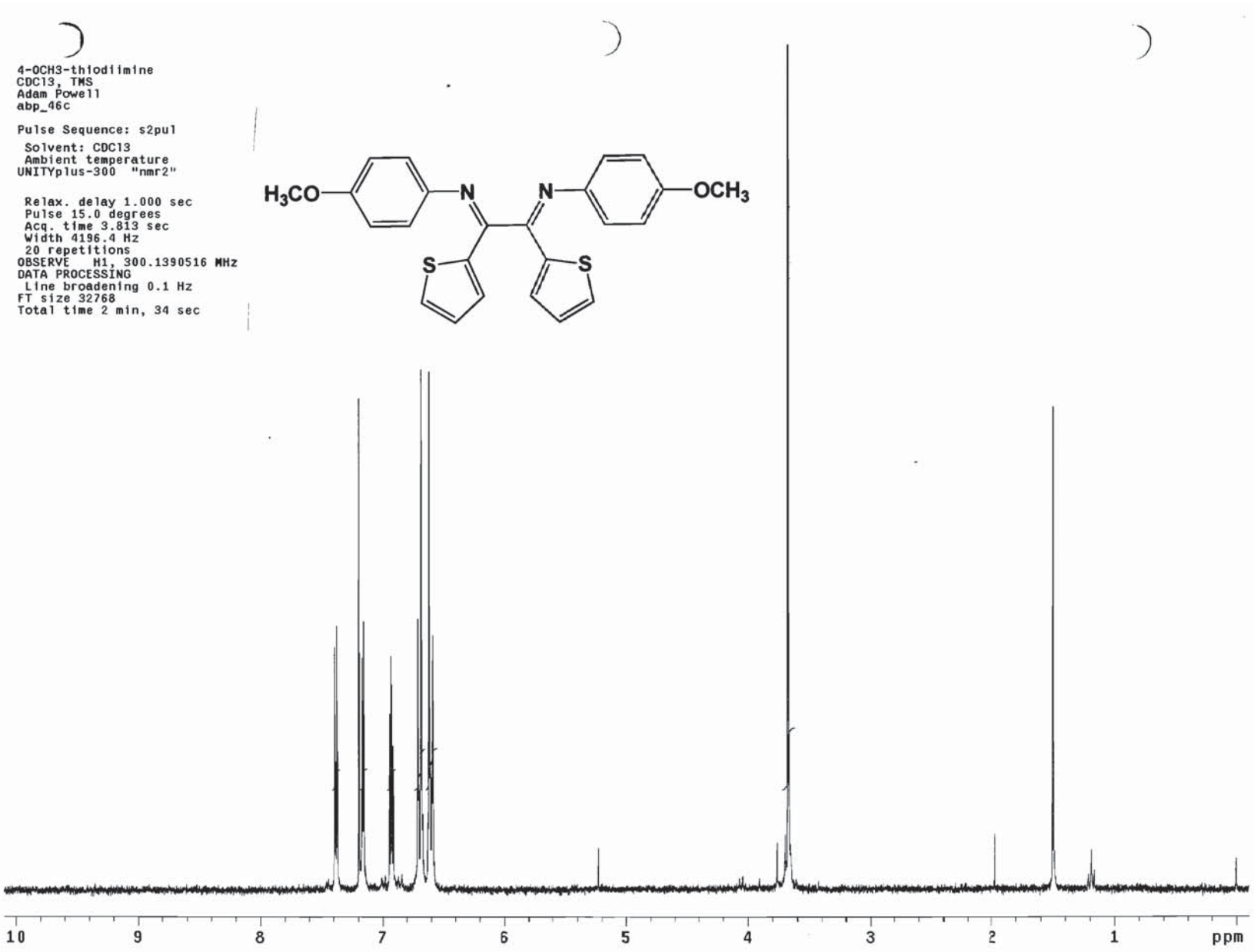
4-OCH3-thiodiimine
CDCl3, TMS
Adam Powell
abp_46c
Pulse Sequence: s2pul
Solvent: CDCl3
Ambient temperature
UNITYplus-300 "nmr2"
Relax. delay 1.000 sec
Pulse 15.0 degrees
Acq. time 3.813 sec
Width 4196.4 Hz
20 repetitions
OBSERVE H1, 300.1390516 MHz
DATA PROCESSING
Line broadening 0.1 Hz
FT size 32768
Total time 2 min, 34 sec
H3CO
N
N
OCH3
S
S
10
9
8
7
6
5
4
3
2
1
ppm

p-OMe diimine
CDCl3
Adam Powell
abp_49c

Pulse Sequence: s2pul
 Solvent: CDCl3
 Ambient temperature
File: abp_49c
INOVA-500 "u5b"

 Relax. delay 2.000 sec
 Pulse 36.0 degrees
 Acq. time 1.777 sec
 Width 18009.9 Hz
 80 repetitions
OBSERVE C13, 75.4700233 MHz
DECOUPLE H1, 300.1409259 MHz
 Power 40 dB
 continuously on
 WALTZ-16 modulated
Single precision data
DATA PROCESSING
 Line broadening 1.0 Hz
FT size 65536
Total time 1 hr, 4 min, 36 sec

INDEX	FREQUENCY	PPM	HEIGHT
1	11888.671	157.528	31.1
2	11810.076	156.487	21.4
3	10881.770	144.187	26.9
4	10671.266	141.397	30.8
5	9893.006	131.085	55.6
6	9829.250	130.240	54.9
7	9657.219	127.961	50.2
8	9264.242	122.754	115.8
9	8584.913	113.753	113.8
10	5843.415	77.427	64.9
11	5811.537	77.005	67.7
12	5779.659	76.582	66.9
13	4172.025	55.281	60.1

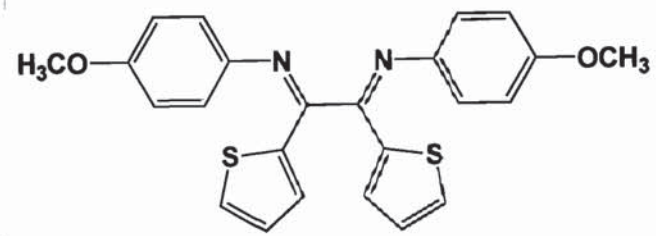

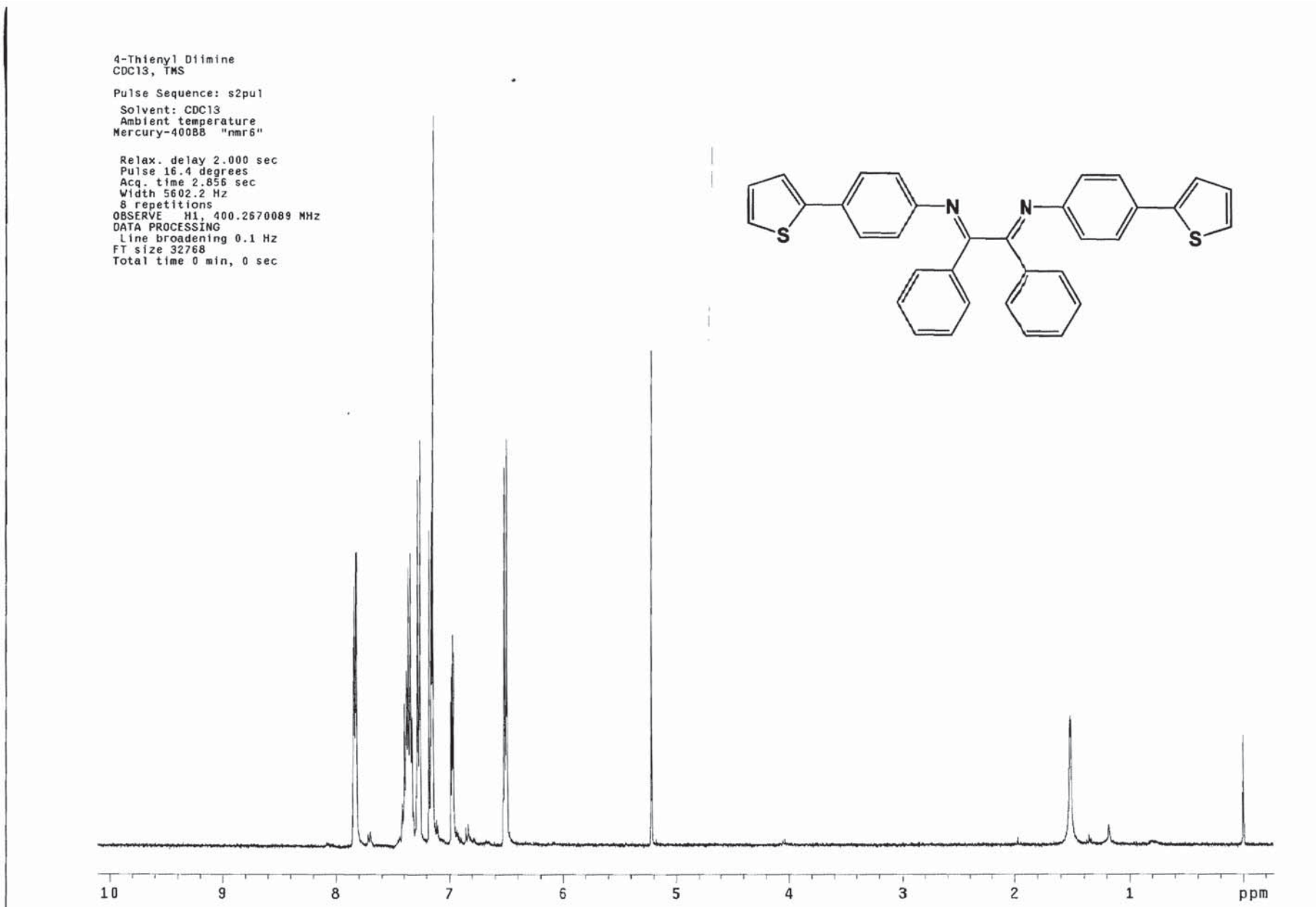
4-Thienyl Diimine
CDCl3, TMS
Pulse Sequence: s2pul
Solvent: CDCl3
Ambient temperature
Mercury-400BB "nmr6"
Relax. delay 2.000 sec
Pulse 16.4 degrees
Acq. time 2.856 sec
Width 5602.2 Hz
8 repetitions
OBSERVE H1, 400.2670089 MHz
DATA PROCESSING
Line broadening 0.1 Hz
FT size 32768
Total time 0 min, 0 sec
N
N
S
S
10
9
8
7
6
5
4
3
2
1
ppm

4-thienylphenyl Ligand
CDCl3
Adam Powell
abp_49d

Pulse Sequence: s2pul
 Solvent: CDCl3
 Ambient temperature
UNITYplus-300 "nmr2"

 Relax. delay 2.000 sec
 Pulse 36.0 degrees
 Acq. time 1.777 sec
 Width 18009.9 Hz
 96 repetitions
OBSERVE C13, 75.4700244 MHz
DECOUPLE H1, 300.1409259 MHz
 Power 40 dB
 continuously on
 WALTZ-16 modulated
Single precision data
DATA PROCESSING
 Line broadening 1.0 Hz
FT size 65536
Total time 1 hr, 4 min, 38 sec

INDEX	FREQUENCY	PPM	HEIGHT
1	12367.244	163.870	40.6
2	11210.261	148.539	43.0
3	10878.281	144.140	38.0
4	10368.769	137.389	49.6
5	9906.526	131.264	64.4
6	9897.182	131.141	54.9
7	9722.398	128.825	150.1
8	9683.923	128.315	150.4
9	9659.190	127.987	85.5
10	9500.345	125.882	153.0
11	9388.220	124.397	80.1
12	9250.261	122.569	85.9
13	9116.700	120.799	139.6
14	5843.071	77.422	122.4
15	5811.192	77.000	129.3
16	5779.313	76.578	125.2

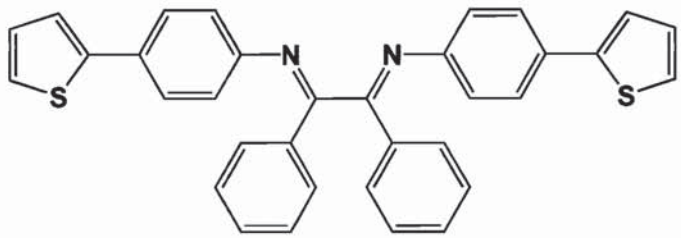

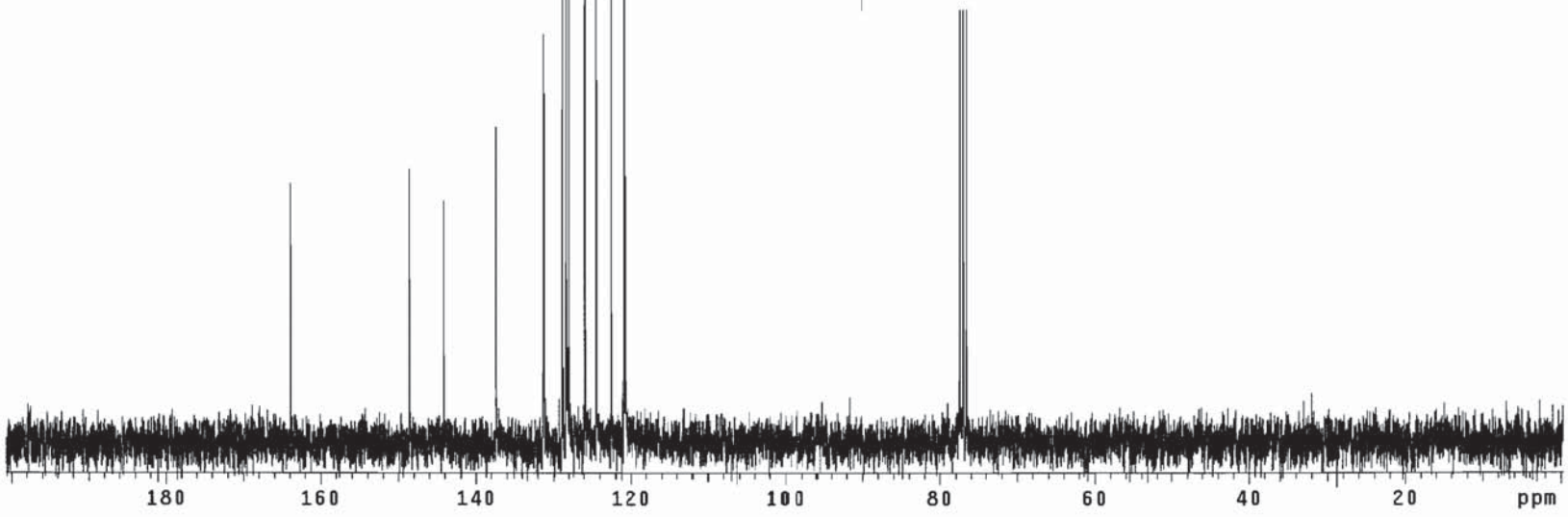

BT-monoimine
CDCl3

Pulse Sequence: s2pul
Solvent: CDCl3
Ambient temperature
File: abp_50e
INOVA-500 "nmrastro"

Relax. delay 2.000 sec
Pulse 16.4 degrees
Acq. time 2.856 sec
Width 5602.2 Hz
16 repetitions
OBSERVE H1, 400.2669856 MHz
DATA PROCESSING
Line broadening 0.1 Hz
FT size 32768
Total time 1 min, 17 sec

INDEX	FREQUENCY	PPM	HEIGHT
1	3405.021	8.507	102.8
2	2934.862	7.332	47.7
3	2930.759	7.322	52.9
4	2914.346	7.281	42.2
5	2911.610	7.274	67.3
6	2910.585	7.272	73.0
7	2906.481	7.261	44.7
8	2905.456	7.259	33.8
9	2897.933	7.240	343.4
10	2876.391	7.186	22.5
11	2870.236	7.171	76.5
12	2867.843	7.165	116.5
13	2866.475	7.161	113.0
14	2863.056	7.153	124.5
15	2854.507	7.132	25.8
16	2819.972	7.045	35.1
17	2816.211	7.036	32.4
18	2814.843	7.032	35.7
19	2811.082	7.023	27.5
20	1049.098	2.621	34.1
21	1041.575	2.602	47.6
22	1033.711	2.583	36.1
23	644.248	1.610	21.4
24	636.384	1.590	36.2
25	628.861	1.571	25.4
26	612.448	1.530	86.2
27	550.217	1.375	21.7
28	542.694	1.356	33.8
29	535.171	1.337	33.7
30	527.649	1.318	19.3
31	373.437	0.933	73.7
32	366.256	0.915	151.8
33	358.734	0.896	60.7

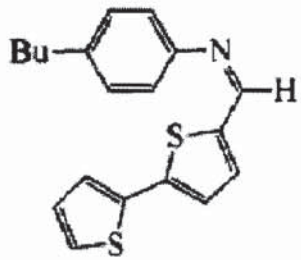

1

Chapter 4

BT-monoimine
CDCl3

Pulse Sequence: s2pul
 Solvent: CDCl3
 Ambient temperature
File: abp_19b
INOVA-500 "nmrastro"

 Relax. delay 2.000 sec
 Pulse 36.0 degrees
 Acq. time 1.777 sec
 Width 18009.9 Hz
 128 repetitions
OBSERVE C13, 75.4700319 MHz
DECOUPLE H1, 300.1409259 MHz
 Power 40 dB
 continuously on
 WALTZ-16 modulated
Single precision data
DATA PROCESSING
 Line broadening 1.0 Hz
FT size 65536
Total time 32 min, 18 sec

INDEX	FREQUENCY	PPM	HEIGHT
1	11438.189	151.559	71.6
2	11221.089	148.683	36.6
3	10683.013	141.553	29.1
4	10668.173	141.356	40.8
5	10637.944	140.956	44.7
6	10332.905	136.914	28.8
7	10004.783	132.566	68.7
8	9736.569	129.012	151.8
9	9661.271	128.015	79.1
10	9471.653	125.502	74.4
11	9415.592	124.759	82.1
12	9342.493	123.791	72.2
13	9122.645	120.878	142.1
14	5843.070	77.422	45.9
15	5811.192	77.000	46.4
16	5778.765	76.570	45.5
17	2649.786	35.110	74.3
18	2532.167	33.552	77.7
19	1680.808	22.271	74.5
20	1049.296	13.903	68.9

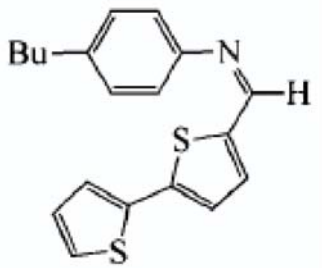

1

BT-ene-diamine
THF-d8, TMS

Pulse Sequence: s2pul

Solvent: THF
Ambient temperature
File: abp_19e
INOVA-500 "nmrastro"

Relax. delay 1.000 sec
Pulse 15.0 degrees
Acq. time 3.813 sec
Width 4196.4 Hz
32 repetitions
OBSERVE H1, 300.1401651 MHz
DATA PROCESSING
Line broadening 0.1 Hz
FT size 32768
Total time 2 min, 34 sec

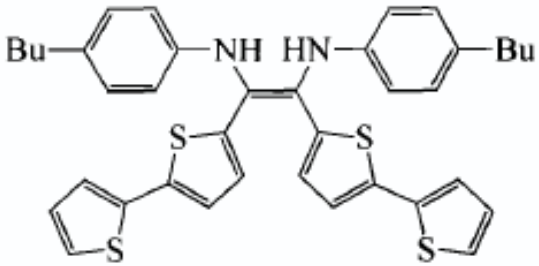

2

INDEX	FREQUENCY	PPM	HEIGHT
1	2139.432	7.128	39.4
2	2134.310	7.111	43.9
3	2087.950	6.957	38.3
4	2087.182	6.954	37.4
5	2084.365	6.945	56.4
6	2083.084	6.940	70.1
7	2078.730	6.926	67.8
8	2054.398	6.845	125.7
9	2050.300	6.831	100.0
10	2046.202	6.817	115.1
11	2041.335	6.801	36.8
12	2025.968	6.750	61.0
13	1977.816	6.590	79.1
14	1969.363	6.561	65.3
15	1041.414	3.470	147.7
16	717.157	2.389	34.2
17	713.315	2.377	36.5
18	709.729	2.365	52.0
19	701.789	2.338	45.4
20	484.849	1.615	116.5
21	436.441	1.454	22.1
22	428.501	1.428	36.6
23	420.817	1.402	27.2
24	378.300	1.260	23.3
25	370.872	1.236	36.0
26	363.189	1.210	34.2
27	356.017	1.186	20.3
28	245.370	0.818	79.6
29	238.198	0.794	151.2
30	230.771	0.769	62.3

BT-ene-diamine
THF-d8

Pulse Sequence: s2pul
Solvent: THF
Ambient temperature
UNITYplus-300 "nmr2"

Relax. delay 2.000 sec
Pulse 36.0 degrees
Acq. time 1.777 sec
Width 18009.9 Hz
192 repetitions
OBSERVE C13, 75.4702215 MHz
DECOUPLE H1, 300.1420244 MHz
Power 40 dB
continuously on
WALTZ-16 modulated
Single precision data
DATA PROCESSING
Line broadening 1.0 Hz
FT size 65536
Total time 32 min, 19 sec

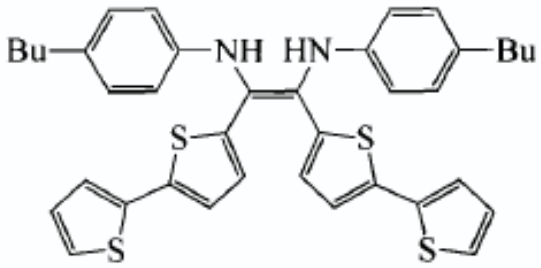

2

INDEX	FREQUENCY	PPM	HEIGHT
1	10962.846	145.261	25.6
2	10593.491	140.366	20.5
3	10518.740	139.376	19.1
4	10460.479	138.604	16.8
5	10051.550	133.186	20.6
6	9789.924	129.719	52.4
7	9765.190	129.391	21.8
8	9726.166	128.874	25.0
9	9697.585	128.496	31.6
10	9437.058	125.043	28.5
11	9359.009	124.009	30.3
12	9330.978	123.638	25.4
13	8692.851	115.183	50.8
14	5131.213	67.990	50.3
15	5108.678	67.691	100.9
16	5086.693	67.400	153.0
17	5064.708	67.109	102.7
18	5042.722	66.817	49.1
19	3760.423	49.827	13.7
20	2696.878	35.734	30.6
21	2635.868	34.926	32.3
22	1949.374	25.830	41.9
23	1929.037	25.560	87.8
24	1908.701	25.291	127.7
25	1888.914	25.029	88.9
26	1868.577	24.759	41.8
27	1755.902	23.266	36.8
28	1082.599	14.345	33.3

BT-diimine
CDCl3, TMS

Pulse Sequence: s2pul

Solvent: CDCl3
Ambient temperature
File: abp_47d
INOVA-500 "nmrastro"

Relax. delay 2.000 sec
Pulse 16.4 degrees
Acq. time 2.856 sec
Width 5602.2 Hz
24 repetitions
OBSERVE H1, 400.2670051 MHz
DATA PROCESSING
Line broadening 0.1 Hz
FT size 32768
Total time 2 min, 35 sec

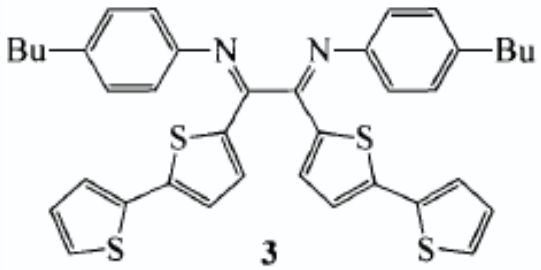

3

INDEX	FREQUENCY	PPM	HEIGHT
1	2895.152	7.233	27.2
2	2891.391	7.224	47.5
3	2886.262	7.211	26.7
4	2878.397	7.191	186.3
5	2861.301	7.148	33.0
6	2857.540	7.139	37.7
7	2814.114	7.031	36.6
8	2810.011	7.020	30.7
9	2798.727	6.992	21.0
10	2794.966	6.983	20.1
11	2793.598	6.979	21.7
12	2790.179	6.971	16.9
13	2743.334	6.854	36.6
14	2735.127	6.833	40.8
15	2618.186	6.541	45.1
16	2609.980	6.521	40.8
17	2093.660	5.231	28.5
18	986.479	2.465	18.8
19	978.956	2.446	30.6
20	971.433	2.427	20.2
21	842.183	2.104	141.2
22	595.990	1.489	302.4
23	587.784	1.468	23.7
24	580.261	1.450	15.7
25	506.746	1.266	12.6
26	499.223	1.247	20.4
27	491.701	1.228	20.4
28	484.520	1.210	11.8
29	341.250	0.853	44.9
30	334.069	0.835	90.2
31	326.547	0.816	39.0

BT-diimine
CDCl3

Pulse Sequence: s2pul

Solvent: CDCl3
Ambient temperature
File: abp_1d
INOVA-500 "nmrastro"

Relax. delay 2.000 sec
Pulse 36.0 degrees
Acq. time 1.777 sec
Width 18009.9 Hz
96 repetitions
OBSERVE C13, 75.4700247 MHz
DECOUPLE H1, 300.1409259 MHz
Power 40 dB
continuously on
WALTZ-16 modulated
Single precision data
DATA PROCESSING
Line broadening 1.0 Hz
FT size 65536
Total time 1 hr, 4 min, 36 sec

INDEX	FREQUENCY	PPM	HEIGHT
1	11792.143	156.249	22.7
2	11010.585	145.893	32.0
3	10767.653	142.675	34.4
4	10723.684	142.092	30.9
5	10578.035	140.162	33.8
6	10328.508	136.856	29.7
7	9976.202	132.188	40.3
8	9693.698	128.444	102.5
9	9667.317	128.095	52.0
10	9487.042	125.706	45.9
11	9427.683	124.920	49.4
12	9367.774	124.126	42.6
13	9124.293	120.900	97.3
14	5843.070	77.422	67.1
15	5811.192	77.000	67.9
16	5779.314	76.578	66.2
17	2644.289	35.038	50.1
18	2529.419	33.516	51.6
19	1668.716	22.111	58.6
20	1050.395	13.918	59.0

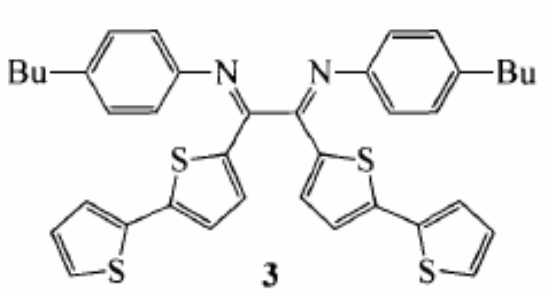

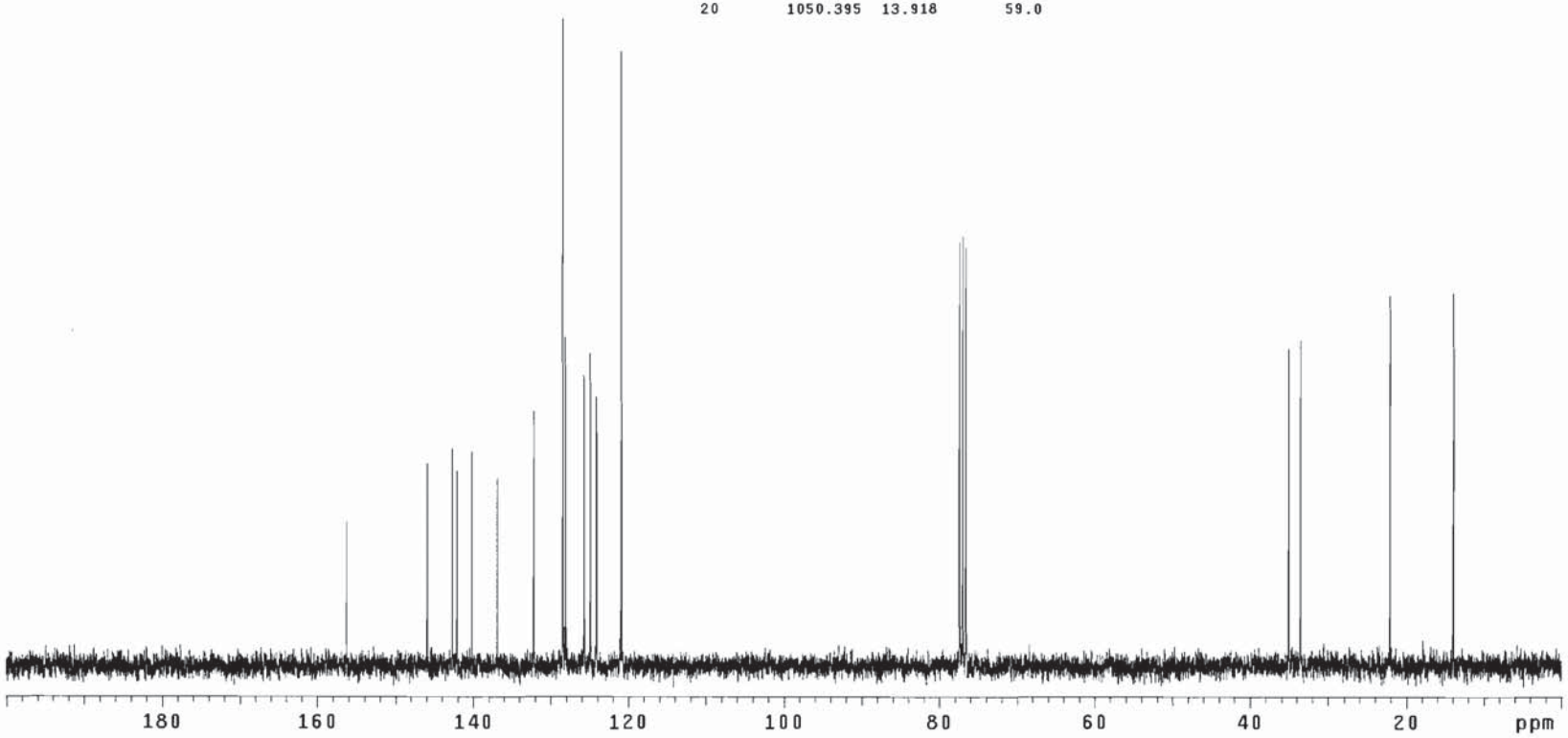

BT-imid-salt
CD2Cl2, TMS

Pulse Sequence: s2pul

Solvent: CD2Cl2
Ambient temperature
File: abp_38a
INOVA-500 "nmrastro"

Relax. delay 2.000 sec
Pulse 16.4 degrees
Acq. time 2.856 sec
Width 5602.2 Hz
8 repetitions
OBSERVE H1, 400.2677959 MHz
DATA PROCESSING
Line broadening 0.1 Hz
FT size 32768
Total time 0 min, 38 sec

INDEX	FREQUENCY	PPM	HEIGHT
1	4165.094	10.406	29.4
2	3056.203	7.635	41.9
3	3047.997	7.615	46.9
4	2887.288	7.213	45.9
5	2878.739	7.192	43.3
6	2859.933	7.145	26.5
7	2858.907	7.142	26.4
8	2854.804	7.132	30.1
9	2853.778	7.130	28.0
10	2797.359	6.989	26.3
11	2796.333	6.986	26.1
12	2793.598	6.979	31.4
13	2792.914	6.978	28.7
14	2763.850	6.905	151.2
15	2746.069	6.861	24.4
16	2742.308	6.851	26.5
17	2740.940	6.848	26.6
18	2737.179	6.838	21.8
19	2090.924	5.224	32.1
20	1024.433	2.559	22.6
21	1016.569	2.540	34.0
22	1009.046	2.521	24.6
23	600.777	1.501	16.0
24	592.913	1.481	27.6
25	585.390	1.462	19.4
26	500.933	1.251	16.3
27	493.410	1.233	27.3
28	485.888	1.214	27.3
29	478.707	1.196	16.0
30	324.837	0.812	54.5
31	317.314	0.793	104.7
32	310.134	0.775	48.0

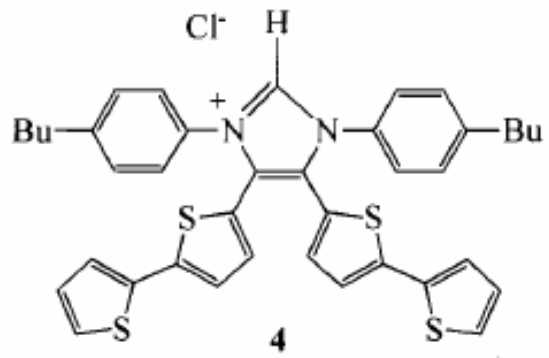

4

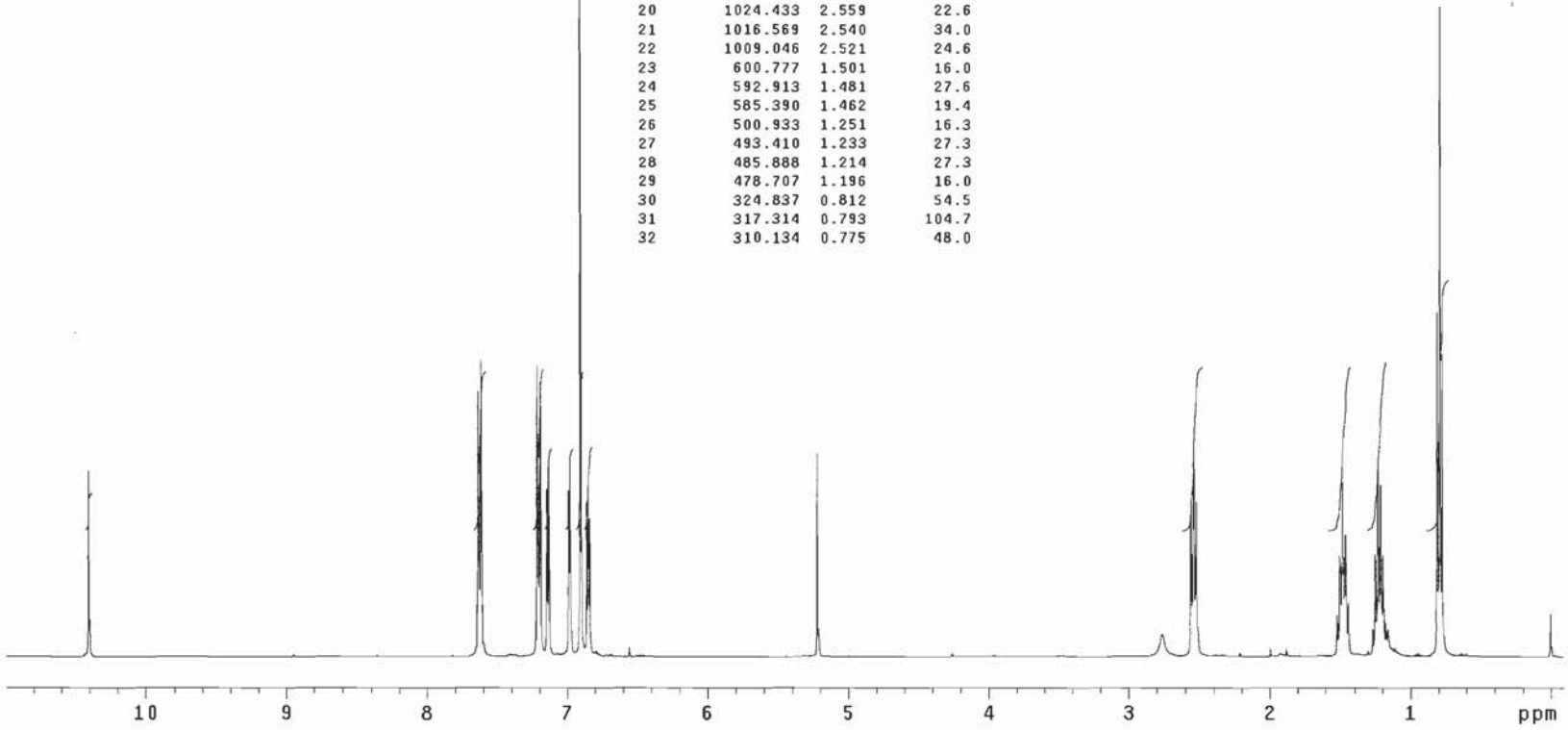

BT-imid-salt
CD2Cl2

Pulse Sequence: s2pul

Solvent: CD2Cl2
Ambient temperature
File: abp_38b
INOVA-500 "nmrastro"

Relax. delay 2.000 sec
Pulse 22.5 degrees
Acq. time 1.280 sec
Width 25188.9 Hz
128 repetitions
OBSERVE C13, 100.6473875 MHz
DECOUPLE H1, 400.2697641 MHz
Power 38 dB
continuously on
WALTZ-16 modulated
DATA PROCESSING
Line broadening 1.0 Hz
FT size 65536
Total time 14 min, 1 sec

INDEX	FREQUENCY	PPM	HEIGHT
1	14746.905	146.520	32.7
2	14345.641	142.534	24.5
3	13937.459	138.478	8.0
4	13662.263	135.744	29.3
5	13473.930	133.873	39.3
6	13185.666	131.009	32.7
7	13071.897	129.878	60.7
8	12906.626	128.236	45.6
9	12813.613	127.312	29.0
10	12754.422	126.724	61.9
11	12686.776	126.052	30.2
12	12590.688	125.097	44.6
13	12463.852	123.837	36.6
14	12321.642	122.424	34.8
15	5469.407	54.342	48.4
16	5441.734	54.067	101.7
17	5414.829	53.800	150.3
18	5387.156	53.525	103.2
19	5360.251	53.258	53.0
20	3566.863	35.439	39.1
21	3357.007	33.354	52.4
22	2264.677	22.501	51.0
23	1398.347	13.894	55.0

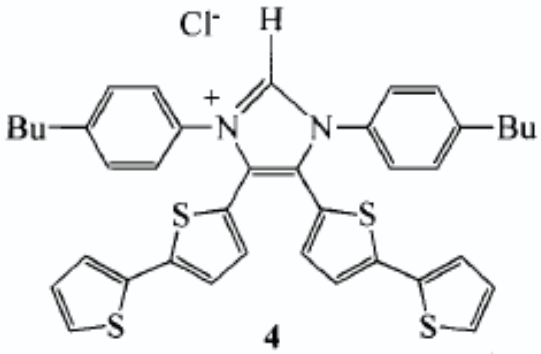

4

BT-Ag-Cl
CD2Cl2, TMS

Pulse Sequence: s2pul

Solvent: CD2Cl2
Ambient temperature
File: abp_36c
INOVA-500 "nmrastro"

Relax. delay 1.000 sec
Pulse 15.0 degrees
Acq. time 3.813 sec
Width 4196.4 Hz
28 repetitions
OBSERVE H1, 300.1396489 MHz
DATA PROCESSING
Line broadening 0.1 Hz
FT size 32768
Total time 2 min, 34 sec

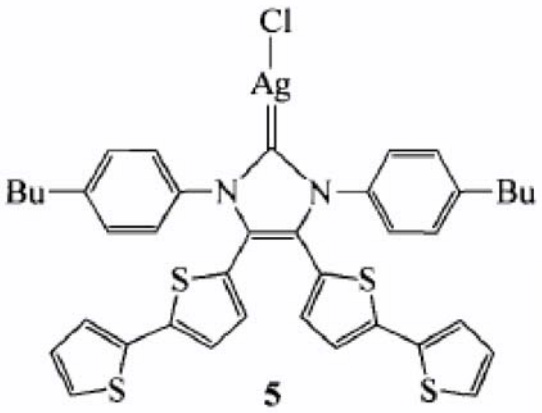

5

INDEX	FREQUENCY	PPM	HEIGHT
1	2181.151	7.267	29.8
2	2172.955	7.240	71.5
3	2162.197	7.204	89.0
4	2153.745	7.176	38.9
5	2140.683	7.132	36.4
6	2139.658	7.129	38.5
7	2135.560	7.115	41.5
8	2134.536	7.112	42.2
9	2096.885	6.986	34.7
10	2095.860	6.983	36.2
11	2093.299	6.974	45.3
12	2092.275	6.971	41.2
13	2066.918	6.887	58.6
14	2064.101	6.877	60.9
15	2063.076	6.874	79.3
16	2060.515	6.865	44.2
17	2059.234	6.861	43.7
18	2055.392	6.848	33.2
19	2005.447	6.682	61.7
20	2001.605	6.669	56.6
21	784.232	2.613	32.9
22	776.804	2.588	48.7
23	768.864	2.562	36.5
24	471.244	1.570	23.3
25	463.304	1.544	38.0
26	455.877	1.519	27.9
27	393.125	1.310	23.7
28	385.698	1.285	37.6
29	378.014	1.259	37.0
30	370.842	1.236	22.8
31	257.122	0.857	80.0
32	249.950	0.833	151.2
33	242.523	0.808	65.1

BT-Ag-Cl
CD2Cl2

Pulse Sequence: s2pul
Solvent: CD2Cl2
Ambient temperature
UNITYplus-300 "nmr2"

Relax. delay 2.000 sec
Pulse 36.0 degrees
Acq. time 1.777 sec
Width 18009.9 Hz
192 repetitions
OBSERVE C13, 75.4701421 MHz
DECOUPLE H1, 300.1415022 MHz
Power 40 dB
continuously on
WALTZ-16 modulated
Single precision data
DATA PROCESSING
Line broadening 1.0 Hz
FT size 65536
Total time 16 min, 9 sec

INDEX	FREQUENCY	PPM	HEIGHT
1	10964.265	145.280	46.8
2	10656.469	141.201	31.9
3	10287.664	136.314	33.6
4	10276.121	136.161	43.4
5	9972.173	132.134	69.0
6	9792.442	129.753	115.8
7	9681.416	128.281	77.6
8	9619.307	127.458	31.9
9	9611.612	127.356	110.2
10	9500.586	125.885	32.6
11	9487.944	125.718	61.3
12	9416.491	124.771	75.1
13	9339.542	123.751	74.7
14	4114.708	54.521	36.4
15	4087.775	54.164	74.6
16	4060.294	53.800	106.0
17	4033.362	53.443	70.8
18	4005.880	53.079	36.6
19	2681.808	35.535	66.3
20	2531.757	33.546	75.4
21	1711.701	22.681	84.7
22	1060.383	14.050	82.3

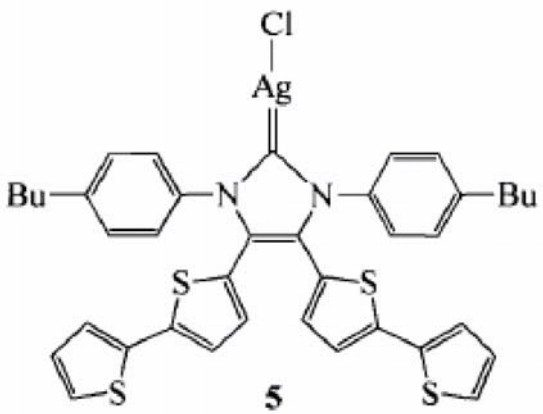

5

BT-Au-Cl
CD2Cl2, TMS

Archive directory:
Sample directory:

Pulse Sequence: s2pul
Solvent: cd2cl2
Temp. 27.0 C / 300.1 K
File: bt_au_cl_h1
INOVA-500 "nmrastro"

Relax. delay 2.000 sec
Pulse 15.0 degrees
Acq. time 4.000 sec
Width 9615.4 Hz
64 repetitions
OBSERVE H1, 599.7509453 MHz
DATA PROCESSING
Line broadening 0.1 Hz
FT size 262144
Total time 6 min, 24 sec

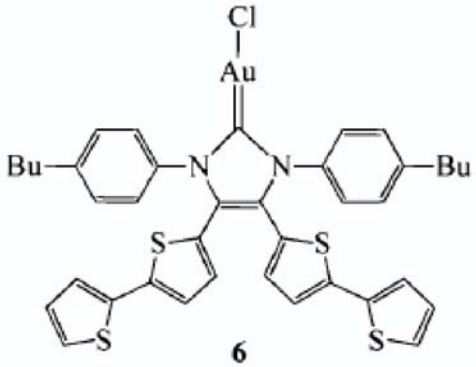

6

INDEX	FREQUENCY	PPM	HEIGHT	INDEX	FREQUENCY	PPM	HEIGHT
1	4403.408	7.342	51.9	40	775.411	1.293	28.2
2	4401.427	7.339	17.3	41	767.855	1.280	28.3
3	4397.025	7.331	20.2	42	760.519	1.268	17.6
4	4394.971	7.328	68.9	43	707.260	1.179	16.1
5	4341.859	7.239	56.4	44	513.664	0.856	70.5
6	4339.805	7.236	17.4	45	506.328	0.844	151.4
7	4335.330	7.229	15.6	46	498.918	0.832	65.7
8	4333.349	7.225	42.9				
9	4290.654	7.154	33.4				
10	4289.554	7.152	34.8				
11	4285.592	7.146	36.3				
12	4284.419	7.144	35.7				
13	4198.441	7.000	30.4				
14	4197.341	6.998	31.0				
15	4194.847	6.994	35.3				
16	4193.673	6.992	33.3				
17	4136.232	6.897	42.4				
18	4132.564	6.890	48.7				
19	4131.977	6.889	66.5				
20	4131.170	6.888	43.1				
21	4128.089	6.883	65.7				
22	4127.502	6.882	43.2				
23	4007.486	6.682	71.6				
24	4003.598	6.675	68.3				
25	3135.534	5.228	21.5				
26	3134.434	5.226	22.9				
27	3133.334	5.224	21.1				
28	1572.756	2.622	22.8				
29	1564.980	2.609	28.4				
30	1557.130	2.596	23.7				
31	947.952	1.581	11.1				
32	946.558	1.578	15.7				
33	944.724	1.575	11.6				
34	940.910	1.569	13.7				
35	938.709	1.565	27.8				
36	936.141	1.561	12.2				
37	932.473	1.555	12.3				
38	931.080	1.552	18.7				
39	782.893	1.305	18.0				

BT-Au-Cl
CDCl3

Pulse Sequence: s2pul

Solvent: CDCl3
Ambient temperature
File: abp_35b
INOVA-500 "nmrastro"

Relax. delay 2.000 sec
Pulse 22.5 degrees
Acq. time 1.280 sec
Width 25188.9 Hz
256 repetitions
OBSERVE C13, 100.6472361 MHz
DECOUPLE H1, 400.2689955 MHz
Power 38 dB
continuously on
WALTZ-16 modulated
DATA PROCESSING
Line broadening 1.0 Hz
FT size 65536
Total time 28 min, 3 sec

INDEX	FREQUENCY	PPM	HEIGHT
1	17337.891	172.264	15.2
2	14536.731	144.432	36.5
3	14171.597	140.805	38.6
4	13668.864	135.810	40.2
5	13557.401	134.702	35.6
6	13243.001	131.578	49.3
7	13000.859	129.173	62.1
8	12855.574	127.729	59.2
9	12810.220	127.278	57.8
10	12719.513	126.377	37.6
11	12592.677	125.117	37.7
12	12586.527	125.056	38.8
13	12505.813	124.254	57.3
14	12399.732	123.200	45.4
15	7782.123	77.321	150.5
16	7749.837	77.000	150.4
17	7718.320	76.687	143.7
18	3533.492	35.108	43.8
19	3307.492	32.862	67.0
20	2230.537	22.162	64.2
21	1387.268	13.783	66.2

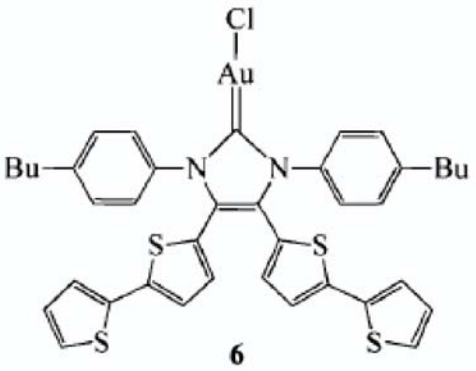

6

BT-Ag-Cl
CD2Cl2, TMS

Archive directory:
Sample directory:

Pulse Sequence: s2pul

Solvent: cd2cl2
Temp. 27.0 C / 300.1 K
File: bt_silver_carbene_h1
INOVA-500 "nmrastro"

Relax. delay 2.000 sec
Pulse 15.0 degrees
Acq. time 4.005 sec
Width 7990.4 Hz
64 repetitions
OBSERVE H1, 499.3997566 MHz
DATA PROCESSING
Line broadening 0.1 Hz
FT size 65536
Total time 6 min, 36 sec

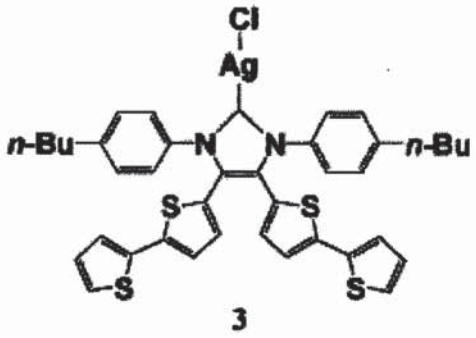

3

INDEX	FREQUENCY	PPM	HEIGHT	INDEX	FREQUENCY	PPM	HEIGHT
1	3637.481	7.284	18.6	40	638.882	1.279	26.7
2	3629.434	7.268	31.0	41	631.566	1.265	16.9
3	3607.975	7.225	49.8	42	429.660	0.860	70.3
4	3599.684	7.208	28.1	43	422.345	0.846	156.1
5	3572.861	7.154	38.1	44	419.419	0.840	7.4
6	3571.642	7.152	36.0	45	415.029	0.831	61.5
7	3567.740	7.144	41.2	46	-0.000	-0.000	10.9
8	3566.521	7.142	36.3				
9	3498.487	7.005	31.8				
10	3497.268	7.003	33.8				
11	3494.830	6.998	38.9				
12	3493.610	6.996	37.4				
13	3446.548	6.901	60.3				
14	3444.841	6.898	45.0				
15	3442.646	6.894	69.9				
16	3441.183	6.891	36.8				
17	3439.720	6.888	37.6				
18	3436.306	6.881	32.7				
19	3340.718	6.689	70.0				
20	3337.060	6.682	63.2				
21	2611.124	5.229	15.1				
22	2609.905	5.226	18.8				
23	2608.930	5.224	15.1				
24	1307.757	2.619	23.1				
25	1300.198	2.604	29.0				
26	1292.151	2.587	24.2				
27	793.238	1.588	8.1				
28	787.141	1.576	10.6				
29	785.922	1.574	15.1				
30	783.971	1.570	11.4				
31	780.070	1.562	13.2				
32	777.875	1.558	27.4				
33	775.437	1.553	12.7				
34	771.779	1.545	12.9				
35	770.316	1.542	19.4				
36	768.365	1.539	10.8				
37	762.513	1.527	10.0				
38	654.000	1.310	17.2				
39	646.441	1.294	26.6				

Chapter 5

BT-Ag-Cl
CD2Cl2

Archive directory:
Sample directory:

Pulse Sequence: s2pul
Solvent: cd2cl2
Temp. 27.0 C / 300.1 K
User: 1-14-87
File: bt_silver_carbene_c13
INOVA-500 "nmrastro"

Relax. delay 2.000 sec
Pulse 23.2 degrees
Acq. time 1.062 sec
Width 30143.2 Hz
3057 repetitions
OBSERVE C13, 125.5741087 MHz
DECOUPLE H1, 499.4021959 MHz
Power 39 dB
continuously on
WALTZ-16 modulated
DATA PROCESSING
Line broadening 1.0 Hz
FT size 65536
Total time 3 hr, 31 min, 16 sec

INDEX	FREQUENCY	PPM	HEIGHT
1	18255.518	145.376	53.5
2	17733.936	141.223	45.1
3	17127.724	136.395	50.2
4	17105.647	136.220	38.0
5	16594.184	132.147	87.9
6	16300.737	129.810	154.9
7	16113.078	128.315	94.6
8	16010.049	127.495	43.9
9	16001.770	127.429	139.2
10	15823.310	126.008	31.1
11	15788.354	125.729	71.6
12	15672.447	124.806	109.9
13	15545.501	123.795	91.8
14	6810.161	54.232	189.1
15	6783.484	54.020	398.2
16	6755.887	53.800	594.1
17	6729.210	53.588	377.3
18	6701.613	53.368	202.3
19	4469.023	35.589	91.4
20	4218.812	33.596	119.3
21	2853.685	22.725	108.4
22	1765.447	14.059	108.4

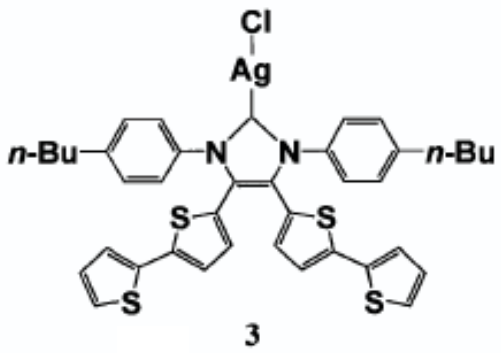

3

BT-Ag-OAc
CDCl3, TMS

Pulse Sequence: s2pul

Solvent: CD2Cl2
Ambient temperature
File: abp_57c
INOVA-500 "nmrastro"

Relax. delay 2.000 sec
Pulse 16.4 degrees
Acq. time 2.856 sec
Width 5602.2 Hz
32 repetitions
OBSERVE H1, 400.2677849 MHz
DATA PROCESSING
Line broadening 0.1 Hz
FT size 32768
Total time 2 min, 35 sec

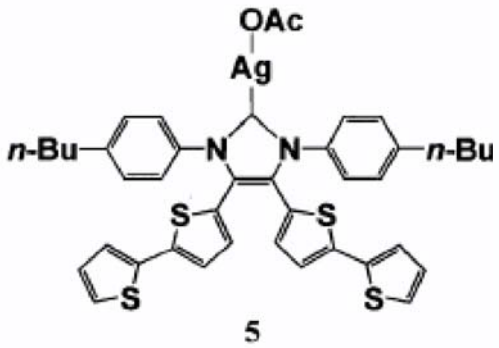

5

INDEX	FREQUENCY	PPM	HEIGHT
1	2917.378	7.289	8.2
2	2882.501	7.201	15.5
3	2869.165	7.168	31.8
4	2864.036	7.155	32.8
5	2806.933	7.013	27.1
6	2803.172	7.003	32.1
7	2766.243	6.911	35.2
8	2764.875	6.908	43.5
9	2761.114	6.898	65.9
10	2757.695	6.890	22.0
11	2673.921	6.680	18.9
12	2670.502	6.672	17.8
13	2102.550	5.253	44.7
14	2101.866	5.251	69.8
15	2097.763	5.241	85.3
16	2096.737	5.238	83.3
17	2095.711	5.236	61.0
18	1052.814	2.630	18.9
19	1045.291	2.611	28.0
20	1037.427	2.592	19.6
21	723.190	1.807	81.5
22	634.287	1.585	14.9
23	626.081	1.564	23.5
24	618.900	1.546	17.1
25	610.693	1.526	7.9
26	529.997	1.324	12.4
27	522.475	1.305	20.5
28	515.294	1.287	20.4
29	507.771	1.269	12.2
30	472.210	1.180	7.6
31	349.798	0.874	36.5
32	342.618	0.856	66.8
33	335.095	0.837	31.3
34	-0.000	-0.000	151.2

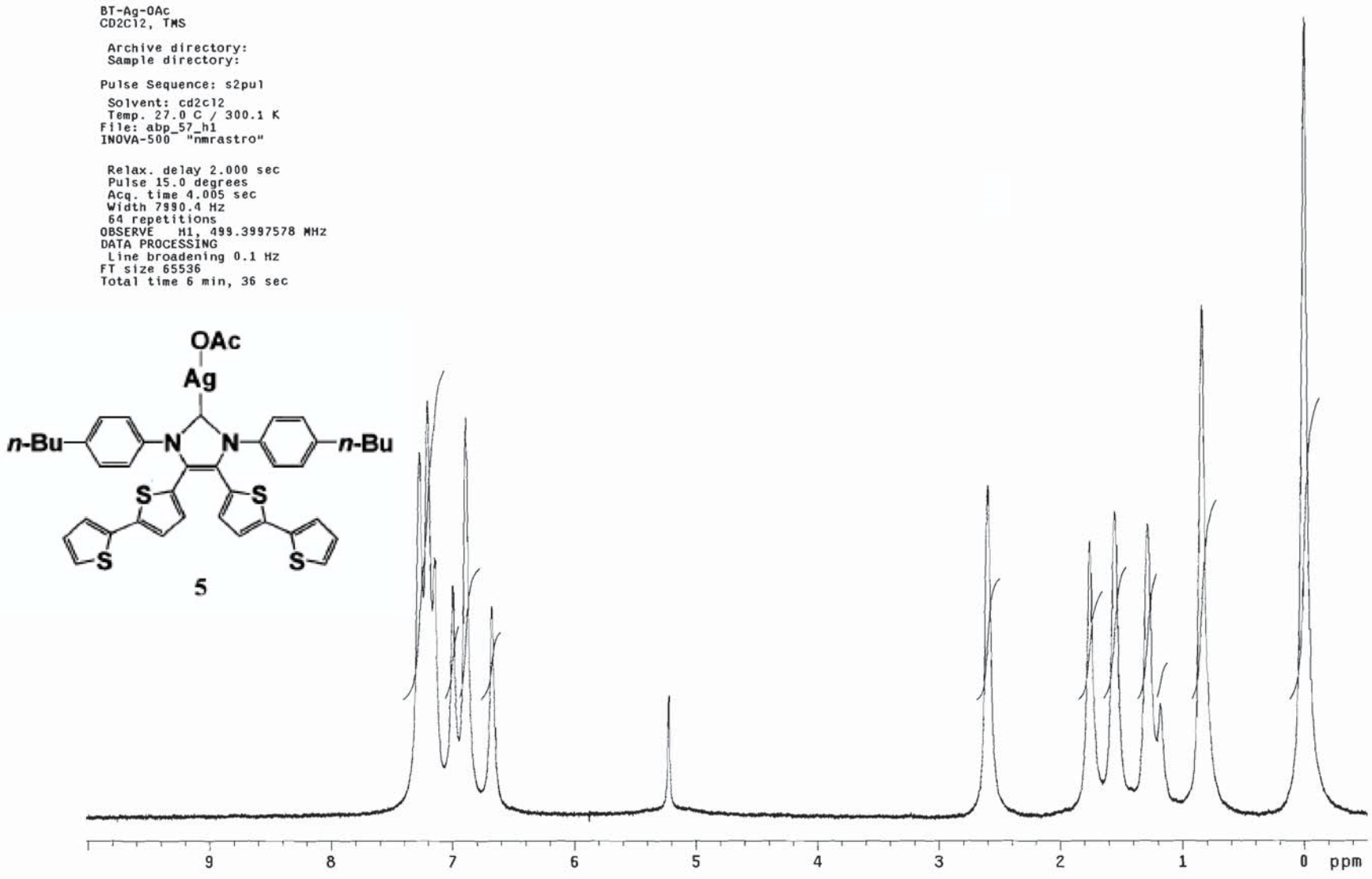
BT-Ag-OAc
CD2Cl2, TMS
Archive directory:
Sample directory:
Pulse Sequence: s2pul
Solvent: cd2cl2
Temp. 27.0 C / 300.1 K
File: abp_57_h1
INOVA-500 "nmrastro"
Relax. delay 2.000 sec
Pulse 15.0 degrees
Acq. time 4.005 sec
Width 7990.4 Hz
64 repetitions
OBSERVE H1, 499.3997578 MHz
DATA PROCESSING
Line broadening 0.1 Hz
FT size 65536
Total time 6 min, 36 sec
OAc
Ag
n-Bu
N
N
n-Bu
S
S
S
S
9
8
7
6
5
4
3
2
1
0
ppm

5

BT-Ag-OAc
CD2Cl2, TMS

Archive directory:
Sample directory:

Pulse Sequence: s2pul

Solvent: cd2cl2
Temp. 27.0 C / 300.1 K
User: 1-14-87
File: abp_57_c13
INOVA-500 "nmrastro"

Relax. delay 2.000 sec
Pulse 23.2 degrees
Acq. time 1.062 sec
Width 30143.2 Hz
1000 repetitions
OBSERVE C13, 125.5742496 MHz
DECOUPLE H1, 499.4021959 MHz
Power 39 dB
continuously on
WALTZ-16 modulated
DATA PROCESSING
Line broadening 1.0 Hz
FT size 65536
Total time 57 min, 43 sec

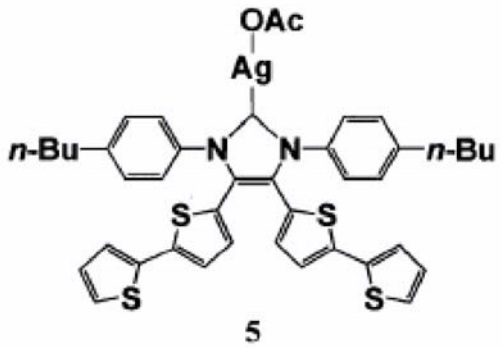

5

INDEX	FREQUENCY	PPM	HEIGHT
1	22083.044	175.856	10.1
2	18089.772	144.056	46.0
3	17589.348	140.071	41.2
4	16989.575	135.295	44.6
5	16977.616	135.200	44.4
6	16451.435	131.010	90.0
7	16152.469	128.629	152.8
8	15971.249	127.186	95.3
9	15872.820	126.402	42.5
10	15856.262	126.270	135.2
11	15694.360	124.981	30.4
12	15643.766	124.578	71.8
13	15529.699	123.669	88.0
14	15402.753	122.659	92.8
15	6668.332	53.103	269.5
16	6640.735	52.883	567.7
17	6614.058	52.670	766.1
18	6586.461	52.451	572.5
19	6558.865	52.231	268.9
20	4326.275	34.452	89.7
21	4078.823	32.481	110.4
22	2710.936	21.588	108.3
23	2696.218	21.471	15.4
24	1624.538	12.937	99.9
25	0.000	0.000	103.0

BT-Thione
CD2Cl2, TMS

Archive directory:
Sample directory:

Pulse Sequence: s2pul

Solvent: cd2cl2
Temp. 27.0 C / 300.1 K
File: abp_7_h1
INOVA-500 "nmrastro"

Relax. delay 2.000 sec
Pulse 15.0 degrees
Acq. time 4.005 sec
Width 7990.4 Hz
64 repetitions
OBSERVE H1, 499.3997595 MHz
DATA PROCESSING
Line broadening 0.1 Hz
FT size 65536
Total time 6 min, 36 sec

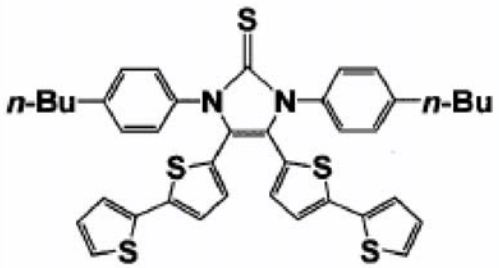

6

INDEX	FREQUENCY	PPM	HEIGHT	INDEX	FREQUENCY	PPM	HEIGHT
1	3619.680	7.248	28.3	40	765.683	1.533	17.8
2	3617.485	7.244	12.0	41	763.732	1.529	9.5
3	3613.340	7.235	20.0	42	757.880	1.518	9.0
4	3611.145	7.231	91.0	43	647.416	1.296	16.9
5	3609.438	7.228	19.6	44	639.857	1.281	26.3
6	3603.098	7.215	74.4	45	632.298	1.266	26.3
7	3600.904	7.210	17.1	46	624.982	1.251	16.3
8	3596.758	7.202	11.0	47	424.539	0.850	65.9
9	3594.563	7.198	24.1	48	417.224	0.835	144.0
10	3556.523	7.122	32.9	49	409.909	0.821	59.4
11	3555.548	7.120	30.3				
12	3551.402	7.111	35.4				
13	3550.427	7.109	32.7				
14	3478.492	6.965	29.3				
15	3477.273	6.963	30.3				
16	3474.834	6.958	35.9				
17	3473.615	6.956	33.5				
18	3433.624	6.876	35.2				
19	3430.210	6.869	31.5				
20	3428.747	6.866	32.6				
21	3425.089	6.858	29.5				
22	3412.897	6.834	53.3				
23	3409.239	6.827	57.8				
24	3309.505	6.627	59.6				
25	3305.604	6.619	64.5				
26	2613.075	5.232	77.0				
27	2607.954	5.222	13.0				
28	2606.979	5.220	14.0				
29	2605.760	5.218	12.4				
30	1298.003	2.599	24.0				
31	1290.200	2.584	31.1				
32	1282.397	2.568	25.2				
33	782.264	1.566	11.0				
34	781.045	1.564	15.2				
35	779.094	1.560	11.2				
36	775.193	1.552	13.2				
37	773.242	1.548	27.6				
38	770.560	1.543	12.1				
39	766.902	1.536	12.8				

BT-Thione
CD2Cl2

Archive directory:
Sample directory:

Pulse Sequence: s2pul

Solvent: cd2cl2
Temp. 27.0 C / 300.1 K
User: 1-14-87
File: abp_7_c13
INOVA-500 "nmrastro"

Relax. delay 2.000 sec
Pulse 23.2 degrees
Acq. time 1.062 sec
Width 30143.2 Hz
400 repetitions
OBSERVE C13, 125.5741106 MHz
DECOUPLE H1, 499.4021959 MHz
Power 39 dB
continuously on
WALTZ-16 modulated
DATA PROCESSING
Line broadening 1.0 Hz
FT size 65536
Total time 22 min, 6 sec

INDEX	FREQUENCY	PPM	HEIGHT
1	20984.852	167.111	10.6
2	18167.208	144.673	42.2
3	17614.350	140.271	27.7
4	17157.161	136.630	31.8
5	16916.148	134.710	35.8
6	16513.233	131.502	70.3
7	16255.662	129.451	118.0
8	16219.786	129.165	116.7
9	16102.959	128.235	63.1
10	15965.894	127.143	31.6
11	15749.719	125.422	67.7
12	15636.571	124.521	72.4
13	15517.905	123.576	67.8
14	15491.228	123.363	29.5
15	6810.161	54.232	103.1
16	6783.484	54.020	197.8
17	6755.887	53.800	314.4
18	6728.290	53.580	187.5
19	6701.613	53.368	104.1
20	4476.383	35.647	64.9
21	4226.171	33.655	84.3
22	2850.925	22.703	79.0
23	1766.367	14.066	70.6

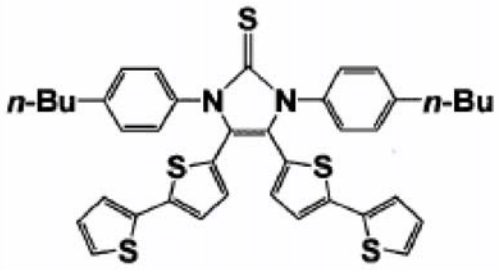

6

BT-Ir-COD
CD2Cl2, TMS

Archive directory:
Sample directory:

Pulse Sequence: s2pul
Solvent: cd2cl2
Temp. 27.0 C / 300.1 K
File: abp_59f_h1
INOVA-500 "nmrastro"

Relax. delay 2.000 sec
Pulse 15.0 degrees
Acq. time 4.005 sec
Width 7990.4 Hz
64 repetitions
OBSERVE H1, 499.3997581 MHz
DATA PROCESSING
Line broadening 0.1 Hz
FT size 65536
Total time 6 min, 36 sec

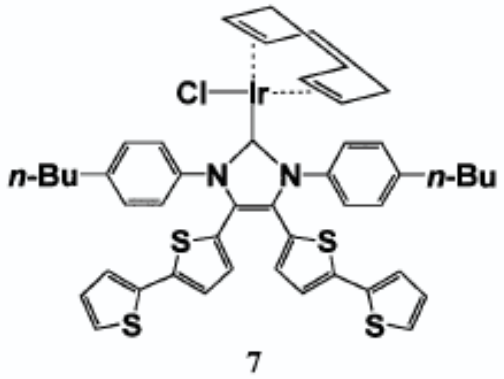

7

INDEX	FREQUENCY	PPM	HEIGHT	INDEX	FREQUENCY	PPM	HEIGHT
1	3784.521	7.578	27.2	40	653.269	1.308	8.2
2	3776.474	7.562	29.6	41	645.710	1.293	23.6
3	3581.152	7.171	51.8	42	638.150	1.278	38.9
4	3572.617	7.154	48.2	43	630.835	1.263	36.2
5	3558.718	7.126	41.4	44	625.714	1.253	13.3
6	3557.499	7.124	41.2	45	623.276	1.248	22.8
7	3553.597	7.116	45.3	46	615.960	1.233	8.9
8	3552.378	7.113	41.9	47	554.754	1.111	7.5
9	3489.953	6.988	33.3	48	553.291	1.108	7.6
10	3488.733	6.986	35.5	49	547.439	1.096	7.3
11	3486.295	6.981	41.2	50	423.320	0.848	72.2
12	3485.076	6.979	39.4	51	416.005	0.833	152.7
13	3436.306	6.881	51.5	52	408.445	0.818	68.0
14	3432.648	6.874	48.8	53	-0.000	-0.000	74.6
15	3431.185	6.871	108.0				
16	3427.528	6.863	92.9				
17	3350.715	6.709	88.3				
18	3346.814	6.702	69.7				
19	2614.538	5.235	87.5				
20	2609.418	5.225	14.3				
21	2608.442	5.223	18.3				
22	2607.467	5.221	13.9				
23	2067.343	4.140	13.4				
24	2064.417	4.134	14.5				
25	2061.491	4.128	13.2				
26	1302.148	2.607	18.9				
27	1294.833	2.593	31.6				
28	1287.030	2.577	21.6				
29	1253.135	2.509	14.7				
30	1250.453	2.504	15.1				
31	1247.770	2.499	13.8				
32	792.018	1.586	8.4				
33	784.703	1.571	21.4				
34	782.752	1.567	11.6				
35	776.900	1.556	30.5				
36	774.949	1.552	16.0				
37	769.340	1.541	26.6				
38	767.634	1.537	15.7				
39	761.781	1.525	15.9				

BT-Ir-COD
CD2Cl2, TMS

Archive directory:
Sample directory:

Pulse Sequence: s2pul
Solvent: cd2cl2
Temp. 27.0 C / 300.1 K
User: 1-14-87
File: abp_59_c13
INOVA-500 "nmrastro"

Relax. delay 2.000 sec
Pulse 23.2 degrees
Acq. time 1.062 sec
Width 30143.2 Hz
1200 repetitions
OBSERVE C13, 125.5742496 MHz
DECOUPLE H1, 499.4021959 MHz
Power 39 dB
continuously on
WALTZ-16 modulated
DATA PROCESSING
Line broadening 1.0 Hz
FT size 65536
Total time 1 hr, 7 min, 58 sec

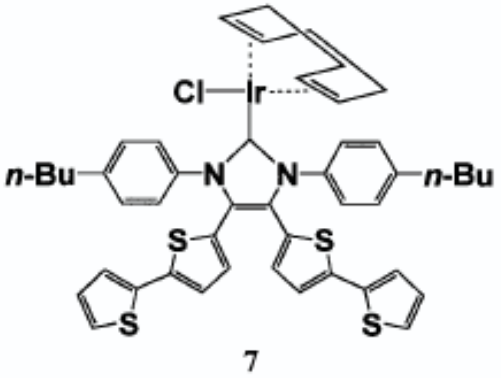

7

INDEX	FREQUENCY	PPM	HEIGHT
1	22932.109	182.618	24.2
2	17940.748	142.870	63.9
3	17501.958	139.375	58.1
4	17019.932	135.537	52.0
5	16934.381	134.856	54.8
6	16428.438	130.826	118.6
7	16078.877	128.043	88.2
8	15999.766	127.413	144.2
9	15962.050	127.112	129.7
10	15814.867	125.940	53.5
11	15809.347	125.896	54.7
12	15610.650	124.314	93.8
13	15504.861	123.472	95.8
14	15384.355	122.512	91.9
15	10315.723	82.148	90.6
16	6668.332	53.103	188.7
17	6641.655	52.890	416.6
18	6614.058	52.670	596.5
19	6587.381	52.458	407.6
20	6559.784	52.238	207.1
21	6373.045	50.751	89.4
22	4331.794	34.496	107.1
23	4111.939	32.745	114.8
24	4026.389	32.064	90.6
25	3527.804	28.093	96.0
26	2681.499	21.354	149.9
27	1624.538	12.937	115.9
28	0.000	0.000	23.6

BT-Ir-CO2Cl
CD2Cl2, TMS

Archive directory:
Sample directory:

Pulse Sequence: s2pul

Solvent: cd2cl2
Temp. 27.0 C / 300.1 K
File: abp_85_h1
INOVA-500 "nmrelroy"

Relax. delay 2.000 sec
Pulse 15.0 degrees
Acq. time 4.005 sec
Width 7990.4 Hz
64 repetitions
OBSERVE H1, 499.3997700 MHz
DATA PROCESSING
Line broadening 0.1 Hz
FT size 65536
Total time 6 min, 36 sec

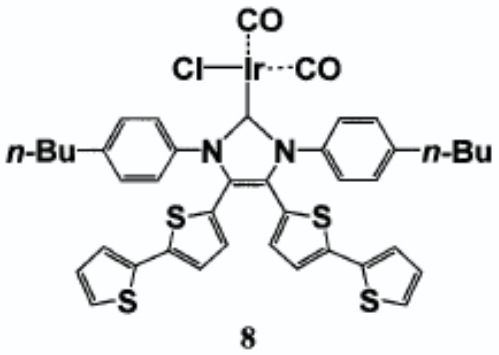

8

INDEX	FREQUENCY	PPM	HEIGHT	INDEX	FREQUENCY	PPM	HEIGHT
1	3679.423	7.368	35.7	40	419.419	0.840	63.2
2	3671.132	7.351	48.5	41	412.103	0.825	124.5
3	3598.709	7.206	53.1	42	404.788	0.811	57.5
4	3590.174	7.189	48.9	43	0.000	0.000	50.2
5	3556.035	7.121	31.1				
6	3554.816	7.118	32.5				
7	3550.915	7.110	34.1				
8	3549.695	7.108	33.9				
9	3481.174	6.971	29.3				
10	3479.955	6.968	30.8				
11	3477.516	6.963	36.0				
12	3476.541	6.961	35.0				
13	3429.235	6.867	32.0				
14	3425.577	6.859	33.9				
15	3423.626	6.855	61.1				
16	3419.724	6.848	59.8				
17	3324.868	6.658	48.8				
18	3320.966	6.650	50.8				
19	2723.538	5.454	28.4				
20	2602.590	5.211	66.7				
21	2597.469	5.201	11.5				
22	2596.494	5.199	12.7				
23	2595.274	5.197	11.2				
24	1302.392	2.608	26.4				
25	1294.589	2.592	39.0				
26	1286.786	2.577	28.8				
27	1122.676	2.248	80.6				
28	1121.701	2.246	79.6				
29	1120.482	2.244	67.9				
30	780.070	1.562	19.5				
31	778.607	1.559	17.8				
32	772.510	1.547	32.7				
33	770.072	1.542	21.1				
34	764.951	1.532	23.8				
35	757.148	1.516	12.4				
36	641.076	1.284	19.6				
37	633.517	1.269	32.2				
38	626.202	1.254	33.0				
39	618.886	1.239	20.9				

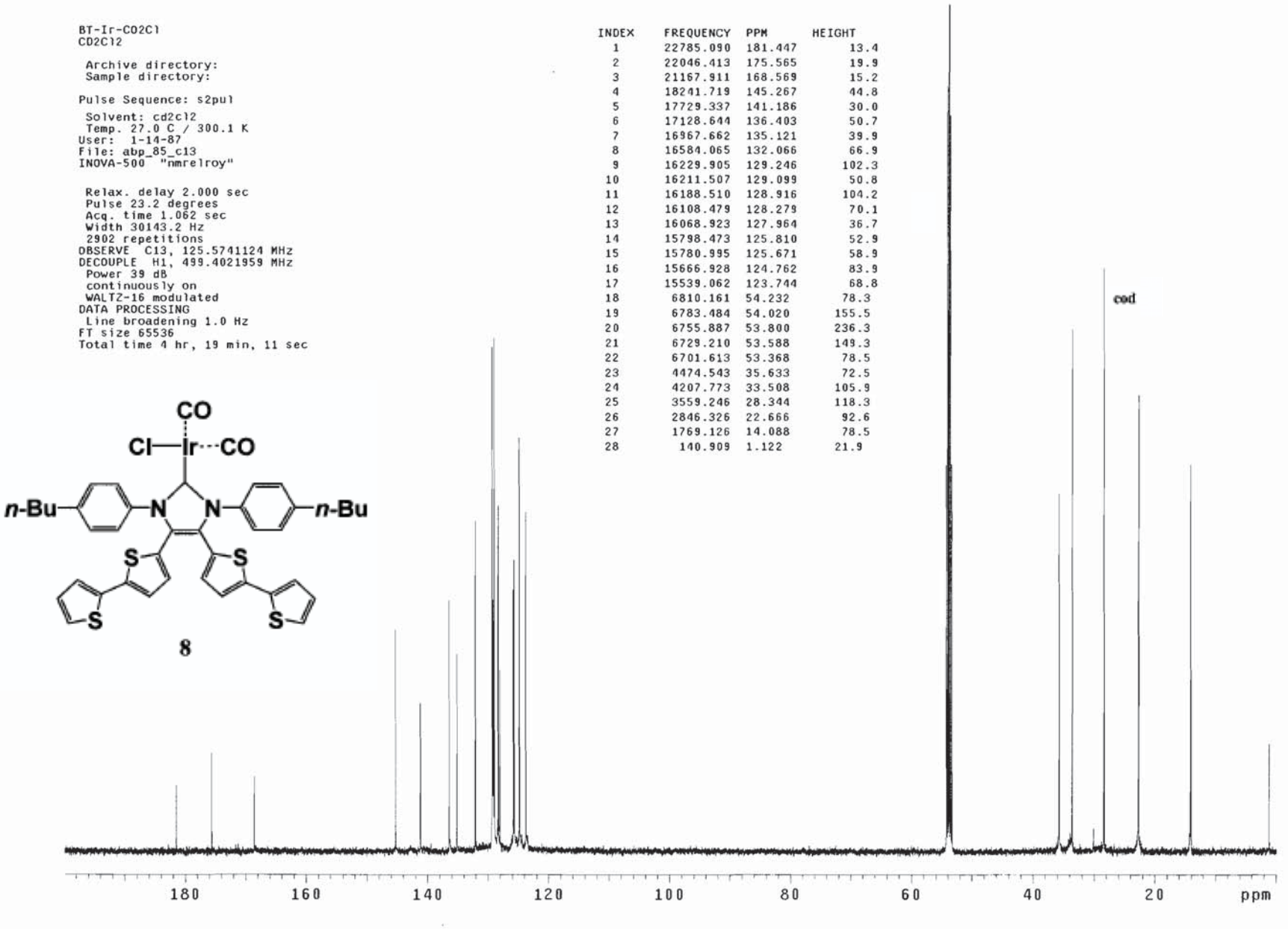
BT-Ir-CO2Cl
CD2Cl2
Archive directory:
Sample directory:
Pulse Sequence: s2pul
Solvent: cd2cl2
Temp. 27.0 C / 300.1 K
User: 1-14-87
File: abp_85_c13
INOVA-500 "nmrelroy"
Relax. delay 2.000 sec
Pulse 23.2 degrees
Acq. time 1.062 sec
Width 30143.2 Hz
2902 repetitions
OBSERVE C13, 125.5741124 MHz
DECOUPLE H1, 499.4021959 MHz
Power 39 dB
continuously on
WALTZ-16 modulated
DATA PROCESSING
Line broadening 1.0 Hz
FT size 65536
Total time 4 hr, 19 min, 11 sec
INDEX FREQUENCY PPM HEIGHT
1 22785.090 181.447 13.4
2 22046.413 175.565 19.9
3 21167.911 168.569 15.2
4 18241.719 145.267 44.8
5 17729.337 141.186 30.0
6 17128.644 136.403 50.7
7 16967.662 135.121 39.9
8 16584.065 132.066 66.9
9 16229.905 129.246 102.3
10 16211.507 129.099 50.8
11 16188.510 128.916 104.2
12 16108.479 128.279 70.1
13 16068.923 127.964 36.7
14 15798.473 125.810 52.9
15 15780.995 125.671 58.9
16 15666.928 124.762 83.9
17 15539.062 123.744 68.8
18 6810.161 54.232 78.3
19 6783.484 54.020 155.5
20 6755.887 53.800 236.3
21 6729.210 53.588 149.3
22 6701.613 53.368 78.5
23 4474.543 35.633 72.5
24 4207.773 33.508 105.9
25 3559.246 28.344 118.3
26 2846.326 22.666 92.6
27 1769.126 14.088 78.5
28 140.909 1.122 21.9
CO
Cl—Ir···CO
n-Bu
N
N
n-Bu
S
S
S
S
cod
180
160
140
120
100
80
60
40
20
ppm

8

Chapter 6

B(4Me-pyridine)4*3Br-
D2O
Adam Powell
abp9-2

Pulse Sequence: s2pul
Solvent: CDCl3
Ambient temperature
UNITYplus-300 "nmr3"

Relax. delay 1.000 sec
Pulse 20.2 degrees
Acq. time 1.814 sec
Width 20000.0 Hz
Single scan
OBSERVE B11, 96.2162650 MHz
DECOUPLE H1, 299.8891221 MHz
Power 40 dB
continuously on
WALTZ-16 modulated
Single precision data
DATA PROCESSING
Line broadening 6.0 Hz
FT size 131072
Total time 0 min, 2 sec

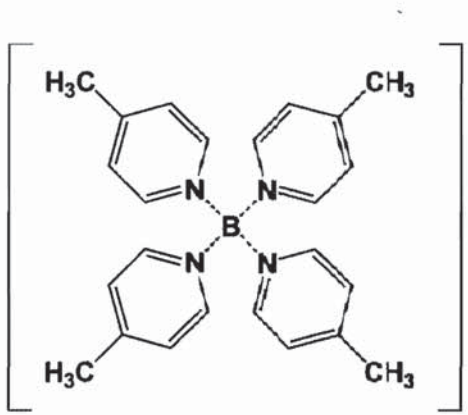

B(py)3Br 2Br-
CD3OD
Adam Powell
abp48

Pulse Sequence: s2pul
Solvent: CDCl3
Ambient temperature
File: abp48
INOVA-500 "nmrelroy"

Relax. delay 1.000 sec
Pulse 12.0 degrees
Acq. time 1.280 sec
Width 50000.0 Hz
160 repetitions
OBSERVE B11, 96.2166237 MHz
DATA PROCESSING
FT size 131072
Total time 39 min, 3 sec

INDEX	FREQUENCY	PPM	HEIGHT
* 1	820.510	8.528	29.5

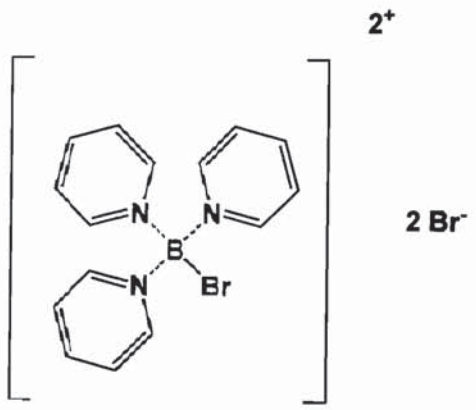

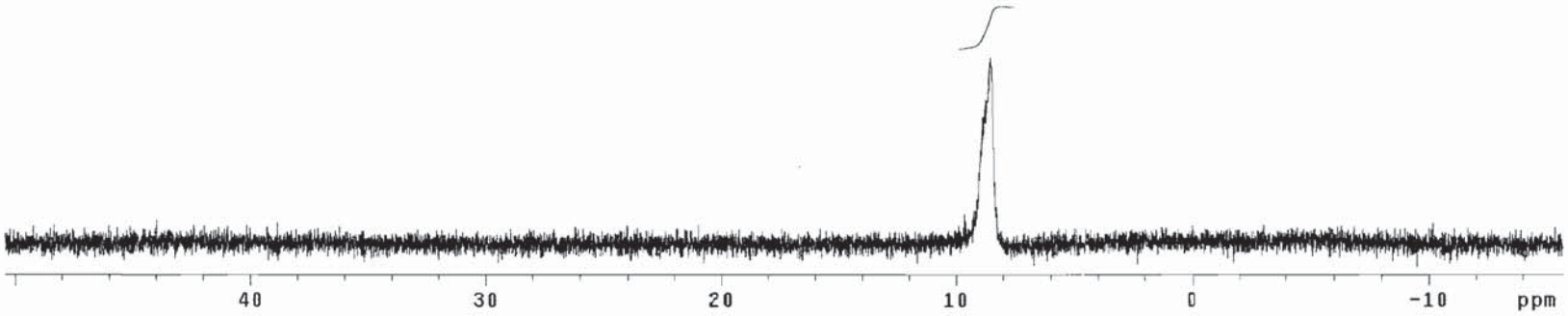

References

Chapter 1

1. (a) Marion, N.; Nolan, S. P. *Chem. Soc. Rev.* **2008**, *37*, 1776-1782. (b) Leyva, A.; Corma, A. *J. Org. Chem.* **2009**, *74*, 2067-2074. (c) Connon, S. J.; Blechert, S. *Bioorg. Med. Chem. Lett.* **2002**, *12*, 1873-1876. (d) McGuinness, D. *Dalton Trans.* **2009**, *35*, 6915-6923.
2. (a) Barnard, P. J.; Berners-Price, S. J. *Coord. Chem. Rev.* **2007**, *251*, 1889-1902. (b) Hindi, K. M.; Panzer, M. J.; Tessier, C. A.; Cannon, C. L. Youngs, W. J. *Chem. Rev.* **2009**, *109*, 3859-3884. (c) Hickey, J. L.; Ruhayel, R. A.; Barnard, P. J.; Murray, V.; Berners-Price, S. J.; Filipovska, A. *J. Am. Chem. Soc.* **2008**, *130*, 12570-12571. (d) Horvath, U. E. I.; Bentivoglio, G.; Hummel, M.; Schottenberger, H.; Wurst, K.; Nell, M. J.; van Rensburg, C. E. J.; Cronje, S.; Raubenheimer, H. G. *New J. Chem.* **2008**, *32*, 533-539.
3. Mercs, L.;Albrecht, M. *Chem. Soc. Rev.* **2010**, *39*, 1903-1912.
4. (a) Sommer, W.; Weck, M. *Coord. Chem. Rev.* **2007**, *251*, 860-873. (b) Vougioukalakis, G. C.; Grubbs, R. H. *Chem. Rev.* **2010**, *110*, 1746-1787. (c) Buchmeiser, M. R. *Chem. Rev.* **2009**, *109*, 303-321.
5. (a) Boydston, A. J.; Williams, K. A.; Bielawski, C. W. *J. Am. Chem. Soc.* **2005**, *127*, 12496-12497. (b) Kamplain, J. W.; Bielawski, C. W. *Chem. Commun.* **2006**, 1727-1729. (c) Boydston, A. J.; Rice, J. D.; Sanderson, M. D.; Dykhno, O. L; Bielawski, C. W. *Organometallics* **2006**, *25*, 6087-6098. (d) Boydston, A. J.; Bielawski, C. W. *Dalton Trans.* **2006**, 4073-4077. (e) Coady, D. J.; Kharmov, D. M.; Norris, B. C.; Tennyson, A. G.; Bielawski, C. W. *Angew. Chem., Int. Ed.* **2009**, *48*, 5187-5190. (f)

Norris, B. C.; Bielawski, C. W. *Macromolecules* **2010**, *43*, 3591-3593. (g) Tennyson, A. G.; Kamplain, J. W.; Bielawski, C. W. *Chem. Commun.* **2009**, 2124-2126. (h) Williams, K. A.; Boydston, A. J.; Bielawski, C. W. *J. R. Soc. Interface* **2007**, *4*, 359-362. (i) Hahn, F. E.; Radloff, C.; Pape, T.; Hepp, A. *Organometallics* **2008**, *27*, 6408-6410.

6. Powell, A. B.; Bielawski, C. W.; Cowley, A. H. *J. Am. Chem. Soc.* **2009**, *131*, 18232-18233.
7. (a) Tennyson, A. G.; Lynch, V. M.; Bielawski, C. W. *J. Am. Chem. Soc.* **2010**, *132*, 9420-9429. (b) Tennyson, A. G.; Rosen, E. L.; Collins, M. S.; Lynch, V. M.; Bielawski, C. W. *Inorg. Chem.* **2009**, 6924-6933.
8. Powell, A. B.; Brown, J. R.; Vasudevan, K. V.; Cowley, A. H. *Dalton Trans.* **2009**, *14*, 2521-2527.
9. (a) Skotheim, T. A.; Reynolds, J. R. *Handbook of Conducting Polymers*; 3rd ed.; CRC Press: Boca Raton, 2007. (b) Farchioni, R.; Grosso, G. *Organic Electric Materials*; Springer-Verlag: Berlin, 2001.
10. Voituriez, A.; Mellah, M.; Schulz, E. *Synth. Met.* **2006**, *156*, 166-175.
11. Powell, A. B.; Bielawski, C. W.; Cowley, A. H. *J. Am. Chem. Soc.* **2010**, *132*, 10184-10194.
12. Milum, K. M.; Kim, Y. N.; Holliday, B. J. *Chem. Mater.* **2010**, *22*, 2414-2416.
13. Beaujuge, P. M.; Reynolds, J. R. *Chem. Rev.* **2010**, *110*, 268-320.
14. Farrell, J. R.; Lavoie, D. P.; Pennell, R. T.; Cetin, A.; Shaw, J. L.; Ziegler, C. J. *Inorg. Chem.* **2007**, *46*, 6840-6842.

Chapter 2

1. (a) Klein, A.; Budnikova, Y. H.; Sinyashin, O. G. *J. Organomet. Chem*. **2007**, *692*, 3156-3166 (b) van Koten, G.; Vrieze, K. *Adv. Organomet. Chem.* **1982**, *21*, 151-239 (c) Uhlig, E. *Pure Appl. Chem.* **1988**, *60*(8), 1235-40 (d) Vlček, A. *Coord. Chem. Rev.* **2002**, *230*, 225-242 (e) Stufkens, D. J.; Vlček, A. *Coord. Chem. Rev.* **1998**, *177*, 127-129 (f) Trifonov, A. A. *Eur. J. Inorg. Chem.* **2007**, *20*, 3151-3167.
2. Moore, J. A.; Cowley, A. H.; Gordon, J. C. *Organometallics* **2006**, *25*, 5207-5209.
3. Chen, X. Y.; Yang, X.; Holliday, B. J. *J. Am. Chem. Soc.* **2008**, *130*, 1546-1547.
4. Faust, R.; Gobelt, H. *Tetrahedron Lett.* **1997**, *38*, 8017-8020.
5. Ogle J.; Zhang, J.; Reibenspies, J. H.; Abboud, K. A.; Miller, S. A. *Organic Lett.* **2008**, *10*(17), 3677-3680.
6. Hermann, W. A.; Kocher, C. *Angew. Chem. Int. Ed.* **1997**, *36*, 2162-2187.
7. (a) Dotz, K. H. *Metal Carbenes in Organic Synthesis*, Springer-Verlag, Berlin, 2004, vol. 13, and references therein (b) Bourissou, D.; Guerret, O.; Gabbaï, F. P.; Bertrand, G. *Chem. Rev.*, **2000**, *100*, 39-91.
8. Boydston, A. J.; Bielawski, C. W. *Dalton Trans.* **2006**, *34*, 4073-4077.
9. (a) Nakazawa, H.; Yamaguchi, Y.; Mizuta, T.; Miyoshi, K. *Organometallics* **1995**, *14*(9), 4173-4182 (b) Yamaguchi, Y.; Nakazawa, H.; Itoh, T.; Miyoshi, K. *Bull. Chem. Soc. Jpn.* **1996**, *69*, 983-985. (c) Nakazawa, H. *J. Organomet. Chem.* **2000**, *611*, 349-363.
10. Spinney, H. A.; Yap, G. P. A.; Korobkov, I.; DiLabio, G.; Richeson, D. S. *Organometallics* **2006**, *25*(15), 3541-3543.
11. Mehrotra, K. N.; Singh, G. *Synthesis* **1980**, 1001-1004.

12. Voituriez, A.; Mellah, M.; Schulz, E. *Synthetic Metals*, **2006**, *156*, 166-175.
13. Tovar, J. D.; Rose, A.; Swager, T. M. *J. Am. Chem. Soc.* **2002**, *124*, 7762-7769.
14. Ellis, B. D.; MacDonald, C. L. B. *Inorg. Chim. Acta* **2007**, *360*, 329-344.
15. (a) Reeske, G.; Hoberg, C. R.; Hill, N. J.; Cowley, A. H. *J. Am. Chem. Soc.* **2006**, *128*, 2800-2801. (b) Reeske, G.; Hoberg, C. R.; Cowley, A. H. *Inorg. Chem.*, **2007**, *46*, 1426-1430.
16. Carmalt, C. J.; Lomeli, V.; McBurnett, B. G.; Cowley, A. H. *Chem. Commun.*, **1997**, *21*, 2095-2096.
17. Sheldrick, G. M. *SHELL-PC*, version 5.03; Siemens Analytical X-ray Instruments, Inc.; Madison, WI, 1994.

Chapter 3

1. (a) Guan, Z.; Popeney, C. S. *Top. Organomet. Chem.* **2009**, *26*, 179-220. (b) Trifonov, A. A. *Russian Chem. Rev.* **2007**, *76*, 617-637. (c) de Bruin, B.; Bill, E.; Bothe, E.; Weyhermüller, T.; Wieghardt, K. *Inorg. Chem.* **2000**, *39*, 2936-2947.
2. Vielle-Petit, L.; Clavier, H.; Linden, A.; Blumentritt, S.; Nolan, S. P.; Dorta, R. *Organometallics* **2010**, *29*, 775-788.
3. (a) Patel, M.; Chhasatia, M.; Parmar, P. *Eur. J. Med. Chem.* **2010**, *45*, 439-446. (b) Pansuriya, P. B.; Patel, M. N. *Applied Organomet. Chem.* **2007**, *21*, 739-749.
4. (a) Ogle, J. W.; Miller, S. A. *Chem. Commun.* **2009**, 5728-5730. (b) Powell, A. B.; Bielawski, C. W.; Cowley, A. H. *J. Am. Chem. Soc.* **2010**, *192*, 10184-10194.
5. Armesto, D.; Bosch, P.; Gallego, M. G.; Martin, J. F.; Ortiz, M. J.; Perez-Ossorio, R.; Ramos, A. *Org. Prep. Proc. Int.* **1987**, *19*, 181-186.
6. (a) Cucinella, S.; Salvatori, T.; Busetto, C.; Perego, G.; Mazzei, A. *J. Organomet.*

Chem. **1974**, *78*, 185-201. (b) Moore, J. A.; Vasudevan, K.; Hill, N. J.; Reeske, G.; Cowley, A. H. *Chem. Commun.* **2006**, 2913-2915.

7. Faust, R.; Göbelt, B. *Tetrahed. Lett.* **1997**, *38*, 8017-8020.
8. Walia, J. S.; Singh, J.; Chattna, M. S.; Satyanarayana, M. *Tetrahed. Lett.* **1969**, *3*, 195-198.
9. Pavia, D. L.; Lampmann, G. M.; Kriz, G. S. Engel, R. G. *Organic Laboratory Techniques 2nd Edition*; Thompson Brooks/Cole; Belmont, CA 2005.
10. Becker, H. D. *J. Org. Chem.* **1970**, *35*, 2099-2102.
11. (a) Reich, B. J. E.; Justice, A. K.; Beckstead, B. T.; Reibenspies, J. H.; Miller, S. A. *J. Org. Chem.* **2004**, *69*, 1357-1359. (b) Walia, J. S.; Guillot, L.; Singh, J.; Chattha, M. S.; Satyanarayana, M. *J. Org. Chem.* **1972**, *37*, 135-137.
12. Reich, B. J. E.; Greenwald, E. E.; Justice, A. K.; Beckstead, B. T.; Reibenspies, J. H.; North, S. W.; Miller, S. A. *J. Org. Chem.* **2005**, *70*, 8409-8416.
13. (a) Ogle, J. W.; Zhang, J.; Reibenspies, J. H.; Abboud, K. A.; Miller, S. A. *Org. Lett.* **2008**, *10*, 3677-3680. (b) Ogle, J. W.; Miller, S. A. *Chem. Commun.* **2009**, 5728-5730.
14. Shimakawa, Y.; Morikawa, T.; Sakaguchi, S. *Tetrahed. Lett.* **2010**, *51*, 1786-1789.
15. Powell, A. B.; Brown, J. R.; Vasudevan, K. V.; Cowley, A. H. *Dalton Trans.* **2009**, 2521-2527.
16. (a) Schlüter, A. D. *J. Polym. Sci. Part A. Polym. Chem.* **2001**, *39*, 1533-1556. (b) Li, Y.; Li, H.; Xu, B.; Li, Z.; Chen, F.; Feng, D.; Zhang, J.; Tian, W. *Polymer* **2010**, *51*, 1786-1795. (c) Charas, A.; Ferreira, Q.; Farinhas, J.; Matos, M.; Alcácer, L.; Morgado, J. *Macromol.* **2009**, *42*, 7903-7912.

17. (a) Stefan, M. C.; Javier, A. E.; Osaka, I.; McCullough, R. D. *Macromol*. **2009**, *42*, 30-32. (b) Jeffries-EL, M.; Sauvé, G. McCullough, R. D. *Adv. Mater.* **2004**, *16*, 1017-1019.

Chapter 4

1. For a recent review, see Sommer, W. J.; Weck, M. *Coord. Chem. Rev.* **2007**, *251*, 860-873.
2. (a) Boydston, A. J.; Williams, K. A.; Bielawski, C. W. *J. Am. Chem. Soc.* **2005**, *127*, 12496-12497. (b) Kamplain, J. W.; Bielawski, C. W. *Chem. Commun.* **2006**, 1727-1729. (c) Boydston, A. J.; Rice, J. D.; Sanderson, M. D.; Dykhno, O. L; Bielawski, C. W. *Organometallics* **2006**, *25*, 6087-6098. (d) Boydston, A. J.; Bielawski, C. W. *Dalton Trans.* **2006**, 4073-4077. (e) Catalano, V. J.; Etogo, A .O. *Inorg. Chem.* **2007**, *46*, 5608-5615. (f) Karimi, B.; Akhavan, P. F. Chem. Commun. 2009, 3750-3752. (g) Coady, D. J.; Kharmov, D. M.; Norris, B. C.; Tennyson, A. G.; Bielawski, C. W. *Angew. Chem., Int. Ed.* **2009**, *48*, 5187-5190.
3. (a) Mercs, L., Neels, A., Stoeckli-Evans, and Albrecht, M. *Dalton Trans.* **2009**, 7168-7178 (b) Chiu, P. L., Chen, C. Y., Zeng, J. Y., Lu, C. Y., Lee, H. M. *J. Organomet. Chem.* **2005**, *690*, 1682-1687.
4. See, for example: (a) Marion, N.; Nolan, S. P. *Chem. Soc. Rev.* **2008**, *37*, 1776-1782. (b) Leyva, A.; Corma, A. *J. Org. Chem.* **2009**, *74*, 2067-2074 (c) Corti, C. W.; Holliday, R. J.; Thompson, D. T. *Topics in Catalysis* **2007**, *44*, 331-343.
5. (a) Barnard, P. J.; Berners-Price, S. J. *Coord. Chem. Rev.* **2007**, *251*, 1889-1902. (b) Hindi, K. M.; Panzer, M. J.; Tessier, C. A.; Cannon, C. L. Youngs, W. J. *Chem. Rev.* **2009**, *109*, 3859-3884. (c) Hickey, J. L.; Ruhayel, R. A.; Barnard, P. J.; Murray, V.; Berners-Price, S. J.; Filipovska, A. *J. Am. Chem. Soc.* **2008**, *130*, 12570-12571. (d) Horvath, U. E. I.; Bentivoglio, G.; Hummel, M.; Schottenberger, H.; Wurst, K.; Nell, M. J.; van Rensburg, C. E. J.; Cronje, S.; Raubenheimer, H. G. *New J. Chem.* **2008**,

32, 533-539. (e) Gold nanoparticles have been used in a variety of medicinal applications, see: Boisselier, E.; Didier, A. *Chem. Soc. Rev.* **2009**, *38*, 1759-1782.

6. Powell, A. B.; Brown, J. R.; Vasudevan, K. V.; Cowley, A. H. *Dalton Trans.* **2009**, 2521-2527.
7. de Frėmont, P.; Scott, N.; Stevens, E. D.; Nolan, S. P. *Organometallics* **2005**, *24*, 2411-2418.
8. (a) Skotheim, T. A.; Reynolds, J. R. *Handbook of Conducting Polymers 3rd Ed.*; CRC Press; Boca Raton, 2007. (b) Farchioni, R.; Grosso, G. *Organic Electric Materials;* Springer-Verlag; Berlin 2001.
9. (a) Decamethylferrocene (Fc*) was used as an external reference and all reported potentials are relative to the Fc^{*0}/Fc^{*+} redox couple (set to zero). (b) Monomer oxidation wave was observed near 1.35 V.
10. (a) Chen, X. Y.; Yang, X.; Holliday, B. J. *J. Am. Chem. Soc.* **2008**, *130*, 1546-1547. (b) González-Tejera, M. J.; de la Blanca, E. S.; Carillo, I.; Redondo, M. I.; Raso, M. A.; Tortajada, J.; Garcia, M. V. *Synthetic Metals* **2005**, *151*, 100-105. (c) Voituriez, A.; Mellah, M.; Schulz, E.; *Synthetic Metals* **2006**, 166-175.
11. We acknowledge that multiple Au···Au interactions may be forming the polymer films and contribute to the stabilities of these materials.
12. (a) Hesse, R.; Strenbel, P.; Szargan, R. *Surf. Interface Anal.* **2005**, *37*, 589-607. (b) Smith, E. L.; Glidle, A.; Mortimer, R. J.; Ryder, K. S. *Phys. Chem. Chem. Phys.* **2007**, *9*, 6098-6105.
13. Guarin, S. A. P.; Bourgeaux, M.; Dufresne, S.; Skene, W. G. *J. Org. Chem.* **2007**, *72*, 2631–2643.

14. Sheldrick, G. M. *SHELL-PC*, version 5.03; Siemens Analytical X-ray Instruments, Inc. Madison, WI, 1994.
15. Ogle, J. W.; Zhang, J.; Reibenspies, J. H.; Abboud, K. A.; Miller, S. A. *Org. Lett.* **2008**, *10*, 3677-3680.

Chapter 5

1. Chiang, C. K.; Fincher, C. R.; Park, Y. W.; Heeger, A. J.; Shirakawa, H.; Louis, E. J.; Gau, S. C.; MacDiarmid, A. G. *Phys. Rev. Lett.* **1977**, *39*(17), 1098-1101.
2. (a) Wong, W. Y.; Wang, X. Z.; He, Z.; Djurisic, A. B.; Yip, C. T.; Cheung, K. Y.; Wang, H.; Mak, C. S. K. Chan, W. K. *Nat. Mater.* **2007**, *6*, 521-527. (b) Knapton, D.; Rowan, S. J.; Weder, C. *Macromolecules* **2006**, *39*, 651-657. (c) Hou, J. H.; Huo, L. J.; He, C.; Yang, C. H.; Li, Y. F. *Macromolecules* **2006**, *39*, 594–603. (d) Zhou, E.; Zhan'ao, T.; Lijun, H.; Youjun, H.; Chunhe, Y.; Yongfang, L; *J. Phys. Chem B*. **2006**, *110*, 26062– 26067.
3. (a) Wong, W. Y. *Dalton Trans.* **2007**, 4495-4510. (b) Holliday, B. J.; Stanford, T. B.; Swager, T. M. *Chem. Mater.* **2006**, *18*, 5649-5651. (c) Tennyson, A. G.; Do, L.; Smith, R. C.; Lippard, S. J. *Polyhedron* **2007**, *26*, 4625–4630. (d) He, S.; Iacono, S.T.; Budy, S.M.; Dennis, A.E.; Smith, D.W.; Smith, R.C. *J. Mater. Chem.* **2008**, *18*, 1970–1976.
4. (a) Boopathi, M.; Won, M. S.; Shim, Y. B. *Anal. Chim. Acta* **2004**, *512*, 191-197. (b) Halldorsson, J. A.; Little, S. J.; Diamond, D.; Spinks, G.; Wallace, G. *Langmuir* **2009**, *25*(18), 11137-11141. (c) Moulton, S. E.; Imisides, M. D.; Shepherd, R. L.; Wallace, G. G. *J. Mater. Chem.* **2008**, *18*(30), 3608-3613. (d) George, P. M.; LaVan, D. A.; Burdick, J. A.; Chen, C. Y.; Liang, E.; Langer, R. *Adv. Mater.* **2006**, *18*(5), 577-581.
5. Moorlag, C.; Clot, O.; Zhu, Y.; Wolf, M. O. *Macromol. Symp.* **2004**, *209*, 133-139.

6. (a) Chen, X. Y.; Yang, X.; Holliday, B. J. *J. Am. Chem. Soc.* **2008**, *130*, 1546-1547. (b) Hesterberg, T. W.; Yang, X.; Holliday, B. J. *Polyhedron*, **2010**, *29*, 110–115.
7. (a) Kingsborough, R. P.; Swager, T. M. *J. Am. Chem. Soc.* **1999**, *121*, 8825-8834. (b) Kurashina, M.; Murata, M.; Watanabe, T.; Hishihara, H. *J. Am. Chem. Soc.* **2003**, *196*, 27-38.
8. For recent reviews see: (a) Eloi, J. C.; Chabanne, L.; Whittel, G. R.; Manners, I. *Materials Today* **2008**, *11*(4), 28–36. (b) Wolf, M. O. *J. Inorganic and Organometallic Polymers and Materials* **2006**, *16*(3), 189-199.
9. (a) Sauvage, J. P.; Kern, J. M.; Bidan, G.; Divisia-Blohorn, B.; Vidal, P. L. *New J. Chem.* **2002**, *26*, 1287–1290. (b) Jousselme, B.; Blanchard, P.; Ocafrain, M.; Allain, M.; Levillain, E.; Roncali, J. *J. Mater. Chem.* **2004**, *14*, 421–427.
10. Powell, A. B.; Brown, J. R.; Vasudevan, K. V.; Cowley, A. H. *Dalton Trans.* **2009**, *14*, 2521–2527.
11. Interestingly, a recent publication revealed a similar outcome with respect to electropolymerizable phosphine-substituted monomers. Velauthamurty, K.; Higgins, S. J.; Rajapakse, R. M. G.; Bacsa, J.; van Zalinge, H.; Nichols, R. J.; Haiss, W. *J. Mater. Chem.* **2009**, *19*(13), 1850–1858.
12. (a) Radloff, C.; Hahn, F. E.; Pape, T.; Frölich *Dalton Trans.* **2009**, *35*, 7215–7222. (b) Hahn, F. E.; Radloff, C.; Pape, T.; Hepp, A. *Organometallics* **2008**, *27*, 6408–6410. (c) Karimi, B.; Akhaven, P. F. *Chem. Commun.* **2009**, *25*, 3750–3752. (d) Bartolome, C.; Ramiro, Z.; Garcia-Cuadrado, D.; Pérez-Galán, Raducan, M.; Bour, C.; Echavarren, A. M.; Espinet, P. *Organometallics* **2010**, *29*, 951–956. For recent reviews see: (e) Diez-Gonzalez, S.; Marion, N.; Nolan, S.P. *Chem. Rev.* **2009**, *109*, 3612-3676. (f) Lin, J. C. Y.; Huang, R. T. W.; Lee, C. S.; Bhattacharyya, A.; Hwang,

W. S.; Lin, I. J. B. *Chem. Rev.* **2009**, *109*, 3561-3598. (g) Kühl, O. *Chem. Soc. Rev.* **2007**, *36*, 592–607. (h) Arnold, P. L.; Pearson, S. *Coord. Chem. Rev.* **2007**, *251*(5-6), 596–609.

13. Winter, A.; Friebe, C.; Chiper, M.; Hager, M. D.; Schubert, U.S. *J. Polym. Sci. Part A.* **2009**, *47*(16), 4083–4098.
14. Leung, A. C. W.; Chong, J. H.; MacLachlan, M. J. *Macromol. Symp.* **2003**, *196*, 229–234.
15. Malinauskas, A. *Synthetic Met.* **1999**, *107*, 75–83.
16. (a) Boydston, A. J.; Williams, K. A.; Bielawski, C. W. *J. Am. Chem. Soc.* **2005**, *127*, 12496-12497. (b) Kamplain, J. W.; Bielawski, C. W. *Chem. Commun.* **2006**, *16*, 1727-1729. (c) Boydston, A. J.; Rice, J. D.; Sanderson, M. D.; Dykhno, O. L; Bielawski, C. W. *Organometallics* **2006**, *25*, 6087-6098. (d) Boydston, A. J.; Bielawski, C. W. *Dalton Trans.* **2006**, 4073-4077. (e) Catalano, V. J.; Etogo, A .O. *Inorg. Chem.* **2007**, *46*, 5608-5615. (f) Karimi, B.; Akhavan, P. F. Chem. Commun. **2009**, *25*, 3750-3752. (g) Coady, D. J.; Kharmov, D. M.; Norris, B. C.; Tennyson, A. G.; Bielawski, C. W. *Angew. Chem. Int. Ed.* **2009**, *48*, 5187-5190. (h) Mercs, L.; Neels, A.; Stoeckli-Evans, H.; Albrecht, M. *Dalton Trans* **2009**, *35*, 7168–7178. (i) Chiu, P. L.; Chen, C. Y.; Zeng, J. Y.; Lu, C. Y.; Lee, H. M. *J. Organomet. Chem.* **2005**, *690*(6), 1682–1687. (j) Guerret, O.; Solé, S.; Gornitzka, H.; Teichert, M.; Trinquier, G.; Bertrand, G. *J. Am. Chem. Soc.* **1997**, *119*, 6668–6669.
17. Powell, A. B.; Bielawski, C. W.; Cowley, A. H. *J. Am. Chem. Soc.* **2009**, *131*, 18232–18233.
18. Farrell, J. R.; Lavoie, D. P.; Pennel, R. T.; Cetin, A.; Shaw, J. L.; Ziegler, C. J. *Inorg. Chem.* **2007,** *46*, 6840–6842.

19. (a) Padilla, J.; Seshadri, V.; Sotzing, G. A.; Otero, T. F. *Electrochem. Commun.* **2007**, *9*(8), 1931–1935. (b) Mecerreyes, D.; Marcilla, R.; Ochoteco, E.; Grande, H.; Pomposo, J. A.; Vergaz, R.; Sánchez Pena, J. M. *Electrochem. Acta* **2004**, *49*(21), 3555–3559.

20. (a) Mortimer, R. G. *Chem. Soc. Rev.* **1997**, *26*(3), 147–156. (b) Granqvist, C. G.; Azens, A.; Isidorsson, J.; Kharrazi, M.; Kullman, L.; Lindstroem, T.; Niklasson, G. A.; Ribbing, C. G.; Roennow, D.; Stromme Mattson, M.; Veszelei, M. *J. Non-Cryst. Solids* **1997**, *218*, 273–279.

21. Kraft, A.; Grimsdale, A. C.; Holmes, A. B. *Angew. Chem. Intl. Ed.* **1998**, *37*(4), 403–428.

22. (a) Sonmez, H.; Meng, H.; Wudl, F. *Chem. Mater.* **2003**, *15*(26), 4923–4929. (b) Meng, H.; Tucker, S.; Chaffins, Y.; Chen, R.; Helgeson, R.; Dunn, B.; Wudl, F. *Adv. Mater.* **2003**, *15*(2), 146–149.

23. Pang, Y.; Li, X.; Ding, H.; Shi, G.; Jin, L. *Electrochim. Acta* **2007**, *52*, 6172–6177.

24. Noviadri, I.; Brown, K. N.; Fleming, D. S.; Gulyas, P. T.; Lay, P. A.; Masters, A. F.; Phillips, L. *J. Phys. Chem. B.* **1999**, *103*, 6713–6722.

25. Sheldrick, G. M. *SHELL-PC*, version 5.03; Siemens Analytical X-ray Instruments, Inc. Madison, WI, 1994.

26. Newman, C. P.; Clarkson, G. J.; Rourke, J. P. *J. Organomet. Chem.* **2007**, *692*, 4962-4968.

27. (a) Chen, F.; Oh, S. W.; Wasylishen, R. E. *Can. J. Chem.* **2009**, *87*, 1090–1101. (b) Ramnial, T.; Abernethy, C. D.; Spicer, M. D.; McKenzie, I. D.; Gay, I. D.; Clyburne, J. A. C. *Inorg. Chem.* **2003**, *42*(5), 1391-1393.

28. Ogle, J. W.; Zhang, J.; Reibenspies, J. H.; Abboud, K. A.; Miller, S. A. *Org. Lett.* **2008**, *10*(17), 3677-3680.
29. Paas, M.; Wibbeling, B.; Fröhlich, R.; Hahn, F.E. *Eur. J. Inorg.* **2006**, *1*, 158–162.
30. Bayler, A.; Schier, A.; Bowmaker, G. A.; Schmidbaur, H. *J. Am. Chem. Soc.* **1996**, *118*, 7006–7007.
31. Lee, C. K; Vasam, C. S.; Huang, T. W.; Wang, H. M. J.; Yang, R. Y.; Lee, C. S.; Lin, I. J. B. *Organometallics* **2006**, *25*, 3768–3775.
32. Chang, Y. H.; Fu, C. F.; Liu, Y. H.; Peng, S. M.; Chen, J. T.; Liu, S. T. *Dalton Trans.* **2009**, 861-867.
33. Ogle, J. W.; Miller, S. A. *Chem. Commun.* **2009**, *38*, 5728–5730.
34. Bittermann, A.; Herdtweck, E.; Härter, P.; Herrmann, W. A. *Organometallics*, **2009**, *28*, 6963–6968.
35. (a) Turkmen, H.; Sahin, O.; Buyukgungor, O.; Cetinkaya, B. *Eur. J. Inorg. Chem.* **2006**, *23*, 4915–4921. (b) Burford, N.; Phillips, A. D.; Spinney, H. A.; Robertson, K. N.; Cameron, T. S. *Inorg. Chem.* **2003**, *42*(16), 4949–4954.
36. Scan rates for poly(**3**)–poly(**8)** above 100 mV/s resulted in distortions of the electrochemical profiles due to kinetic limitations on the counterion diffusion in and out of the polymer matrix.
37. XPS analysis of the monomers was unsuccessful due to their inability to form thin films.
38. The diimine thin film poly(**1**) could not be deposited on either stainless steel or ITO glass for further characterization.
39. The cyclization succeeded in eliminating the reduction of the diimine moiety, but no thin film poly(**2**) was detected on the electrode in monomer-free solution.

40. de Frémont, P.; Scott, N. M.; Stevens, E. D.; Ramnial, T.; Lightbody, O. C.; MacDonald, C. L. B.; Clyburne, J. A. C.; Abernethy, C. D.; Nolan, S. P. *Organometallics* **2005**, *24*, 6301–6309.
41. Hesse, R.; Streubel, P.; Szargan, R. *Surf. Interface Anal.* **2005**, *37*, 589-607.
42. For a recent review see: Hindi, K. M.; Panzer, M. J.; Tessier, C. A.; Cannon, C. L.; Youngs, W. J. *Chem. Rev.* **2009**, *109*, 3859–3884.
43. Moulder, J. F.; Stickle, W. F.; Sobol, P. E.; Bomben, K. *Handbook of X-ray Photoelectron Spectroscopy 2nd Ed.*; Perkin–Elmer; Eden Prarie, 1992.
44. Bates, J. R.; Kathirgamanathan, P.; Miles, R. W. *Thin Solid Films* **1997**, *299*, 18–24.
45. To further strengthen this explanation the thione analogue of the Kühn carbene was synthesized, analyzed by cyclic voltammetry and shown to possess similar electrochemical features as described in the literature for other thione compounds. The electrochemistry of Kühn thione is shown in supporting information.
46. Tennyson, A. G.; Rosen, E. L.; Collins, M. S.; Lynch, V. M.; Bielawski, C. W. *Inorg. Chem.* **2009**, *48*, 6924–6933.
47. Deng, Y. D.; Liu, S. J.; Fan, Q. L.; Fang, C.; Zhu, R.; Pu, K. Y.; Yuwen, L. H.; Wang, L. H.; Huang, W. *Synthetic Met.* **2007**, *157*, 813-822.
48. For a recent review see: Beaujuge, P. M.; Reynolds, J. R. *Chem. Rev.* **2010**, *110*, 268–320.
49. (a) Skotheim, T. A.; Reynolds, J. R. *Handbook of Conducting Polymers 3rd Ed.*; CRC Press; Boca Raton, 2007. (b) Farchioni, R.; Grosso, G. *Organic Electric Materials;* Springer-Verlag; Berlin 2001.
50. Tehrani, P.; Robinson, N. D.; Kugler, T.; Romonen, T.; Hennerdal, L. O.; Häll, J.; Malström, A.; Leenders, L.; Berggren, M. *Smart Mater. Struct.* **2005**, *14*, N21–N25.

Chapter 6

1. Chen, E. Y.; Marks, T. J. *Chem. Rev.* **2000**, *100*(4), 1391-1434. (b) Piers, W. E. *Adv. Organomet. Chem.* **2005**, *52*, 1-76. (c) Satyanarayana, T.; Kagan, H. B. *Adv. Synth. Catal.* **2005**, *347*, 737-748.
2. (a) Piers, W. E.; Bourke, S. C.; Conroy, K. D. *Angew. Chem. Int. Ed.* **2005**, *44*(32), 5016-5036. (b) Ryu, D. H.; Zhou, G.; Corey, E. J. *J. Am. Chem. Soc.* **2004**, *126*, 4800-4802.
3. Sowa, F. J. *US Pat.*, 2 655 524 1953; *Chem. Abs.* 19544813704f.
4. (a) Prasad, S.; Singh, N. P. *Z. Anorg. Chem.* **1966**, *346*, 217. (b) Prasad, S.; Singh, N. P. *Z. Anorg. Chem.* **1967**, *350*, 332.
5. (a) Makosky, C. W.; Galloway, Ryschkewitsch, G. E. *Inorg. Chem.* **1967**, *6*, 1972-1974. (b) Ryschkewitsch, G. E.; Galloway, G. E. *Inorg. Synth.* **1970**, *12*, 141-143. (c) Nainan, K. C.; Ryschkewitsch, G. E. *J. Am. Chem. Soc.* **1969**, *91*(2), 330-336.
6. (a) Nöth, H.; Wrackmeyer, B. *Nuclear Magenetic Resonance of Boron Compounds*, Springer Verlag, Berlin, 1978. (b) Findlater, M.; Hill, N. J.; Cowley, A. H. *Dalton Trans.* **2008**, 4419-4423.
7. Hanasaka, F.; Fujita, K.; Yamaguchi, R. *Organometallics* **2005**, *24*(14), 3422-3433.
8. (a) Cowley, A. H.; Lu, Z.; Jones, J. N.; Moore, J. A. *J. Organomet. Chem.* **2004**, *689*, 2562-2564. (b) Vidovic, D.; Findlater, M.; Cowley, A. H. *J. Am. Chem. Soc.* **2007**, *129*, 8436-8437.
9. Kölle, P.; Nöth, H. *Chem. Rev.* **1985**, *85*, 399-348.

Vita

Adam B. Powell was born in Charleston, South Carolina on June 10, 1983, the son of Edward and Carolyn Powell. After completing his work at Winter Springs High School in Winter Springs, Florida, he received an Associate of Arts degree from Valencia Community College in May 2003. Following that Adam earned a Bachelor of Science in Chemistry from the University of Central Florida in December 2005. In August 2006, he entered the graduate program in Chemistry at the University of Texas at Austin.

Permanent address: 1480 Connors Lane
Winter Springs, FL 32708

This dissertation was typed by the author.